UNCLASSIFIED

AD NUMBER

AD355284

CLASSIFICATION CHANGES

TO: unclassified

FROM: confidential

LIMITATION CHANGES

TO:

Approved for public release, distribution unlimited

FROM:

Distribution authorized to U.S. Gov't. agencies and their contractors; Specific Authority; Oct 64. Other requests shall be referred to Air Force Flight Dynamics Lab., Research and Technology Div., Air Force Systems Command, Wright-Patterson AFB, OH 45433.

AUTHORITY

AFFDL ltr., dtd July 13, 1971.; AFFDL ltr., dtd July 13, 1971.

THIS PAGE IS UNCLASSIFIED

UNCLASSIFIED

AD 355284L

CLASSIFICATION CHANGED
TO: UNCLASSIFIED
FROM: CONFIDENTIAL
AUTHORITY: AFFDL - ltr, 13 - July - 71

UNCLASSIFIED

government or other drawings, speci-
other data are used for any purpose
connection with a definitely related
government operation, the U. S.
Army incurs no responsibility, nor any
whatsoever; and the fact that the Govern-
formulated, furnished, or in any way
such drawings, specifications, or other
be regarded by implication or other-
wise in any manner licensing the holder or any
corporation, or conveying any rights
to manufacture, use or sell any
that may in any way be related

NOTICE:

DOCUMENT CONTAINS INFORMATION
AFFECTING THE NATIONAL DEFENSE OF
UNITED STATES WITHIN THE MEAN-
OF THE ESPIONAGE LAWS, TITLE 18,
, SECTIONS 793 and 794. THE
TRANSMISSION OR THE REVELATION OF
CONTENTS IN ANY MANNER TO AN
UNAUTHORIZED PERSON IS PROHIBITED

355284

RTD-TDR-63-4219

(Unclassified Title)

HYPERSONIC FLUTTER MODEL TESTS OF ADVANCED WING CONFIGURATIONS AT INITIAL ANGLES OF ATTACK

TECHNICAL DOCUMENTARY REPORT NO. RTD-TDR-63-4219

October 1964

CATALOGED BY DDC
AS AD No.

Air Force Flight Dynamics Laboratory
Research and Technology Division
Air Force Systems Command
Wright-Patterson Air Force Base, Ohio

Project No. 1370, Task No. 137003

DOWNGRADED AT 3 YEAR INTERVALS;
DECLASSIFIED AFTER 12 YEARS
DOD DIR. 5200.10

(Prepared under Contract No. AF33(616)-7770
by North American Aviation, Inc.,
4300 East Fifth Avenue
Columbus, Ohio
Author: S. R. Hurley)

THIS DOCUMENT CONTAINS INFORMATION AFFECTING THE NATIONAL DEFENSE OF THE UNITED STATES WITHIN THE MEANING OF THE ESPIONAGE LAWS TITLE 18 U.S.C. SECTIONS 793 AND 794, ITS TRANSMISSION OR THE REVELATION OF ITS CONTENTS IN ANY MANNER TO AN UNAUTHORIZED PERSON IS PROHIBITED BY LAW.

355284

AF-WP-8-NOV 64 6 1

64FD-724

UNCLASSIFIED

NOTICES

When Government drawings, specifications, or other data are used for any purpose other than in connection with a definitely related Government procurement operation, the United States Government thereby incurs no responsibility nor any obligation whatsoever; and the fact that the Government may have formulated, furnished, or in any way supplied the said drawings, specifications, or other data, is not to be regarded by implication or otherwise as in any manner licensing the holder or any other person or corporation, or conveying any rights or permission to manufacture, use, or sell any patented invention that may in any way be related thereto.

This document contains information affecting the National defense of the United States within the meaning of the Espionage Laws, Title 18, U.S.C., Sections 793 and 794. Its transmission or the revelation of its contents in any manner to an unauthorized person is prohibited by law.

Qualified requesters may obtain copies of this report from the Defense Documentation Center (DDC), (formerly ASTIA), Cameron Station, Bldg. 5, 5010 Duke Street, Alexandria, Virginia, 22314.

Copies of this report should not be returned to the Research and Technology Division, Wright-Patterson Air Force Base, Ohio, unless return is required by security considerations, contractual obligations, or notice on a specific document.

UNCLASSIFIED

FOREWORD

The research work in this report was performed by North American Aviation, Inc., Columbus, Ohio, for the Aerospace Dynamics Branch, Vehicle Dynamics Division, Air Force Flight Dynamics Laboratory, Wright-Patterson Air Force Base, Ohio under Contract AF33(616)-7770. This research is part of a continuing effort to advance the aeroelastic state-of-the-art for flight vehicles and is part of the Research and Technology Division, Air Force Systems Command's exploratory development program. This work was performed under Project No. 1370, "Dynamic Problems in Flight Vehicles" and Task No. 137003, "Prediction and Prevention of Aerothermoelastic Instabilities." Mr. James J. Olsen of the Aerospace Dynamics Branch was Task Engineer. The research program was conducted by the Dynamics Group of the Applied Mechanics Section, Research and Development Division, of North American Aviation, Inc., Columbus, Ohio. This work was performed by the Contract Project Engineer, Mr. S. R. Hurley and with the assistance of Mr. D. A. Brown.

The author wishes to express his appreciation to all personnel at the Columbus Division of North American Aviation who have contributed to the accomplishment of the work reported herein. Additionally, mention should be made of the excellent assistance and services provided by the personnel at Arnold Engineering Development Center during the experimental phases of this contract.

This report is classified CONFIDENTIAL since it contains experimental test data and significant results and conclusions which are pertinent to the development of military weapon systems, the unauthorized disclosure of which is considered to be prejudicial to the defense interests of the United States.

This technical documentary report has been reviewed and is approved.

Walter J. Mykytow

WALTER J. MYKYTOW
Asst. for Research & Technology
Vehicle Dynamics Division

This abstract is classified CONFIDENTIAL

ABSTRACT

This report presents an experimental and analytical flutter investigation of a low aspect ratio lifting surface with a 70° leading edge sweep angle, and thickness ratios of 3%, 6%, and 9% in the hypersonic speed range from M = 5.0 to M = 8.0. The 6% thickness ratio models were tested at uncoupled frequency ratios of .60, .75, and .90. The models used were of the semi-rigid type with a double wedge leading edge to 15% chord with constant thickness from the 15% chord to a blunt trailing edge.

All experimental flutter configurations were analyzed using an analog representation of a quasi-steady flutter solution. The aerodynamic representations investigated were experimentally obtained static aerodynamic force coefficients and aerodynamic force coefficients derived from steady-state, two-dimensional, "shock-expansion" techniques with sweep angle corrections. Additionally, the relative effect on the flutter characteristics of inclusion of "piston theory" derived rate terms in the aerodynamics was investigated for several configurations.

The results indicate that some aerodynamic flow disturbance was generated by the splitter plate mounting system which influenced certain aerodynamic force coefficients. A pronounced effect on the pitching moment coefficient was observed at M = 7.0 due to shock detachment and was reflected in flutter characteristics. It was concluded that the "modified shock-expansion" theory predictions exhibit poor correlation with experiment in the case of pitching moment coefficient, but excellent agreement with experiment in the case of rolling moment coefficient. Increasing airfoil thickness ratio and angle-of-attack result in depreciating agreement between experimental and "shock-expansion" aerodynamics.

A stabilizing effect in flutter velocity is noted at M = 7.0, relative to M = 5, 6, and 8. The effect of increasing angle-of-attack was found to be slightly destabilizing at all Mach numbers over the experimental range investigated. For the modal frequency ratios investigated, a slight destabilizing effect was noted with increasing frequency ratio.

Abstract Continued on page iv

ABSTRACT CONT'D

In general, flutter analyses using experimental aerodynamic force coefficients are sufficiently accurate to predict flutter speed trends for preliminary design purposes. The prediction of flutter frequencies using this technique, however, is inadequate.

Flutter analyses using "modified shock-expansion" techniques are a very inexpensive, simple preliminary design tool and resulted in increased accuracy over results obtained from "piston theory."

The effect of including aerodynamic rate terms, as derived from "piston theory," in the theoretical studies performed was negligible.

Certain improvements in similar experimental studies are recommended.

TABLE OF CONTENTS

SECTION		PAGE
	INTRODUCTION	1
I	MODEL DESIGN AND CONSTRUCTION	3
	A. Environmental Conditions	3
	B. Static Force Models	3
	C. Semi-Rigid Flutter Models	3
II	SUSPENSION SYSTEM DESIGN AND CONSTRUCTION	4
III	PRELIMINARY TEST PROCEDURES	5
	A. Mass Characteristics	5
	B. Environmental Temperature Tests	5
	C. Preliminary Vibration Tests	6
IV	WIND TUNNEL TESTS	7
	A. General	7
	B. Static Aerodynamic Force Tests	7
	C. Flutter Tests	7
V	EXPERIMENTAL AND THEORETICAL RESULTS	10
	A. Static Aerodynamic Forces	10
	B. Flutter Results	10
VI	THEORETICAL ANALYSES	11
	A. General	11
	B. Equations of Motion	11

TABLE OF CONTENTS (CONT'D)

SECTION		PAGE
	C. Quasi-Steady Flutter Analysis Methods	17
	D. Quasi-Steady Flutter Analyses Using Experimental Aerodynamics	18
	E. Quasi-Steady Flutter Analyses Using Modified "Shock-Expansion" Aerodynamics	18
	F. Analog Analysis Techniques	22
VII	DISCUSSION OF RESULTS	25
	A. Evaluation of Flow Characteristics in the Vicinity of the Splitter Plate	25
	B. Experimental Static Aerodynamic Force Coefficients	25
	C. Comparison of Experimental and Shock Expansion Aerodynamic Force Coefficients	27
	D. Experimental and Theoretical Flutter Characteristics	28
	E. Effect of Variations in System Product of Inertia	32
VIII	CONCLUSIONS	34
IX	RECOMMENDATIONS	37
	REFERENCES	38
	APPENDIX	150

LIST OF ILLUSTRATIONS

Figure No.	Description	Page No.
1	Model Configuration Geometry	41
2	Photograph of Static Aerodynamic Force Measurement Components and Rigid Models	42
3	Basic Spar and Completed Semi-Rigid Flutter Model	43
4	Suspension System Roll Mode Mechanism	44
5	Suspension System Pitch Mode Mechanism	45
6	Zero Airspeed Vibration Test Set-Up	46
7	Photograph of Suspension System Unit	47
8	Photograph of Pitch and Roll Mechanism	48
9	Axis System and Data Reduction Equations for Static Aerodynamic Force Data	49
10	Experimental Lift Coefficient vs. Angle-of-Attack; Basic Planform, t/c = .06, Mach Number = 6.0	50
11	Experimental Pitching Moment Coefficient vs. Angle-of-Attack; Basic Planform, t/c = .06, Mach Number = 6.0	51
12	Experimental Rolling Moment Coefficient vs. Angle-of-Attack; Basic Planform, t/c = .06, Mach Number = 6.0	52
13	Experimental Chordwise Center-of-Pressure vs. Angle-of-Attack; Basic Planform, t/c = .06, Mach Number = 6.0	53

Figure No.	Description	Page No.
14	Experimental Spanwise Center-of-Pressure vs. Angle-of-Attack; Basic Planform, t/c = .06, Mach Number = 6.0	54
15	Experimental Lift Coefficient vs. Angle-of-Attack; Basic Planform, t/c = .06, Mach Number = 7.0	55
16	Experimental Pitching Moment Coefficient vs. Angle-of-Attack; Basic Planform, t/c = .06, Mach Number = 7.0	56
17	Experimental Rolling Moment Coefficient vs. Angle-of-Attack; Basic Planform, t/c = .06, Mach Number = 7.0	57
18	Experimental Chordwise Center-of-Pressure vs. Angle-of-Attack; Basic Planform, t/c = .06, Mach Number = 7.0	58
19	Experimental Spanwise Center-of-Pressure vs. Angle-of-Attack; Basic Planform, t/c = .06, Mach Number = 7.0	59
20	Experimental Lift Coefficient vs. Angle-of-Attack; Basic Planform, t/c = .06, Mach Number = 8.0	60
21	Experimental Pitching Moment Coefficient vs. Angle-of-Attack; Basic Planform, t/c = .06, Mach Number = 8.0	61
22	Experimental Rolling Moment Coefficient vs. Angle-of-Attack; Basic Planform, t/c = .06, Mach Number = 8.0	62
23	Experimental Chordwise Center-of-Pressure vs. Angle-of-Attack; Basic Planform, t/c = .06, Mach Number = 8.0	63

Figure No.	Description	Page No.
24	Experimental Spanwise Center-of-Pressure vs. Angle-of-Attack; Basic Planform, t/c = .06, Mach Number = 8.0	64
25	Experimental Lift Coefficient vs. Angle-of-Attack; Basic Planform, t/c = .03, Mach Number = 6.0	65
26	Experimental Pitching Moment Coefficient vs. Angle-of-Attack; Basic Planform, t/c = .03, Mach Number = 6.0	66
27	Experimental Rolling Moment Coefficient vs. Angle-of-Attack; Basic Planform, t/c = .03, Mach Number = 6.0	67
28	Experimental Chordwise Center-of-Pressure vs. Angle-of-Attack; Basic Planform, t/c = .03, Mach Number = 6.0	68
29	Experimental Spanwise Center-of-Pressure vs. Angle-of-Attack; Basic Planform, t/c = .03, Mach Number = 6.0	69
30	Experimental Lift Coefficient vs. Angle-of-Attack; Basic Planform, t/c = .03, Mach Number = 8.0	70
31	Experimental Pitching Moment Coefficient vs. Angle-of-Attack; Basic Planform, t/c = .03, Mach Number = 8.0	71
32	Experimental Rolling Moment Coefficient vs. Angle-of-Attack; Basic Planform, t/c = .03, Mach Number = 8.0	72
33	Experimental Chordwise Center-of-Pressure vs. Angle-of-Attack; Basic Planform, t/c = .03, Mach Number = 8.0	73

Figure No.	Description	Page No.
34	Experimental Spanwise Center-of-Pressure vs. Angle-of-Attack; Basic Planform, t/c = .03, Mach Number = 8.0	74
35	Experimental Lift Coefficient vs. Angle-of-Attack; Basic Planform, t/c = .09, Mach Number = 6.0	75
36	Experimental Pitching Moment Coefficient vs. Angle-of-Attack; Basic Planform, t/c = .09, Mach Number = 6.0	76
37	Experimental Rolling Moment Coefficient vs. Angle-of-Attack; Basic Planform, t/c = .09, Mach Number = 6.0	77
38	Experimental Chordwise Center-of-Pressure vs. Angle-of-Attack; Basic Planform, t/c = .09, Mach Number = 6.0	78
39	Experimental Spanwise Center-of-Pressure vs. Angle-of-Attack; Basic Planform, t/c = .09, Mach Number = 6.0	79
40	Experimental Lift Coefficient vs. Angle-of-Attack; Basic Planform, t/c - .09, Mach Number = 8.0	80
41	Experimental Pitching Moment Coefficient vs. Angle-of-Attack; Basic Planform, t/c = .09, Mach Number = 8.0	81
42	Experimental Rolling Moment Coefficient vs. Angle-of-Attack; Basic Planform, t/c = .09, Mach Number = 8.0	82
43	Experimental Chordwise Center-of-Pressure vs. Angle-of-Attack; Basic Planform, t/c = .09, Mach Number = 8.0	83

Figure No.	Description	Page No.
44	Experimental Spanwise Center-of-Pressure vs. Angle-of-Attack; Basic Planform, t/c = .09, Mach Number = 8.0	84
45	Photograph of Model Excitation System	85
46	Comparison of Experimental and Shock Expansion Pitching Moment Coefficient vs. Angle-of-Attack at Mach Number = 5.0; Basic Planform, t/c = .06	86
47	Comparison of Experimental and Shock Expansion Pitching Moment Coefficient vs. Angle-of-Attack at Mach Number = 6.0; Basic Planform, t/c = .06	87
48	Comparison of Experimental and Shock Expansion Pitching Moment Coefficient vs. Angle-of-Attack at Mach Number = 7.0; Basic Planform, t/c = .06	88
49	Comparison of Experimental and Shock Expansion Pitching Moment Coefficient vs. Angle-of-Attack at Mach Number = 8.0; Basic Planform, t/c = .06	89
50	Comparison of Experimental and Shock Expansion Rolling Moment Coefficient vs. Angle-of-Attack at Mach Number = 5.0; Basic Planform, t/c = .06	90
51	Comparison of Experimental and Shock Expansion Rolling Moment Coefficient vs. Angle-of-Attack at Mach Number = 6.0; Basic Planform, t/c = .06	91
52	Comparison of Experimental and Shock Expansion Rolling Moment Coefficient vs. Angle-of-Attack at Mach Number = 7.0; Basic Planform, t/c = .06	92

Figure No.	Description	Page No.
53	Comparison of Experimental and Shock Expansion Rolling Moment Coefficient vs. Angle-of-Attack at Mach Number = 8.0; Basic Planform, t/c = .06	93
54	Comparison of Experimental and Shock Expansion Pitching Moment Coefficient vs. Angle-of-Attack at Mach Number = 6.0; Basic Planform, t/c = .03	94
55	Comparison of Experimental and Shock Expansion Pitching Moment Coefficient vs. Angle-of-Attack at Mach Number = 8.0; Basic Planform, t/c = .03	95
56	Comparison of Experimental and Shock Expansion Rolling Moment Coefficient vs. Angle-of-Attack at Mach Number = 6.0; Basic Planform, t/c = .03	96
57	Comparison of Experimental and Shock Expansion Rolling Moment Coefficient vs. Angle-of-Attack at Mach Number = 8.0; Basic Planform, t/c = .03	97
58	Comparison of Experimental and Shock Expansion Pitching Moment Coefficient vs. Angle-of-Attack at Mach Number = 6.0; Basic Planform, t/c = .09	98
59	Comparison of Experimental and Shock Expansion Pitching Moment Coefficient vs. Angle-of-Attack at Mach Number = 8.0; Basic Planform, t/c = .09	99
60	Comparison of Experimental and Shock Expansion Rolling Moment Coefficient vs. Angle-of-Attack at Mach Number = 6.0; Basic Planform, t/c = .09	100

Figure No.	Description	Page No.
61	Comparison of Experimental and Shock Expansion Rolling Moment Coefficient vs. Angle-of-Attack at Mach Number = 8.0; Basic Planform, t/c = .09	101
62	Effect of Thickness Ratio on Pitching Moment Coefficient vs. Angle-of-Attack; "Shock-Expansion" Theory - Mach Number = 5.0	102
63	Effect of Thickness Ratio on Pitching Moment Coefficient vs. Angle-of-Attack; "Shock-Expansion" Theory - Mach Number = 6.0	103
64	Effect of Thickness Ratio on Pitching Moment Coefficient vs. Angle-of-Attack; "Shock-Expansion" Theory - Mach Number = 7.0	104
65	Effect of Thickness Ratio on Pitching Moment Coefficient vs. Angle-of-Attack; "Shock-Expansion" Theory - Mach Number = 8.0	105
66	Effect of Thickness Ratio on Rolling Moment Coefficient vs. Angle-of-Attack; "Shock-Expansion" Theory - Mach Number = 6.0	106
67	Effect of Thickness Ratio on Rolling Moment Coefficient vs. Angle-of-Attack; "Shock-Expansion" Theory - Mach Number = 8.0	107
68	Experimental and Theoretical, Quasi-Steady (Using Experimental Aerodynamics) Flutter Velocity Parameter vs. Mach Number; Basic Planform, t/c = .06, $\omega_{h_1}/\omega_{\alpha_1}$ = .60, $\alpha_o = 0^\circ$	108

Figure No.	Description	Page No.
69	Experimental and Theoretical, Quasi-Steady (Using Experimental Aerodynamics) Flutter Frequency Ratio vs. Mach Number; Basic Planform, t/c = .06, $\omega_{h_1}/\omega_{\alpha_1}$ = .60, $\alpha_o = 0°$	109
70	Experimental and Theoretical, Quasi-Steady (Using Experimental Aerodynamics) Flutter Velocity Parameter vs. Angle-of-Attack at Mach Number = 6.0; Basic Planform, t/c = .06, $\omega_{h_1}/\omega_{\alpha_1}$ = .60	110
71	Experimental and Theoretical, Quasi-Steady (Using Experimental Aerodynamics) Flutter Frequency Ratio vs. Angle-of-Attack at Mach Number = 6.0; Basic Planform, t/c = .06, $\omega_{h_1}/\omega_{\alpha_1}$ = .60	111
72	Theoretical, Quasi-Steady (Using Experimental Aerodynamics) Flutter Velocity Parameter vs. Angle-of-Attack at Mach Number = 7.0; Basic Planform Nominal Model, t/c = .06, $\omega_{h_1}/\omega_{\alpha_1}$ = .60	112
73	Theoretical Quasi-Steady (Using Experimental Aerodynamics) Flutter Frequency Ratio vs. Angle-of-Attack at Mach Number = 7.0; Basic Planform, Nominal Model, t/c = .06, $\omega_{h_1}/\omega_{\alpha_1}$ = .60	113
74	Experimental and Theoretical, Quasi-Steady (Using Experimental Aerodynamics) Flutter Velocity Parameter vs. Angle-of-Attack at Mach Number = 8.0; Basic Planform, t/c = .06, $\omega_{h_1}/\omega_{\alpha_1}$ = .60	114
75	Experimental and Theoretical, Quasi-Steady (Using Experimental Aerodynamics) Flutter Frequency Ratio vs. Angle-of-Attack at Mach Number = 8.0; Basic Planform, t/c = .06, $\omega_{h_1}/\omega_{\alpha_1}$ = .60	115

Figure No.	Description	Page No.
76	Experimental and Theoretical, Quasi-Steady (Using Experimental Aerodynamics) Flutter Velocity Parameter vs. Modal Frequency Ratio at Mach Number = 6.0; Basic Planform, t/c = .06, $\alpha_0 = 0°$	116
77	Experimental and Theoretical, Quasi-Steady (Using Experimental Aerodynamics) Flutter Frequency Ratio vs. Modal Frequency Ratio at Mach Number = 6.0; Basic Planform, t/c = .06; $\alpha_0 = 0°$	117
78	Experimental and Theoretical, Quasi-Steady (Using Experimental Aerodynamics) Flutter Velocity Parameter vs. Modal Frequency Ratio at Mach Number = 8.0; Basic Planform, t/c = .06, $\alpha_0 = 0°$	118
79	Experimental and Theoretical, Quasi-Steady (Using Experimental Aerodynamics) Flutter Frequency Ratio vs. Modal Frequency Ratio at Mach Number = 8.0; Basic Planform, t/c = .06, $\alpha_0 = 0°$	119
80	Experimental and Theoretical, Quasi-Steady (Using Experimental Aerodynamics) Flutter Velocity Parameter vs. Mach Number; Basic Planform, t/c = .09, $\omega_{h_1}/\omega_{\alpha_1} = .60$; $\alpha_0 = 0°$	120
81	Experimental and Theoretical, Quasi-Steady (Using Experimental Aerodynamics) Flutter Frequency Ratio vs. Mach Number; Basic Planform, t/c = .09, $\omega_{h_1}/\omega_{\alpha_1} = .60$; $\alpha_0 = 0°$	121
82	Experimental and Theoretical, Quasi-Steady (Using Experimental Aerodynamics) Flutter Velocity Parameter vs. Thickness Ratio at Mach Number = 6.0; Basic Planform, $\omega_{h_1}/\omega_{\alpha_1} = .60$; $\alpha_0 = 0°$	122

Figure No.	Description	Page No.
83	Experimental and Theoretical, Quasi-Steady (Using Experimental Aerodynamics) Flutter Frequency Ratio vs. Thickness Ratio at Mach Number = 6.0; Basic Planform, $\omega_{h_1}/\omega_{\alpha_1}$ = .60; $\alpha_0 = 0°$	123
84	Experimental and Theoretical, Quasi-Steady (Using Experimental Aerodynamics) Flutter Velocity Parameter vs. Thickness Ratio at Mach Number = 7.0; Basic Planform, $\omega_{h_1}/\omega_{\alpha_1}$ = .60; $\alpha_0 = 0°$	124
85	Experimental and Theoretical, Quasi-Steady (Using Experimental Aerodynamics) Flutter Frequency Ratio vs. Thickness Ratio at Mach Number = 7.0, Basic Planform, $\omega_{h_1}/\omega_{\alpha_1}$ = .60; $\alpha_0 = 0°$	125
86	Experimental and Theoretical, Quasi-Steady (Using Experimental Aerodynamics) Flutter Velocity Parameter vs. Thickness Ratio at Mach Number = 8.0; Basic Planform, $\omega_{h_1}/\omega_{\alpha_1}$ = .60; $\alpha_0 = 0°$	126
87	Experimental and Theoretical, Quasi-Steady (Using Experimental Aerodynamics) Flutter Frequency Ratio vs. Thickness Ratio at Mach Number = 8.0; Basic Planform, $\omega_{h_1}/\omega_{\alpha_1}$ = .60; $\alpha_0 = 0°$	127
88	Experimental and Theoretical, Quasi-Steady (Using Shock-Expansion Aerodynamics) Flutter Velocity Parameter vs. Mach Number; Basic Planform, t/c = .06, $\omega_{h_1}/\omega_{\alpha_1}$ = .60; $\alpha_0 = 0°$	128
89	Experimental and Theoretical, Quasi-Steady (Using Shock-Expansion Aerodynamics) Flutter Frequency Ratio vs. Mach Number; Basic Planform, t/c = .06, $\omega_{h_1}/\omega_{\alpha_1}$ = .60, $\alpha_0 = 0°$	129

Figure No.	Description	Page No.
90	Experimental and Theoretical, Quasi-Steady (Using Shock-Expansion Aerodynamics) Flutter Velocity Parameter vs. Angle-of-Attack at Mach Number = 6.0; Basic Planform, t/c = .06, $\omega_{h_1}/\omega_{\alpha_1}$ = .60	130
91	Experimental and Theoretical, Quasi-Steady (Using Shock-Expansion Aerodynamics) Flutter Frequency Ratio vs. Angle-of-Attack at Mach Number = 6.0; Basic Planform, t/c = .06, $\omega_{h_1}/\omega_{\alpha_1}$ = .60	131
92	Theoretical, Quasi-Steady (Using Shock-Expansion Aerodynamics) Flutter Velocity Parameter vs. Angle-of-Attack at Mach Number = 7.0; Basic Planform, Nominal Model, t/c = .06, $\omega_{h_1}/\omega_{\alpha_1}$ = .60	132
93	Theoretical, Quasi-Steady (Using Shock-Expansion Aerodynamics) Flutter Frequency Ratio vs. Angle-of-Attack at Mach Number = 7.0; Basic Planform, t/c = .06, $\omega_{h_1}/\omega_{\alpha_1}$ = .60	133
94	Experimental and Theoretical, Quasi-Steady (Using Shock-Expansion Aerodynamics) Flutter Velocity Parameter vs. Angle-of-Attack at Mach Number = 8.0; Basic Planform, t/c = .06, $\omega_{h_1}/\omega_{\alpha_1}$ = .60	134
95	Experimental and Theoretical, Quasi-Steady (Using Shock-Expansion Aerodynamics) Flutter Frequency Ratio vs. Angle-of-Attack at Mach Number = 8.0; Basic Planform, t/c = .06, $\omega_{h_1}/\omega_{\alpha_1}$ = .60	135
96	Experimental and Theoretical, Quasi-Steady (Using Shock-Expansion Aerodynamics) Flutter Velocity Parameter vs. Modal Frequency Ratio at Mach Number = 6.0; Basic Planform, t/c = .06, $\alpha_0 = 0°$	136

Figure No.	Description	Page No.
97	Experimental and Theoretical, Quasi-Steady (Using Shock-Expansion Aerodynamics) Flutter Frequency Ratio vs. Modal Frequency Ratio at Mach Number = 6.0; Basic Planform, $t/c = .06$, $\alpha_0 = 0°$	137
98	Experimental and Theoretical, Quasi-Steady (Using Shock-Expansion Aerodynamics) Flutter Velocity Parameter vs. Modal Frequency Ratio at Mach Number = 8.0; Basic Planform; $t/c = .06$, $\alpha_0 = 0°$	138
99	Experimental and Theoretical, Quasi-Steady (Using Shock-Expansion Aerodynamics) Flutter Frequency Ratio vs. Modal Frequency Ratio at Mach Number = 8.0; Basic Planform, $t/c = .06$, $\alpha_0 = 0°$	139
100	Experimental and Theoretical, Quasi-Steady (Using Shock-Expansion Aerodynamics) Flutter Velocity Parameter vs. Mach Number; Basic Planform, $t/c = .09$, $\omega_{h_1}/\omega_{\alpha_1} = .60$; $\alpha_0 = 0°$	140
101	Experimental and Theoretical, Quasi-Steady (Using Shock-Expansion Aerodynamics) Flutter Frequency Ratio vs. Mach Number; Basic Planform, $t/c = .09$, $\omega_{h_1}/\omega_{\alpha_1} = .60$, $\alpha_0 = 0°$	141
102	Experimental and Theoretical, Quasi-Steady (Using Shock Expansion Aerodynamics) Flutter Velocity Parameter vs. Thickness Ratio at Mach Number = 6.0; Basic Planform $\omega_{h_1}/\omega_{\alpha_1} = .60$; $\alpha_0 = 0°$	142

Figure No.	Description	Page No.
103	Experimental and Theoretical, Quasi-Steady (Using Shock-Expansion Aerodynamics) Flutter Frequency Ratio vs. Thickness Ratio at Mach Number = 6.0; Basic Planform $\omega_{h_1}/\omega_{\alpha_1}$ = .60; $\alpha_0 = 0°$	143
104	Experimental and Theoretical, Quasi-Steady (Using Shock-Expansion Aerodynamics) Flutter Velocity Parameter vs. Thickness Ratio at Mach Number = 8.0; Basic Planform $\omega_{h_1}/\omega_{\alpha_1}$ = .60; $\alpha_0 = 0°$	144
105	Experimental and Theoretical, Quasi-Steady (Using Shock-Expansion Aerodynamics) Flutter Frequency Ratio vs. Thickness Ratio at Mach Number = 8.0; Basic Planform $\omega_{h_1}/\omega_{\alpha_1}$ = .60; $\alpha_0 = 0°$	145
106	Theoretical, Quasi-Steady (Using Shock-Expansion Aerodynamics) Flutter Velocity Parameter vs. Modal Frequency Ratio at Mach Number = 7.0; Basic Planform, t/c = .06, $\alpha_0 = 0°$	146
107	Theoretical, Quasi-Steady (Using Shock-Expansion Aerodynamics) Flutter Frequency Ratio vs. Modal Frequency Ratio at Mach Number = 7.0; Basic Planform, t/c = .06, $\alpha_0 = 0°$	147
108	Theoretical Quasi-Steady Flutter Velocity Parameter vs. Product of Inertia (Using Shock-Expansion Aerodynamics and Experimental Aerodynamics) Mach Number = 8.0, Basic Planform, t/c = .06	148
109	Shock Expansion Aerodynamic Areas of Influence	149

Figure No.	Description	Page No.
A1	Experimental Lift Coefficient vs. Angle-of-Attack; Configuration #4, Mach Number = 6.0	151
A2	Experimental Pitching Moment Coefficient vs. Angle-of-Attack; Configuration #4, Mach Number = 6.0	152
A3	Experimental Rolling Moment Coefficient vs. Angle-of-Attack; Configuration #4, Mach Number = 6.0	153
A4	Experimental Lift Coefficient vs. Angle-of-Attack; Configuration #4, Mach Number = 8.0	154
A5	Experimental Pitching Moment Coefficient vs. Angle-of-Attack; Configuration #4, Mach Number = 8.0	155
A6	Experimental Rolling Moment Coefficient vs. Angle-of-Attack; Configuration #4, Mach Number = 8.0	156
A7	Experimental Lift Coefficient vs. Angle-of-Attack; Configuration #5, Mach Number = 6.0	157
A8	Experimental Pitching Moment Coefficient vs. Angle-of-Attack; Configuration #5, Mach Number = 6.0	158
A9	Experimental Rolling Moment Coefficient vs. Angle-of-Attack; Configuration #5, Mach Number = 6.0	159
A10	Experimental Lift Coefficient vs. Angle-of-Attack; Configuration #5, Mach Number = 8.0	160

Figure No.	Description	Page No.
A11	Experimental Pitching Moment Coefficient vs. Angle-of-Attack; Configuration #5, Mach Number = 8.0	161
A12	Experimental Rolling Moment Coefficient vs. Angle-of-Attack; Configuration #5, Mach Number = 8.0	162
A13	Experimental Lift Coefficient vs. Angle-of-Attack; Configuration #6, Mach Number = 6.0	163
A14	Experimental Pitching Moment Coefficient vs. Angle-of-Attack; Configuration #6, Mach Number = 6.0	164
A15	Experimental Rolling Moment Coefficient vs. Angle-of-Attack; Configuration #6, Mach Number = 6.0	165
A16	Experimental Lift Coefficient vs. Angle-of-Attack; Configuration #6, Mach Number = 8.0	166
A17	Experimental Pitching Moment Coefficient vs. Angle-of-Attack; Configuration #6, Mach Number = 8.0	167
A18	Experimental Rolling Moment Coefficient vs. Angle-of-Attack; Configuration #6, Mach Number = 8.0	168
A19	Experimental Lift Coefficient vs. Angle-of-Attack; Configuration #7, Mach Number = 6.0	169
A20	Experimental Pitching Moment Coefficient vs. Angle-of-Attack; Configuration #7, Mach Number = 6.0	170

Figure No.	Description	Page No.
A21	Experimental Rolling Moment Coefficient vs. Angle-of-Attack; Configuration #7, Mach Number = 6.0	171
A22	Experimental Lift Coefficient vs. Angle-of-Attack; Configuration #7, Mach Number = 8.0	172
A23	Experimental Pitching Moment Coefficient vs. Angle-of-Attack; Configuration #7, Mach Number = 8.0	173
A24	Experimental Rolling Moment Coefficient vs. Angle-of-Attack; Configuration #7, Mach Number = 8.0	174

LIST OF TABLES

Table No.	Description	Page No.
I	Tabulation of Experimental and Theoretical Flutter Results	39
II	Tabulation of Theoretical Flutter Results Using Nominal Constant Model	40

SUMMARY

A series of semi-rigid flutter models were tested in the Mach number range 5.0 to 8.0 to evaluate the effects of:

1. Initial angle-of-attack
2. Thickness ratio
3. Modal frequency ratio

on the flutter characteristics of highly swept, low aspect ratio lifting surfaces having roll and pitch degrees of freedom.

Correlative analog studies were performed using the quasi-steady flutter analysis techniques in conjunction with

1. Experimentally determined total aerodynamic force coefficients
2. Aerodynamic force coefficients derived from "shock-expansion" techniques, modified by sweep angle corrections and an assumed elliptical spanwise lift distribution

Generalized aerodynamic trends are noted with certain deviation phenomena occurring in the experimental coefficients. The analog studies were concluded to predict flutter velocities and trends sufficient for preliminary design purposes, the use of "shock-expansion" aerodynamics providing the least complex and inexpensive tool.

Recommendations were made to initiate further research relative to the aerodynamic representation in the interest of providing further refinements to the techniques used during this investigation.

LIST OF SYMBOLS

a	Speed of sound, in/sec
AR	Aspect ratio, $\frac{b^2}{2 S_W}$, non-dimensional
BC	Bellcrank
$(b/2)$	Model semi-span, inches
b	Model span, inches
b_o	Root semi-chord, inches
C	Local chord, inches
C_R	Root chord, inches
C_T	Tip chord, inches
$\bar{C}$	Mean aerodynamic chord, inches
$C_{avg.}$	Average chord, inches
C_m	Pitching moment coefficient, measured about pitch axis, positive nose up, nondimensional
C_ζ	Rolling moment coefficient about root chord, non-dimensional, positive tip up, nondimensional
C_ζ'	Rolling moment coefficient referenced to the roll axis, positive tip up, nondimensional
C_L	Lift coefficient, non-dimensional
C_{L_α}	Lift curve slope, per degree
d_P	Length of forward arms of pitch bellcranks, inches
d_R	Length of forward arms of roll bellcranks, inches
g_{h1}	Damping in first un-coupled mode, non-dimensional

g_{α_1}	Damping in second un-coupled mode, non-dimensional
G_R	Equivalent viscous damping in roll, inch-lb.-second
G_P	Equivalent viscous damping in pitch, inch-lb.-second
h_{1_R}, h_{2_R}	Roll arm heights, upper and lower, inches
h_{1_P}, h_{2_P}	Pitch arm heights, upper and lower, inches
I_φ	Total system roll inertia about roll axis, inch-lb.-second^2
I_{φ_o}	Model roll inertia about center of gravity, inch-lb.-second^2
$I_{\varphi_{BC}}$	Inertia of roll bellcrank about its axis of rotation, inch-lb.-second^2
I_α	Total system pitch inertia about the pitch axis, inch-lb.-second^2
I_{α_o}	Model pitch inertia about center of gravity, inch-lb.-second^2
$I_{\alpha_{BC}}$	Inertia of pitch bellcrank about its axis of rotation, inch-lb.-second^2
$I_{\alpha\varphi}$	Product of inertia with respect to intersection of roll axis and pitch axis, inch-lb.-second^2
$(I_{\alpha\varphi})_{NM}$	Product of inertia of nominal constant model with respect to intersection of roll axis and pitch axis, inch-lb.-second^2
$(I_{\alpha\varphi})_o$	Product of inertia of model with respect to center of gravity axis parallel to pitch axis and roll axis, inch-lb.-second^2
K_φ	Roll stiffness, inch-lb./radian
$(K_\varphi)_{EFF}$	Effective roll stiffness, inch-lb./radian
K_θ	Pitch stiffness, inch-lb./radian
$(K_\theta)_{EFF}$	Effective pitch stiffness, inch-lb./radian

K_{RS_1}	Linear spring rate of upper roll spring, lb./inch
K_{RS_2}	Linear spring rate of lower roll spring, lb./inch
K_{PS_1}	Linear spring rate of upper pitch spring, lb./inch
K_{PS_2}	Linear spring rate of lower pitch spring, lb./inch
L	Lift, lb.
l_R	Roll arm length, distance from roll axis to point of attachment of roll bellcranks, inches
l_p	Pitch arm length, inches
l_t	Spanwise distance from roll axis to tip chord of model, measure normal to roll axis, inches
M	Mach Number, U/a, non-dimensional
M_{model}	Mass of Model, lb.-second^2/inch
M_{RS_1}, M_{RS_2}	Mass of upper and lower roll springs, lb.-second^2/inch
M_{SH_1}, M_{SH_2}	Mass of upper and lower spring hooks, lb.-second^2/inch
M_{RC}	Mass of roll collar, lb.-second^2/inch
M_{PS_1}, M_{PS_2}	Mass of upper and lower pitch springs, lb.-second^2/inch
P_o	Wind tunnel stagnation pressure, lb./inch^2
P	Local pressure, lb./inch^2
P_∞	Freestream pressure, lb/inch^2
ΔP	Pressure difference between upper and lower surfaces, lb./inch^2
P_1, P_2	Motor cable pulleys
P.M.	Pitching moment about pitch axis, inch-lb.
PB	Pitch bearing

Q_R	Generalized aerodynamic force in roll, in.-lb.
Q_P	Generalized aerodynamic force in pitch, in-lb.
Q_i	Generalized aerodynamic force
q	Dynamic pressure, lb./inch^2
q_F	Dynamic pressure at flutter condition, lb./inch^2
R.M.	Rolling moment about root chord, inch-lb.
R.M.$'$	Rolling moment about model roll axis, inch-lb.
r_α	Effective system pitch radius of gyration, inches
$(r_\alpha)_{AIR}$	Effective pitch radius of gyration for V_{AIR}, inches
RT	Roll tube
R_{BC_1}, R_{BC_2}	Roll bellcranks, upper and lower
RS_1, RS_2	Roll spring, upper and lower
RMD	Roll motor drum
RB_1, RB_2	Roll bearings, upper and lower
RC	Roll collar
RF	Roll flexure
RLO	Roll lock out mechanism
S.E.T.	Shock expansion theory
SS	Suspension system
S_W	Area of one wing panel, inches^2
SH_1, SH_2	Spring hooks
t/c	Thickness ratio, non-dimensional
U	Free-stream velocity, inches/second

U_F	Free-stream velocity at flutter condition, inches/second
$\frac{U_F}{b_o \omega_{\alpha_1} \sqrt{u}}$	Flutter velocity parameter, non-dimensional
V_{AIR}	Volume of air contained within the frustrum of a truncated cone with the maximum radius being the root semi-chord, the minimum radius being the tip semi-chord and the height being the model semi-span, inches^3
X	Chordwise coordinate variable, positive aft of the pitch axis, inches
X_o	Distance from intersection of the model root chord and leading edge to the pitch axis, inches
X_1	Chordwise coordinate variable, positive aft of leading edge, inches
X_{cg}	Chordwise center of gravity, positive aft of pitch axis, inches
$(X_{CP}/\bar{C})_{TOTAL}$	Chordwise center of pressure, fraction of mean aerodynamic chord
X_{CP}/C	Chordwise center of pressure, fraction of local chord
X_{cg}/C	Center of gravity, fraction of local chord
Y_{cg}	Spanwise center of gravity measured from model root chord, inches
y	Spanwise coordinate variable, positive outboard of root chord, inches
y_1	Spanwise coordinate variable, positive outboard of roll axis, inches
y_o	Distance from roll axis to model root chord, inches
α_o	Model angle of attack, degrees .

γ	Ratio of specific heats, non-dimensional
η_{CP}	Spanwise center of pressure, non-dimensional
η	Non-dimensional spanwise coordinate variable, $\frac{y}{b/2}$
$\eta_{\bar{c}}$	Spanwise location of mean aerodynamic chord, non-dimensional
θ_{WS}	Leading edge wedge angle of model in streamwise direction, degrees
θ_{WN}	Leading edge wedge angle of model normal to leading edge, degrees
θ_R	Roll angle, positive tip up, degrees
$\dot{\theta}_R$	Roll rate, radians/second
$\ddot{\theta}_R$	Roll acceleration, radians/second^2
θ_P	Pitch angle, positive leading edge up, radians
$\dot{\theta}_P$	Pitch rate, radians/second
$\ddot{\theta}_P$	Pitch acceleration, radians/second^2
θ_{PYLON}	Wedge angle of splitter plate pylon section, 22° 24'
θ'_{WS}	Leading edge wedge semi-angle, degrees
θ_{SP}	Splitter plate wedge angle, 3.5°
λ	Taper ratio, C_T/C_R, non-dimensional
$\Lambda_{L.E.}$	Leading edge sweep angle, degrees
μ	Ratio of total system pitch inertia to pitch inertia of the volume of air as defined for V_{AIR}, non-dimensional
ρ	Density of air, $\frac{\text{Lb.-second}^2}{\text{inch}}$/inch^3

ω_{h_1}	Uncoupled roll frequency, radians/second
ω_{α_1}	Uncoupled pitch frequency, radians/second
ω_1	First coupled frequency, radians/second
ω_2	Second coupled frequency, radians/second
$\omega_{h_1}/\omega_{\alpha_1}$	Ratio of uncoupled roll frequency to uncoupled pitch frequency, non-dimensional
ω_F	Flutter frequency, radians/second
$\omega_F/\omega_{\alpha_1}$	Ratio of flutter frequency to uncoupled pitch frequency, non-dimensional

INTRODUCTION

The current and near future class of ultra-performance flight vehicles such as missiles and re-entry vehicles with lifting surfaces has produced an urgent need for advancing the state-of-the-art relative to reliable prediction of the flutter characteristics in the early design stages of such vehicles. Typical lifting surfaces of such vehicles tend to employ configurations having low aspect ratios, large leading edge sweep angles and wedge type leading edges. Each of these configuration characteristics amplifies the difficulties encountered by the aeroelastician in the mathematical representation of the unsteady aerodynamic forces experienced by these surfaces in the hypersonic speed range. A further complication evolves from the fact that the vehicles under consideration must perform flight missions which include operation with the lifting surfaces oriented at relatively large angles of attack.

Reference 1 reports the results of an investigation made by Mr. D. A. Brown relative to planform configurations identical to those investigated in the study covered by this report. The investigation made by Mr. Brown covered the transonic and supersonic speed range; evaluating the adequacy of "piston theory" flutter analyses, "quasi-steady" flutter analyses using experimentally obtained static aerodynamic force coefficients, and "subsonic kernel function" flutter analyses. The conclusions reached in Reference 1 state that "piston theory" is inadequate to reliably predict the flutter characteristics of the configuration investigated. In view of this conclusion it was apparent that the mathematical limitations inherent in "piston theory" would be more seriously violated as Mach number increased. It was therefore elected to investigate the reliability of "shock-expansion" techniques as recommended in Reference 1.

The theoretical methods evaluated in this report make use of an analog computer simulation of the dynamic system using quasi-steady flutter analyses techniques based on

A. Experimentally determined static aerodynamic force coefficients.

B. Steady-state, two-dimensional aerodynamic force coefficients based on "shock-expansion" techniques with sweep angle corrections and assumed spanwise variations.

Manuscript released by the author 1 April 1964 for publication as an RTD Technical Documentary Report.

C. The aerodynamics defined in A and B, above, were also investigated with and without the inclusion of rate terms derived from "piston theory" methods.

The parameter variations investigated during this study include initial angle of attack, thickness ratio, frequency ratio, and Mach number.

SECTION I

MODEL DESIGN AND CONSTRUCTION

A. Environmental Conditions

The design and construction of wind tunnel models relative to this study was radically different than the construction techniques used during the study reported in Reference (1). These differences were necessitated to obtain proper model life while subjected to the high stagnation temperatures experienced in tunnel E-2 at the Arnold Engineering Development Center. Test section stagnation temperatures experienced were as high as 900°F.

B. Static Force Models

Static force models of all model configurations were machined from a solid plate of PH15-7MO stainless steel. The geometry of the model configurations which were fabricated for use in the static aerodynamic force tests is presented in Figures 1 and 2.

C. Semi-Rigid Flutter Models

The final construction techniques used for the semi-rigid flutter models consisted of machining a basic root chord-tip chord-double spar in one piece, using titanium stock (Comp 6AL-4V Cond STA) - see Figure 3 . Titanium skins, .005" thick, were then spot welded to the one piece spars using a stabilizing core of ceramic foam (Eccofoam LM-43A). The stabilizing core was bonded to the spar and skin using a high temperature bonding agent. A titanium cap on the trailing edge, spot welded to the skin, was eventually employed to prolong model life. Tungsten and platinum balance weights were used to obtain the proper dynamic mass characteristics. The balance weights were attached to the rear spar using press-fit locating pins and attachment screws. This construction technique proved to be very satisfactory, making possible repeated usage of the same model while retaining structural stability under the severe temperature and dynamic stresses experienced during the divergent flutter conditions. Semi-rigid flutter models of the basic planform (double wedge leading edge, blunt trailing edge) were constructed for the 3%, 6% and 9% thick configurations only.

SECTION II

SUSPENSION SYSTEM DESIGN AND CONSTRUCTION

The suspension system used during this study was the identical system described in Reference (1) with the addition of a minor modification to the servo control electronics. This modification provided the capability of sinusoidally exciting the model by superimposing a sinusoidal voltage on the pitch motor sensing circuit and causing a small sinusoidal motion of the model in the pitch mode, the intention being to overcome the break-away forces inherent in the bearing system.

A diagram of the roll and pitch mechanism is presented in Figures 4 and 5 . In addition Figures 6 , 7 , and 8 are photographs of the actual suspension system used with the major functional components indicated. A more complete description of the suspension system and its design considerations may be found in Section II of Reference (1).

SECTION III

PRELIMINARY TEST PROCEDURES

A. Mass Characteristics

As described elsewhere in this report, the semi-rigid flutter model design criteria required that the mass coupling parameter of the models maintain a constant ratio of pitch inertia to product of inertia about the pitch axis and roll axis. To accomplish this objective the mass and inertia characteristics of the machined spar alone were determined experimentally. The inertia characteristics of the appropriate suspension system components were determined experimentally or mathematically. Mathematical equations were then evolved to determine the size and mass of appropriate mass balance weights to maintain a constant $\frac{I_\alpha}{I_{\alpha\varphi}}$ and $\frac{I_\varphi}{I_{\alpha\varphi}}$. Subsequent to fabrication of the completed model, including the foam stabilizing core, titanium skins, and mass balance weights, the model mass characteristics were determined experimentally using a bifilar pendulum.

B. Environmental Temperature Tests

During the static aerodynamic force tests, a thermocouple was installed on the model-to-balance connecting link to determine the maximum temperature to be expected. It was determined from this test that the maximum temperature experienced in the model-to-suspension system connecting link was 650°F.

It was decided that any adverse temperature effects would be limited to the roll and pitch bearings, such effects being important only insofar as they would change the frequency and/or damping characteristics of the system. A copper heat sink link was therefore fabricated to be placed between a simulated model and the roll arm carry thru. This heat sink was subjected to intense heat from a propane torch for approximately 5 minutes, during which time the heat transfer from the heat sink to the end of the roll arm adjacent to the bearings attained a maximum temperature of approximately 950°F. During this heating process system frequency and damping rates were recorded at 30 second intervals. It was found that no

change in the system vibration characteristics was noted until seizure of the bearings at about the 5 minute elapsed time condition. Since normal flutter runs have a time duration of about two minutes and the environmental temperature of the parts involved attain maximum temperatures of only 650°F., it was concluded that no adverse effects would be experienced by the system during the actual flutter runs in the wind tunnel.

C. Preliminary Vibration Tests

Prior to each wind tunnel flutter run, vibration tests were performed to determine the following experimental values:

a. Uncoupled roll frequency

b. Uncoupled roll mode damping rate

c. Uncoupled pitch frequency

d. Uncoupled pitch mode damping rate

e. First coupled frequency

f. Second coupled frequency

It was determined during the study reported in Reference (1) that the suspension system springs displayed linear rate characteristics over the range of aerodynamic loads encountered in the wind tunnel, but that the loads expected above $\alpha_o = 10°$ at M = 6.0 and $\alpha_o = 15°$ at M = 8.0 would exceed the linearity range of the springs used. Angle-of-attack runs greater than those mentioned above were therefore not investigated.

SECTION IV

WIND TUNNEL TESTS

A. General

All static force tests and semi-rigid flutter model tests were conducted in the E-2 tunnel at Arnold Engineering Development Center, Tullahoma, Tennessee. The E-2 tunnel has a 12" x 12" test section and is an intermittent variable density wind tunnel utilizing manually adjusted flexible nozzle plates. Mach number was variable from 5 to 8 with maximum stagnation pressures from 400 to 1300 psia. A more detailed description of the E-2 wind tunnel may be found in Reference (2).

B. Static Aerodynamic Force Tests

Solid stainless steel force models were used to obtain static aerodynamic force data in the E-2 wind tunnel at A.E.D.C. A beam balance designed for sting mounting was used to measure the desired aerodynamic forces by modifying the mounting system to a sidewall mount. A splitter plate was used to project the model outside the boundary layer of the tunnel. All tests were made with the splitter plate mounted 2.5 inches from the tunnel sidewall. The beam balance, splitter plate, mounting hardware and rigid force models are shown in Figure 2 . The beam balance used was enclosed in a water-cooled jacket to prevent any thermal effects from influencing the strain gage outputs. A closed vessel vented to the test section ambient pressure was used to equalize the pressure inside the splitter plate pylon and the test section, thus minimizing airflow thru the clearance space around the model attachment carry-thru. During the static force tests, pressure surveys were made to determine any existing flow disturbances in the model occupancy area. A more detailed discussion of the static force tests, installation, and testing techniques may be found in Reference (3). The results of the tests are presented in Figures 10 thru 44 and in Appendix A. A discussion of these results may be found in Section VII of this report.

C. Flutter Tests

The semi-rigid flutter model tests were performed as follows:

1. Based upon flutter boundaries determined during the course of tests reported in Reference (1), an uncoupled system pitch frequency was assumed which would cause the model to become divergent near the mid-range pressure of the E-2 wind tunnel.

2. A set of roll and pitch spring systems was then chosen and installed in the suspension system which would produce the desired uncoupled frequencies while maintaining a constant system inertia ratio.

3. Zero airspeed vibration tests were performed by exciting the model with a set of opposing loudspeakers (8" diameter) modified with a baffle plate allowing a pulsating jet of air to impinge upon the model, see Figure 45. The frequency of this pulsating jet was varied manually using an audio oscillator to drive the loudspeaker amplifier until the uncoupled roll and pitch mode resonances were determined. The system damping rate was then determined by disconnecting the amplifier circuit to the speaker system while recording, on a direct-writing oscillograph, the damped motion of the model as sensed by the roll and pitch flexures. The coupled roll and pitch resonant frequencies were determined in the same manner described above.

4. The model and suspension system were then installed in the wind tunnel in the desired roll and pitch attitude. With the model retracted inside the splitter plate pylon section, flow was then established in the test section. After stabilization of flow, the model was injected into the airstream by actuating the pneumatic injection system. The flow was normally established at a low P_0 value. Subsequent to injection, sufficient time was allowed for the pitch and roll attitude motors to react and stabilize the model at the desired attitude. P_0 was then increased gradually at constant Mach number until a divergent flutter condition was reached.

5. Mechanical amplitude limiting stops were incorporated into the system which allowed an oscillatory response of $\pm 10^\circ$ from the equilibrium position of the model. As soon as these amplitude limits were reached, P_0 was rapidly decreased to regain a stable condition. By using this

procedure, the model was subjected to the extreme environmental and dynamic load conditions for the shortest possible duration.

6. The data recording system used in conjunction with the flutter runs resulted in a tabulation of pressure and temperature readouts at 1.9 second intervals. A manually activated flutter indicate switch was used to correlate the time of divergence between the pressure-temperature data recording system and the direct writing oscillograph record which recorded the output of the response flexures. Stagnation pressure and stagnation temperature conditions were then determined at the time of divergence.

7. High speed motion pictures were taken during each flutter run to verify the divergence. The E-2 wind tunnel was equipped with a double window on the observation wall, requiring a camera angle of approximately 30° with respect to the pitch axis. As a result, the roll motion coverage of the model was somewhat limited.

8. During the flutter runs, the model was excited sinusoidally in the pitch degree of freedom to overcome the bearing starting friction torque. The amplitude of oscillation was approximately $\pm$ 1.5° about the equilibrium position and was held, as nearly as practical, constant for each run.

A tabulation of each experimental flutter run and associated characteristics is presented in Table I.

SECTION V

EXPERIMENTAL AND THEORETICAL RESULTS

A. Static Aerodynamic Forces

The static aerodynamic force coefficients determined experimentally for all configurations are presented in Figures 10 thru 44 and in Appendix A. The reference axis system, geometric constants and non-dimensionalizing equations used to compute the force coefficients are presented as Figure 9 . It should be noted that the rolling moment coefficients presented in Figures 10 thru 44 are computed about the model root chord.

The static aerodynamic pitching moment and rolling moment coefficients as computed theoretically using a modified "shock-expansion" theory are presented in comparison with experimentally determined coefficients in Figures 46 thru 61 . These figures present rolling moment coefficients computed about the actual roll axis and are the force coefficients used in conjunction with the respective quasi-steady, analog, theoretical study. The details of the "shock-expansion" theory techniques are presented in Section VI. The effects of thickness ratio on pitching moment and rolling moment coefficient are presented in Figures 62 thru 67.

B. Flutter Results

The results of the experimental flutter tests are presented in comparison with theoretical analyses results obtained from an analog study utilizing two types of aerodynamic representations, (see Figures 68 thru 107).

SECTION VI

THEORETICAL ANALYSES

A. General

All theoretical, correlative analyses were performed on an operational analog computer using quasi-steady flutter analysis techniques. With the exception of the aerodynamic representations investigated, the equations of motion and analog mechanization used were identical to those used by Mr. D. A. Brown during the study reported in Reference (1). That section of Reference (1) which is directly applicable to the current study is repeated briefly herein for the convenience of the reader.

During this study, the two aerodynamic representations used as the system forcing function were:

1. Experimentally determined pitching moment and rolling moment.

2. Pitching moment and rolling moment coefficients computed from "shock-expansion" theory techniques, Reference (6), modified to reflect the effect of leading edge sweep, Reference (7), and an assumed elliptical lift distribution in the spanwise direction based on the two-dimensional root chord value.

B. Equations of Motion

The equations of motion which represent the two degree-of-freedom system under consideration are as follows:

$$I_{\varphi}\ddot{\theta}_R + I_{\alpha\varphi}\ddot{\theta}_P + G_R\dot{\theta}_R + K_{\varphi}\theta_R = Q_R \qquad \text{(Eq. 1)}$$

$$I_{\alpha}\ddot{\theta}_P + I_{\alpha\varphi}\ddot{\theta}_R + G_P\dot{\theta}_P + K_{\theta}\theta_P = Q_P \qquad \text{(Eq. 2)}$$

It should be noted that the steady state aerodynamic term associated with initial angle of attack, α_0, is omitted from the right side of equations 1 and 2. This omission is justified by also omitting the the corresponding motor force terms on the left side which is a force term equal and opposite to the α_0 aerodynamic term. The flutter solution of these equations is unaffected by these omissions.

The terms in Equations (1) and (2) are defined as:

I_φ = Total roll inertia about the roll axis

I_α = Total pitch inertia about the pitch axis

$I_{\alpha\varphi}$ = Total product of inertia

K_φ = Roll stiffness

K_θ = Pitch stiffness

G_R = Equivalent viscous damping in the roll mode = $g_{h_1}\ \omega_{h_1}\ I_\varphi$

G_P = Equivalent viscous damping in the pitch mode = $g_{\alpha_1}\ \omega_{\alpha_1}\ I_\alpha$

Q_R = Generalized aerodynamic force in the roll degree-of-freedom

Q_P = Generalized aerodynamic force in the pitch degree-of-freedom

θ_P = Pitch angle, positive leading edge up

θ_R = Roll angle, positive tip up

The inertia, stiffness, and damping terms used in Equations (1) and (2) above are defined as total system characteristics, including contributions from all components in the suspension system (bellcranks, pitch and roll arms, connecting links, springs, etc.) which are subjected to any motion in space as the system experiences motion in either of its two degrees of freedom independently.

Since all system components do not necessarily exhibit motion ratios of unity with respect to the model, it was necessary to determine "effective" values for all components as they function in the system.

Considering the roll mechanism shown in Figure 4, the effective roll inertia, I_φ may be determined by evaluating the inertial components of the system as the model is rotated one radian about the roll axis. The effective system roll inertia may therefore be expressed as:

$$I_\varphi = (I_\varphi)_M + (I_\varphi)_{SS} + \left(\frac{\ell_R}{d_R}\right)^2 \Big[\frac{1}{3} M_{RS_1} h_{1R}^2 + \frac{1}{3} M_{RS_2} h_{2R}^2 + M_{SH_1} h_{1R}^2 + M_{SH_2} h_{2R}^2 + 2\,(I_\varphi)_{BC} \Big] + M_{RC}\,\ell_R^2 \qquad \text{(Eq. 3)}$$

Similarly, the effective pitch inertia may be expressed as:

$$I_\alpha = (I_\alpha)_M + (I_\alpha)_{SS} + \left(\frac{\ell_P}{d_P}\right)^2 \Big[\frac{1}{3} M_{PS_1} h_{1P}^2 + \frac{1}{3} M_{PS_2} h_{2P}^2 + M_{SH_1} h_{1P}^2 + M_{SH_1} h_{2P}^2 + 2\,(I_\alpha)_{BC} \Big] \qquad \text{(Eq. 4)}$$

where $(I_i)_M$ = Experimentally determined inertia, in the ith mode, of the model alone, inch-lb.-second^2.

$(I_i)_{SS}$ = i^{th} mode inertia of those suspension system parts which exhibit a motion ratio of unity relative to the model, inch-lb.-second^2.

M_{RS_1} = Mass of upper roll spring, lb.-second^2/inch.

M_{RS_2} = Mass of lower roll spring, lb.-second^2/inch.

M_{PS_1} = Mass of upper pitch spring, lb.-second^2/inch.

M_{PS_2} = Mass of lower pitch spring, lb.-second^2/inch.

M_{SH_1}, M_{SH_2} = Mass of upper and lower spring hooks, lb.-second^2/inch.

$(I_i)_{BC}$ = Inertia of ith mode bellcrank about its axis of rotation, inch-lb./second^2.

M_{RC} = Mass of roll collar and connecting cable, lb.-second^2/inch.

Based on an energy analysis of a coil spring fixed at one end and elongating axially, the effective mass in motion was found to be 1/3 of the total spring mass, as indicated in Equations (3) and (4). The product of inertia of the model, ($I_{\alpha\varphi}$), was experimentally determined as previously mentioned in Section III.

The "effective" roll and pitch stiffnesses, K_φ and K_θ used in the analog analyses were determined from the experimental uncoupled frequencies and experimental/theoretical inertias indicated above as follows:

$$(K_\varphi)_{EFF.} = (\omega_{h_1})^2 I_\varphi$$

$$(K_\alpha)_{EFF.} \quad (\omega_{\alpha_1})^2 I_\alpha$$

Rewriting Equations (1) and (2) in matrix form,

$$\begin{bmatrix} I_\varphi & I_{\alpha\varphi} \\ I_{\alpha\varphi} & I_\alpha \end{bmatrix} \begin{Bmatrix} \ddot{\theta}_R \\ \ddot{\theta}_P \end{Bmatrix} + \begin{bmatrix} (g_{h_1}\omega_{h_1} I_\varphi) & 0 \\ 0 & g_{\alpha_1}\omega_{\alpha_1} I_\alpha \end{bmatrix} \begin{Bmatrix} \dot{\theta}_R \\ \dot{\theta}_P \end{Bmatrix} + \begin{bmatrix} (K_\varphi)_{EFF} & 0 \\ 0 & (K_\alpha)_{EFF.} \end{bmatrix} \begin{Bmatrix} \theta_R \\ \theta_P \end{Bmatrix}$$

$$= \begin{bmatrix} 1 & 0 \\ 0 & 1 \end{bmatrix} \begin{Bmatrix} Q_R \\ Q_P \end{Bmatrix} \qquad \text{(Eq. 5)}$$

Considering Equation (5), it is apparent that no stiffness coupling exists and that the mass coupling is a function of only the relationship between I_φ, I_α, and $I_{\alpha\varphi}$. Further, an examination of the physical system reveals that $I_{\alpha\varphi}$ is fully defined by the product of inertia of the model only, $(I_{\alpha\varphi})_M$, about the pitch and roll axis. It shall also be noted that calculations of r_α^2 and x_{cg}/c, as they are classically defined, are indeterminate relative to the system under consideration due to inclusion of the effective mass properties of the suspension system components which do not have motion ratios of unity relative to the model. However, as described in Reference (1), if it is assumed that the total effective inertia of the system is distributed along the exposed span of the model such that the spanwise mass distribution is proportional to the square of the local chord and the spanwise distribution of pitch inertia is proportional to the fourth power of the local chord, then:

$$\left(r_\alpha^2\right)_{EFF.} = .1228 \frac{I_\alpha}{I_\varphi} \qquad \text{and}$$

$$\left(\frac{x_{cg}}{c}\right)_{EFF.} = .2979 + .24398 \frac{I_{\alpha\varphi}}{I_\varphi}$$

Computed values of r_α^2 and x_{cg}/c are presented in Tables I and II.

Since the classical definition of μ is dependent upon the implicit knowledge of total and constant mass, its value becomes indeterminate also; the effective mass in the roll mode being unequal to the effective mass in the pitch mode. The following definition of μ was used to reduce the flutter data presented herein and in Reference (1):

$$\mu = \frac{I_\alpha}{\rho V_{AIR} \left(r_\alpha^2\right)_{AIR}} \qquad \text{(Eq. 6)}$$

where:

I_α = Total pitch inertia of the system, inch-lb.-second^2

ρ = Density of air, $\frac{\text{lb.-second}^2}{\text{inch}}$/inch^3

V_{AIR} = Volume of air contained within the frustum of a cone with the maximum radius being the semi-root chord and the minimum radius being the semi-tip chord and the height of the frustum equal to the model semi-span, inches^3

$(r_\alpha)_{AIR}$ = Effective pitch radius of gyration for V_{AIR}, inches

Using the definition above, V_{AIR} is then given by:

$$V_{AIR} = \frac{\pi}{3}\left(\frac{\ell}{2}\right)\left[\left(\frac{C_R}{2}\right)^2 + \frac{C_R C_T}{2} + \left(\frac{C_T}{2}\right)^2\right] \qquad \text{(Eq. 7)}$$

The value of $(r_\alpha^2)_{AIR}$ is given by:

$$(r_\alpha^2)_{AIR} = \frac{(C_{AVG.}/2)^2}{2} \qquad \text{(Eq. 8)}$$

The terms remaining to be defined in the basic equations of motion are the generalized aerodynamic forces, Q_R and Q_P. As stated in Reference (1), the principle of virtual work results in the following:

Q_R = Aerodynamic rolling moment about the roll axis

Q_P = Aerodynamic pitching moment about the pitch axis

C. Quasi-Steady Flutter Analysis Methods

The quasi-steady flutter analysis techniques presented in Reference (4) state that displacements, rates and accelerations yield all the aerodynamic forces required in the solution of the flutter equation using the quasi-steady technique. For the case of the two degree-of-freedom dynamic system under consideration these force generation parameters are:

$$\theta_R, \ \dot{\theta}_R, \ \ddot{\theta}_R, \ \theta_P, \ \dot{\theta}_P, \ \ddot{\theta}_P$$

Neglecting the virtual mass terms associated with roll and pitch accelerations, all circulation lag effects, and static displacements in roll, θ_R, the remaining force generation parameters are:

$$\theta_P, \ \dot{\theta}_R, \ \text{AND} \ \dot{\theta}_P$$

greatly simplifying the aerodynamic representation. The forcing functions - rolling moment and pitching moment - may now be expressed as:

$$R.M. = q S_W \ell_T \left[C_{1R} \dot{\theta}_P + C'_{2R} \dot{\theta}_R + C'_{3R} \theta_P \right] \quad \text{(Eq. 9)}$$

$$P.M. = q S_W \bar{C} \left[C_{1P} \dot{\theta}_P + C'_{2P} \dot{\theta}_R + C_{3P} \theta_P \right] \quad \text{(Eq. 10)}$$

Since no experimental measurements of aerodynamic moments due to modal rate functions $\dot{\theta}_R$ and $\dot{\theta}_P$ were made, it was necessary to utilize theoretically determined rate terms to fully represent Equations (9) and (10). The rate term values were determined by "piston theory" techniques. Since the details of the development of these terms is fully described in Reference (1), they shall not be restated herein. Additionally, it was subsequently determined, during the initial phase of the analog analyses, that the rate dependent terms produced a change of less than one percent in the flutter characteristics of the systems being analyzed. By establishing this conclusion in the early stages of the analog study, an economy of operation was realized by eliminating all aerodynamic forcing function terms dependent upon rates.

D. Quasi-Steady Flutter Analyses Using Experimental Aerodynamics

The required forcing functions were, for the major portion of the analog studies, generated by the relatively simple relationships:

$$Q_R = R.M. = q S_W l_T C'_{3R} \theta_P = q S_W l_T C'_\zeta \quad \text{(Eq. 11)}$$

$$Q_P = P.M. = q S_W \bar{C} C_{3P} \theta_P = q S_W \bar{C} C_m \quad \text{(Eq. 12)}$$

where C'_ζ is merely the experimentally determined rolling moment coefficient referenced to the roll axis and C_m is the experimentally determined pitching moment coefficient measured about the pitch axis. As evidenced by Figures 10 thru 44, the aerodynamic coefficients of concern are non-linear functions of θ_P. Diode function generators were utilized in the analog mechanization to simulate these non-linear forcing functions.

E. Quasi-Steady Flutter Analyses Using Modified "Shock-Expansion" Aerodynamics

Quasi-steady flutter analyses were also performed during the analog study using the aerodynamic forcing functions specified in Equations (11) and (12) with C'_ζ and C_m being obtained by modified "Shock-expansion theory" techniques.

The basic theory used the techniques presented in Reference (6) for two dimensional supersonic flow. This method essentially calculates the flow at the nose of the airfoil using oblique-shock equations and progresses downstream of the nose using the Prandtl-Meyer equations. A basic assumption of the "Shock-expansion" method is that disturbances incident on the nose shock, or on any other shock, are almost entirely consumed in changing the direction of the shock.

The techniques presented in Reference (6) are as follows:

$$\theta_{N_L} = \left(\frac{dz_L}{dx}\right)_{x=0} + \alpha_0$$

$$\theta_{N_U} = \left(\frac{dz_U}{dx}\right)_{x=0} - \alpha_0$$

$$\frac{p(x)}{p_\infty} = \left\{\frac{\bar{p}_N}{p_\infty}\right\}\left\{1 + \frac{\gamma-1}{2}\,\bar{M}_N\,(\Delta(x))\right\}^{\frac{2\gamma}{\gamma-1}}$$

$$\left(\frac{p_L - p_U}{p_\infty}\right)_{(x)} = \left\{\frac{p_{N_L}}{p_\infty}\right\}\left\{1+\left(\frac{\gamma-1}{2}\right)\bar{M}_{N_L}\,\Delta_L(x)\right\}^{\frac{2\gamma}{\gamma-1}} - \left\{\frac{p_{N_U}}{p_\infty}\right\}\left\{1 + \frac{\gamma-1}{2}\bar{M}_{N_U}\Delta_U(x)\right\}^{\frac{2\gamma}{\gamma-1}}$$

The following relationships must then be solved to determine the net pressure on the airfoil:

$$M_\infty\bar{\beta} = .6(M_\infty\theta_N) + \sqrt{[.6M_\infty\theta_N]^2 + 1}$$

$$\frac{\bar{p}_N}{p_\infty} = 1.16667\,(M_\infty\bar{\beta})^2 - .01667$$

$$\frac{\bar{M}_N}{M_\infty} = 1.2\,\frac{M_\infty\bar{\beta}}{[1.4(M_\infty\bar{\beta})^2 - .2]^{1/2}\,[.2\,(M_\infty\bar{\beta})^2 + 1]^{1/2}}$$

and

$$\frac{p_L - p_U}{p_\infty} = \left\{\frac{\bar{p}_{N_L}}{p_\infty}\right\}\left\{1 + .2\,\bar{M}_{N_L}\left(\theta_L(x) - \theta_{N_L}\right)\right\}^7 - \left\{\frac{\bar{p}_{N_U}}{p_\infty}\right\}\left\{1 + .2\,\bar{M}_{N_U}\left(\theta_U(x) - \theta_{N_U}\right)\right\}^7$$

where:

γ	=	Specific heat ratio = 1.40 = constant
M_∞	=	Free stream Mach number
$\bar{\beta}$	=	The shock inclination corresponding to the turning angle
θ_N	=	"Mean inclination" of the surface (at the nose) for all fluid slabs
$\Delta(x)$	=	$(\theta(x) - \theta_N)$
x	=	Distance aft of leading edge
$\bar{p}_N$	=	Pressure at the nose
p_∞	=	Free stream pressure
$\bar{M}_N$	=	Mach number at the nose
$(\ )_L$	=	Quantity defined on the lower surface
$(\ )_U$	=	Quantity defined on the upper surface
$p_L - p_U$	=	$\Delta p(x)$

L = Lift = $\iint \Delta p(x,y)\, dA$

$R.M.$ = Rolling moment = $\iint y\, \Delta p(x)\, dA$

$P.M.$ = Pitching moment = $\iint x\, \Delta p(x)\, dA$

A pressure coefficient sweep angle correction factor was applied to the pitching moment and rolling moment as follows. The assumption was made that the flow condition acting upon the model was predominantly flow existing outside the apex influence zone. The sweep angle correction factor established in Reference (7) was applied as follows:

$$C_N = \frac{2K_i}{\gamma M_\infty^2 S}\left\{\sum_{i=1}^{4} \frac{\Delta p_N}{p_\infty} A_{N_i} + \sum_{j=1}^{4} \frac{\Delta p_{AB}}{p_\infty} A_{AB_j}\right\} \quad \text{(Eq. 13)}$$

where,

K_i = Correction factor for leading edge sweep = $\left[1 - \left(\frac{\tan \Lambda}{\sqrt{M_\infty^2 - 1}}\right)^2\right]^{1/2}$ *

M_∞ = Free stream Mach number

A_N = Area of the nose section from leading edge to the shoulder

A_{AB} = Area of the airfoil between the shoulder and the trailing edge

Λ = Leading edge sweep angle

* K_i is not valid when $M \rightarrow 1$ or as $\Lambda \rightarrow 90°$.

The airfoil was divided into eight aerodynamic areas as indicated on Figure 109 . The aerodynamic rolling moment and pitching moments for all Mach numbers and configurations studied were calculated by the method indicated above. The technique proved to be relatively simple and easily adaptable to calculations by small Recomp II computers.

F. Analog Analysis Techniques

As stated previously, the generalized aerodynamic forcing functions of interest were found to be non-linear functions of angle-of-attack. For this reason, and in view of the number of system parameter variations to be investigated, it was elected to utilize an analog computer to solve the system equations.

The aerodynamic forcing functions were reproduced by use of diode function generators. Since the equations of motion do not include terms representative of the static load compensation motors, it was necessary to eliminate the static aerodynamic forces resulting from initial angle-of-attack. This was accomplished by biasing the diode function generator output such that only those forces generated by time dependent motion were realized as the forcing function.

Execution of the analog analyses was performed in the following manner:

1. The particular experimental system characteristics were simulated on the analog computer.

2. Appropriate aerodynamic functions were entered on the diode function generators and all static airloads were biased to zero.

3. With the aerodynamic forces removed from the system, the dynamic system was sinusoidally excited at a frequency near one of the expected modal frequencies. A record of the damped sinusoidal motion was recorded for the following:

   (a) Roll motion, θ_R, with no coupling terms - gave uncoupled roll frequency and damping.

   (b) Pitch motion, θ_P, with no coupling terms - gave uncoupled pitch frequency and damping.

   (c) Roll motion, θ_R, with coupling terms in - gave first coupled modal frequency and damping.

   (d) Pitch motion, θ_P, with coupling terms in - gave second coupled modal frequency and damping.

4. The coupled system was then subjected to the unsteady aerodynamic forces, generated as indicated by the generalized force equations previously presented, at some nominal dynamic pressure.

5. The dynamic pressure associated with the aerodynamics was then increased at a constant rate equivalent to the actual rate used experimentally in the wind tunnel.

6. The system was subjected to a constant sinusoidal forcing function representative of that used experimentally. The amplitude of response to this sinusoidal excitation was held constant, ($\pm$ 1.5°), for all analog solutions.

7. The dynamic pressure existing at the time of model divergence was noted as the flutter dynamic pressure, q_F.

8. The flutter frequency was computed from the model response records at the time where $q = q_F$.

A brief investigation was made to determine the effect of excitation amplitude on the system flutter characteristics. It was concluded that response amplitudes up to $\pm 5^{\circ}$ were relatively ineffective in changing the flutter characteristics of the system.

It was further determined during the zero airspeed vibration analyses that the coupled frequencies resulting from matching the uncoupled experimental frequencies and using the experimental/theoretical system mass characteristics did not match the experimental coupled frequencies in all cases. The product of inertia, $I_{\alpha\varphi}$, was varied to match the experimental coupled frequencies within $\pm$ 10%. The uncoupled analog frequencies matched the uncoupled experimental frequencies within $\pm$ 1.0%. The practice of varying $I_{\alpha\varphi}$ was determined to cause very small changes in the flutter characteristics, as evidenced by Figure 108, which indicates that the nominal inertia ratio studies coincidentally correspond to the relatively constant, minimum portion of the curve. In addition, the accuracy of the experimental determination of $I_{\alpha\varphi}$ was compromised somewhat by the relatively small inertias being measured. The determination of coupled experimental frequencies was subject to certain inaccuracies by reason of the relatively broad band resonance of the system in its coupled modes. The adjustment of $I_{\alpha\varphi}$ was therefore considered to yield the most reasonable representation of the dynamic system being analyzed.

Analyses were conducted for all conditions, except frequency ratio variations, using a constant nominal model. The experimental model used in run number 17, (see Table I), was chosen as the nominal model. The results of analyses made using the nominal model are presented in Table II.

SECTION VII

DISCUSSION OF RESULTS

A. Evaluation of Flow Characteristics in the Vicinity of the Splitter Plate

An evaluation of the flow characteristics associated with the splitter plate used during the investigation reported in Reference (1) with a 1.5" projection indicated undesirable disturbances in the E-2 wind tunnel. Extension of the splitter plate plane to 2.5" and elimination of certain surface irregularities reduced these disturbances to an acceptable level. The results of this investigation are competently presented in Reference (3) by Mr. J. L. Burk of Arnold Engineering Development Center. It was concluded that a flow disturbance did exist in the model-occupancy space. As indicated by Mr. Burk, a variation of approximately 5% in Mach number over a narrow zone of the model existed. The magnitude and location of this disturbance is considered to have negligible effect upon the flutter characteristics investigated, due to the very small surface area influenced by the disturbance.

B. Experimental Static Aerodynamic Force Coefficients

The results of the static aerodynamic force tests are presented in Figures 10 thru 44 as well as in Reference (3). The purpose of obtaining static force coefficients during this investigation was to provide experimental aerodynamic forcing functions compatible with the quasi-steady flutter analysis study. Experimental flutter tests were conducted only on the double wedge leading edge - blunt trailing edge configurations number 1, 2, and 3 of Figure 1. The discussion of the force coefficients shall therefore be limited to those three configurations. Data relative to the additional configurations is, however, included in Appendix A for information.

It should be noted that at $M = 6.0$ and $M = 7.0$, (see Figures 10 and 15), a loss of lift is experienced near $\alpha_0 = 20^\circ$ with a negligible corresponding influence on the rolling moment and pitching moment, as evidenced by Figures 11, 12, and 16. The aerodynamic center of pressure in this angle-of-attack region is seen to shift outboard and aft, indicating that the lift loss occurs in the area near the root chord and leading edge.

It is believed that at these relatively high angles-of-attack and high pressures, some flow between the root chord and splitter plate is established, causing a loss of lift in the indicated area. As evidenced by Figure 20 , this phenomenon is not observed at M = 8.0. This is believed to be due to the boundary layer growth at the higher Mach number which reduces the flow at the root chord gap.

In general, for configurations 1, 2, and 3 aerodynamic force trends are as follows:

1. With the exception of the lift loss at M = 6.0 and 7.0 already noted, the lift curve slope in general decreases with increasing Mach number.

2. The pitching moment coefficient for configurations 2 and 3 was measured only at small angles-of-attack since flutter tests for these configurations were performed only at $\alpha_o = 0°$. The available data was sufficient to define the force coefficients only over the expected flutter-definition amplitudes, but insufficient to resolve aerodynamic trends as functions of α_o with any degree of reliability. Configuration 1, however, was investigated over a relatively wide range of α_o. The results presented in Figures 10 thru 24 may be discussed as follows:

   a. The pitching moment coefficient data indicates small slope variations at approximately 2° and 6° at M = 6.0 and M = 8.0, respectively. At M = 7.0, a significant change in slope is noted, Figure 16 , at approximately 4° angle-of-attack. It is expected that a more intense investigation at M = 6.0 and 8.0 with increased accuracy and sensitivity would also disclose a rather pronounced slope change at the angles indicated above. This pitching moment slope change is believed due to a shock detachment condition occurring at the leading edge as angle-of-attack is increased beyond the values indicated. As a matter of interest, observations were made during the wind tunnel flutter tests which indicated a condition of neutral stability at dynamic pressures below the actual divergent condition. Visual estimates of the neutral stability condition indicate amplitudes of $\pm$ 3-5° which may indicate a stabilizing influence due to the shock detachment condition explained above.

b. The pitching moment coefficient shows a decrease in slope with increasing Mach number.

c. Since considerable data scatter was unavoidable in the measurement of rolling moment using the available force balance, all centers of pressures, $x_{c.p.}/\bar{c}$ and $\eta_{c.p.}$, were calculated from the faired curves of C_N, C_m, and C rather than using direct point by point data values. The centers of pressure require little discussion, other than to point out the center of pressure shift mentioned previously in discussing the lift loss experienced at M = 6.0 and 7.0 at the high angles-of-attack.

C. Comparison of Experimental and Shock Expansion Aerodynamic Force Coefficients

Figures 46 thru 61 present the pitching moment and rolling moment coefficients obtained from the modified shock expansion methods, as functions of angle-of-attack, in comparison with those obtained experimentally.

In general the comparisons show that "shock-expansion" predictions indicate rather poor correlation with experiment in the case of the pitching moment coefficient. Since the "shock-expansion" method used is a two-dimensional theory, and does not include viscous effects, errors of this nature are to be expected in the chordwise pressure distribution. Additionally, due to the large leading edge sweep angle and blunt trailing edge effect, rather poor correlation is expected to exist in the pressure predictions on the area near the tip, trailing edge; this area having a large influence on pitching moment.

The comparison of rolling moment coefficient predicted by "shock-expansion" techniques with experimental results is considered very good for the t/c = .03 and t/c = .06 configuration. The comparison of rolling moment coefficient for the t/c = .09 configuration is somewhat poorer. This condition is due primarily to the fact that a detached shock condition exists for the 9% thickness configuration at all Mach numbers and angles-of-attack investigated.

Figures 62 thru 65 present the effect of thickness ratio on the pitching moment coefficient as predicted by the modified "shock expansion" theory. It should be noted that, in the case of pitching moment coefficient, the slope changes from negative values

to positive values as thickness increases. Again, the detached shock involved is believed to cause large errors in the pressure distribution in the area of the trailing edge. It is concluded that the modified "shock-expansion" theory does not accurately predict pitching moment, the error being greatly magnified when applied to relatively thick airfoils. Additionally, the error is further amplified with increasing Mach number.

Figures 66 thru 67 present the effect of thickness ratio on the rolling moment coefficient as predicted by the modified "shock-expansion" methods. The slope of rolling moment versus angle-of-attack increases somewhat with increasing thickness.

The remaining static aerodynamic force data has been briefly described in Reference (3), and shall not be discussed in further detail.

D. Experimental and Theoretical Flutter Characteristics

1. Flutter tests were performed only on the "basic" planform and thickness variations, Configurations 1, 2, and 3. The parameter variations investigated were:

   1. Mach number
   2. Angle-of-attack
   3. Uncoupled modal frequency ratio
   4. Thickness ratio

2. The results obtained for configuration number 1 - basic planform, t/c = .06, $\omega_{h_1}/\omega_{\alpha_1}$=.60, $\alpha_0 = 0°$ - at varying Mach number are presented in Figures 68 and 69 . It should be noted that these figures present the flutter velocity parameter and flutter frequency parameter as functions of Mach number. The experimental results indicate that the flutter velocity exhibits a pronounced increase at M = 7.0 and decreases again at M = 8.0. It is believed that this radical increase in flutter velocity at M = 7.0 is due to the very small pitching moment coefficient slope observed in the range of 0° to about 4° angle of attack and previously discussed as being caused by shock detachment at the leading edge. Figure 68 also shows the analog results obtained by using quasi-steady analyses with experimental static force coefficients for the actual model used and for a nominal model having constant mass and dynamic characteristics. The

analog results in this case agree very well with experiment and produce a similar trend with Mach number, indicating that a relatively good representation of the aerodynamics was used. It is felt that further investigation of the flow characteristics in this low angle-of-attack region is necessary to more completely understand the phenomena observed at M = 7.0. Although some experimental scatter is obviously present, it is felt that the faired curve shown on the figure is a relatively accurate indication of the Mach number trend of the basic planform investigated. Figure 69 presents the non-dimensionalized flutter frequency trend with Mach number. Again, at M = 7.0, a noticeably higher level of flutter frequency is observed relative to the other test Mach numbers.

3. The flutter velocity parameter and flutter frequency parameter as a function of angle-of-attack are presented as Figures 70 and 71 for configuration number 1, t/c = .06, $\omega_{h_1}/\omega_{\alpha_1}$ = .60, and Mach number = 6.0. As previously discussed, the system linearity limits precluded the attainment of experimental data at angles-of-attack greater than 10°. The effect of angle of attack within the experimental range investigated was slightly destabilizing. As indicated, a similar destabilizing effect was exhibited in the quasi-steady analog results which were about 22% conservative in the prediction of flutter velocity. The flutter frequencies obtained theoretically were in this case generally higher than those obtained experimentally, with rather large scatter noted in the experimental results.

4. Figures 72 and 73 present the variation of flutter velocity and frequency with angle-of-attack at Mach number = 7.0 for the nominal, basic planform with t/c = .06 and $\omega_{h_1}/\omega_{\alpha_1}$ = .60. Since angle-of-attack variations were not made at M = 7.0, the curve presented is for the nominal model. Only the $\alpha_0 = 0°$ experimental data is noted. The general theoretical trend for this configuration is destabilizing between $\alpha_0 = 0°$ and 5°, relatively constant between $\alpha_0 = 5°$ and 12°, with the destabilizing trend reestablished above 12°. The frequency trends indicate a gradual increase to about 15°, at which point a decreasing frequency trend is noted to exist to the limits investigated.

5. Figures 74 and 75 present the flutter characteristics of the basic planform with t/c = .06, $\omega_{h_1}/\omega_{\alpha_1}$ = .60 at M = 8.0 as they vary with angle-of-attack. Excellent agreement between experiment and theory is observed for this case. As indicated by the differences between actual model results and constant nominal model results, the increase in flutter velocity indicated at $\alpha_0 = 10°$ is believed due primarily to variations of model mass and modal damping characteristics relative to the models utilized at $\alpha_0 = 0°$ and $\alpha_0 = 5°$. It is therefore concluded that a general destabilizing effect is to be expected between $\alpha_0 = 0°$ and 15° with a possible stabilizing effect occurring between $\alpha_0 = 15°$ and $\alpha_0 = 20°$. A relatively large decrease in the slope of the aerodynamic rolling moment is indicated in Figure 22 between 15° and 20° which may be the cause of the above described stabilizing trend in that range of α_0. The analog predictions for this case are very close to the experimental results, but slightly conservative. Figure 75 presents the variation of flutter frequency with angle-of-attack. It will be noted that the flutter frequency observed at $\alpha_0 = 10°$ and 15° indicates a radical increase in flutter frequency with the ratio $\omega_F/\omega_{\alpha_1}$ exceeding unity. This frequency increase may be due to change in the flutter mode occurring at the higher angles-of-attack.

6. Figures 76 and 77 present the flutter characteristics of the basic planform, configuration number 1, M = 6.0 t/c = .06, $\alpha_0 = 0°$; as they vary with modal frequency ratio. The modal frequency ratios investigated were .60, .75, and .90. The nominal, constant model was not analyzed for varying frequency ratio; therefore, the data presented consists only of experimental data and model by model quasi-steady analyses.

   For the configuration in question, the variation of modal frequency ratio over the range investigated reflects a negligible effect on the flutter velocity, but a nearly linear increase in flutter frequency with increasing modal frequency ratio. The results of the analyses indicate very good agreement with experiment in the case of flutter velocity, but rather large error in predicting flutter frequency.

7. Figures 78 and 79 present a comparison of experimental to theoretical flutter characteristics for the basic planform, configuration number 1, t/c = .06. $\alpha_0 = 0°$ at Mach number = 8.0, as they vary with modal frequency ratio. Both

experiment and theory indicate a very small destabilizing effect with increasing modal frequency ratio over the angle-of-attack range investigated. At this Mach number, $\omega_F/\omega_{\alpha_1}$ is less than unity and indicates a small increase in flutter frequency with increasing modal frequency ratio.

8. Figures 80 and 81 present the flutter characteristics of the basic planform, configuration number 3, t/c = .09, $\omega_{h_1}/\omega_{\alpha_1}$ = .60, $\alpha_0 = 0^\circ$ as they vary with Mach number. The experimental trend observed indicates that as Mach number is increased from M = 6.0 to M = 8.0, a destabilizing effect is observed. The decrease in flutter speed between M = 6.0 to M = 8.0 is approximately 17%. The quasi-steady analyses, using experimental aerodynamic coefficients, however, indicate a stabilizing effect with increasing Mach number. This stabilizing effect in the case of the quasi-steady analyses is believed due to the decreasing pitching moment slope with increasing Mach number observed in the experimentally derived aerodynamics used in the analyses. The trend observed relative to flutter frequency may be seen in Figure 81.

9. The variations of flutter velocity and flutter frequency with airfoil thickness ratio using the basic planform at M = 6.0, $\omega_{h_1}/\omega_{\alpha_1}$ = .60 and $\alpha_0 = 0^\circ$ are presented as Figures 82 and 83. In general, the experimental results indicate that the 3% and 9% thickness ratio configurations are slightly less stable than the 6% thickness ratio configuration. As noted in Table I, very large differences in modal damping existed between the particular configurations tested. As reported in Reference (1), the modal damping rates have large influences on the flutter characteristics of the configurations under investigation; however, it is believed that the destabilizing effect noted as thickness ratio is increased from 6% to 9% is due primarily to a shock detachment condition occurring in this region.

The theoretical analysis results associated with this variation indicate a general destabilizing effect over the entire thickness range investigated.

10. In addition to analyzing all experimental flutter configurations using experimentally obtained static aerodynamic force coefficients in conjunction with a quasi-steady analysis, additional studies were made using static aerodynamic force coefficients obtained from a modified "shock-expansion" theory technique. The details of the modified "shock-expansion" technique have been previously discussed.

    Figures 88 thru 107 present a comparison of experimental and theoretical flutter characteristics obtained from a quasi-steady flutter analysis using "shock-expansion" aerodynamics. In general, it is concluded that the use of this very simple aerodynamic theory shows good agreement with the experimental results for the parameter variations presented, with the exception of the variation shown in Figure 88, which shows a relatively large difference in flutter velocity at M = 7.0. As previously explained, and shown in Figure 16, the aerodynamic pitching moment coefficient at M = 7.0, $\alpha_0 = 4^\circ$ exhibits a shallow slope with angle-of-attack. The effect of this condition is stabilizing. The modified "shock-expansion" technique does not predict the aerodynamic phenomena experienced by the model at the Mach number and angle-of-attack region in question. As previously stated, a shock detachment condition is believed to induce the non-linear behavior of the aerodynamics of this configuration.

    With the above exception, "shock-expansion" theory generally is conservative in predicting flutter velocities of the system investigated.

E. Effect of Variations In System Product of Inertia

A brief investigation of the effect of variations in product of inertia on the flutter velocity parameter was made during the analog study. The need for this study was predicated by the extremely small model scale used which in turn compromised the experimental accuracy of determining the product of inertia of the models.

Figure 108 presents the flutter velocity parameter as a function of the ratio $I_{\alpha\varphi}/I_{\alpha\varphi_{NOM}}$, where $I_{\alpha\varphi}$ is the variable product of

inertia and $I_{\alpha\varphi_{NOM}}$, is the actual product of inertia of the nominal constant model. All other system characteristics were those representing the constant nominal model at $\alpha = 0°$, $\omega_{h_1}/\omega_{\alpha_1} = .597$ and M = 8.0. Both experimental aerodynamic coefficients and "shock-expansion" aerodynamic coefficients were used in the study.

The results of the study indicate that variations of $I_{\alpha\varphi}$ of $\pm$ 25% result in negligible changes in the flutter velocity predictions.

SECTION VIII

CONCLUSIONS

A. The following conclusions may be drawn relative to the static aerodynamic force coefficients obtained during this investigation for the double wedge leading edge-blunt trailing edge configurations

1. At M = 6.0 and M = 7.0 a loss of lift is experienced between $\alpha_0 = 20^\circ$ and $\alpha_0 = 21^\circ$ with a negligible corresponding influence on pitching moment and rolling moment. This phenomena is believed to be a function of the finite space between the model and splitter plate.

2. The lift curve slope, relative to the configurations tested, indicates a general decrease with increasing Mach number.

3. The pitching moment coefficients suggest relatively small slope deviations at M = 6.0 and 8.0 as the shock detaches from the leading edge. These slope deviations occur near the theoretically predicted shock detachment angles of attack.

4. A rather significant inflection in the pitching moment is observed at $\alpha_0 \approx 4^\circ$, Mach number = 7.0. This inflection may also be concluded to be caused by shock detachment.

5. The "modified shock-expansion" aerodynamic predictions indicate poor correlation with experiment in the case of pitching moment coefficient, but excellent agreement with experiment in the case of rolling moment coefficient.

6. "Shock-expansion" techniques indicate that the correlation between theory and experiment depreciates with increasing airfoil thickness ratio and increasing angle of attack.

B. The following conclusions may be made relative to the flutter characteristics of the configurations investigated.

1. The variation of flutter velocity with increasing Mach number from $M = 5.0$ to $M = 8.0$ indicates an increase at $M = 7.0$. This increase is due to the very small pitching moment slope observed in the $\alpha_0 \approx 4^\circ$ range. This phenomena is apparent not only in the experimental flutter velocity variation, but also in the trends predicted by the quasi-steady flutter analyses using experimental aerodynamic coefficients.

2. The effect of increasing initial angle-of-attack was slightly destabilizing at all Mach numbers over the experimental range investigated.

3. For the range of modal frequency ratios investigated, both experimental and theoretical flutter velocities reflect very small destabilizing effects with increasing modal frequency ratio.

4. For the 9% thick model, the flutter velocity decreased with increasing Mach number experimentally; but increased with increasing Mach number theoretically.

5. The experimental results indicate that the 3% and 9% thickness variations investigated are less stable than the 6% thickness variation at $\alpha_0 = 0^\circ$, due primarily to the detached shock associated with the 9% configuration. Theoretical analyses, however, indicate a general destabilizing effect with increasing thickness ratio over the entire range investigated.

6. In general, the quasi-steady flutter analysis technique, using experimentally obtained aerodynamic force coefficients, is considered sufficiently accurate in predicting flutter trends for preliminary design purposes. The prediction of flutter frequencies using this technique, however, is considered inadequate.

7. The quasi-steady flutter analysis technique using modified "shock-expansion" aerodynamics is considered a reliable, inexpensive method for predicting flutter velocities and trends in the preliminary design stages of vehicle development, within the range of parameters investigated. Flutter frequencies are not accurately predicted by this technique.

8. In the case of the two aerodynamic forcing functions investigated, the effect of including the rate terms derived from "piston theory" techniques is insignificant.

9. The effect of moderate variations in system product of inertia for the 6% thick configuration at $M = 8.0$ is negligible.

SECTION IX

RECOMMENDATIONS

During the course of this investigation and in consideration of the objectives and results, the following recommendations are made:

A. The primary difficulties experienced during the experimental portion of this investigation were amplified greatly by the small scale models and associated adaptations of the suspension system to the extremely small splitter plate pylon section. It is therefore recommended that any continuation of this study be made using a much larger scale and larger wind tunnel. It is expected that with less restrictive space requirements, considerably better control over system damping, frequency range, ease and speed of operation, and improved parameter constancy would be obtained.

B. It is recommended that additional research be initiated to further develop the use of the basic "shock-expansion" aerodynamic theory in conjunction with quasi-steady flutter analyses. It is believed that chordwise pressure distribution data relative to practical airfoil configurations could be used to evolve reasonable empirical corrections to the two-dimensional results in order to more nearly predict the pitching moment coefficient. The modified theory used in this study proved to be very accurate in predicting static aerodynamic rolling moment coefficients.

C. It is recommended that research be done to specifically determine shock detachment effects on airfoil pressure distributions, both statically and dynamically.

REFERENCES

1. Brown, D. A., "Flutter Model Tests of Advanced Wing Configurations at Initial Angles of Attack," ASD-TDR-62-498, Dated July, 1962

2. Arnold Engineering Development Center, "Arnold Center Facilities Handbook," Vol. 4, Dated July, 1962

3. Burk, Jack L., "Force Tests of Semispan, 70-Deg Swept Wings at Hypersonic Speeds," AEDC-TDR-62-235, Dated December, 1962

4. Bryce, W. W., Cooper, R. E., and Gravitz, S. I., "Development of a Quasi-Steady Flutter Approach and Correlation of Quasi-Steady, Quasi-Unsteady, and Kernel Function Flutter Analyses with Experimental Data," WADD-TR-60-367, Dated May, 1960

5. Uselton, B. L., and Urban, R. H., "Flutter Tests of Highly Swept Wings at Mach Numbers 5 Through 8," AEDC-TDR-63-133, Dated July, 1963

6. Zartarian, G., "Unsteady Airloads on Pointed Airfoils and Slender Bodies at High Mach Numbers," WADC-TR-59-583, Dated December, 1959

7. Sheppard, L. M., Thomson, K. D., "A Shock Expansion Theory Applicable to Wings with Attached Shock Waves," Aeronautical Research Council Technical Report C. P. No. 392, Dated January, 1957

EXPERIMENTAL RUN NUMBER	MACH NUMBER	INITIAL ANGLE-OF-ATTACK α_0 (DEGREES)	THICKNESS RATIO t/c	EQUAL FREQUENCY RATIO $\omega_{\alpha_1}/\omega_{h_1}$	MODAL DAMPING g_{h_1}	MODAL DAMPING g_{α_1}	EXTERNAL EXCITATION	UNCOUPLED ROLL FREQUENCY ω_{α_1} (C.P.S.)	UNCOUPLED PITCH FREQUENCY ω_{h_1} (C.P.S.)	COUPLED ROLL FREQUENCY ω_1 (C.P.S.)	COUPLED PITCH FREQUENCY ω_2 (C.P.S.)	ROLL INERTIA RATIO $I_{y'}/I_{y_{OC}}$	PITCH INERTIA RATIO $I_{x'}/I_{x_{OC}}$	PRODUCT OF INERTIA $I_{xy'} \times 10^{-6}$ (SLUG-FT-LB-SEC^2)	$\frac{x_{ac}}{c}$	$\frac{x_{cg}}{c}$	FLUTTER VELOCITY V_F (FT./SEC.)	EXPERIMENTAL $\frac{V_F}{b_0\omega_{\alpha_1}\sqrt{\mu}}$	EXPERIMENTAL ω_1 (C.P.S.)	EXPERIMENTAL $\frac{\omega_1}{\omega_{\alpha_1}}$	QUASI-STEADY ANALOG (USING EXPER. AERO.) $\frac{V_F}{b_0\omega_{\alpha_1}\sqrt{\mu}}$	QUASI-STEADY ANALOG (USING EXPER. AERO.) ω_1 (C.P.S.)	QUASI-STEADY ANALOG (USING EXPER. AERO.) $\frac{\omega_1}{\omega_{\alpha_1}}$	QUASI-STEADY ANALOG (USING SHOCK EXPAN. AERO.) $\frac{V_F}{b_0\omega_{\alpha_1}\sqrt{\mu}}$	QUASI-STEADY ANALOG (USING SHOCK EXPAN. AERO.) ω_1 (C.P.S.)	QUASI-STEADY ANALOG (USING SHOCK EXPAN. AERO.) $\frac{\omega_1}{\omega_{\alpha_1}}$
17	8.0	0	.06	.195	.150	.071		16.6	27.9	16.9	36.7	1.466	2.430	6.472	.204	.4843	3930	1.191	24.5	.878	1.141	23.0	.827	1.083	23.4	.849
18	8.0		.06	.198	.110	.076		14.1	23.6	13.6	35.5	1.332	2.418	6.472	.223	.4809	3900	1.336	21.4	.997	1.111	19.0	.811	1.081	19.5	.829
19	7.0		.06	.198	.110	.076		14.1	23.6	13.8	32.8	1.333	2.418	6.472	.223	.4809	3500	1.496	21.6	.915	1.372	20.1	.852	1.000	19.6	.831
22	7.0	0	.02	.195	.074	.157		15.4	25.9	15.8	39.2	1.482	2.457	6.543	.204	.4835	3489	1.084	23.2	.896				1.009	20.2	.783
24	8.0	10	.06	.191	.183	.067		14.2	24.5	13.5	33.5	1.293	2.647	5.797	.251	.4806	3919	1.202	18.7	1.316	1.092	21.3	.866	.939	22.7	.682
25A	8.0	5	.06	.198	.159	.076		14.9	24.5	15.0	38.5	1.215	2.621	6.052	.265	.4987	3929	1.046	21.4	.874	1.051	21.5	.873	1.028	21.1	.861
25B	8.0	5		.198	.159	.076		14.9	24.5	15.0	38.5	1.215	2.621	6.052	.265	.4987	3929	1.106	21.4	.874	1.051	21.9	.894	1.093	21.9	.894
26	8.0	15		.196	.157	.122		14.7	24.8	15.8	36.8	1.242	2.647	5.797	.262	.4944	3855	1.374	32.4	1.396	.844	21.1	.861	.902	21.6	.871
27	8.0	0		.197	.179	.179		15.9	26.5	15.9	36.4	1.570	2.660	5.797	.208	.4533	3082	1.350	18.9	.714	1.164	21.3	.813	1.075	21.7	.828
28	8.0	5	.06	.189	.314	.110		16.2	26.8	16.2	37.1	1.579	2.660	5.797	.208	.4533	3098	1.360	17.5	.665	1.096	24.1	.896	1.063	24.4	.907
29	8.0	0	.03	.189	.367	.105		14.3	23.7	13.8	33.6	1.359	2.478	4.109	.225	.4763	3940	1.071	24.6	1.038	1.215	22.3	.927	1.293	22.0	.924
30	8.0		.03	.189	.359	.183		14.4	23.5	13.8	34.8	1.359	2.478	4.109	.225	.4763	3200	1.212	22.4	.954	1.506	22.7	.966	1.325	22.3	.949
31	8.0		.03	.189	.359	.056		14.7	24.5	13.9	31.5	1.389	2.481	8.849	.221	.4747	3040	1.143	20.1	.820	1.035	20.9	.816	.956	20.4	.813
32	8.0		.02	.194	.209	.119		14.7	24.6	13.1	33.7	1.357	2.476	3.649	.222	.4764	3683	.947	17.1	.695	1.458	21.5	.874	1.046	21.8	.889
33	8.0		.06	.191	.143	.147		20.5	22.4	18.0	31.4	1.455	2.457	5.616	.207	.4656	3910	.977	20.7	.925	1.053	21.8	.973	1.051	22.0	.982
34	8.0			.191	.129	.129		21.5	23.6	19.0	31.2	1.495	2.457		.208	.4611	3140	1.159	23.9	.973	1.064	23.3	.987	1.002	23.5	.996
35	8.0			.196	.275	.143		18.0	23.7	18.2	30.1	1.371	2.457		.220	.4759	3123	1.063	19.0	.802	1.106	23.0	.971	1.009	22.9	.966
36	8.0			.196	.366	.119		17.8	23.4	17.4	31.2	1.371	2.457		.220	.4759	3880	1.202	20.5	.876	1.093	22.1	.945	1.074	21.5	.919
37	8.0			.191	.220	.157		17.6	29.2	17.2	36.5	1.371	2.454		.220	.4759	2650	1.111	20.5	.702	1.297	25.0	.862	1.342	24.8	.915
38	6.0			.614	.200	.061		16.2	26.4	15.5	32.3	1.344	2.422		.221	.4794	3160	1.107	20.0	.756	1.173	23.2	.879	1.049	23.1	.872
39	6.0			.601	.158	.064		15.[illegible]	26.3	17.4	33.9	1.291			.230	.4849	3060	1.200	18.5	.703	1.172	22.7	.863	1.053	23.0	.876
40	6.0	5		.607	.220	.059		19.3	31.5	17.7	42.7	1.290			.231	.4870										
41	6.0			.600	.157	.183		18.9	31.5	17.6	43.1	1.290			.231		3026	1.147	25.6	.819	1.007	24.1	.768	1.002	24.6	.783
42	6.0	10		.620	.320	.027		18.5	31.4	17.6	42.3	1.290			.231		3061	1.118	25.5	.812	.998	25.2	.803	.948	29.2	.930
43	6.0	0		.600	.275	.063		18.5	31.5	14.2	36.4	1.290	2.422		.231	.4870	3095	1.037	18.6	.590	1.162	28.2	.895	1.038	27.8	.883
44	6.0	0		.598	.054	.105		24.0	26.8	20.1	40.7	1.385	2.426		.225	.4820	3107	1.103	23.8	.692	.997	25.8	.970	.954	26.2	.989
45	8.0	5		.594	.105	.039		17.0	24.6	15.9	34.1	1.297	2.425		.230	.4860	3946	1.002	19.6	.625	1.075	24.0	.839	1.054	24.4	.853
46	8.0	0	.06	.595	.105	.039		16.9	24.4	16.6	33.4	1.297	2.425	5.518	.230	.4860	3910	1.070	19.3	.580	1.098	23.2	.817	1.063	23.8	.838

TABLE I TABULATION OF EXPERIMENTAL AND THEORETICAL FLUTTER RESULTS

EXPERIMENTAL RUN NUMBER	MACH NUMBER	INITIAL ANGLE-OF-ATTACK (DEGREES)	THICKNESS RATIO t/c	MODAL FREQUENCY RATIO ω_θ/ω_h	ROLL INERTIA RATIO I_α/I_{α_0}	PITCH INERTIA RATIO I_θ/I_{θ_0}	PRODUCT OF INERTIA $I_{\alpha\theta} \times 10^4$ (IN-LB-SEC²)	x_α/c	FLUTTER VELOCITY V_F (FT/SEC)	QUASI-STEADY ANALOG (USING EXPER. AERO.) $V_F/b\omega_\theta$	ω_F (C.P.S.)	ω_F/ω_θ	QUASI-STEADY ANALOG (USING SHOCK EXPAN. AERO.) $V_F/b\omega_\theta$	ω_F (C.P.S.)	ω_F/ω_θ	EXPERIMENTAL $V_F/b\omega_\theta$	ω_F (C.P.S.)	ω_F/ω_θ	THE FOLLOWING PARAMETERS ARE CONSTANT FOR NOMINAL MODEL RUN NUMBER 17	VALUE
17-200	.8	0	.06	.597	1.466	2.430	6.472	.4643	3930	1.141	23.0	.827	1.081	23.4	.842	1.191	24.5	.873	UNCOUPLED ROLL FREQUENCY ~ ω_α (C.P.S.)	16.6
17-205		5								1.116	23.3	.838	1.035	23.2	.838					
17-210		10								1.048	23.7	.845	.982	23.9	.860					
17-215		15								.947	23.6	.833	.958	23.0	.859				UNCOUPLED PITCH FREQUENCY ~ ω_θ (C.P.S.)	27.0
17-220		20							3930	1.053	28.1	1.013	.738	25.3	.910					
17-700	7	5							3500	1.168	24.4	.878	1.001	23.6	.845					
17-705		5								1.104	24.2	.875	1.061	23.6	.849				COUPLED ROLL FREQUENCY ~ ω_α (C.P.S.)	15.6
17-710		10								1.105	25.9	.932	1.048	25.0	.899					
17-715		15								1.029	27.1	.975	.895	25.6	.906					
17-720	7	20							3500	.744	22.4	.802	.860	24.2	.906				COUPLED PITCH FREQUENCY ~ ω_θ (C.P.S.)	34.6
17-600	6	0							3100	1.212	23.5	.845	1.072	23.8	.854					
17-605		5								1.070	23.7	.853	1.038	24.0	.862					
17-610		10								1.039	24.2	.871	.988	24.0	.862				MODAL DAMPING, $\sim g_\alpha$	.150
17-615		15								.937	24.6	.892	.959	24.6	.885					
17-620	6	20							3100	.871	26.1	.939	.867	24.2	.870				MODAL DAMPING, $\sim g_\theta$	.071
17-500	5	0							2650	1.321	23.5	.842	1.064	24.0	.860					
17-505		5								1.087	24.1	.867	1.051	23.8	.856				r_α^2	.004
17-510		10								1.015	24.5	.871	1.014	24.6	.885				$I_\alpha \times 10^4$ (IN-LB-SEC²)	15.73
17-515		15								1.002	25.3	.910	.932	25.1	.903					
17-520		20				1.466	2.430	6.472	2650	1.034	25.7	.924	.891	24.4	.878				$I_\theta \times 10^4$ (IN-LB-SEC²)	.487
17-801		0				1.466	2.430	6.472	.4643	3930	2.162	23.0	.827	1.097	23.5	.845				
17-802						1.210	5.931	2.250	.3558		1.473	23.7	.853	1.293	22.6	.811				
17-803						2.162	5.243	3.091	.3751		1.314	23.6	.849	1.192	22.6	.811				
17-804						2.530	4.194	3.750	.3943		1.225	23.3	.838	1.138	22.8	.819				
17-805						2.092	3.489	4.134	.4145		1.182	23.3	.838	1.115	23.1	.829				
17-806						1.581	2.601	6.931	.4522		1.139	23.2	.835	1.100	23.3	.836				
17-807						1.265	2.097	7.931	.4900		1.146	23.0	.827	1.115	23.8	.854				
17-808						1.150	1.906	8.251	.5101		1.150	22.9	.824	1.132	24.1	.865				
17-809						1.094	1.741	9.071	.5294		1.191	23.2	.835	1.162	24.0	.862				
17-810						.973	1.611	9.751	.5487		1.202	23.7	.853	1.183	24.7	.887				
17-820			.06			.903	1.493	10.502	.5680	3930	1.211	22.9	.824	1.210	25.2	.905				
17-790	7		.09			1.466	2.430	6.472	.4643	3500				1.063	24.6	.885				
17-8[illegible]	8		.09							3930	1.472	24.6	.892	1.096	24.9	.896				
17-[illegible]	8		.09							3930	1.251	24.8	.892	1.295	24.5	.881				
17-[illegible]	6	0	.09	.597	1.466	2.430	6.472	.4643	3100	1.104	24.4	.878	1.284	24.4	.878					
17-[illegible]	5	0	.09	.597	1.466	2.430	6.472	.4643	3100	1.473	24.0	.863	1.263	25.1	.891					
17-[illegible]	7	0	.09	.597					3500	1.372	23.1	.458	1.000	19.6	.831					
17-75	7	0	.06	.754					3500				.961	21.9	.898					
17-90	7	0	.06	.989	1.466	2.430	6.472	.4643	3100				.974	23.7	1.004					

TABLE II TABULATION OF THEORETICAL FLUTTER RESULTS USING NOMINAL CONSTANT MODEL

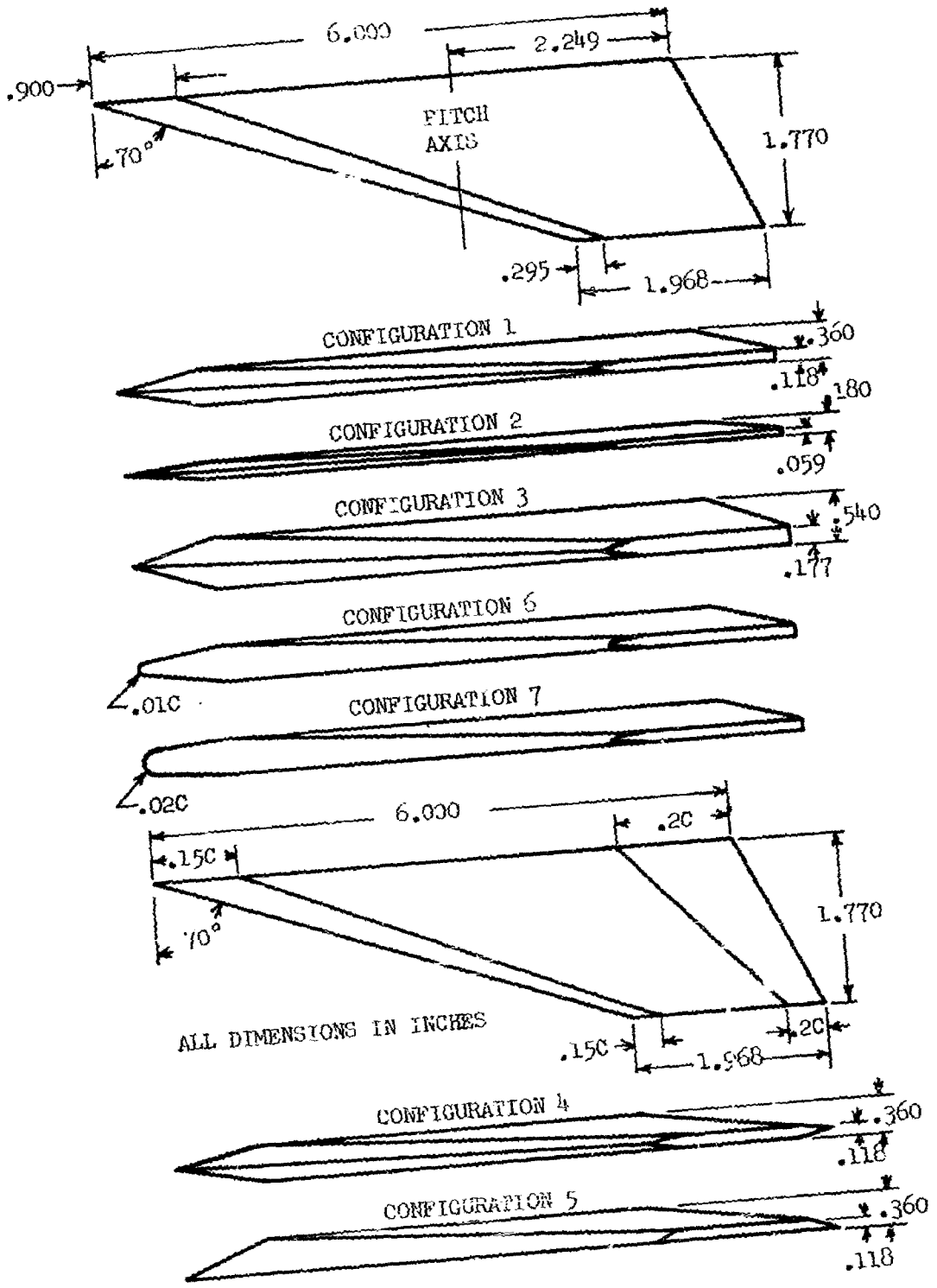

FIGURE 1 MODEL CONFIGURATION GEOMETRY

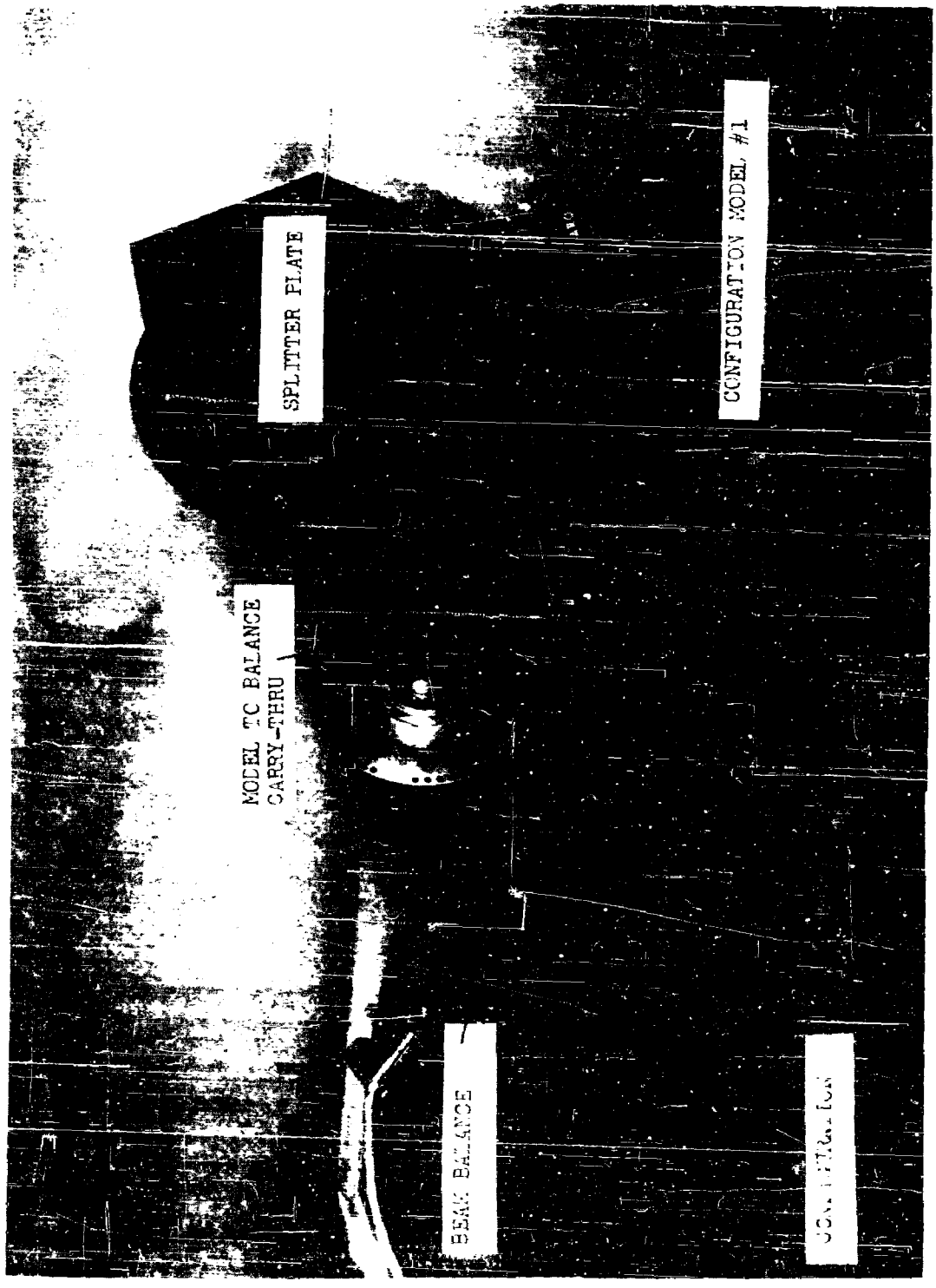

FIGURE 2 PHOTOGRAPH OF STATIC AERODYNAMIC FORCE MEASUREMENT COMPONENTS AND RIGID MODELS

FIGURE 3 BASIC SPAR AND COMPLETED SEMI-RIGID FLUTTER MODEL

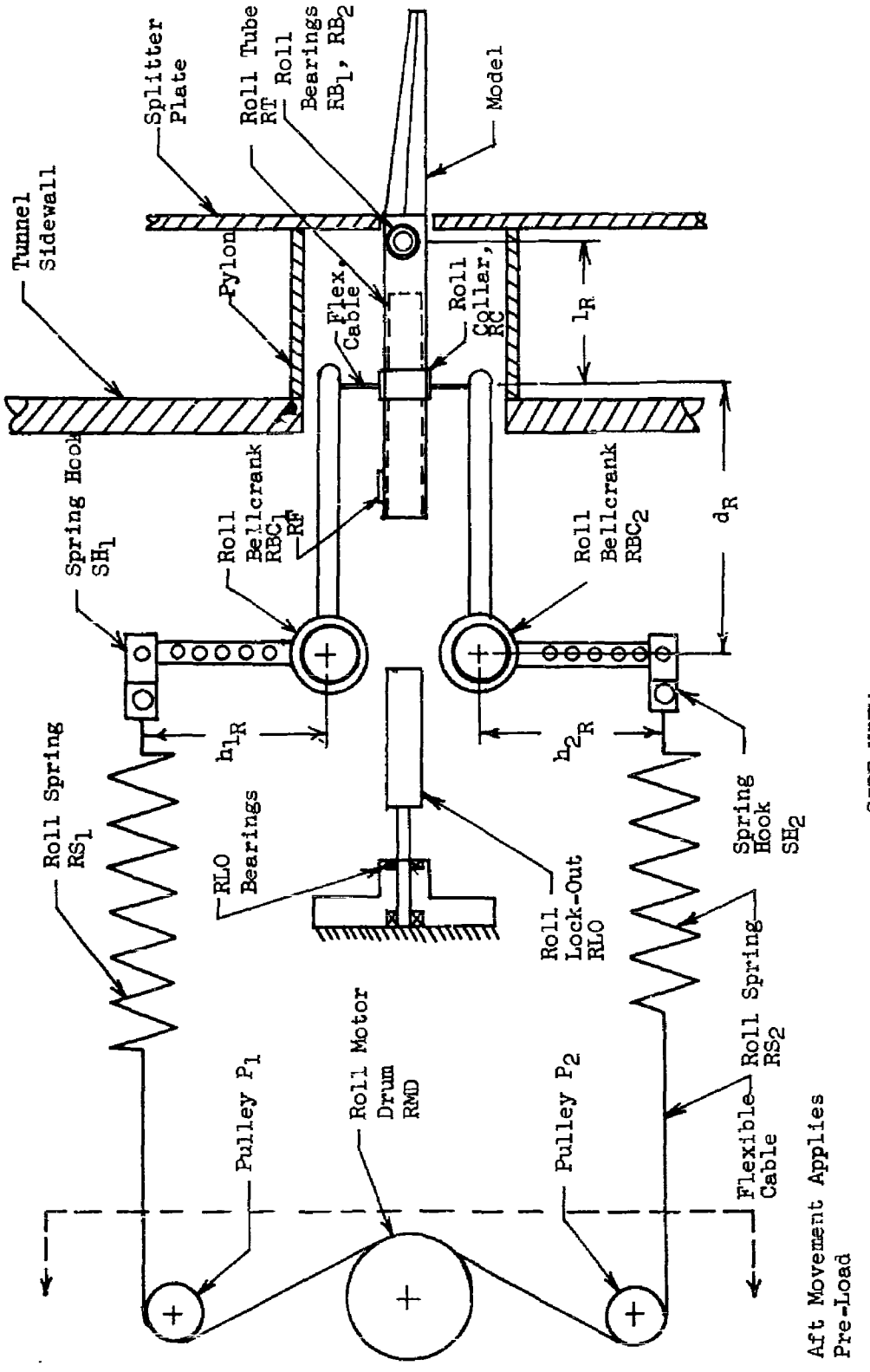

SIDE VIEW

FIGURE 4 SUSPENSION SYSTEM ROLL MODE MECHANISM

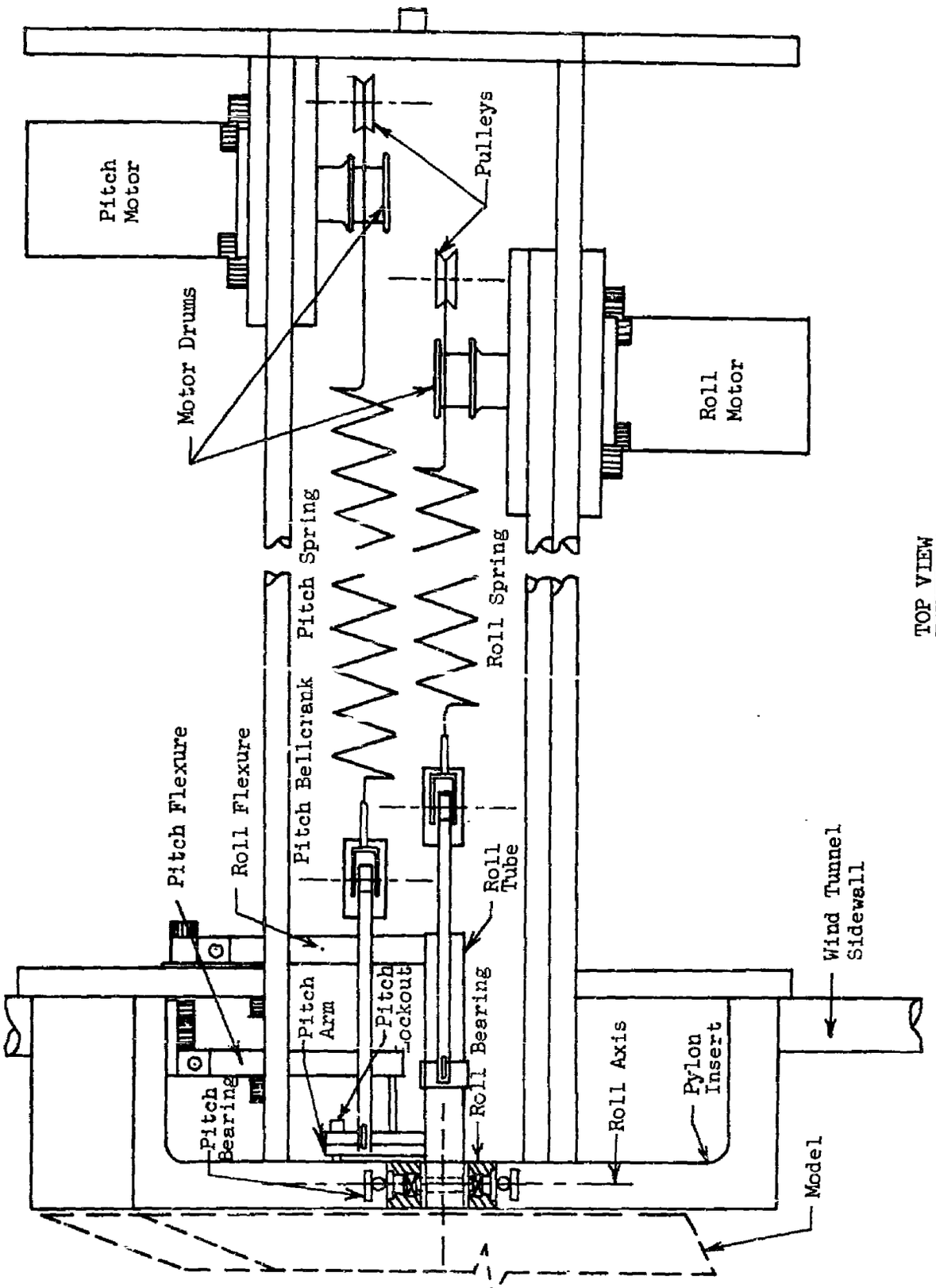

TOP VIEW

FIGURE 5 SUSPENSION SYSTEM PITCH MODE MECHANISM

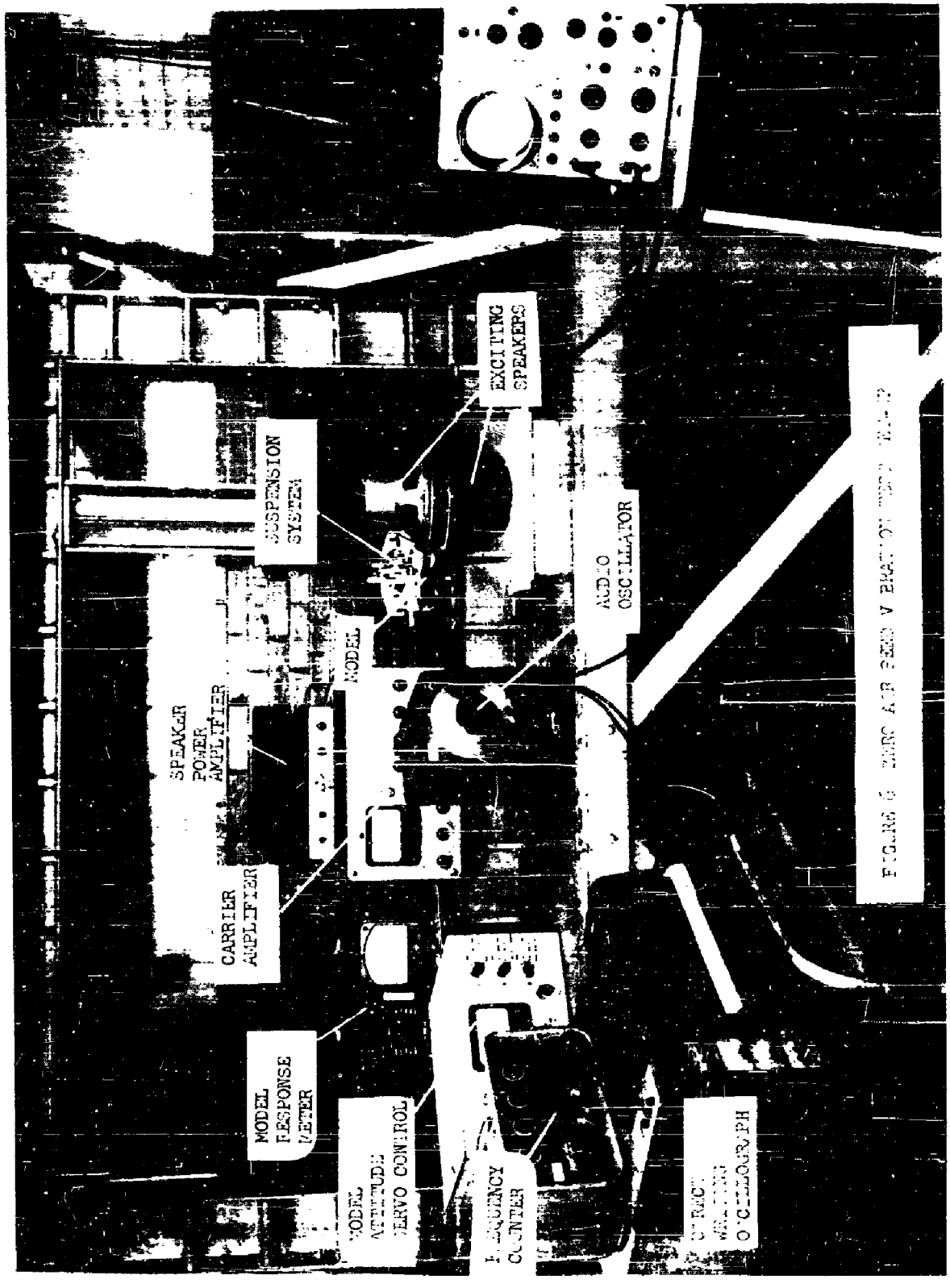
SUSPENSION SYSTEM
EXCITING SPEAKERS
SPEAKER POWER AMPLIFIER
MODEL
AUDIO OSCILLATOR
CARRIER AMPLIFIER
MODEL RESPONSE METER
MODEL ATTITUDE SERVO CONTROL
FREQUENCY COUNTER

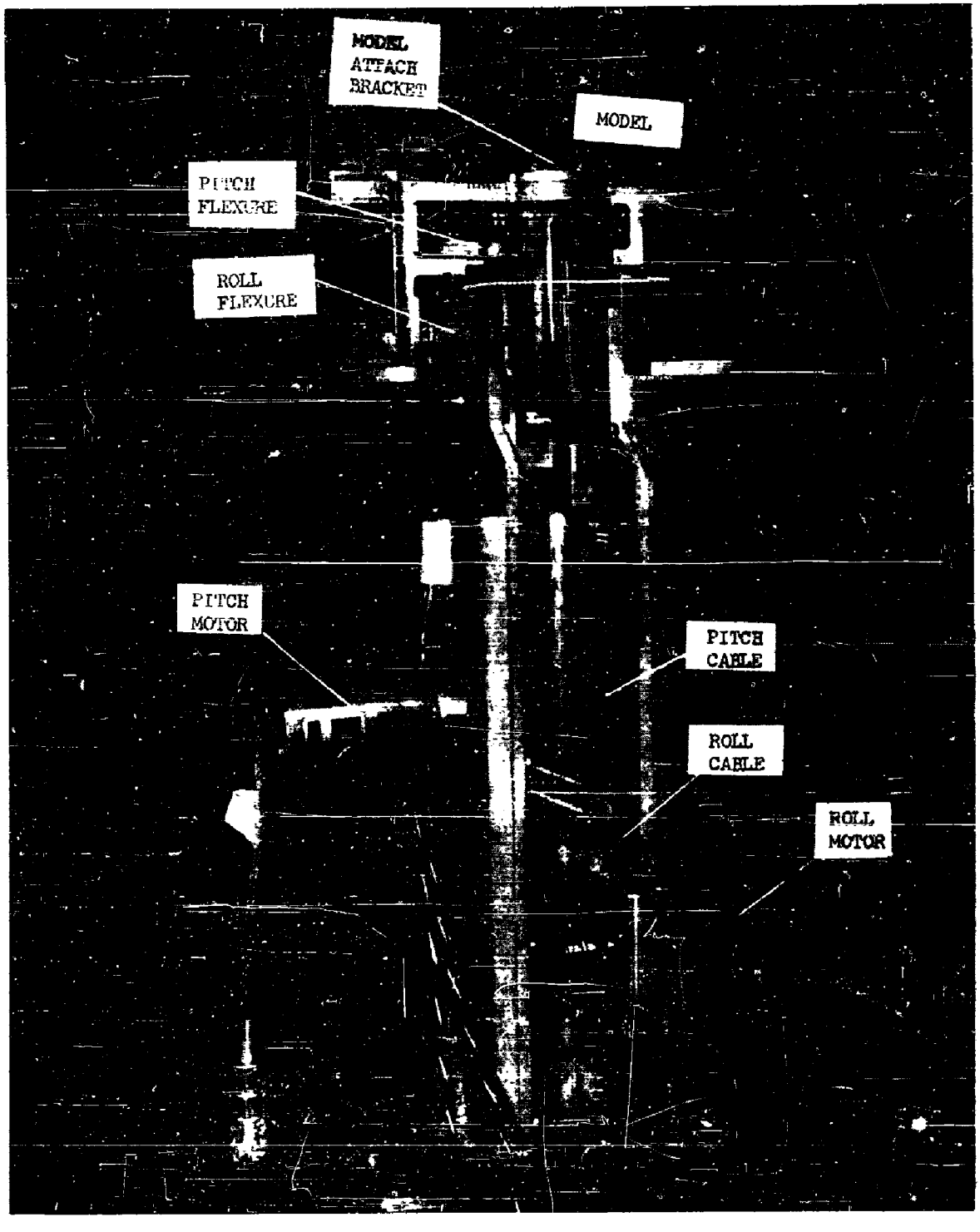

FIGURE 7 PHOTOGRAPH OF SUSPENSION SYSTEM UNIT

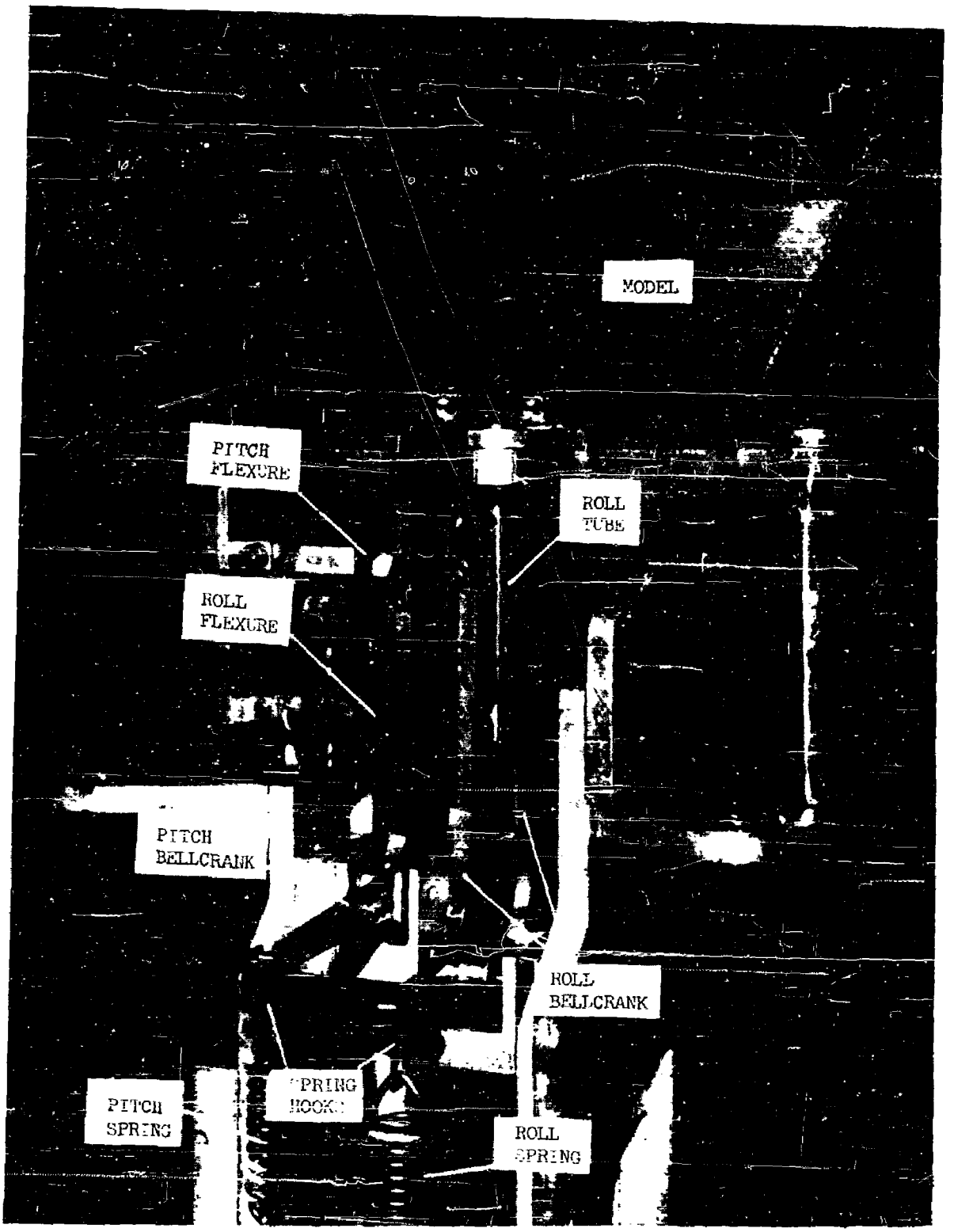

FIGURE 8 PHOTOGRAPH OF PITCH AND ROLL MECHANISM

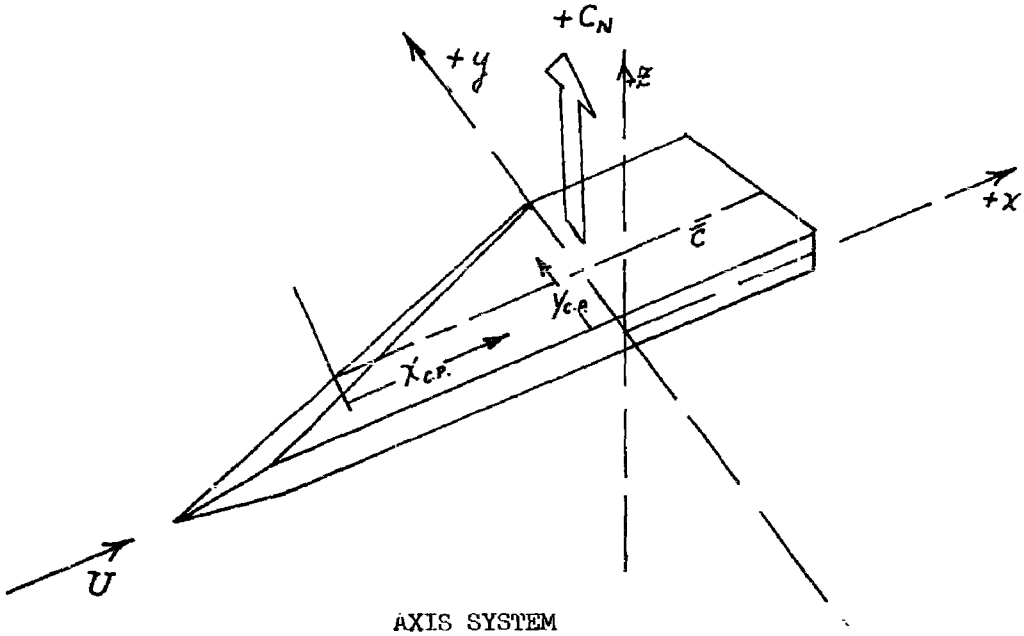

AXIS SYSTEM

DATA REDUCTION EQUATIONS

$$C_N = \frac{\text{Normal Force}}{qS_W}$$

$$C_m = \frac{\text{Pitching Moment}}{qS_W\bar{c}}$$, Positive leading edge up

$$C_\ell = \frac{\text{Rolling Moment}}{qS_W(b/2)}$$, Positive tip up - about model root chord

$$\eta_{C.P.} = \frac{C_\ell}{C_N}$$

$$\frac{X_{C.P.}}{\bar{c}} = .400 - \frac{C_m}{C_N}$$

FIGURE 9 AXIS SYSTEM AND DATA REDUCTION EQUATIONS FOR STATIC AERODYNAMIC FORCE DATA

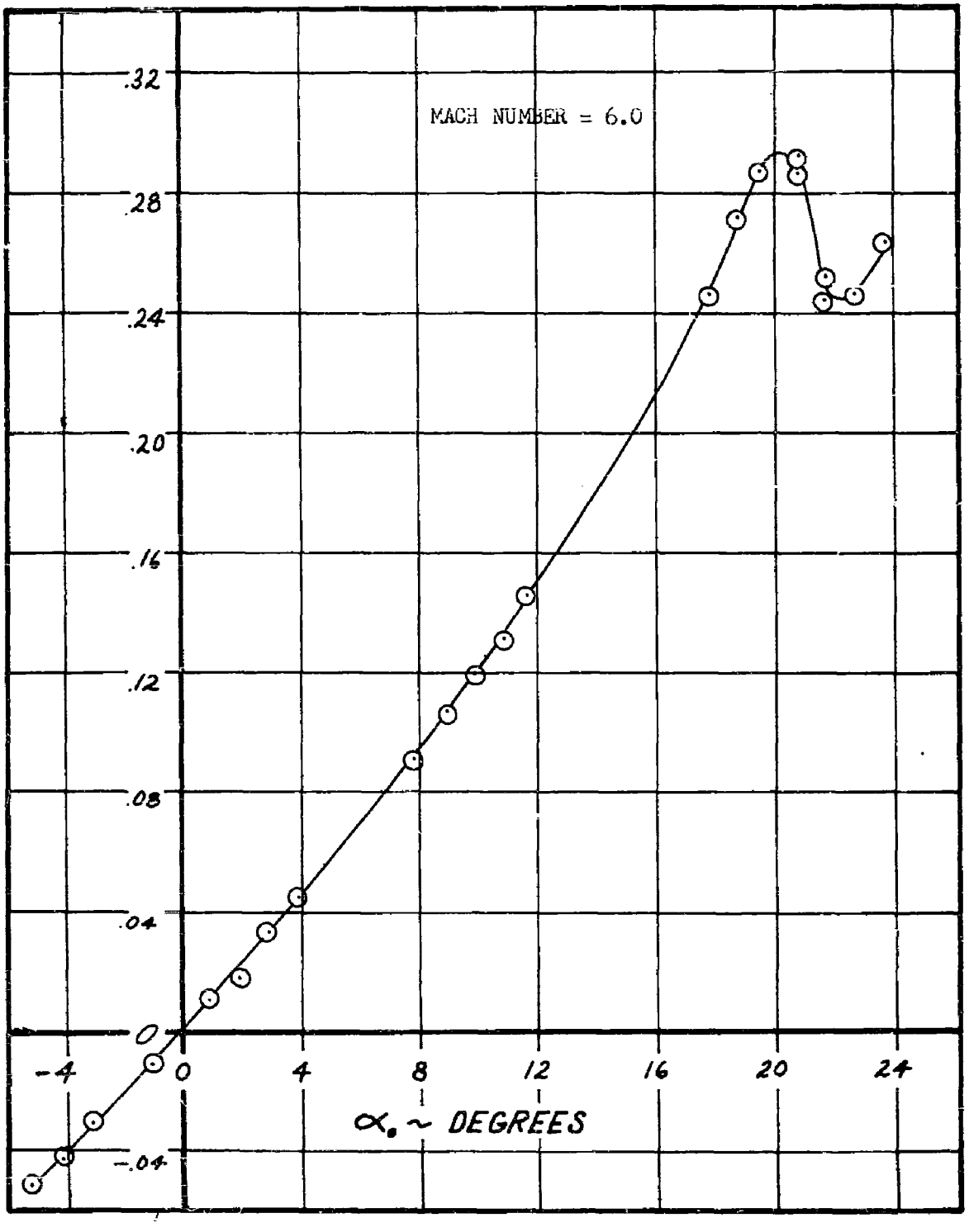

FIGURE 10 EXPERIMENTAL LIFT COEFFICIENT VS. ANGLE-OF-ATTACK; BASIC PLANFORM, t/c = .06, MACH NUMBER = 6.0

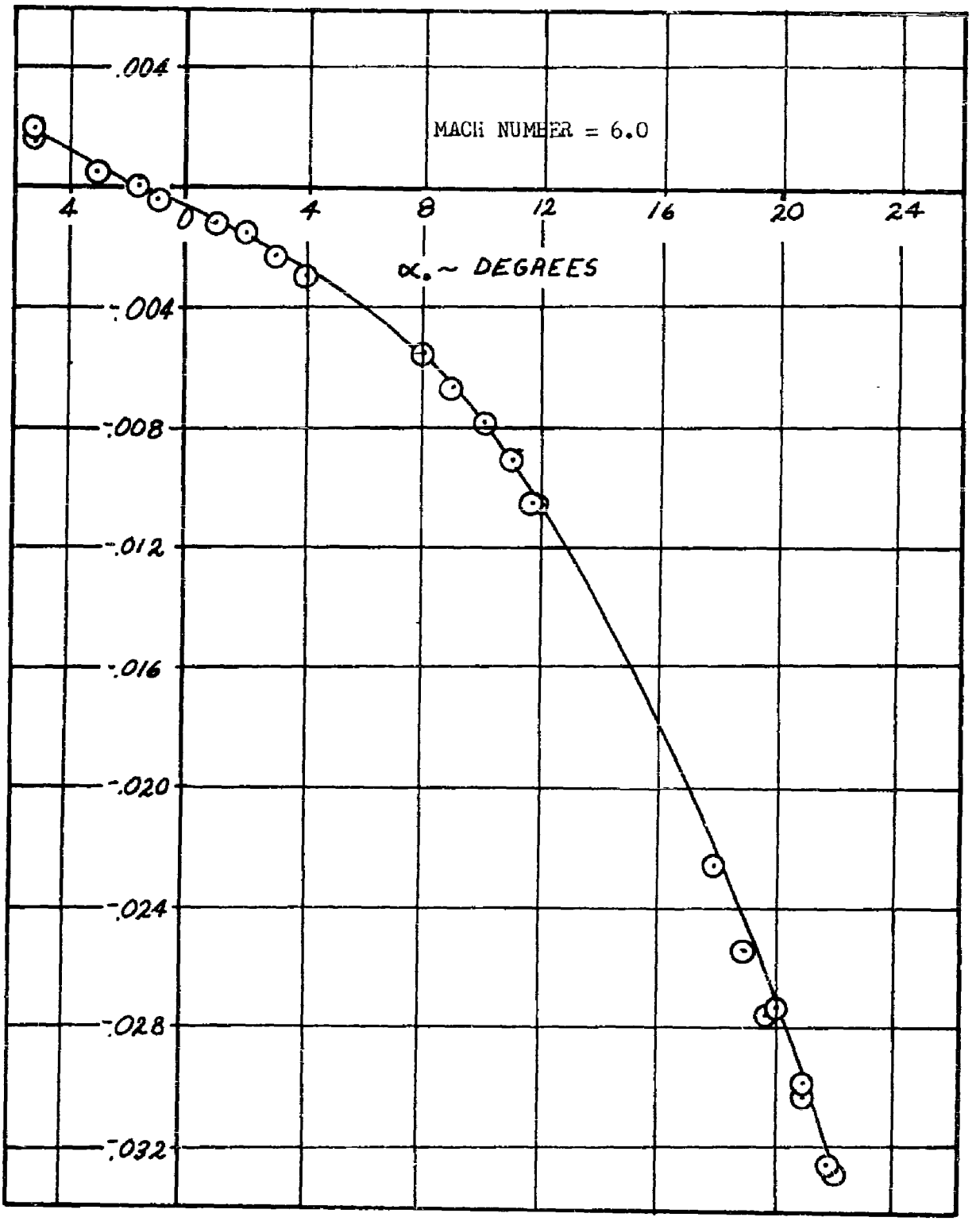

FIGURE 11 EXPERIMENTAL PITCHING MOMENT COEFFICIENT VS. ANGLE-OF-ATTACK; BASIC PLANFORM, t/c = .06, MACH NUMBER = 6.0

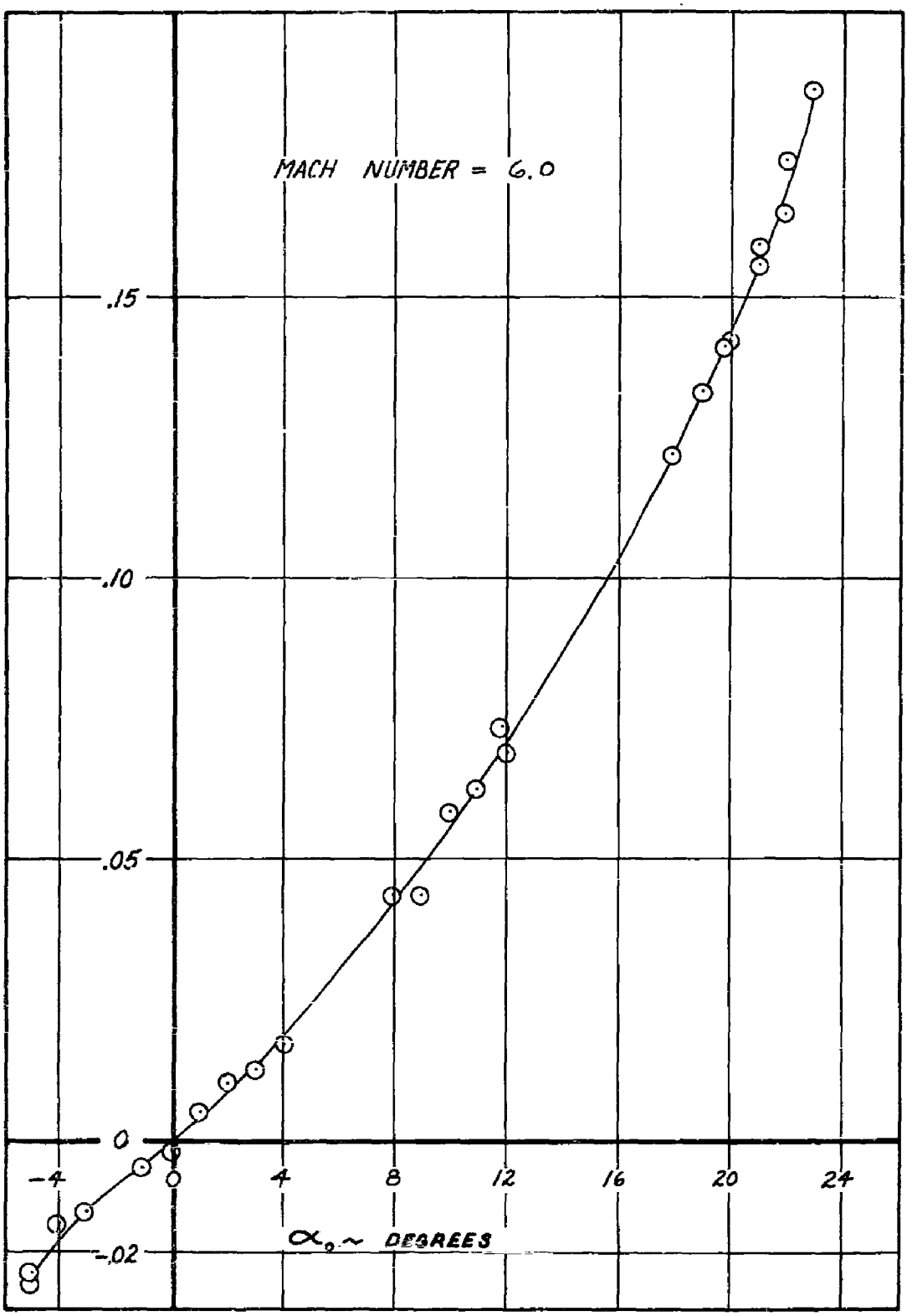

FIGURE 12 EXPERIMENTAL ROLLING MOMENT COEFFICIENT VS. ANGLE-OF-ATTACK; BASIC PLANFORM, t/c = .06, MACH NUMBER = 6.0

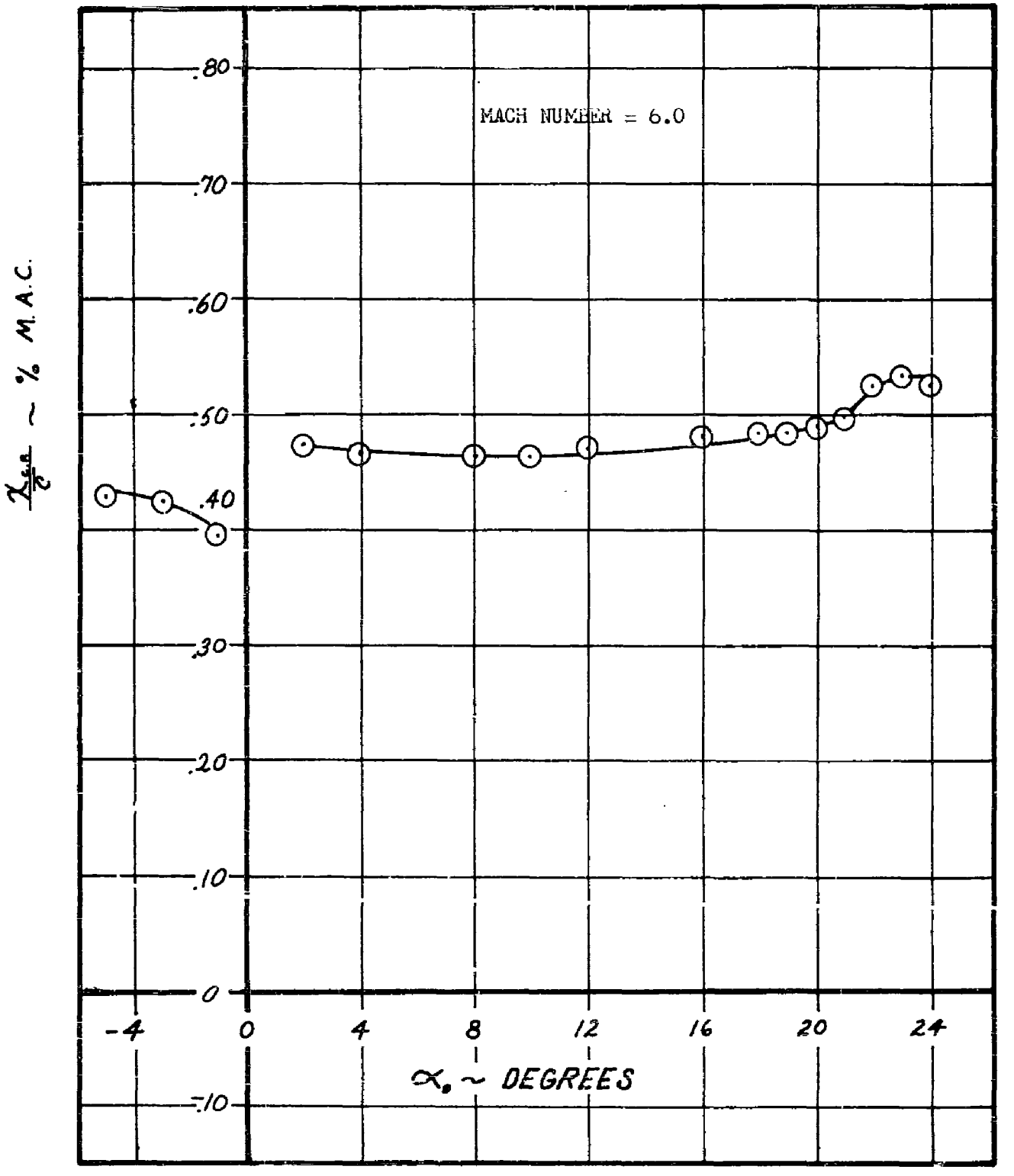

FIGURE 13 EXPERIMENTAL CHORDWISE CENTER-OF-PRESSURE VS. ANGLE-OF-ATTACK; BASIC PLANFORM, t/c = .06, MACH NUMBER = 6.0

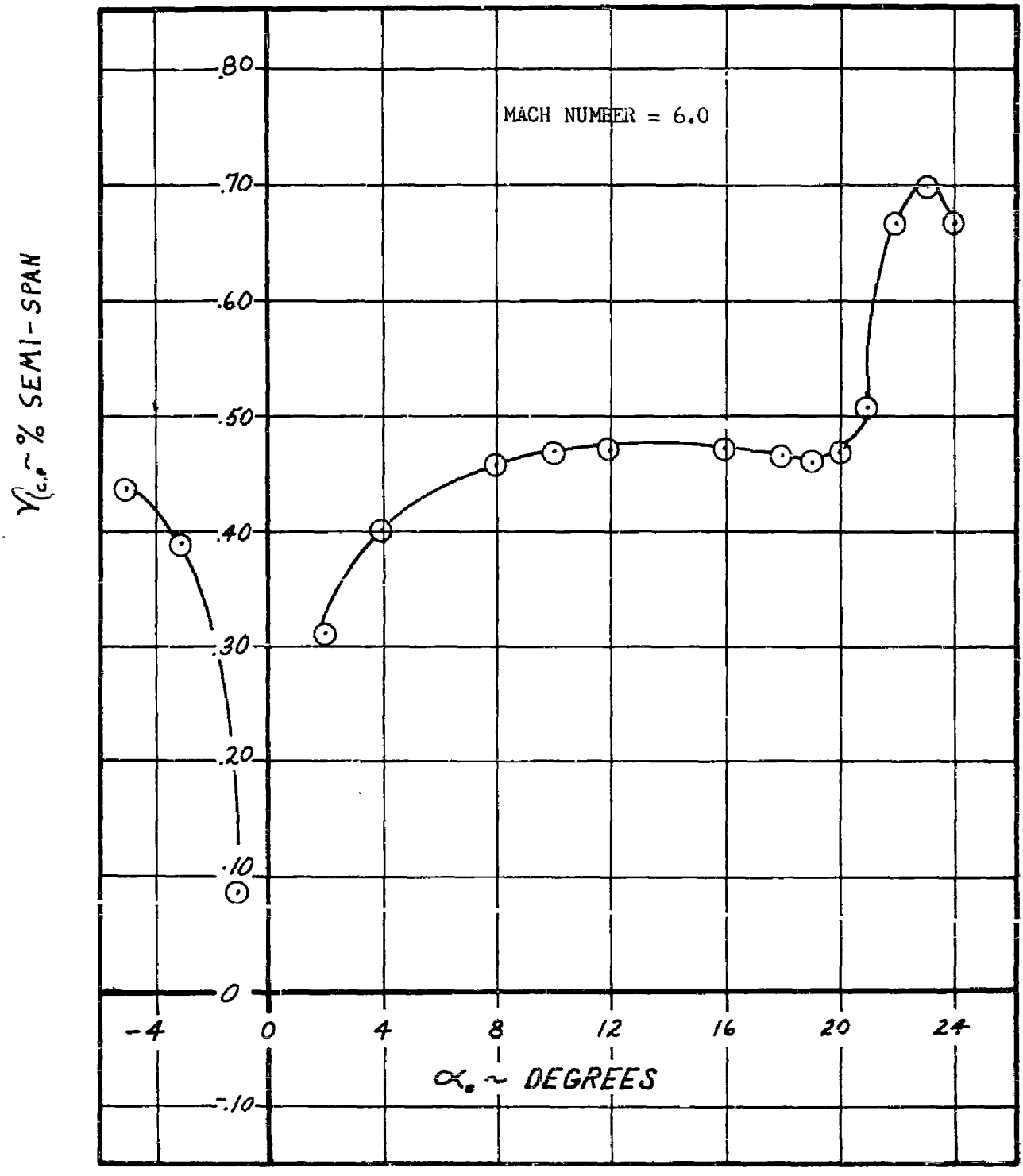

FIGURE 14 EXPERIMENTAL SPANWISE CENTER-OF-PRESSURE VS. ANGLE-OF-ATTACK; BASIC PLANFORM, t/c = .06, MACH NUMBER = 6.0

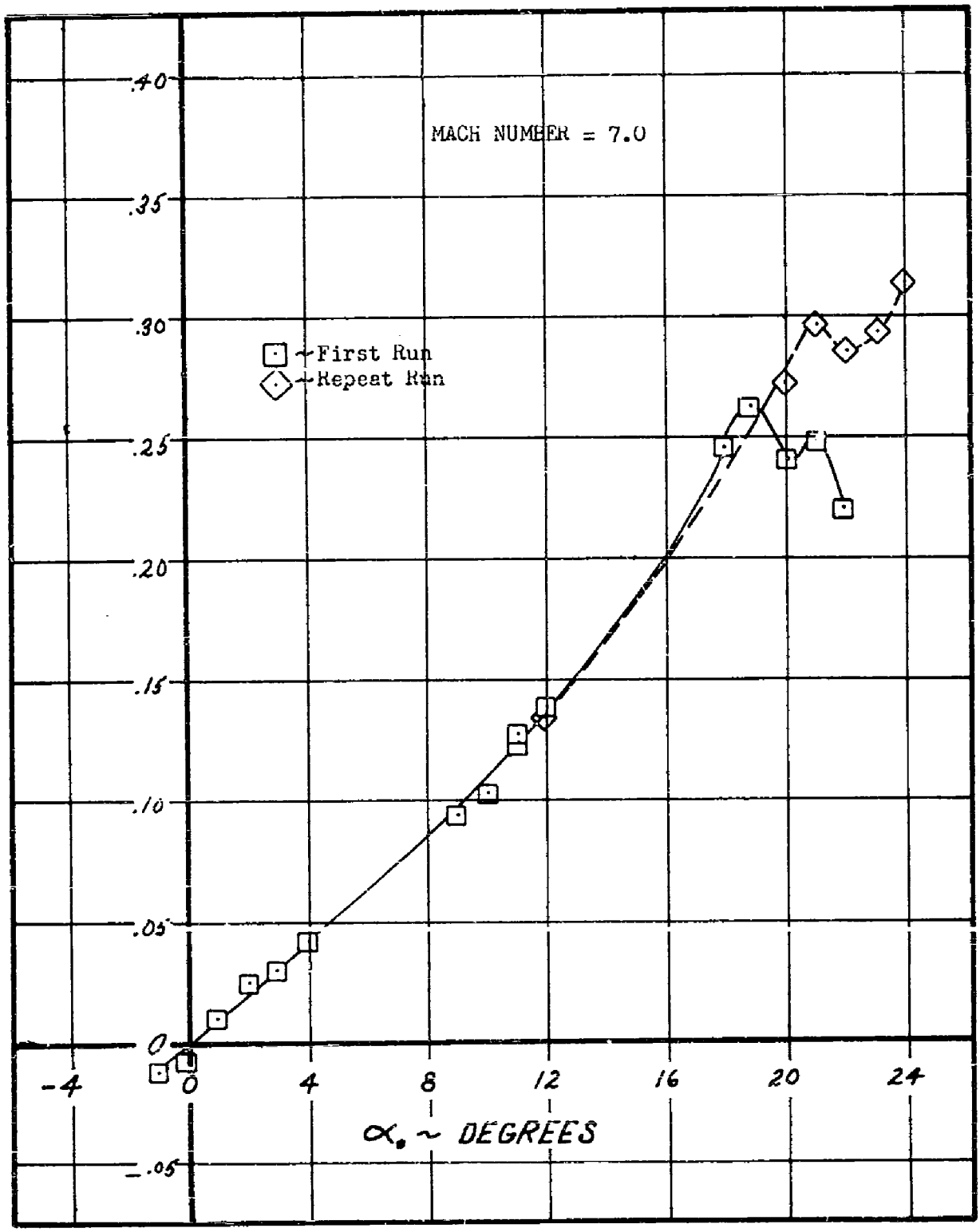

FIGURE 15 EXPERIMENTAL LIFT COEFFICIENT VS. ANGLE-OF-ATTACK; BASIC PLANFORM, t/c = .06, MACH NUMBER = 7.0

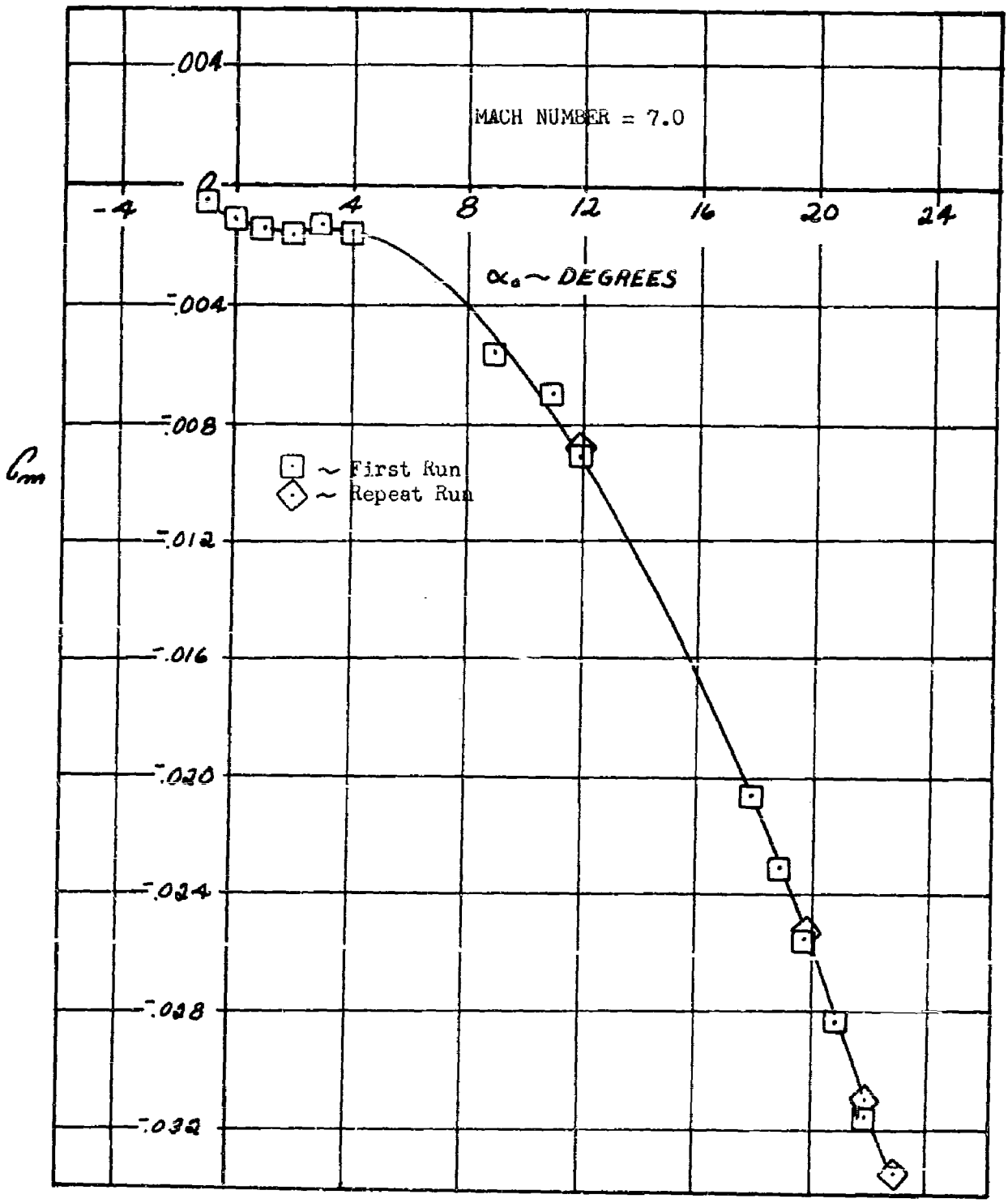

FIGURE 16 EXPERIMENTAL PITCHING MOMENT COEFFICIENT VS. ANGLE-OF-ATTACK; BASIC PLANFORM, t/c = .06, MACH NUMBER = 7.0

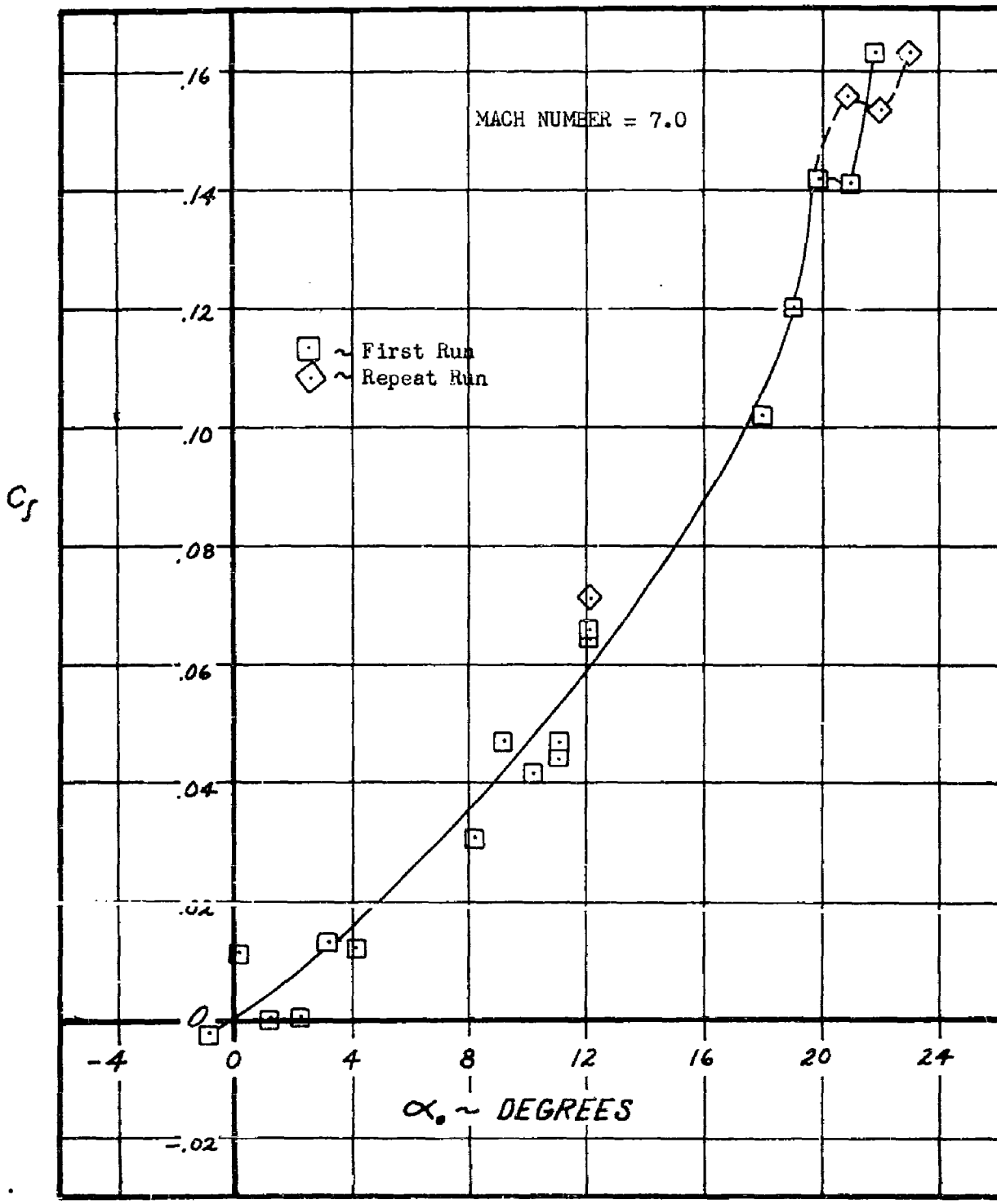

FIGURE 17 EXPERIMENTAL ROLLING MOMENT COEFFICIENT VS. ANGLE-OF-ATTACK; BASIC PLANFORM, t/c = .06, MACH NUMBER = 7.0

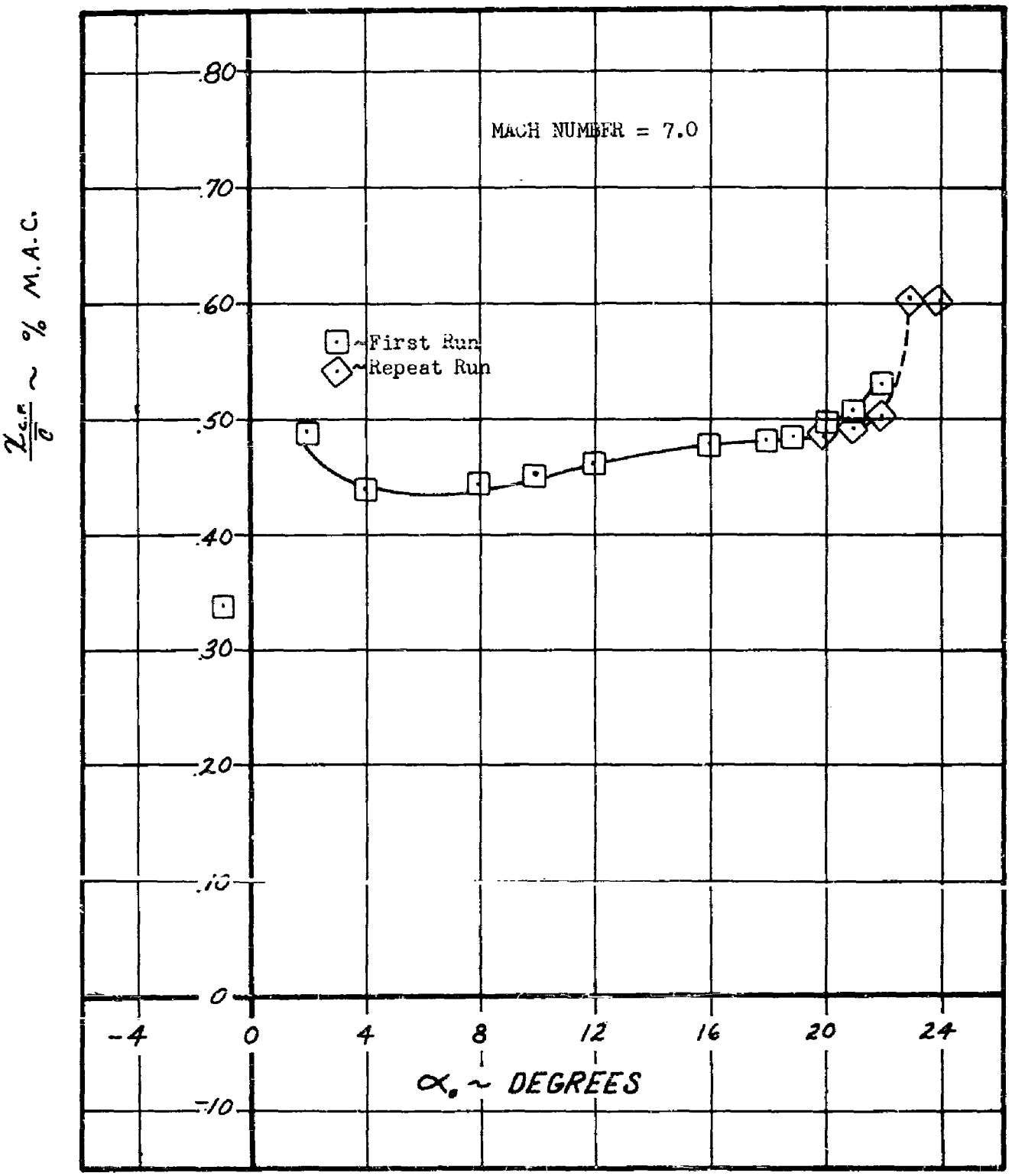

FIGURE 18 EXPERIMENTAL CHORDWISE CENTER-OF-PRESSURE VS. ANGLE-OF-ATTACK; BASIC PLANFORM, t/c = .06, MACH NUMBER = 7.0

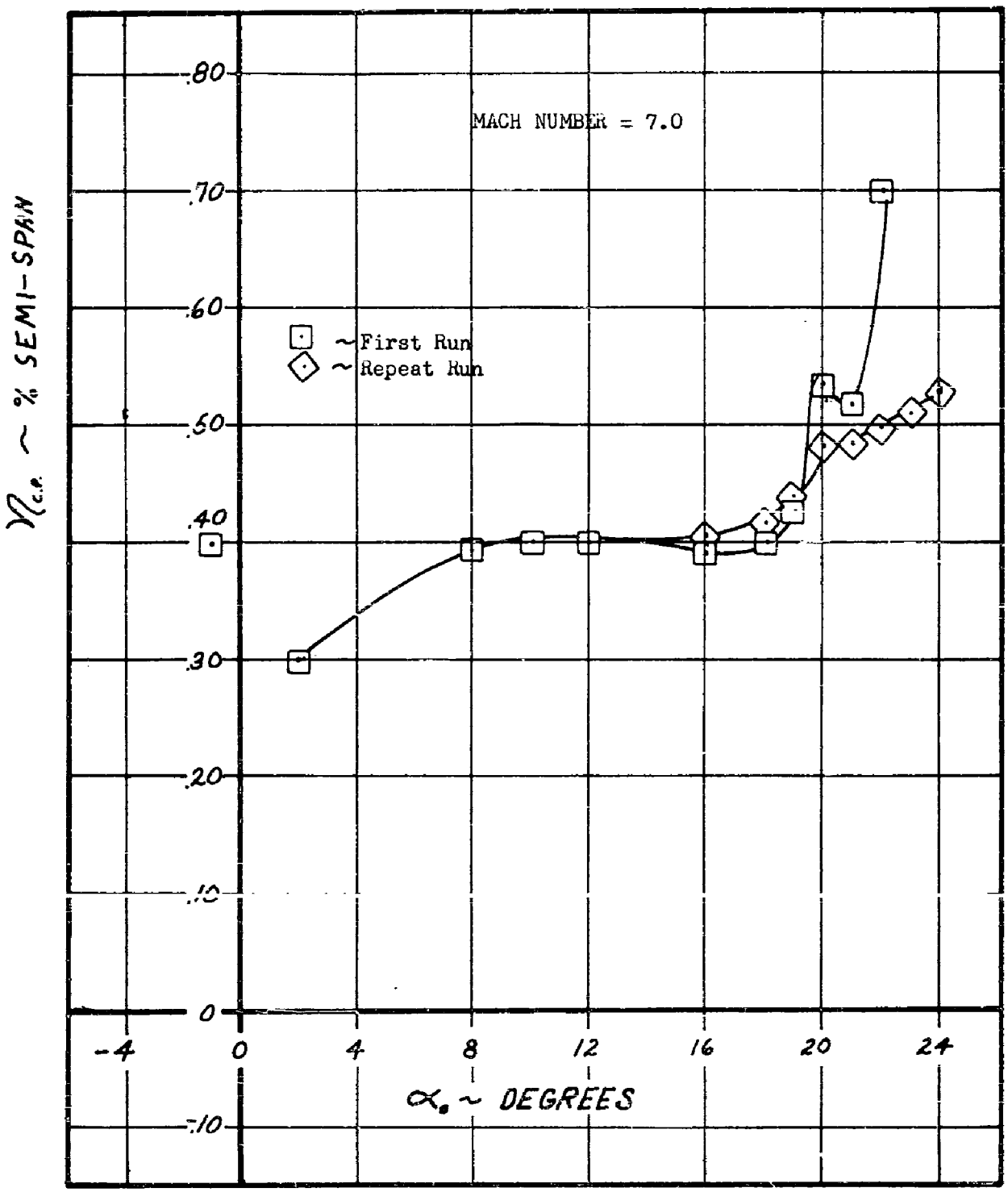

FIGURE 19 EXPERIMENTAL SPANWISE CENTER-OF-PRESSURE VS. ANGLE-OF-ATTACK; BASIC PLANFORM, t/c = .06, MACH NUMBER = 7.0

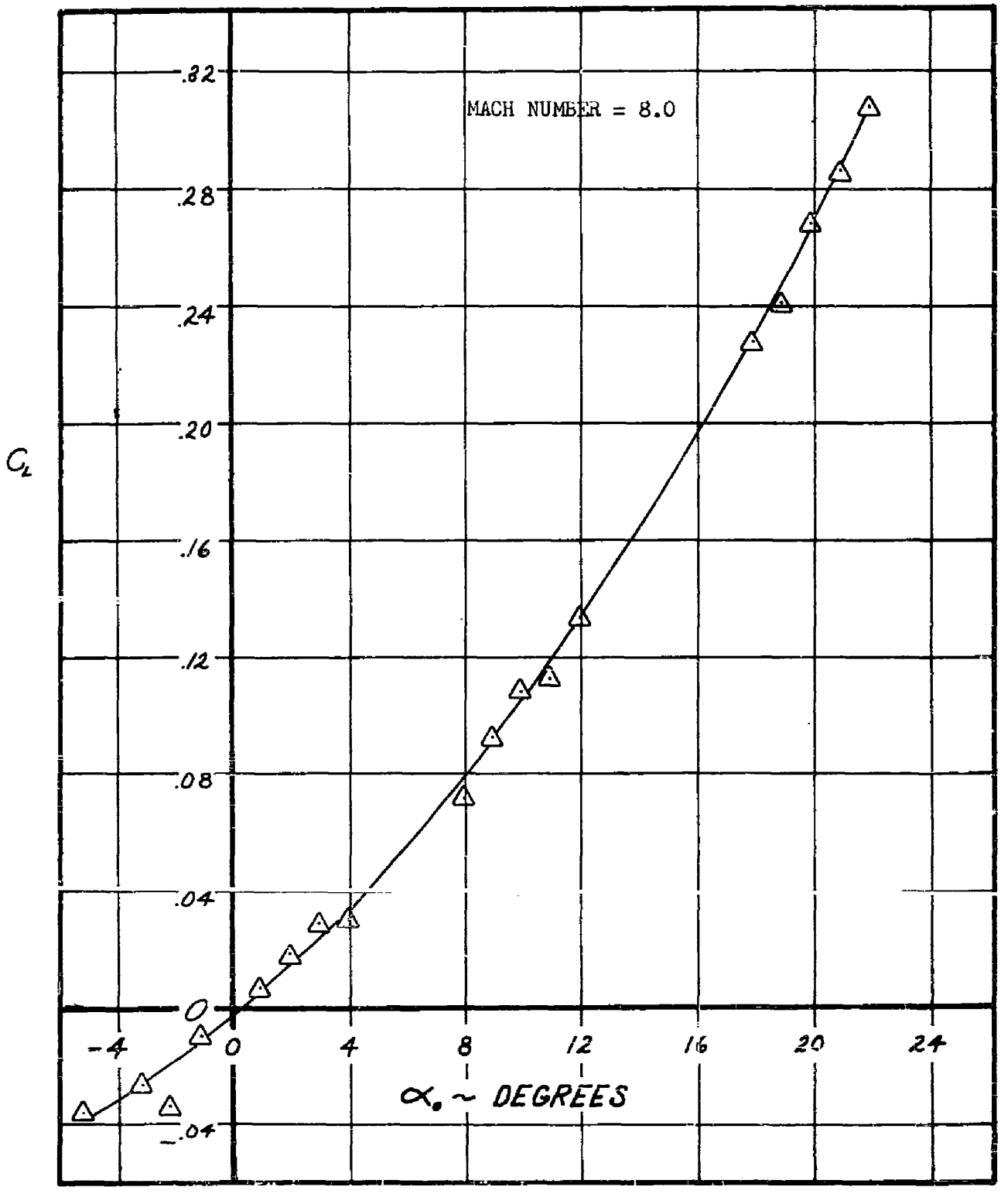

FIGURE 20 EXPERIMENTAL LIFT COEFFICIENT VS. ANGLE-OF-ATTACK; BASIC PLANFORM, t/c = .06, MACH NUMBER = 8.0

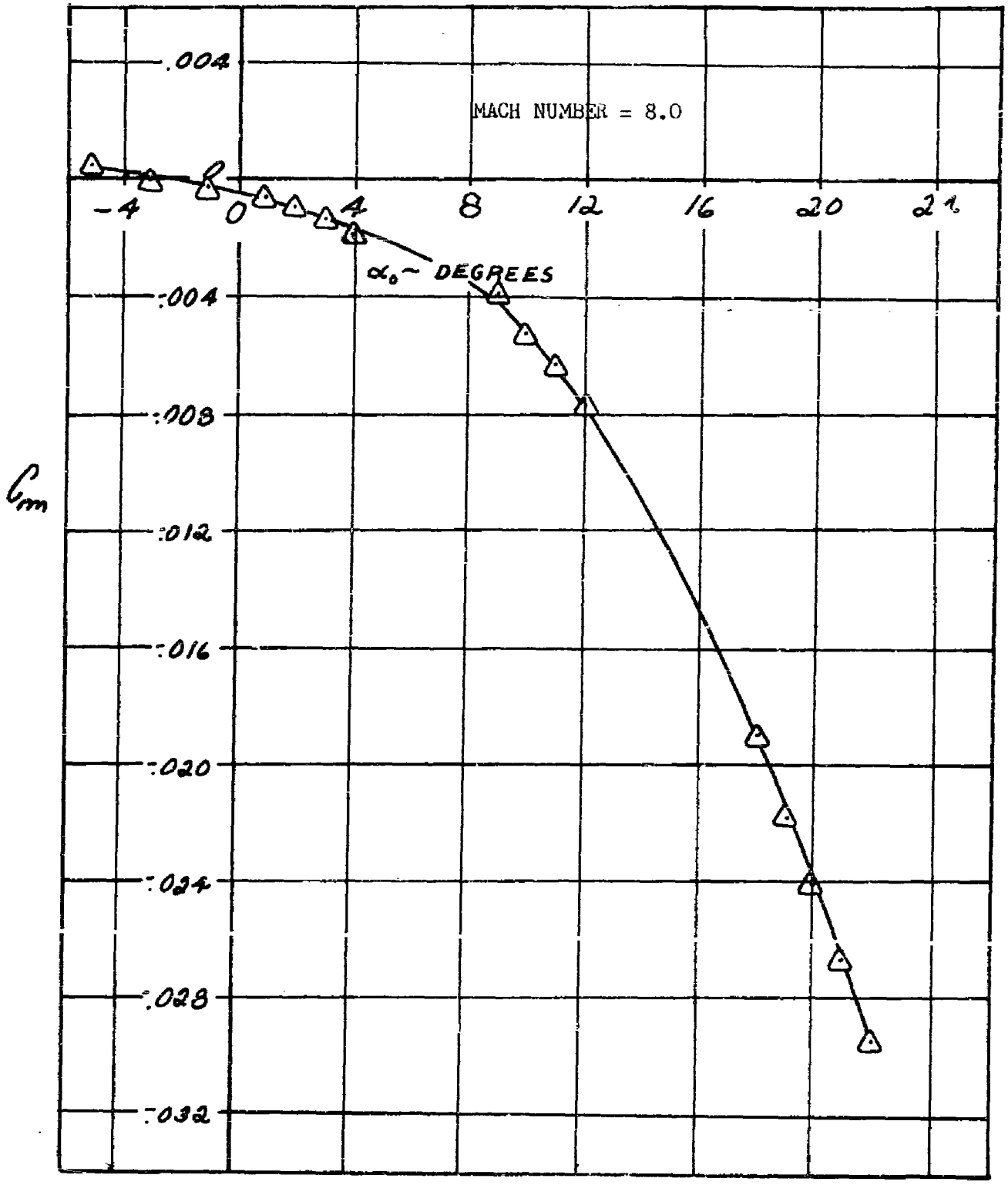

FIGURE 21 EXPERIMENTAL PITCHING MOMENT COEFFICIENT VS. ANGLE-OF-ATTACK; BASIC PLANFORM, t/c = .06, MACH NUMBER = 8.0

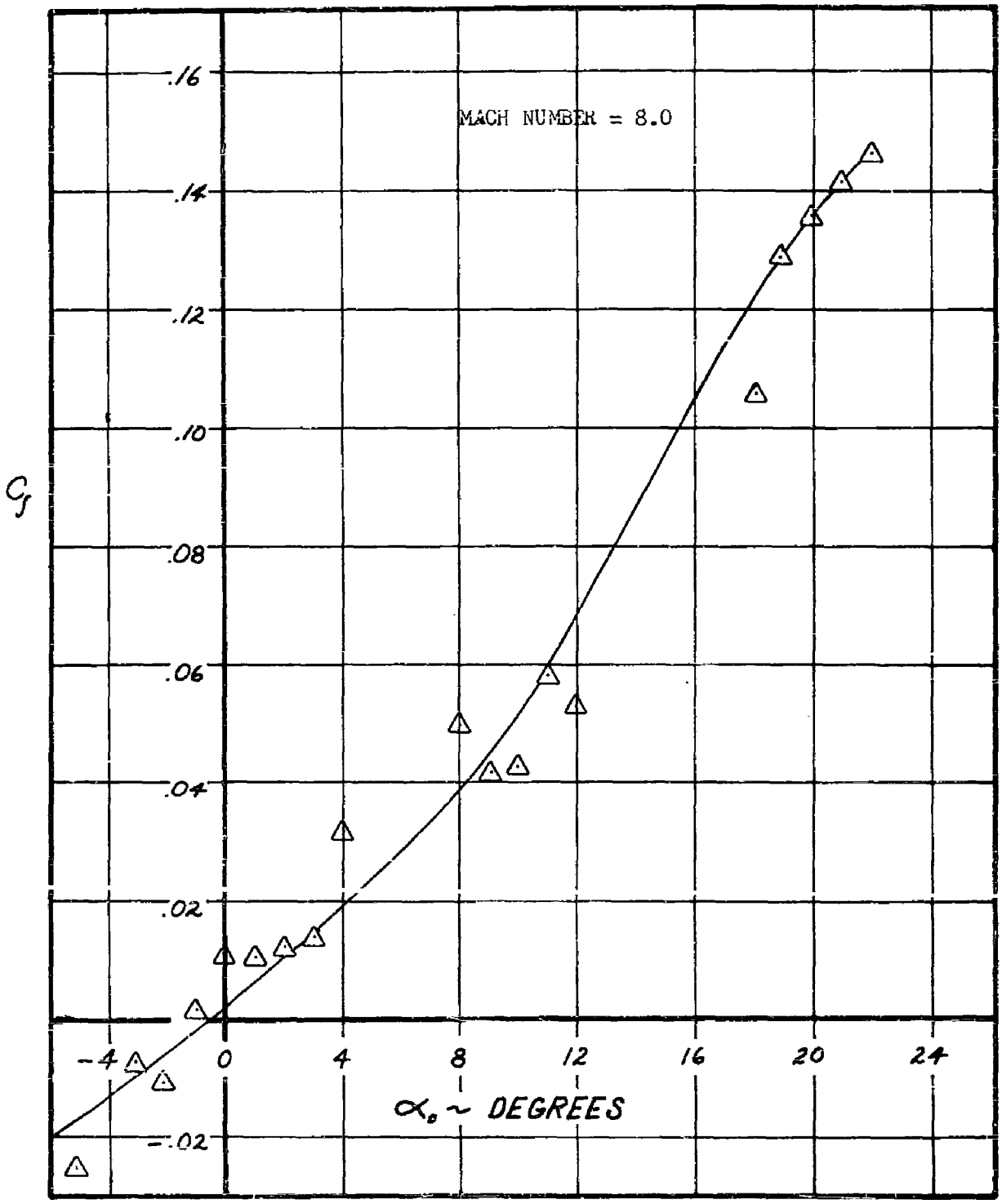

FIGURE 22 EXPERIMENTAL ROLLING MOMENT COEFFICIENT VS. ANGLE-OF-ATTACK; BASIC PLANFORM, t/c = .06, MACH NUMBER = 8.0

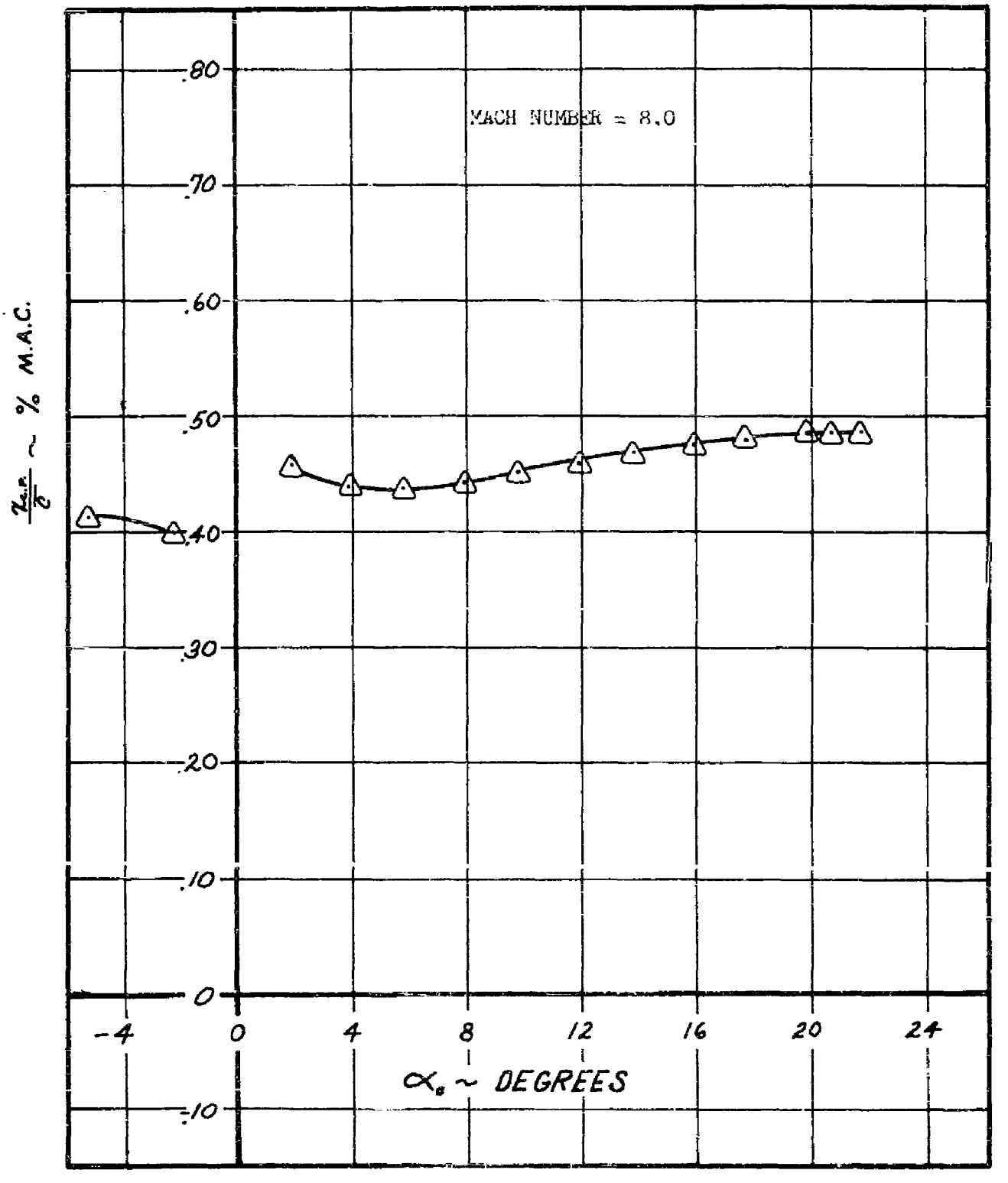

FIGURE 23 EXPERIMENTAL CHORDWISE CENTER-OF-PRESSURE VS. ANGLE-OF-ATTACK; BASIC PLANFORM, t/c = .06, MACH NUMBER = 8.0

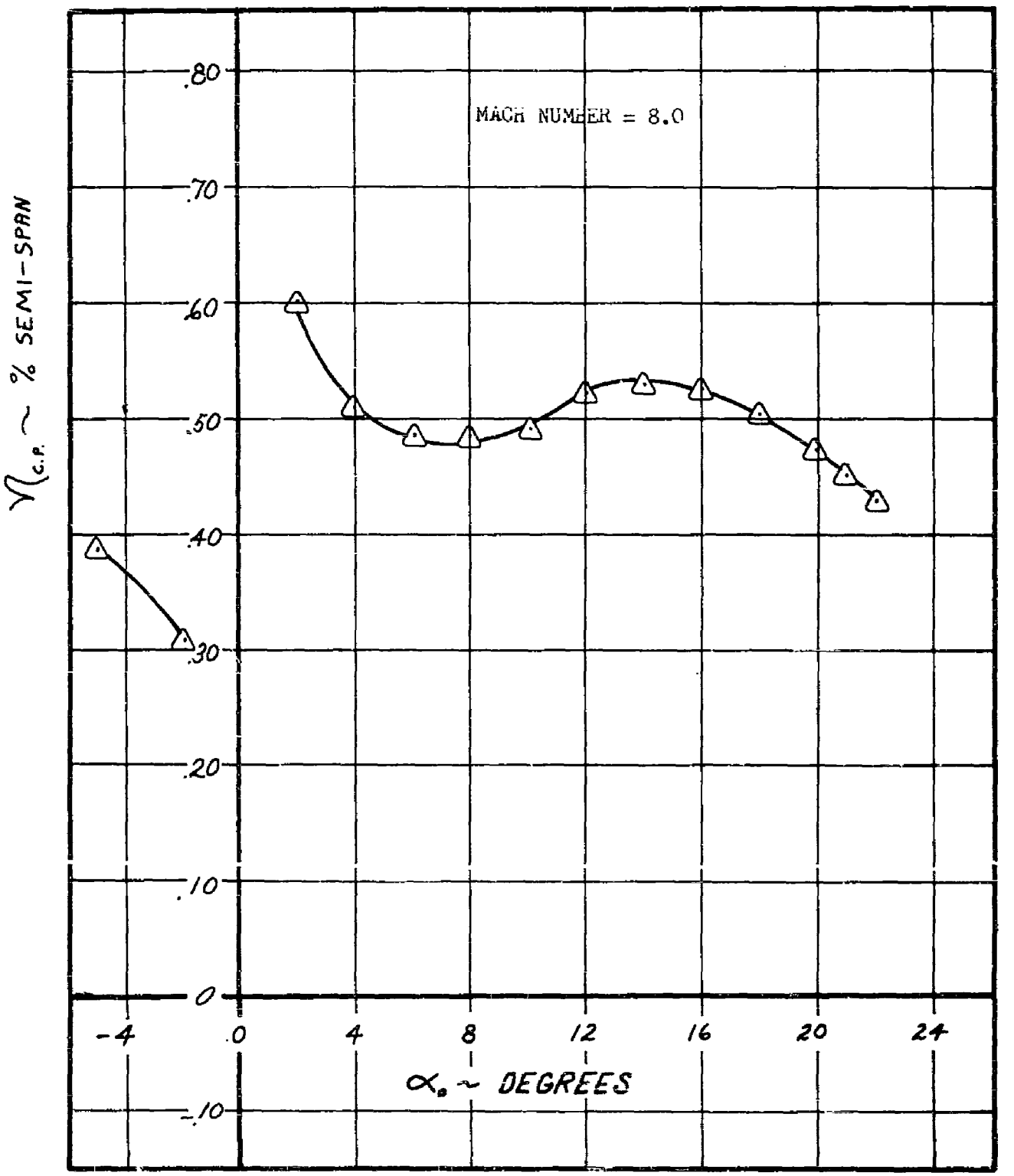

FIGURE 24 EXPERIMENTAL SPANWISE CENTER-OF-PRESSURE VS. ANGLE-OF-ATTACK: BASIC PLANFORM, t/c = .06, MACH NUMBER = 8.0

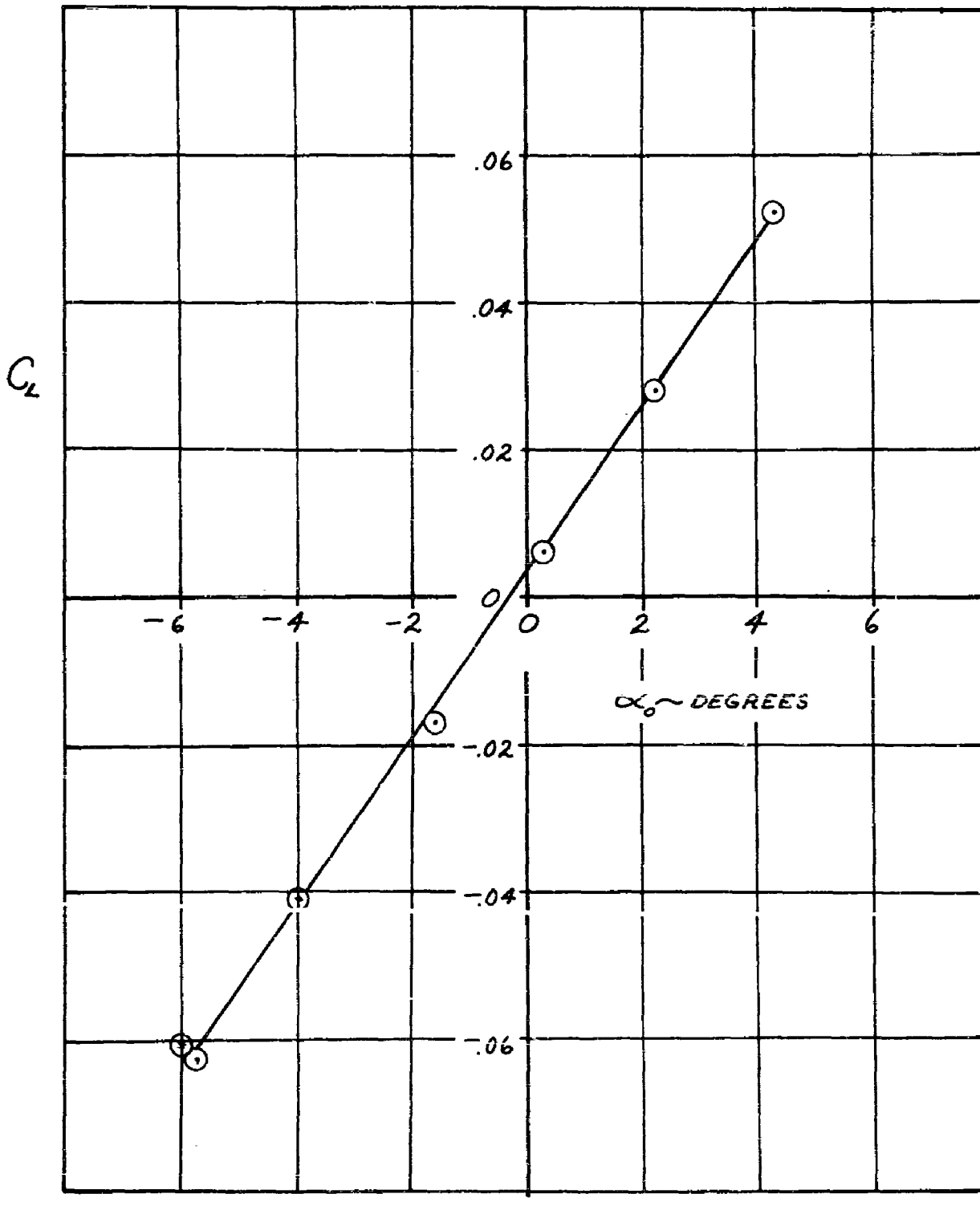

FIGURE 25 EXPERIMENTAL LIFT COEFFICIENT VS. ANGLE-OF-ATTACK; BASIC PLANFORM, t/c = .03, MACH NUMBER = 6.0

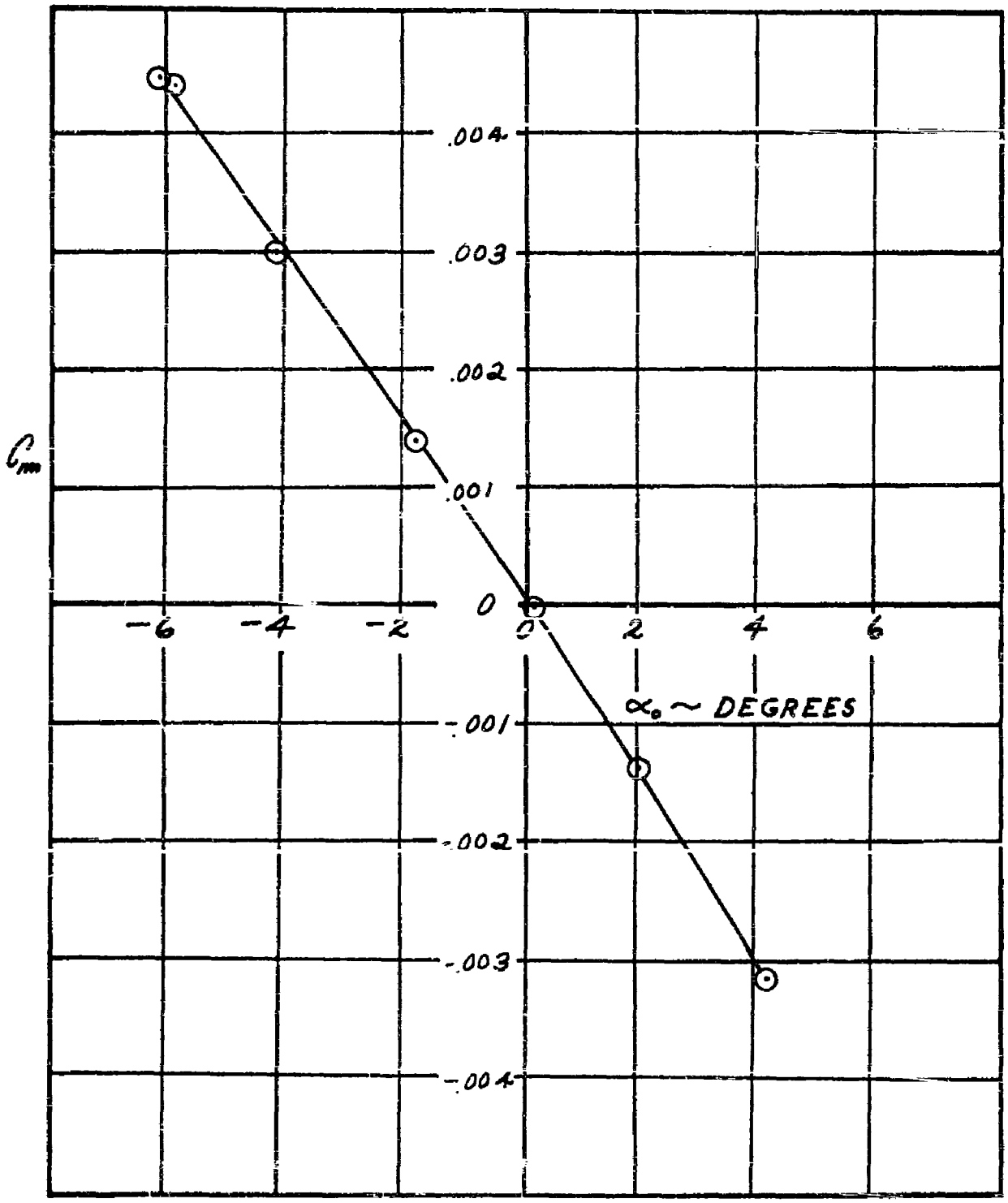

FIGURE 26 EXPERIMENTAL PITCHING MOMENT COEFFICIENT VS. ANGLE-OF-ATTACK; BASIC PLANFORM, t/c = .03, MACH NUMBER = 6.0

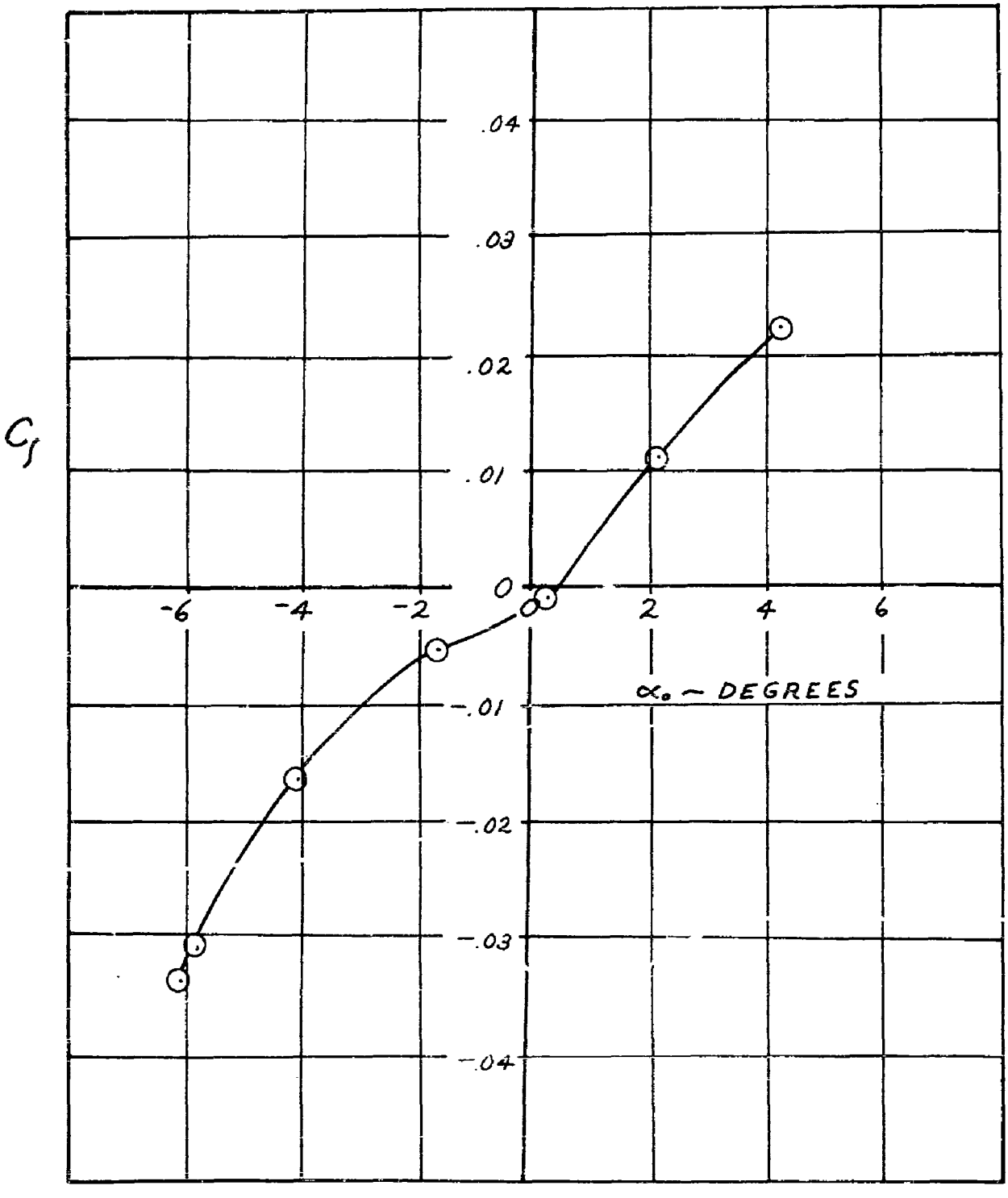

FIGURE 27 EXPERIMENTAL ROLLING MOMENT COEFFICIENT VS. ANGLE-OF-ATTACK; BASIC PLANFORM, t/c = .03, MACH NUMBER = 6.0

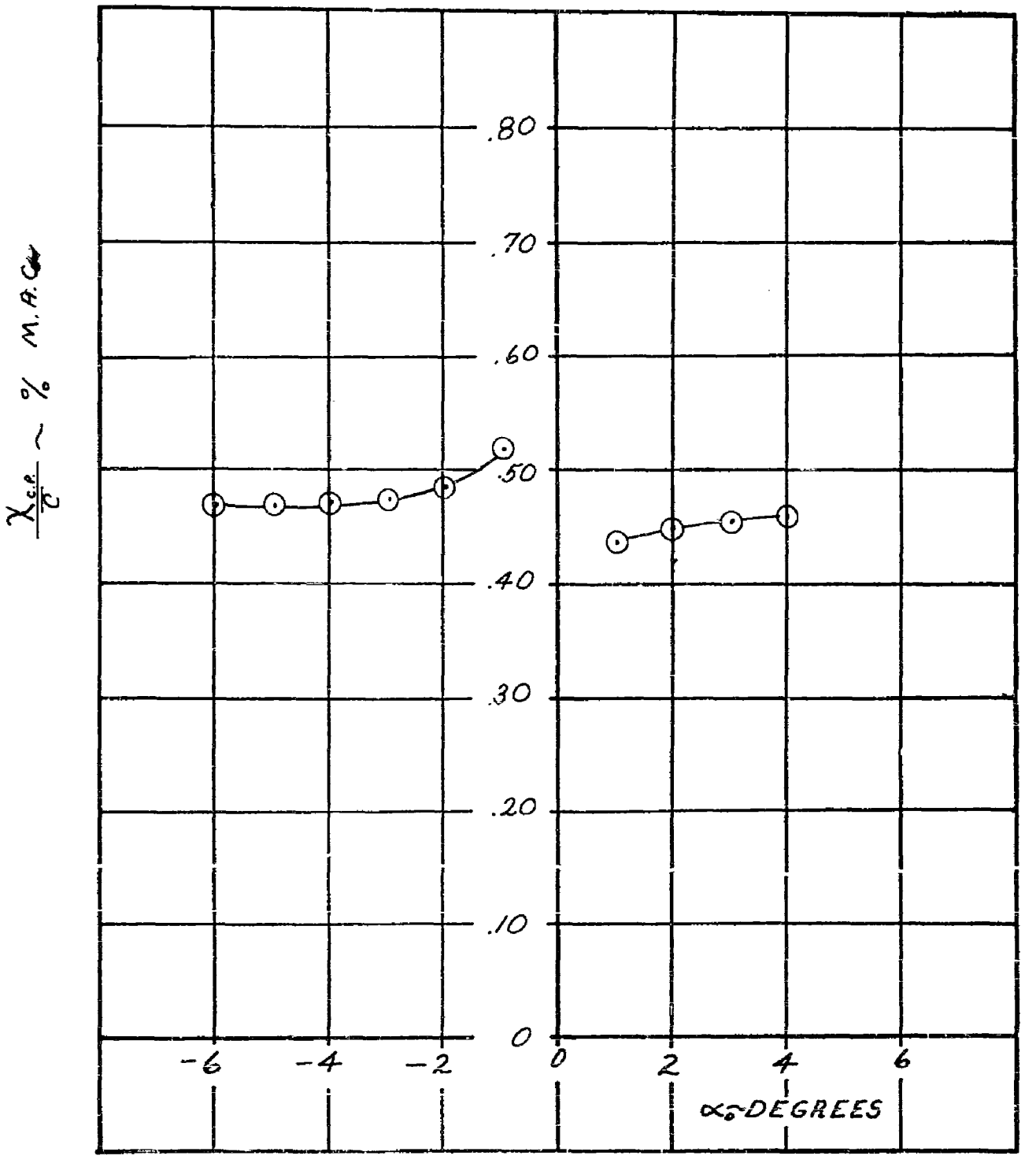

FIGURE 28 EXPERIMENTAL CHORDWISE CENTER-OF-PRESSURE VS. ANGLE-OF-ATTACK; BASIC PLANFORM, t/c = .03, MACH NUMBER = 6.0

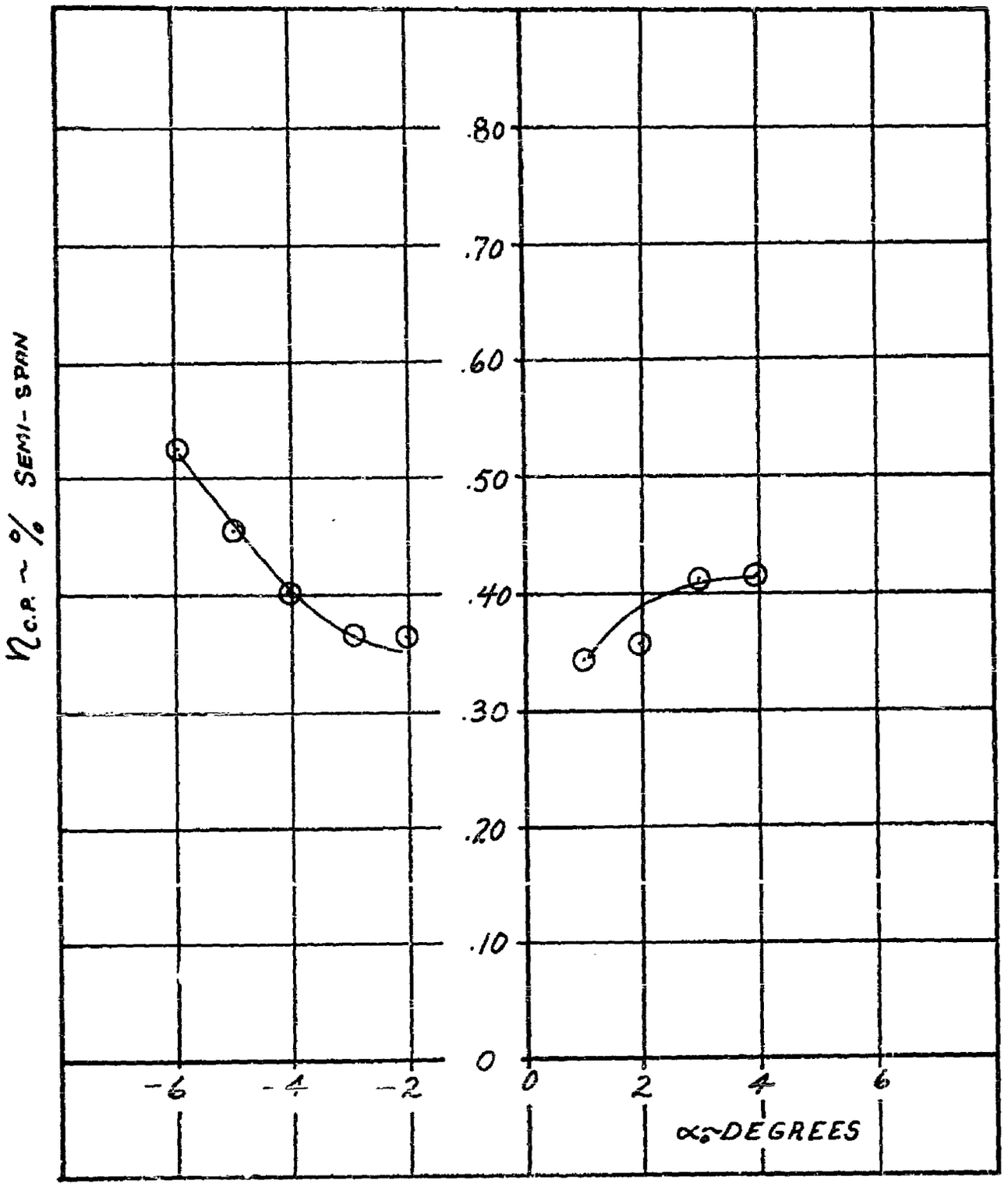

FIGURE 29 EXPERIMENTAL SPANWISE CENTER-OF-PRESSURE VS. ANGLE-OF-ATTACK; BASIC PLANFORM, t/c = .03, MACH NUMBER = 6.0

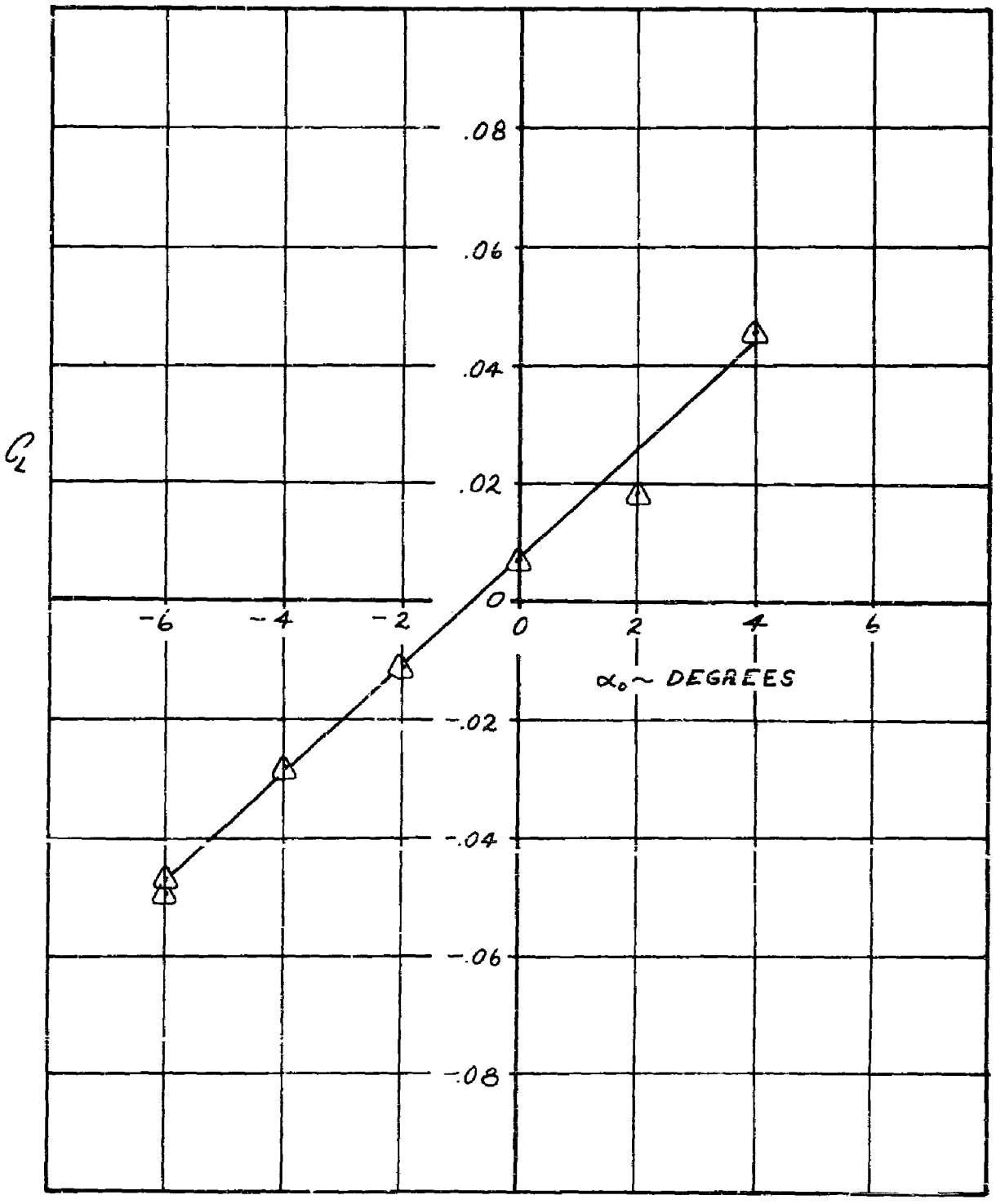

FIGURE 30 EXPERIMENTAL LIFT COEFFICIENT VS. ANGLE-OF-ATTACK; BASIC PLANFORM, t/c = .03, MACH NUMBER = 8.0

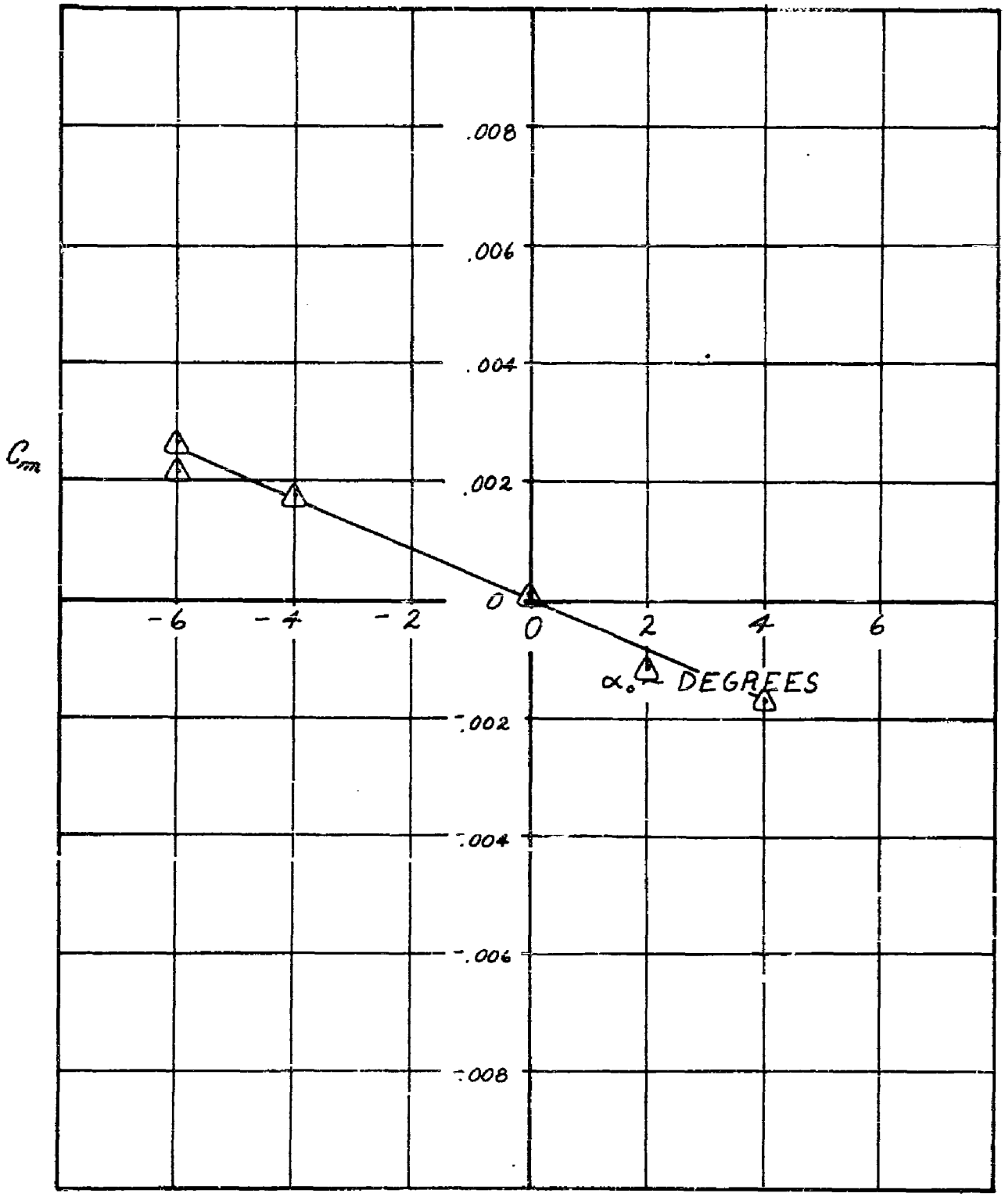

FIGURE 31 EXPERIMENTAL PITCHING MOMENT COEFFICIENT VS. ANGLE-OF-ATTACK; BASIC PLANFORM, t/c = .03, MACH NUMBER = 8.0

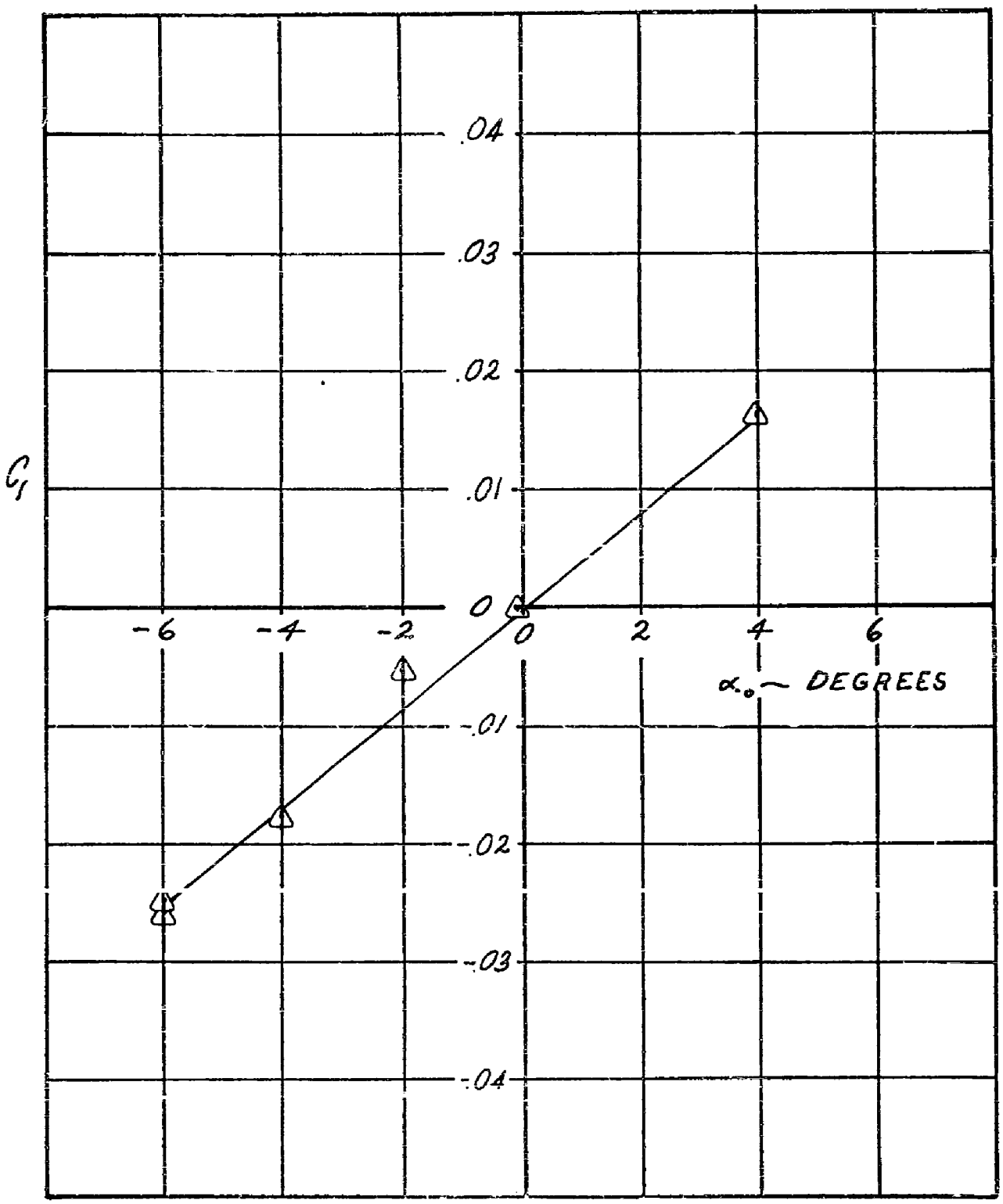

FIGURE 32 EXPERIMENTAL ROLLING MOMENT COEFFICIENT VS. ANGLE-OF-ATTACK; BASIC PLANFORM, t/c = .03, MACH NUMBER = 8.0

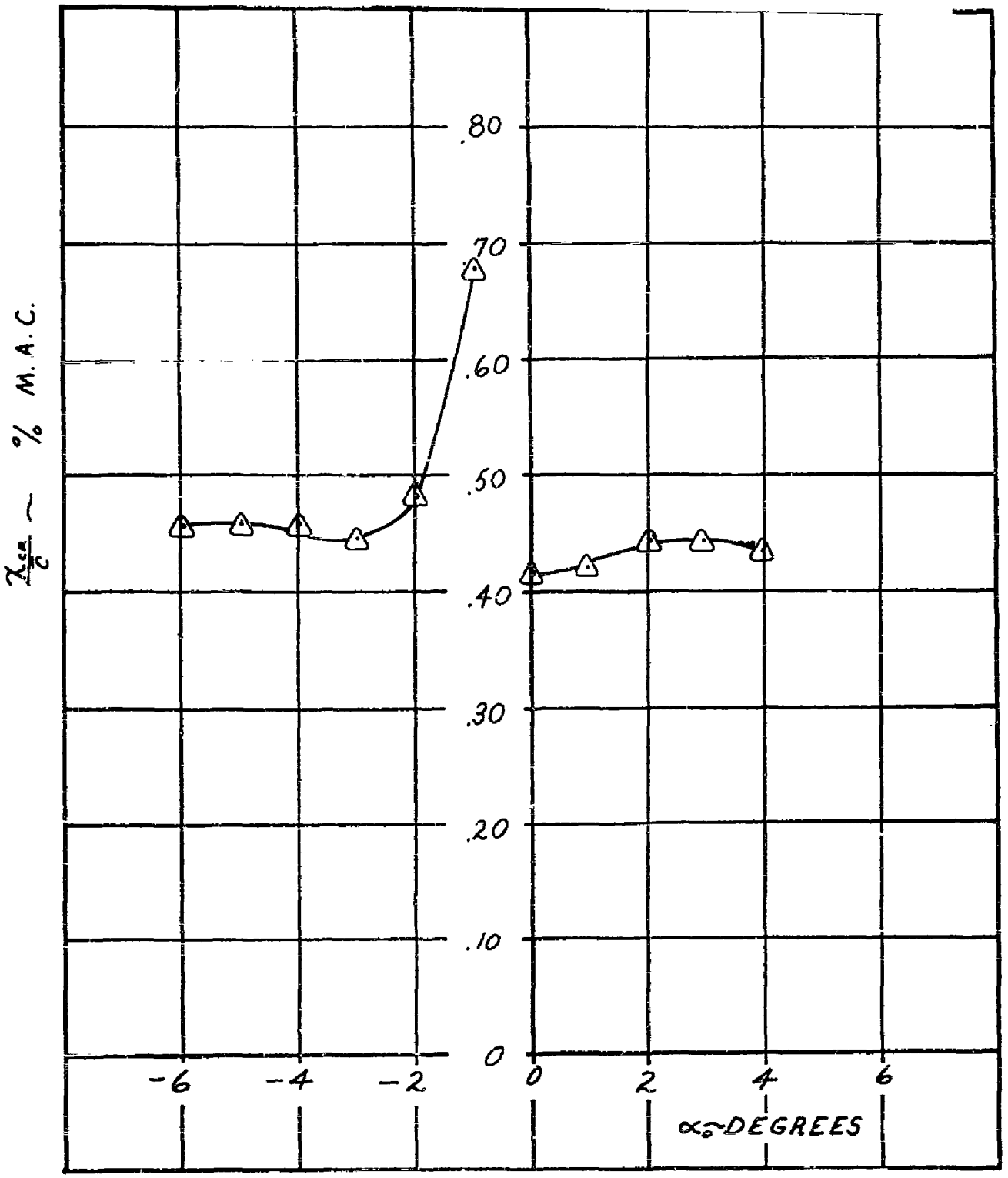

FIGURE 33 EXPERIMENTAL CHORDWISE CENTER-OF-PRESSURE VS. ANGLE-OF-ATTACK; BASIC PLANFORM, t/c = .03, MACH NUMBER = 8.0

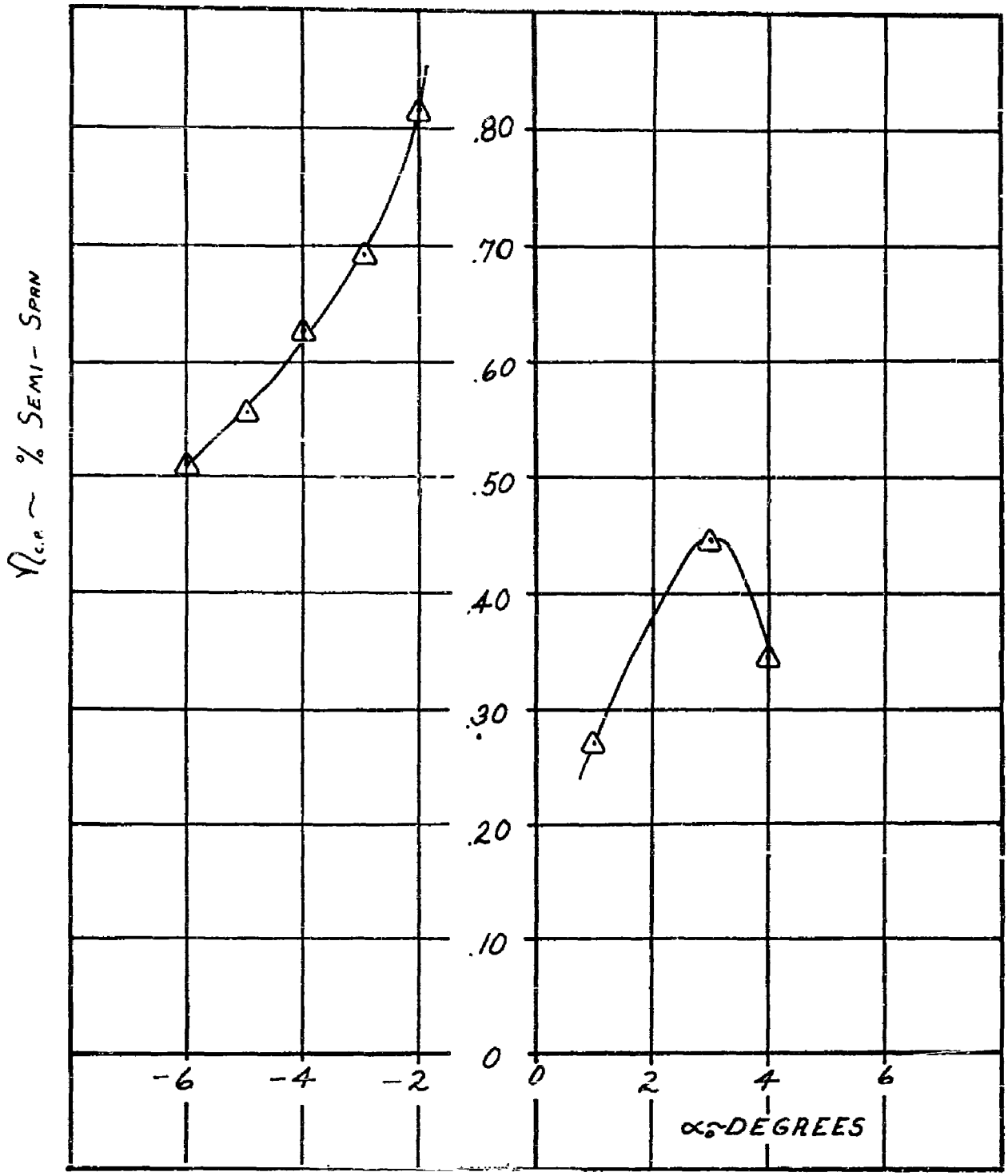

FIGURE 34 EXPERIMENTAL SPANWISE CENTER-OF-PRESSURE VS. ANGLE-OF-ATTACK; BASIC PLANFORM, t/c = .03, MACH NUMBER = 8.0

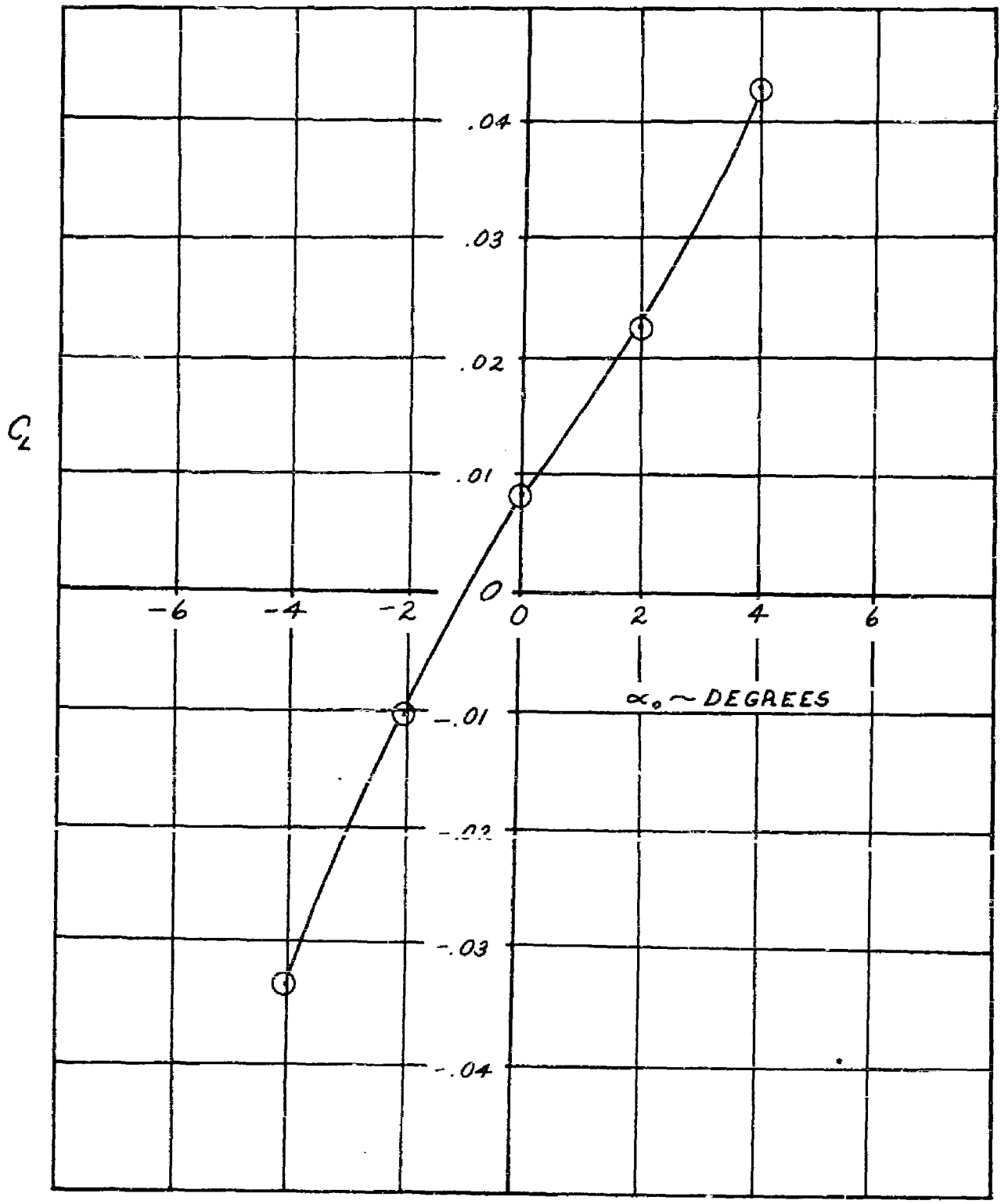

FIGURE 35 EXPERIMENTAL LIFT COEFFICIENT VS. ANGLE-OF-ATTACK; BASIC PLANFORM, t/c = .09, MACH NUMBER = 6.0

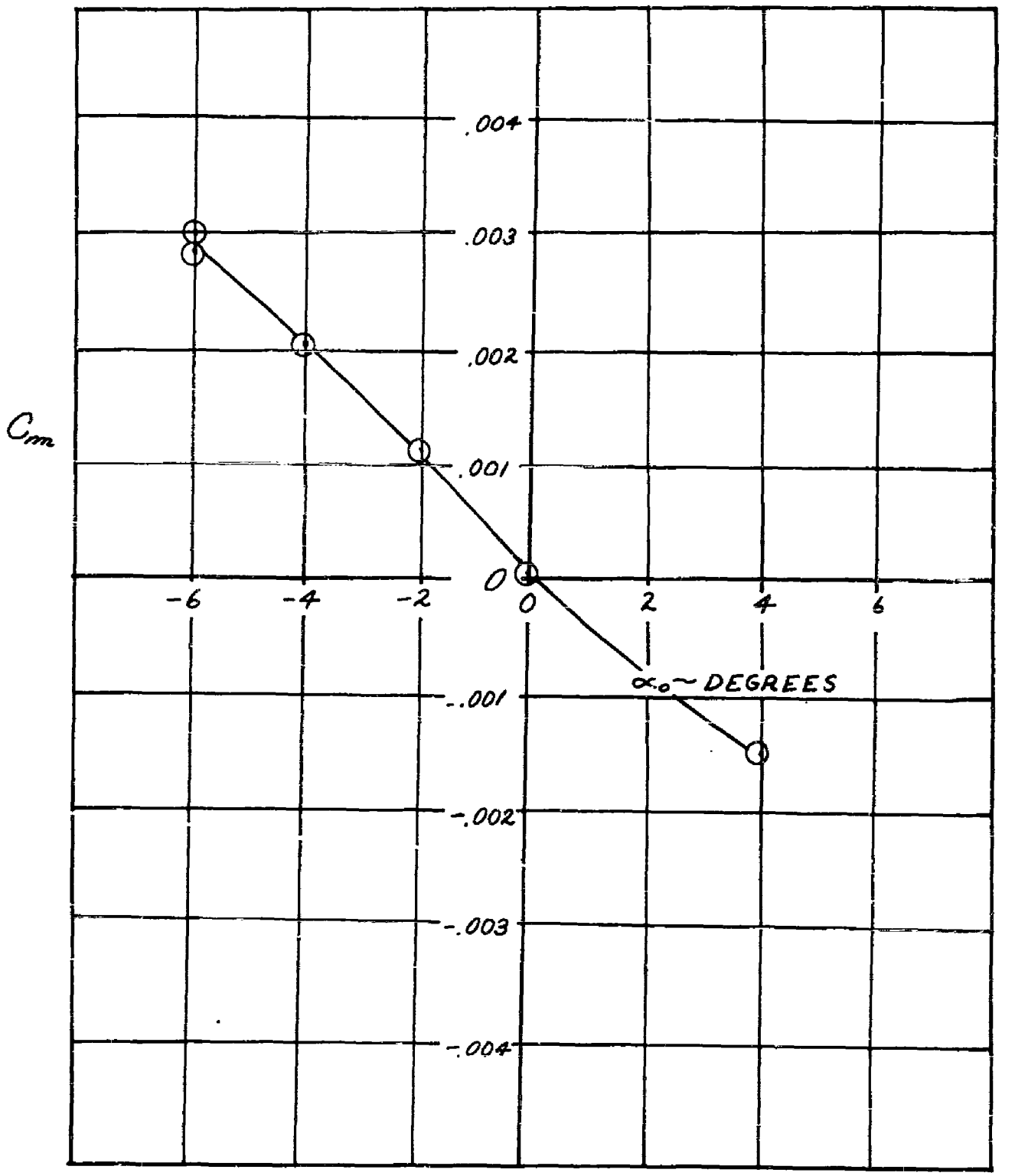

FIGURE 36 EXPERIMENTAL PITCHING MOMENT COEFFICIENT VS. ANGLE-OF-ATTACK; BASIC PLANFORM, t/c = .09, MACH NUMBER = 6.0

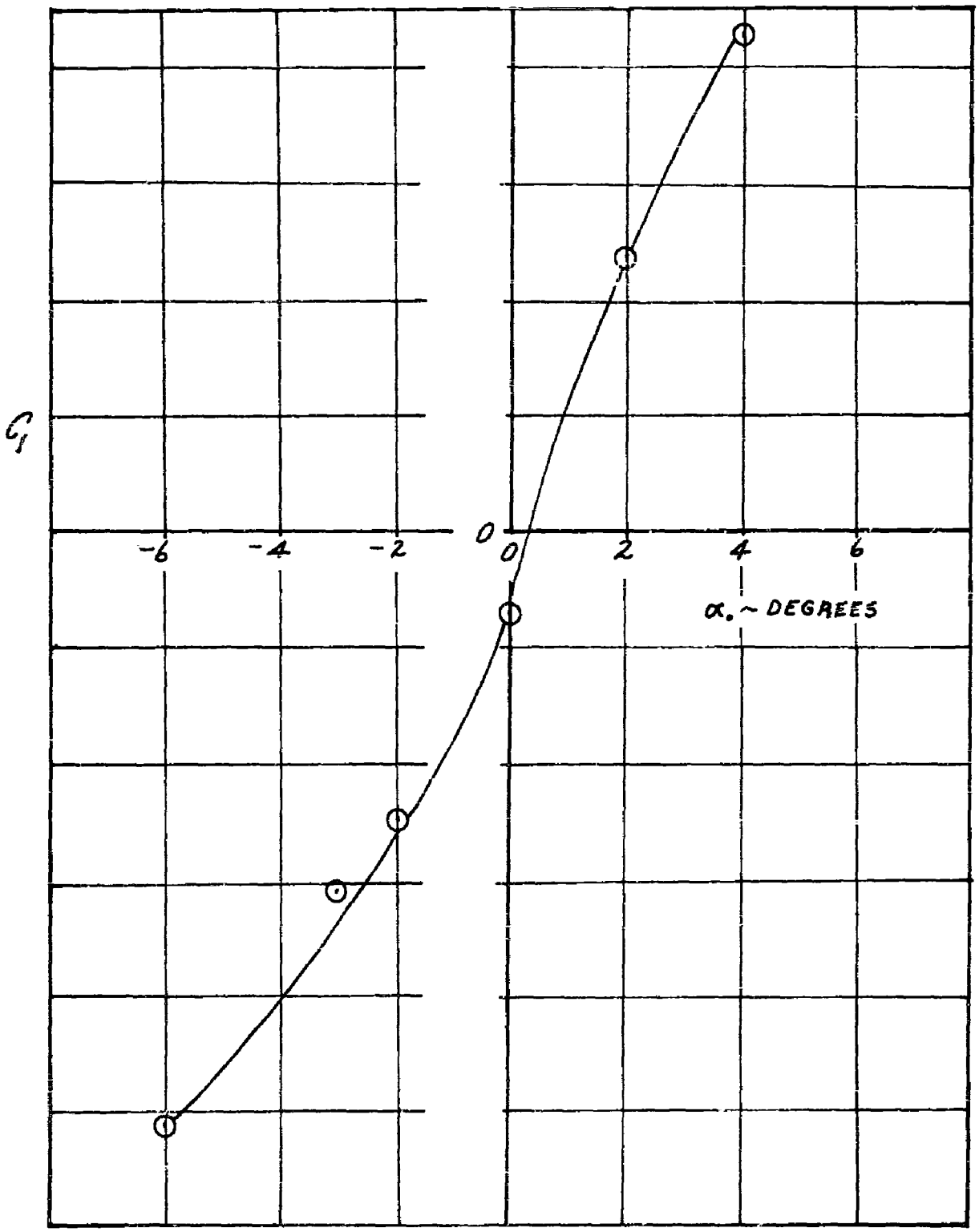

FIGURE 37 EXPERIMENTAL ROLLING MOMENT COEFFICIENT VS. ANGLE-OF-ATTACK; BASIC PLANFORM, t/c = .09, MACH NUMBER = 6.0

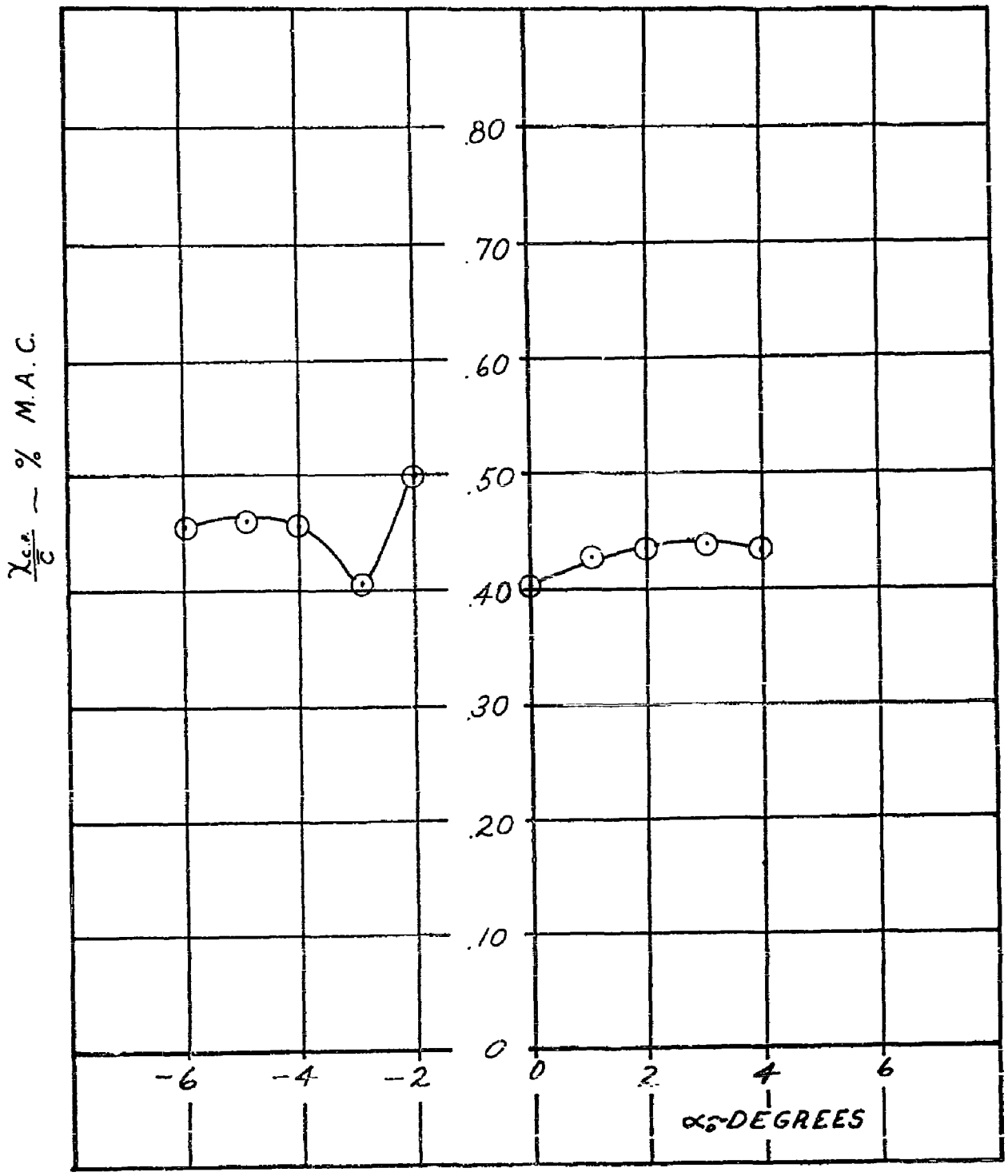

FIGURE 38 EXPERIMENTAL CHORDWISE CENTER-OF-PRESSURE VS. ANGLE-OF-ATTACK; BASIC PLANFORM, t/c = .09, MACH NUMBER = 6.0

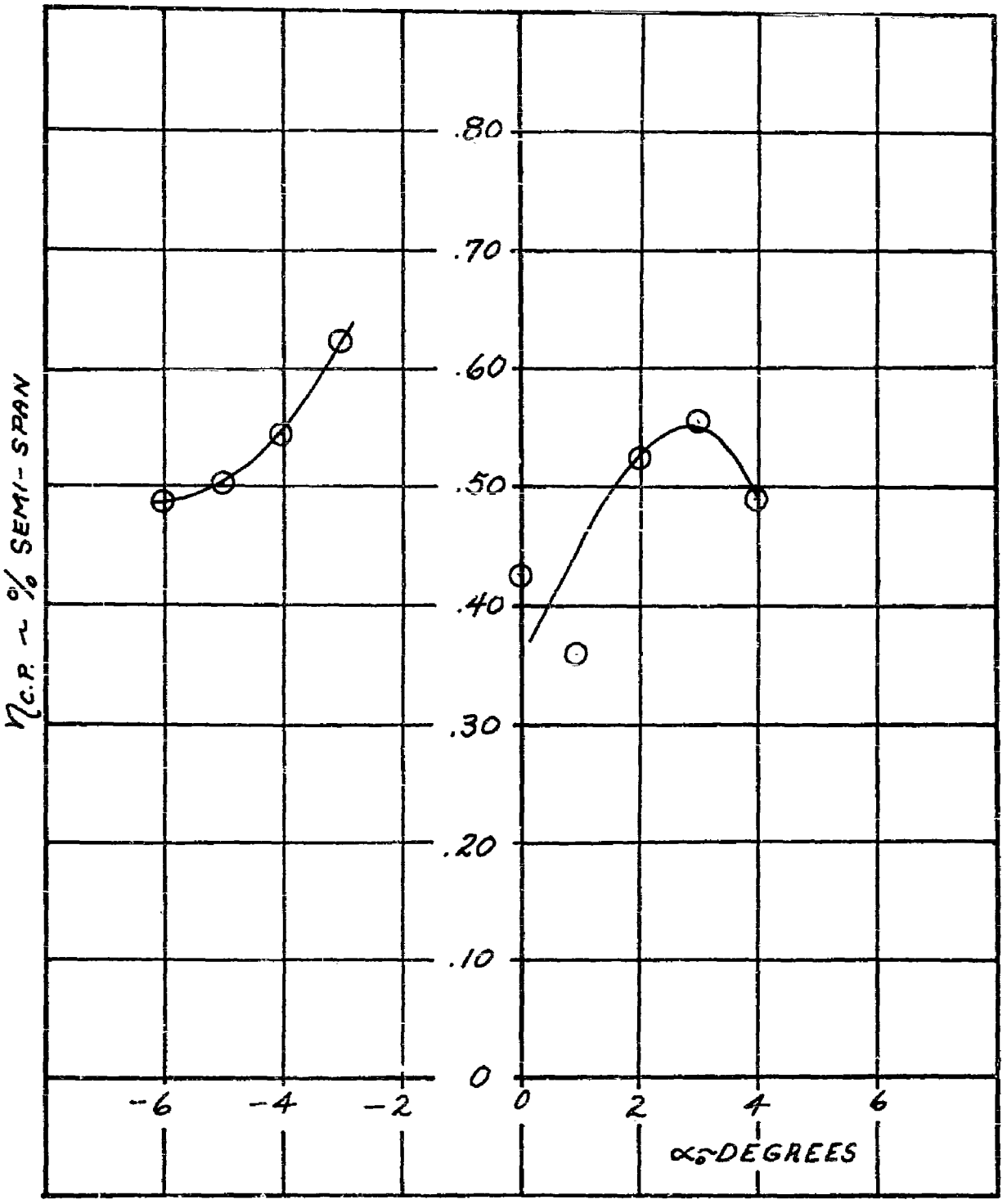

FIGURE 39 EXPERIMENTAL SPANWISE CENTER-OF-PRESSURE VS. ANGLE-OF-ATTACK; BASIC PLANFORM, t/c = .09, MACH NUMBER = 6.0

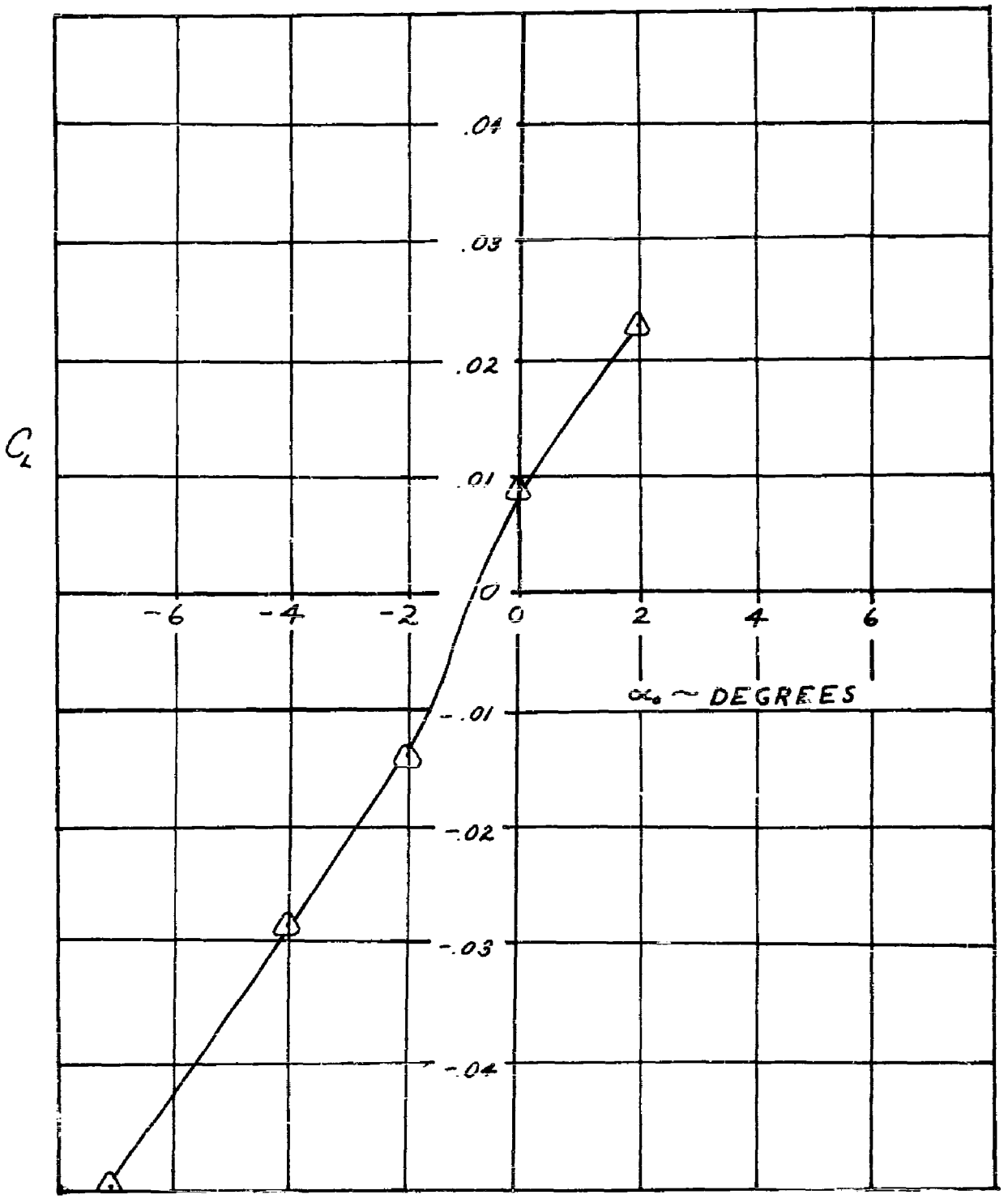

FIGURE 40 EXPERIMENTAL LIFT COEFFICIENT VS. ANGLE-OF-ATTACK; BASIC PLANFORM, t/c = .09, MACH NUMBER = 8.0

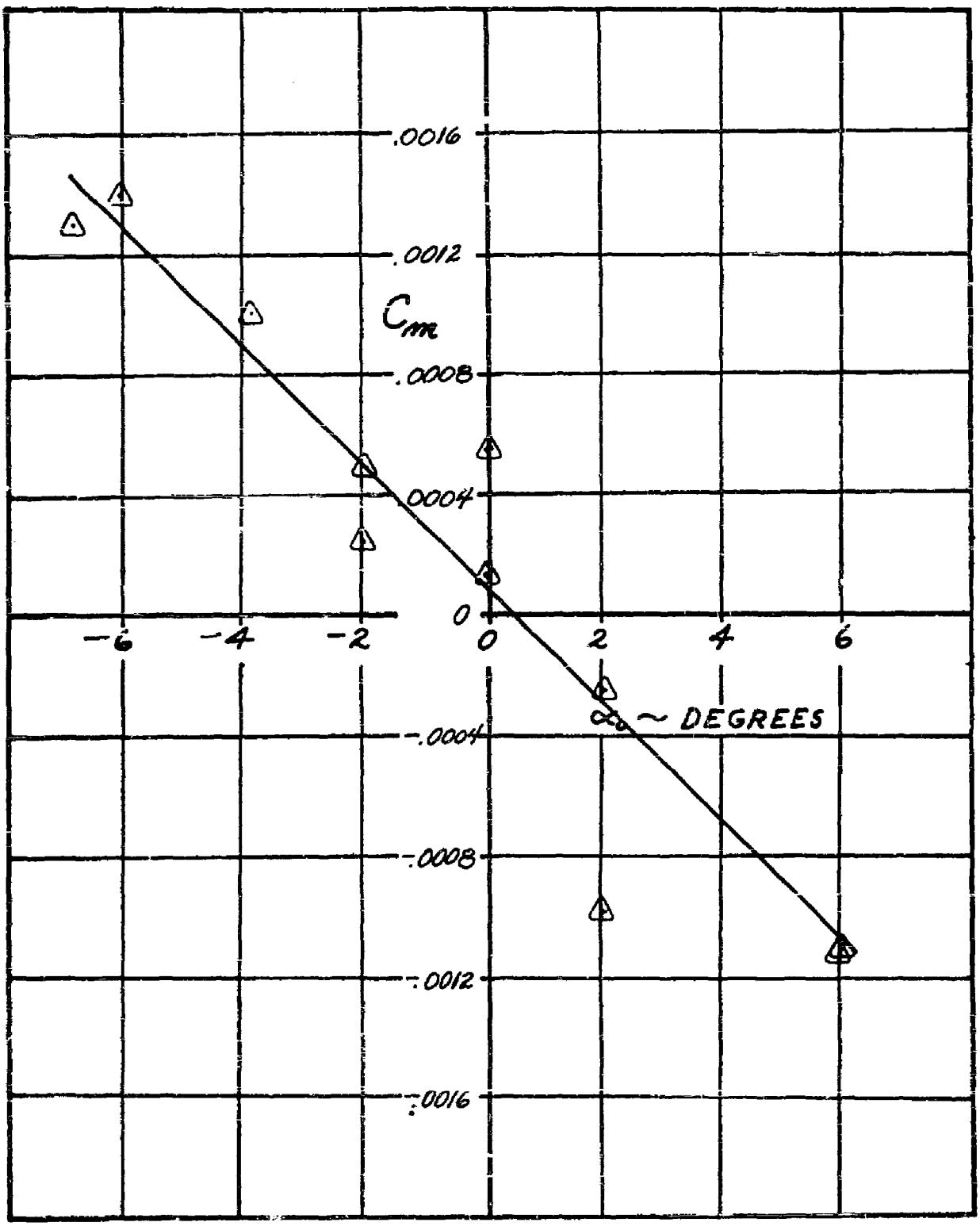

FIGURE 41 EXPERIMENTAL PITCHING MOMENT COEFFICIENT VS. ANGLE-OF-ATTACK; BASIC PLANFORM, t/c = .09, MACH NUMBER = 8.0

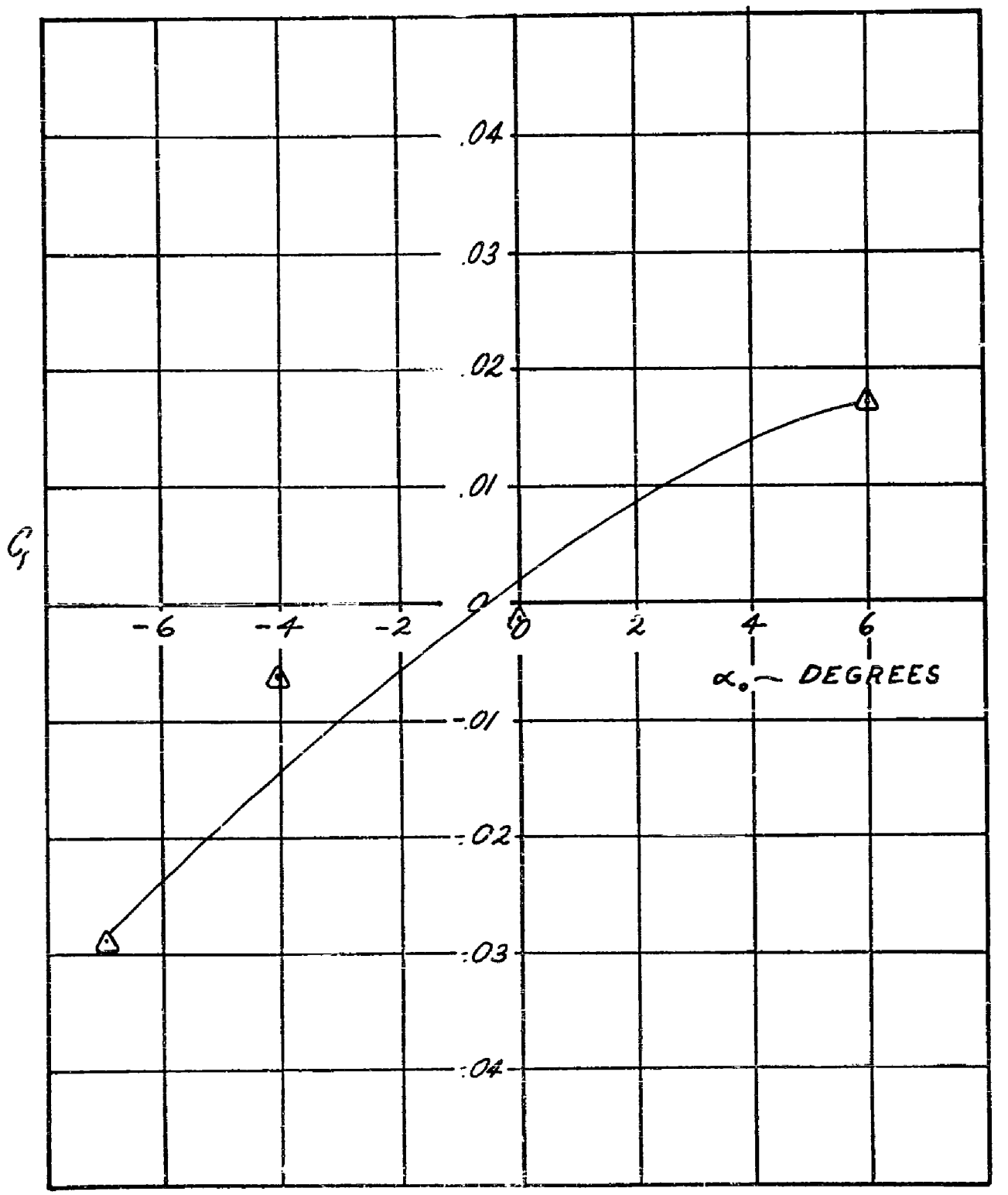

FIGURE 42 EXPERIMENTAL ROLLING MOMENT COEFFICIENT VS. ANGLE-OF-ATTACK; BASIC PLANFORM, t/c = .09, MACH NUMBER = 8.0

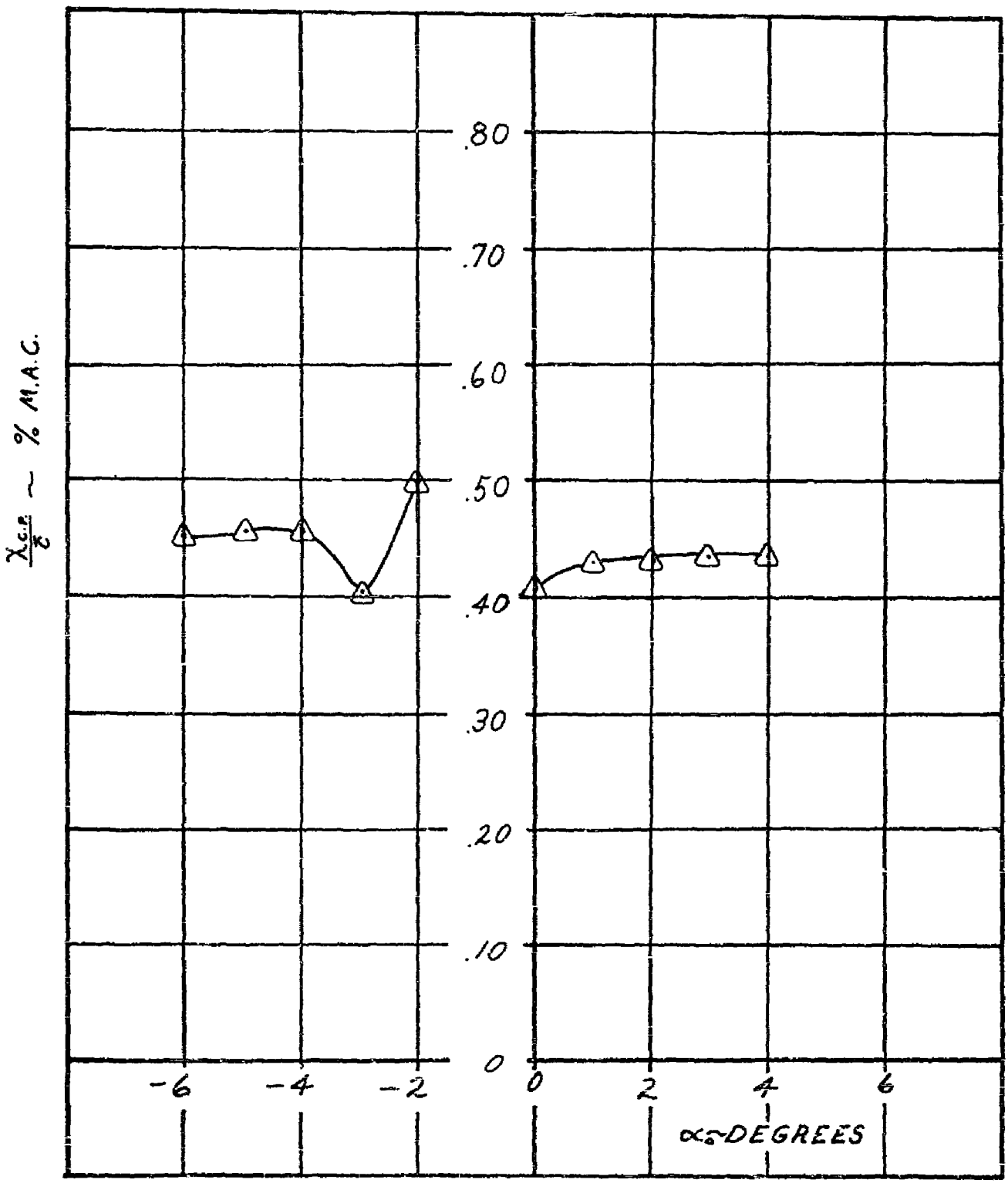

FIGURE 43 EXPERIMENTAL CHORDWISE CENTER-OF-PRESSURE VS. ANGLE-OF-ATTACK; BASIC PLANFORM, t/c = .09, MACH NUMBER = 8.0

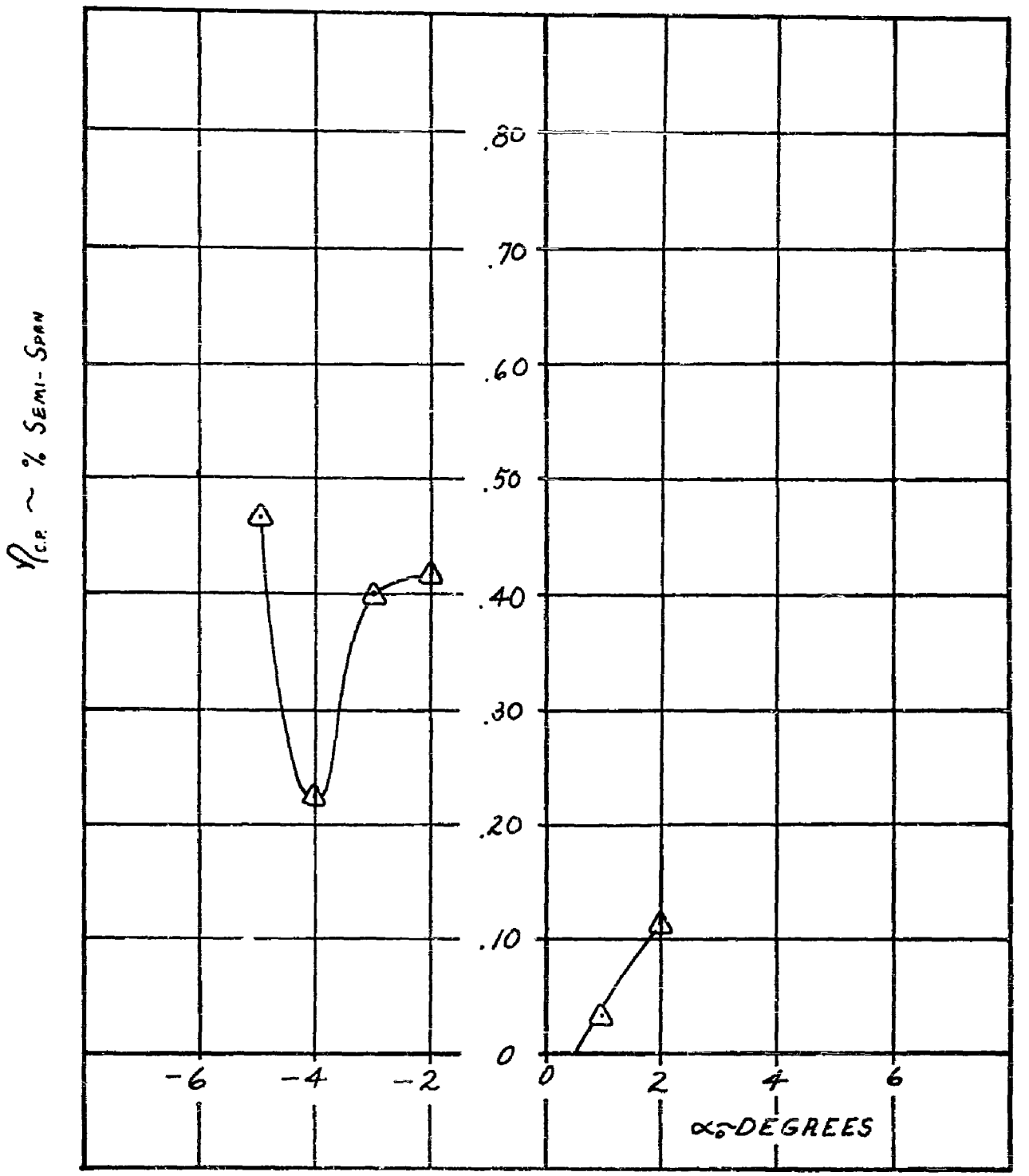

FIGURE 44 EXPERIMENTAL SPANWISE CENTER-OF-PRESSURE VS. ANGLE-OF-ATTACK; BASIC PLANFORM, t/c = .09, MACH NUMBER = 8.0

SUSPENSION
SYSTEM

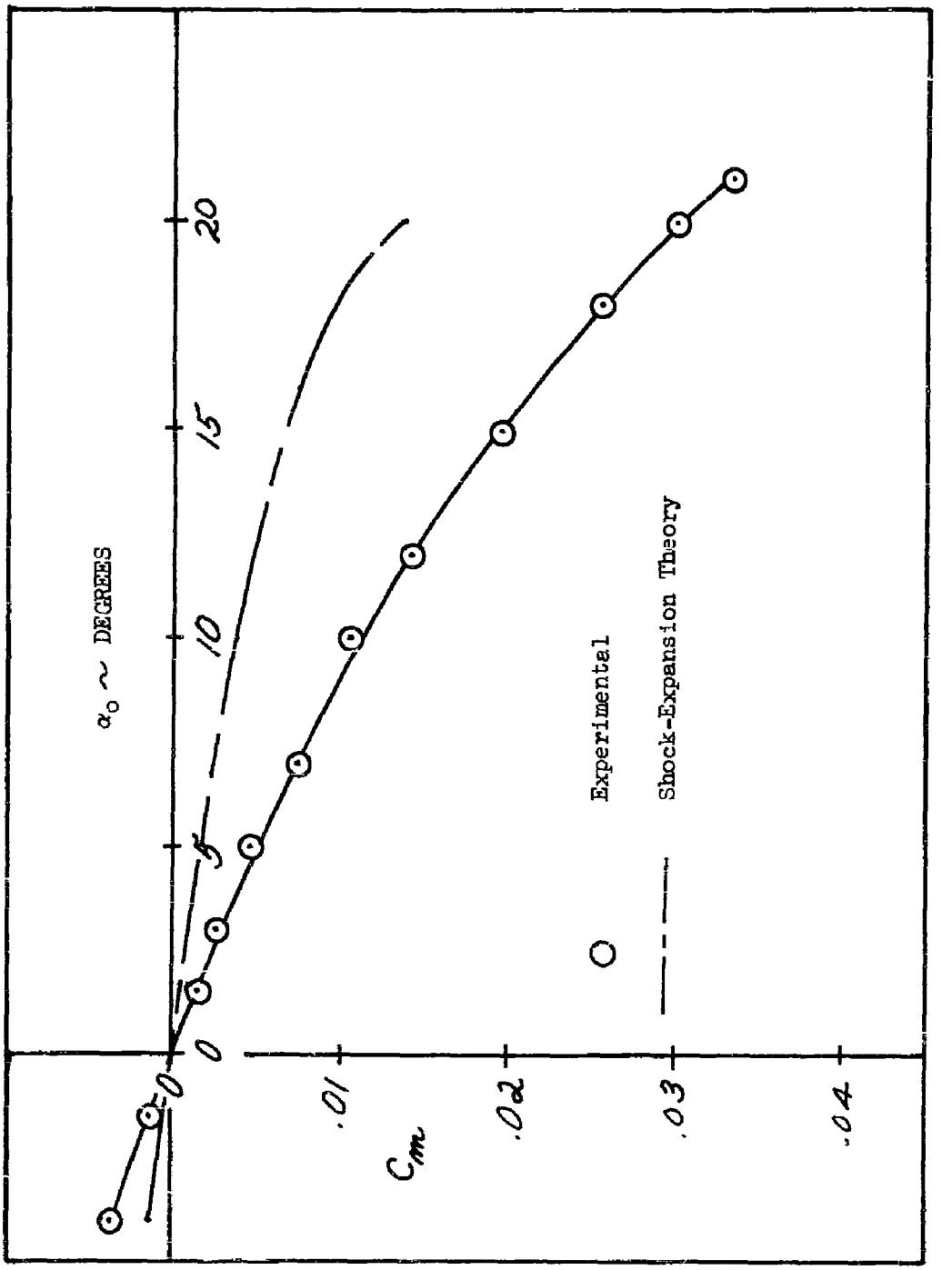

FIGURE 46. COMPARISON OF EXPERIMENTAL AND SHOCK EXPANSION PITCHING MOMENT COEFFICIENT VS. ANGLE-OF-ATTACK AT MACH NUMBER = 5.0; BASIC PLANFORM, t/c = .06

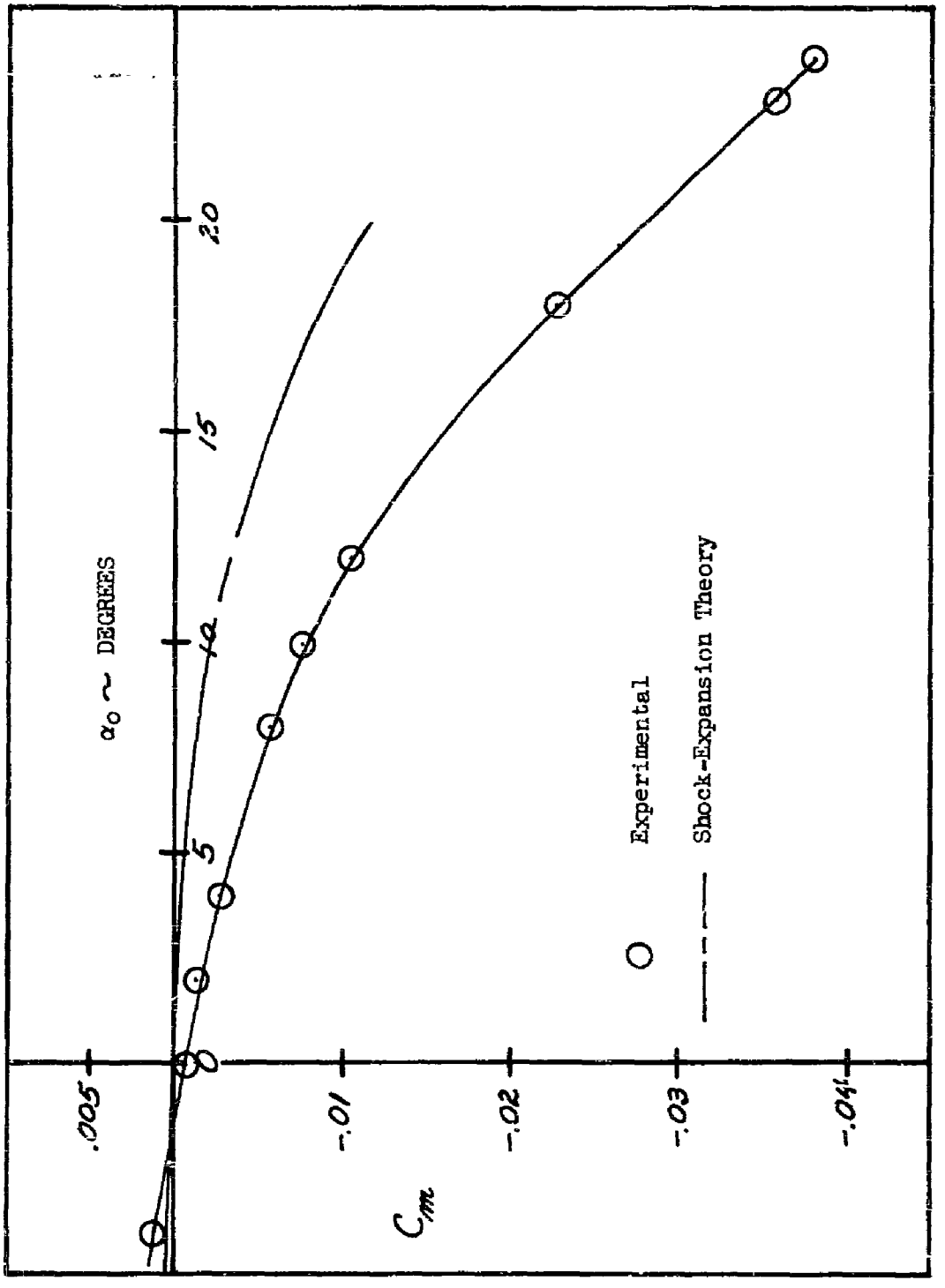

FIGURE 47 COMPARISON OF EXPERIMENTAL AND SHOCK EXPANSION PITCHING MOMENT COEFFICIENT VS. ANGLE-OF-ATTACK AT MACH NUMBER = 6.0; BASIC PLANFORM, t/c = .06

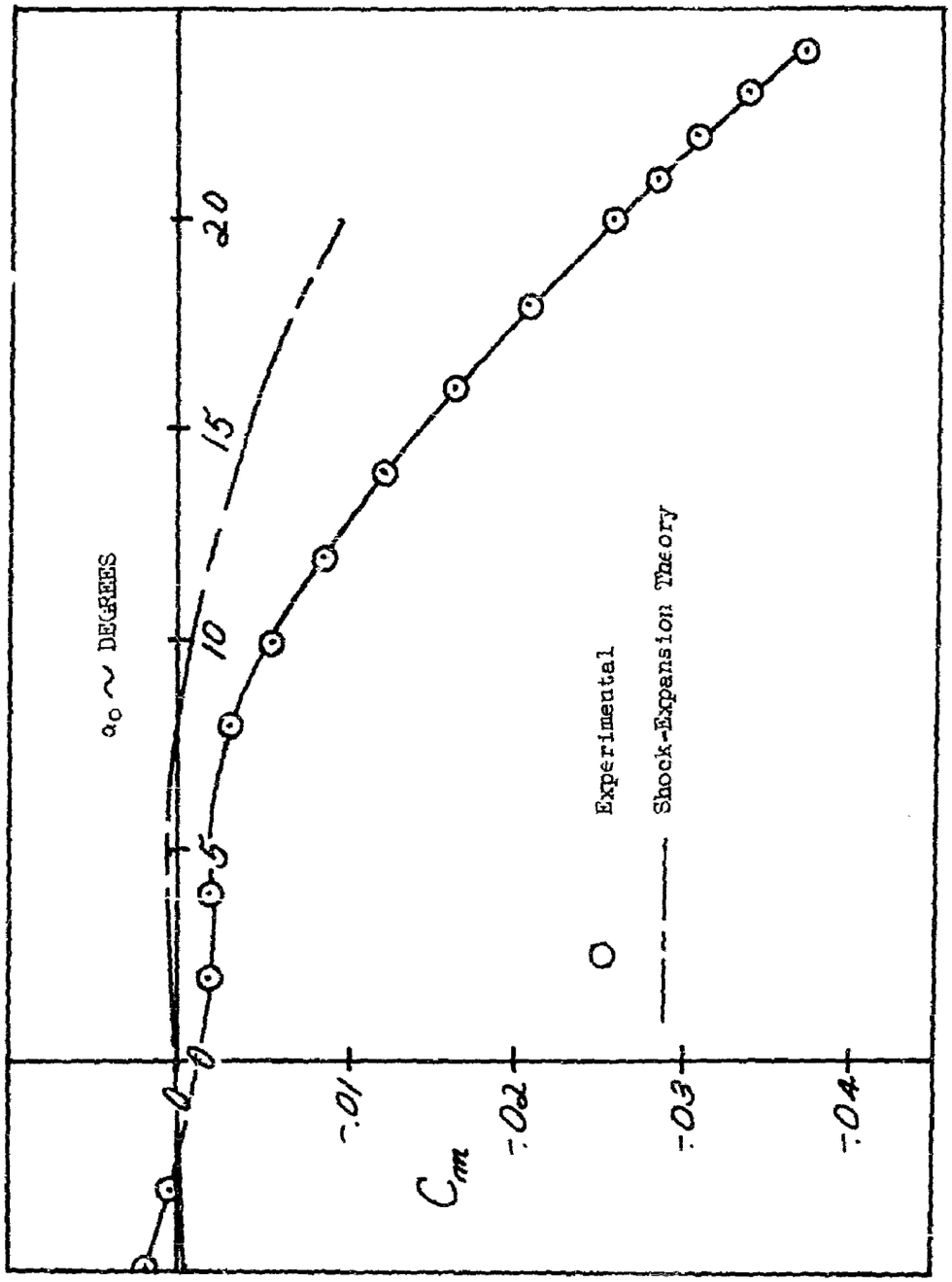

FIGURE 48 COMPARISON OF EXPERIMENTAL AND SHOCK EXPANSION PITCHING MOMENT COEFFICIENT VS. ANGLE-OF-ATTACK AT MACH NUMBER = 7.0; BASIC PLANFORM, t/c = .06

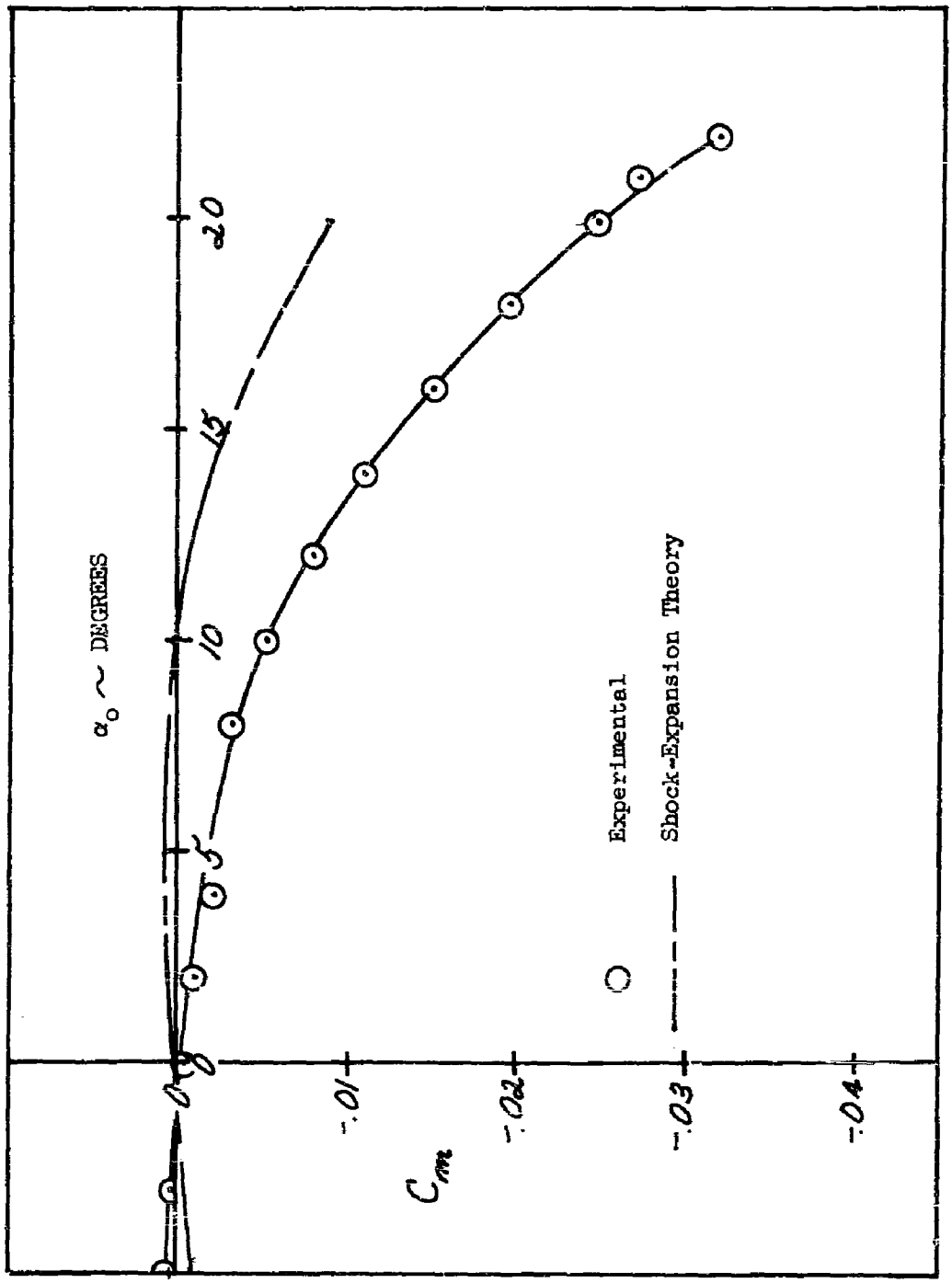

FIGURE 49 COMPARISON OF EXPERIMENTAL AND SHOCK EXPANSION PITCHING MOMENT COEFFICIENT VS. ANGLE-OF-ATTACK AT MACH NUMBER = 8.0; BASIC PLANFORM, t/c = .06

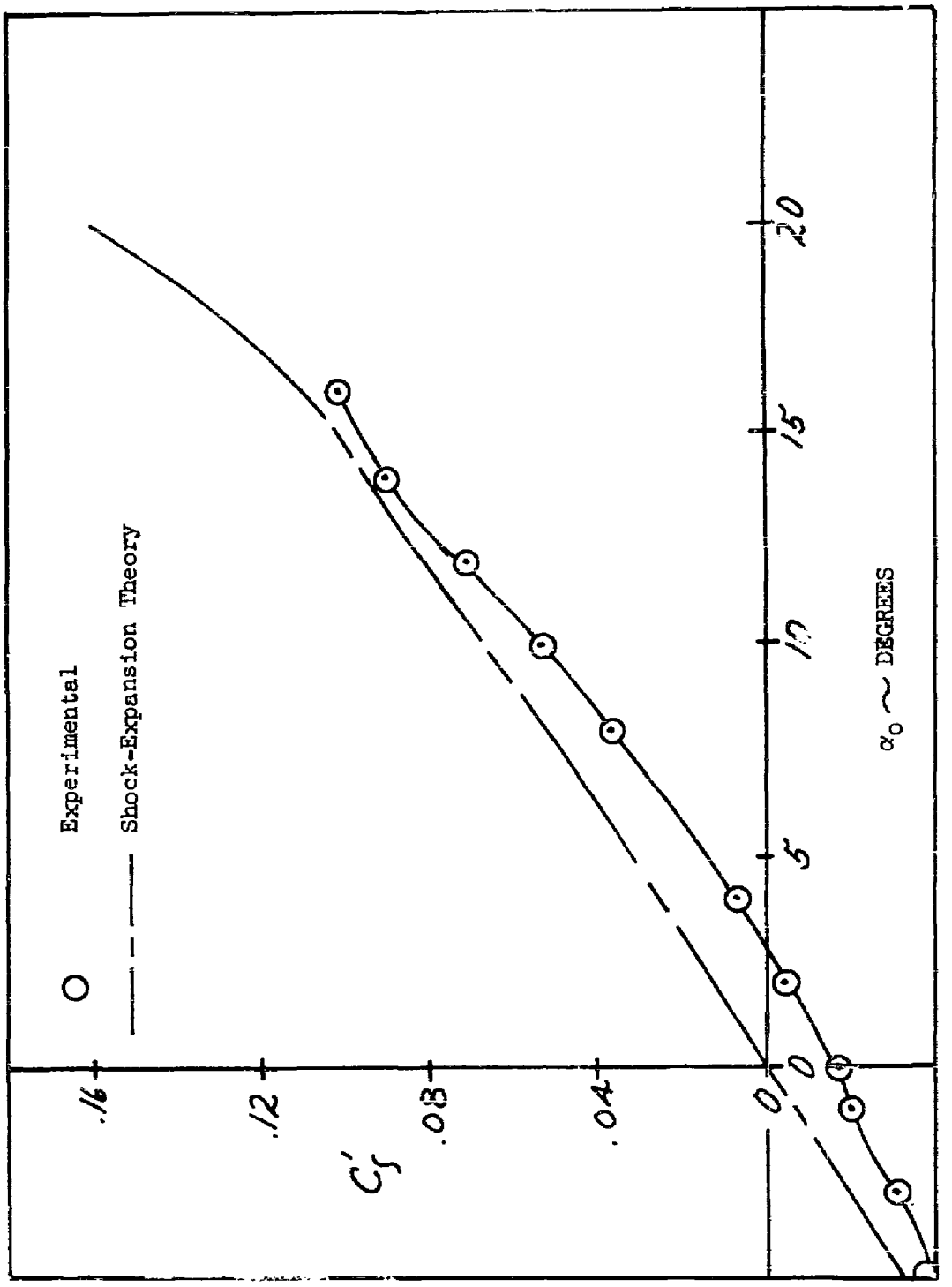

FIGURE 50 COMPARISON OF EXPERIMENTAL AND SHOCK EXPANSION ROLLING MOMENT COEFFICIENT VS. ANGLE-OF-ATTACK AT MACH NUMBER = 5.0; BASIC PLANFORM, t/c = .06

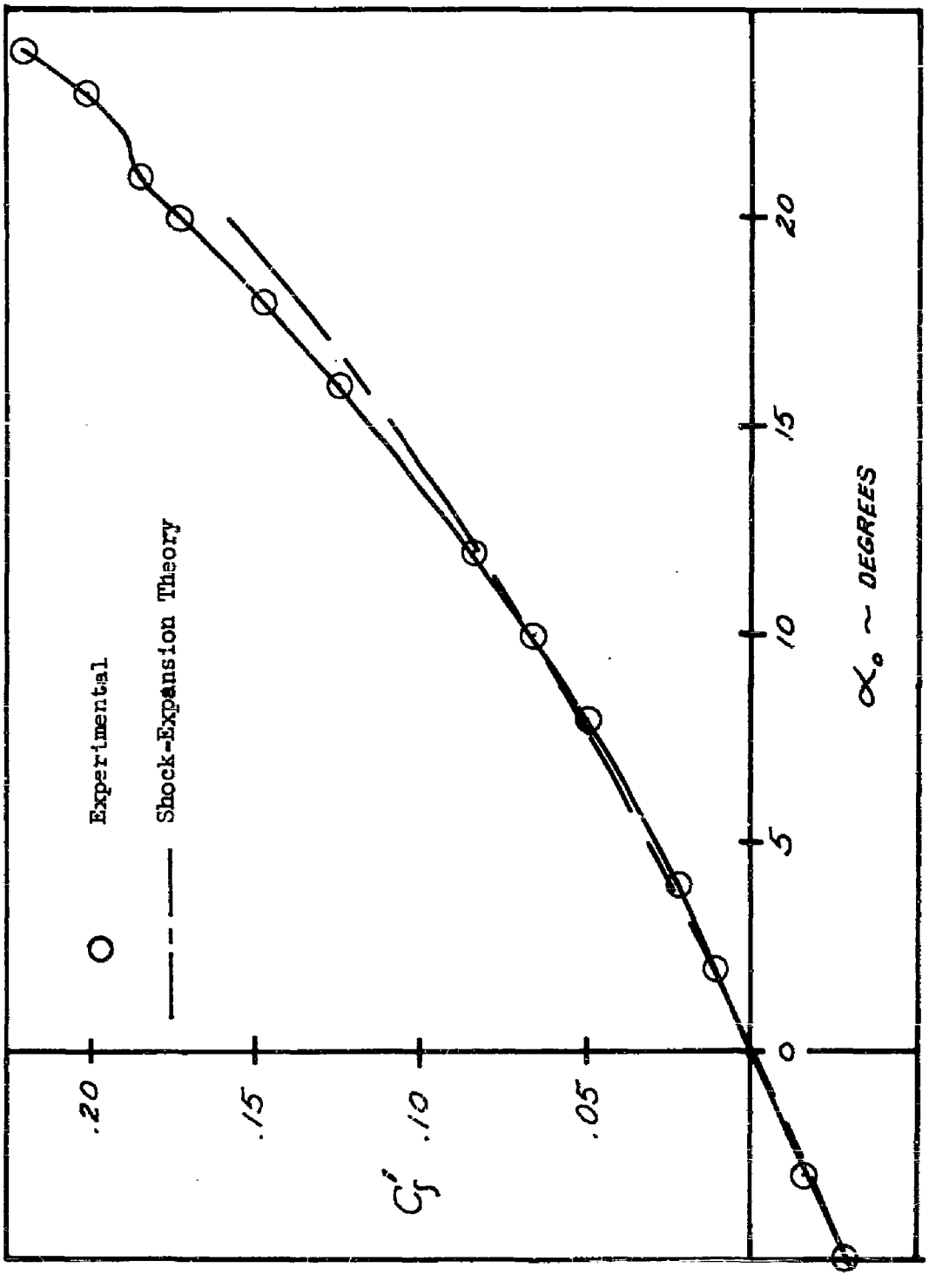

FIGURE 51 COMPARISON OF EXPERIMENTAL AND SHOCK EXPANSION ROLLING MOMENT COEFFICIENT VS. ANGLE-OF-ATTACK AT MACH NUMBER = 6.0; BASIC PLANFORM, t/c = .06

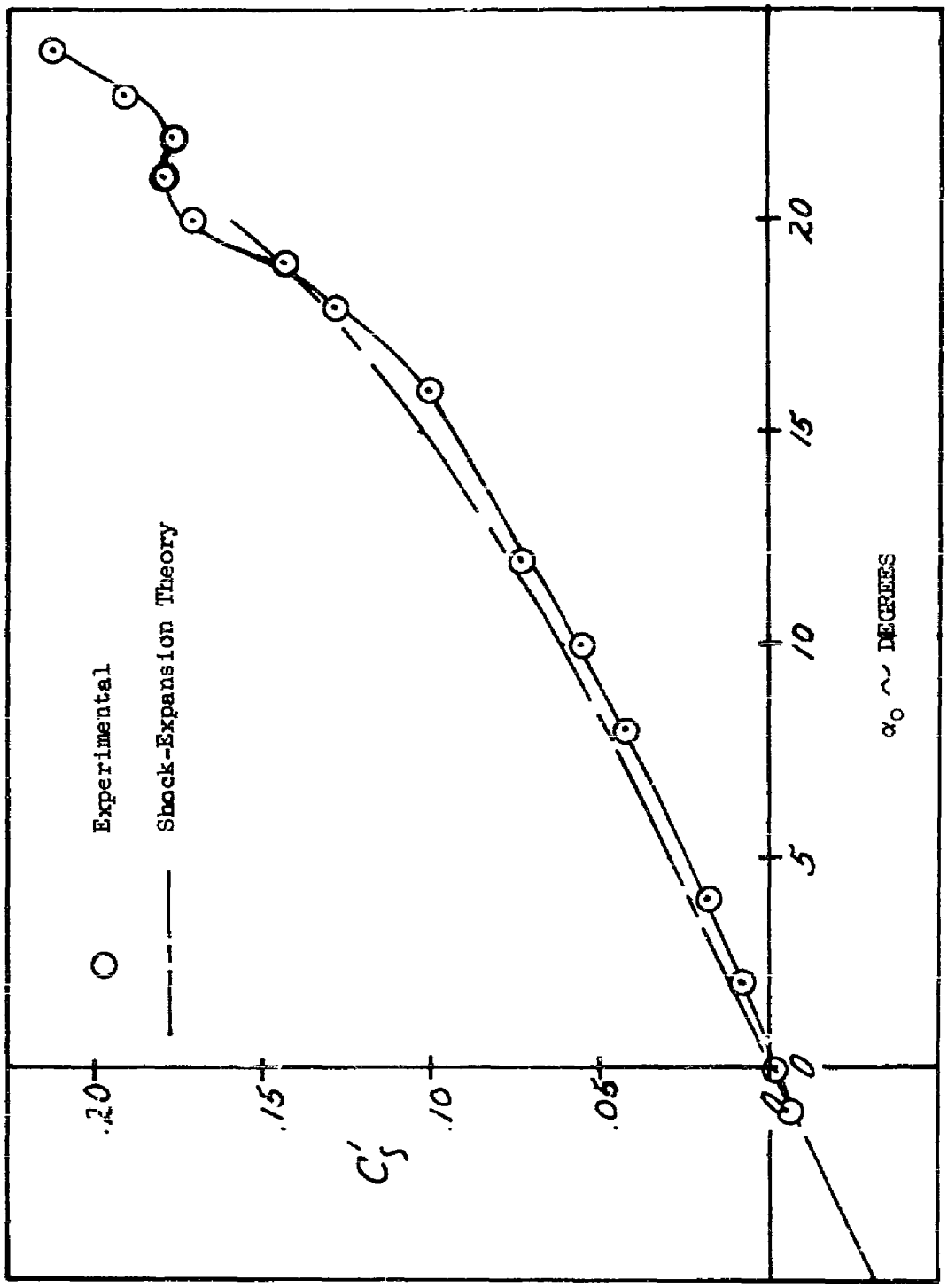

FIGURE 52 COMPARISON OF EXPERIMENTAL AND SHOCK EXPANSION ROLLING MOMENT COEFFICIENT VS. ANGLE-OF-ATTACK AT MACH NUMBER = 7.0; BASIC PLANFORM, t/c = .06

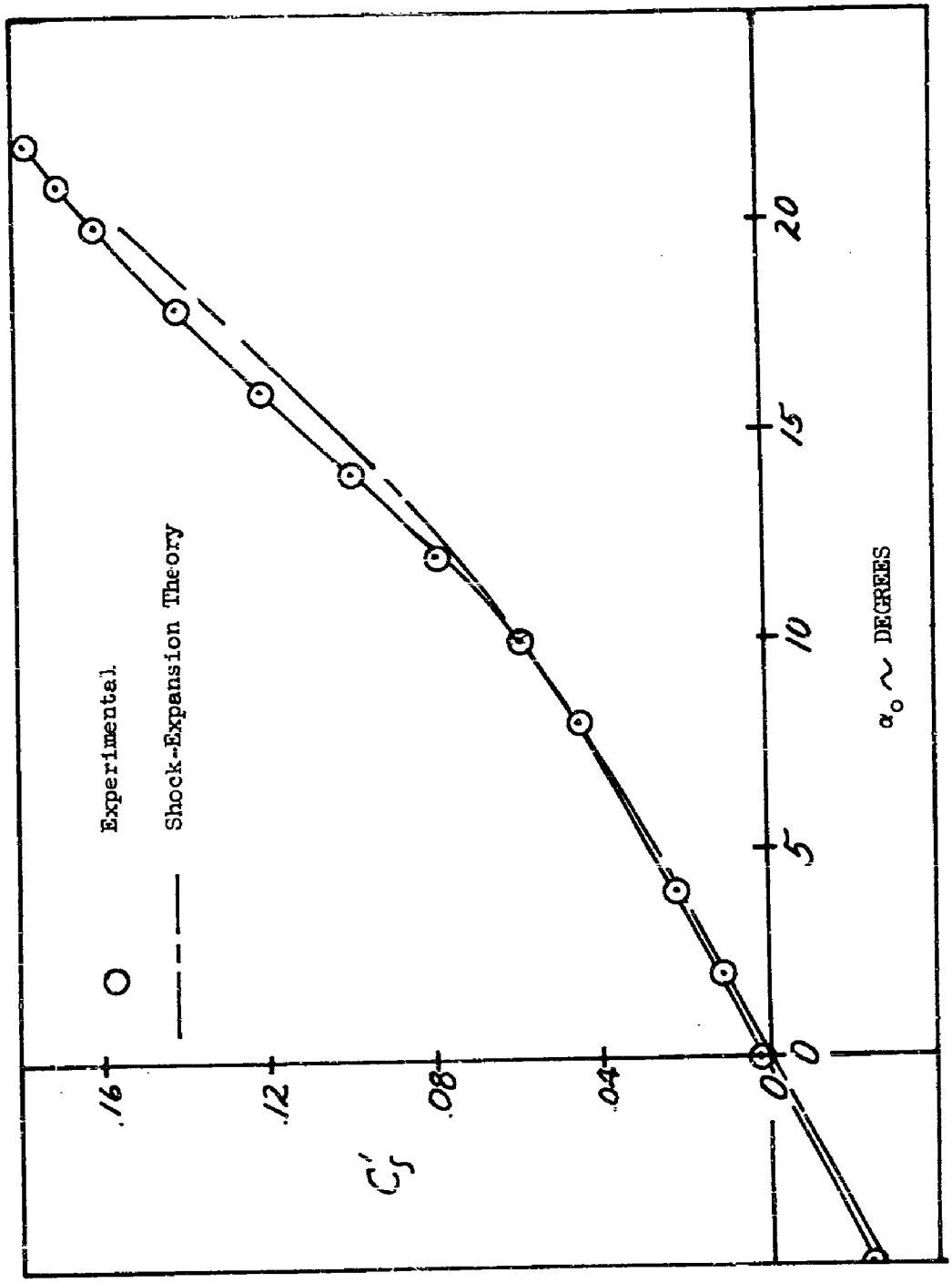

FIGURE 53 COMPARISON OF EXPERIMENTAL AND SHOCK EXPANSION ROLLING MOMENT COEFFICIENT VS. ANGLE-OF-ATTACK AT MACH NUMBER = 8.0; BASIC PLANFORM, t/c = .06

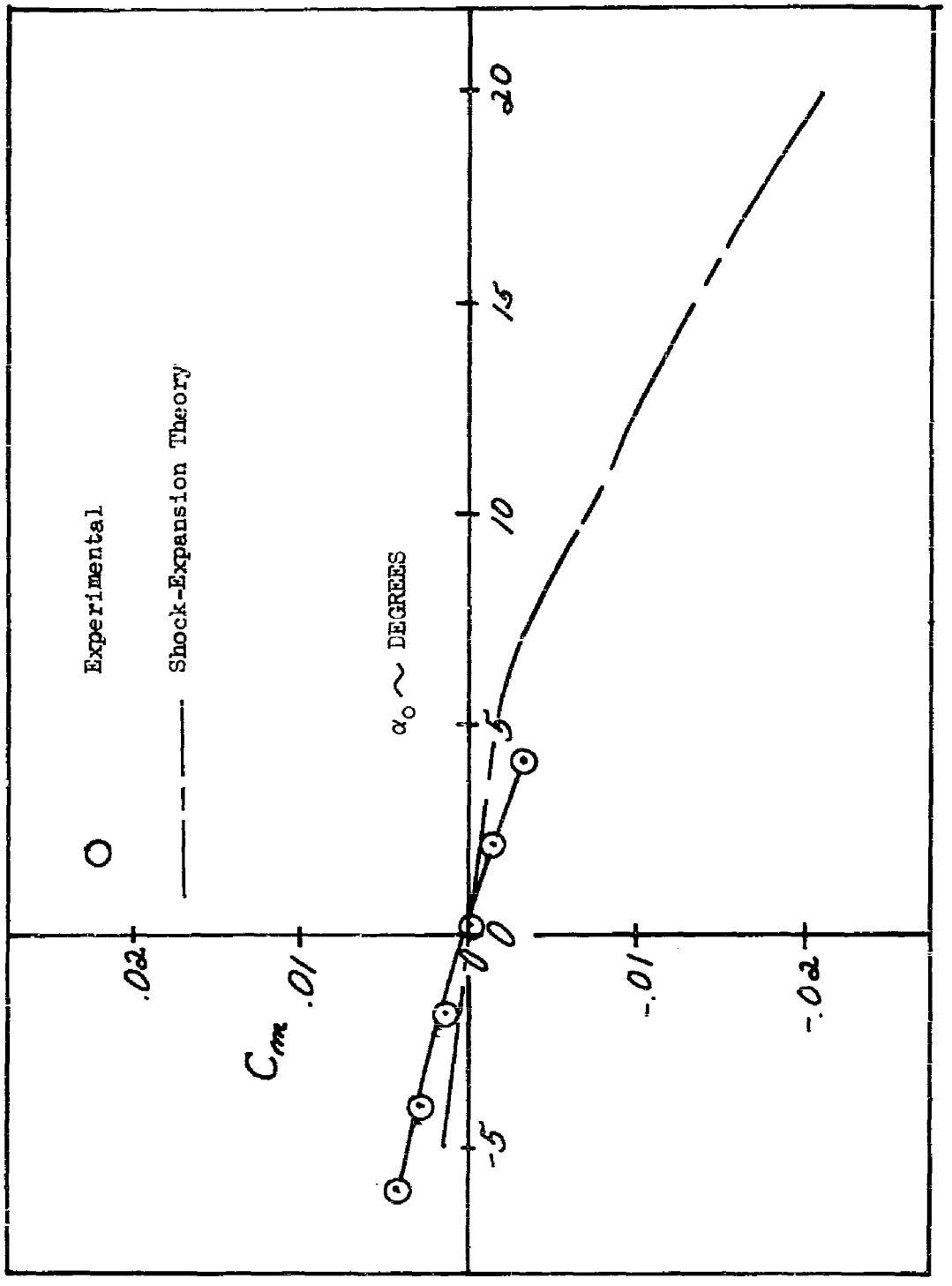

FIGURE 54 COMPARISON OF EXPERIMENTAL AND SHOCK EXPANSION PITCHING MOMENT COEFFICIENT VS. ANGLE-OF-ATTACK AT MACH NUMBER = 6.0; BASIC PLANFORM, t/c = .03

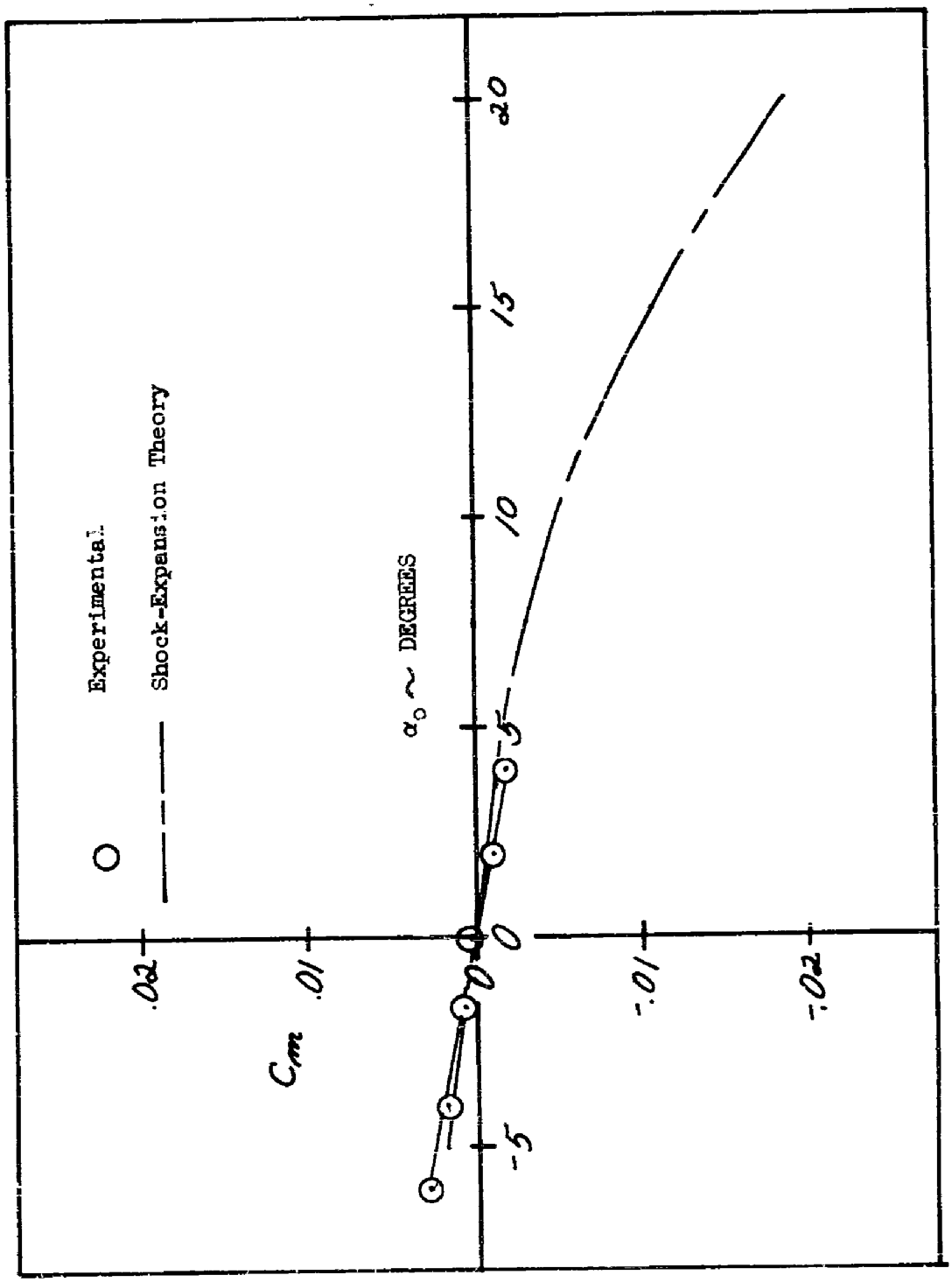

FIGURE 55 COMPARISON OF EXPERIMENTAL AND SHOCK EXPANSION PITCHING MOMENT COEFFICIENT VS. ANGLE-OF-ATTACK AT MACH NUMBER = 8.0; BASIC PLANFORM, t/c = .03

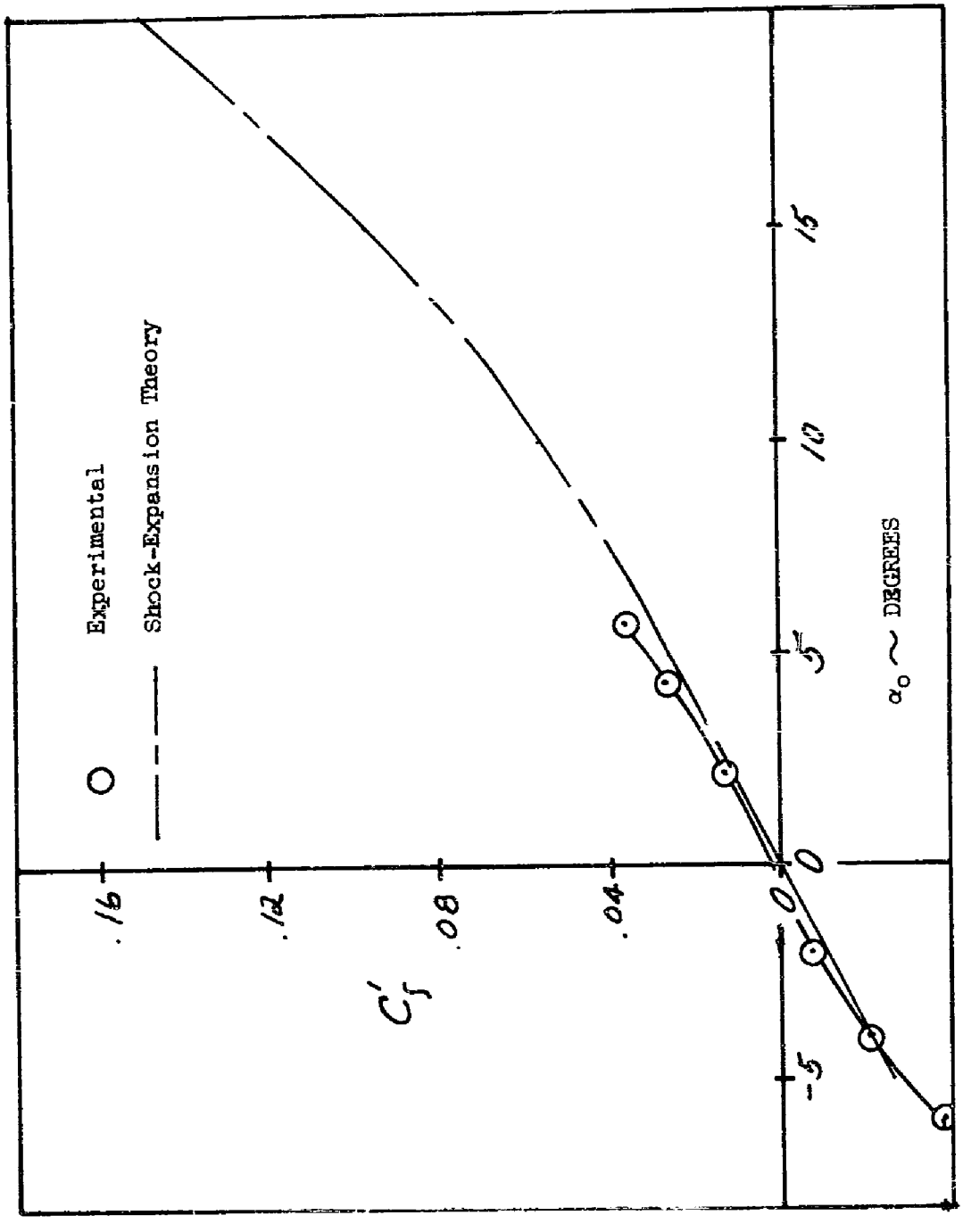

FIGURE 56 COMPARISON OF EXPERIMENTAL AND SHOCK EXPANSION ROLLING MOMENT COEFFICIENT VS. ANGLE-OF-ATTACK AT MACH NUMBER = 6.0; BASIC PLANFORM, t/c = .03

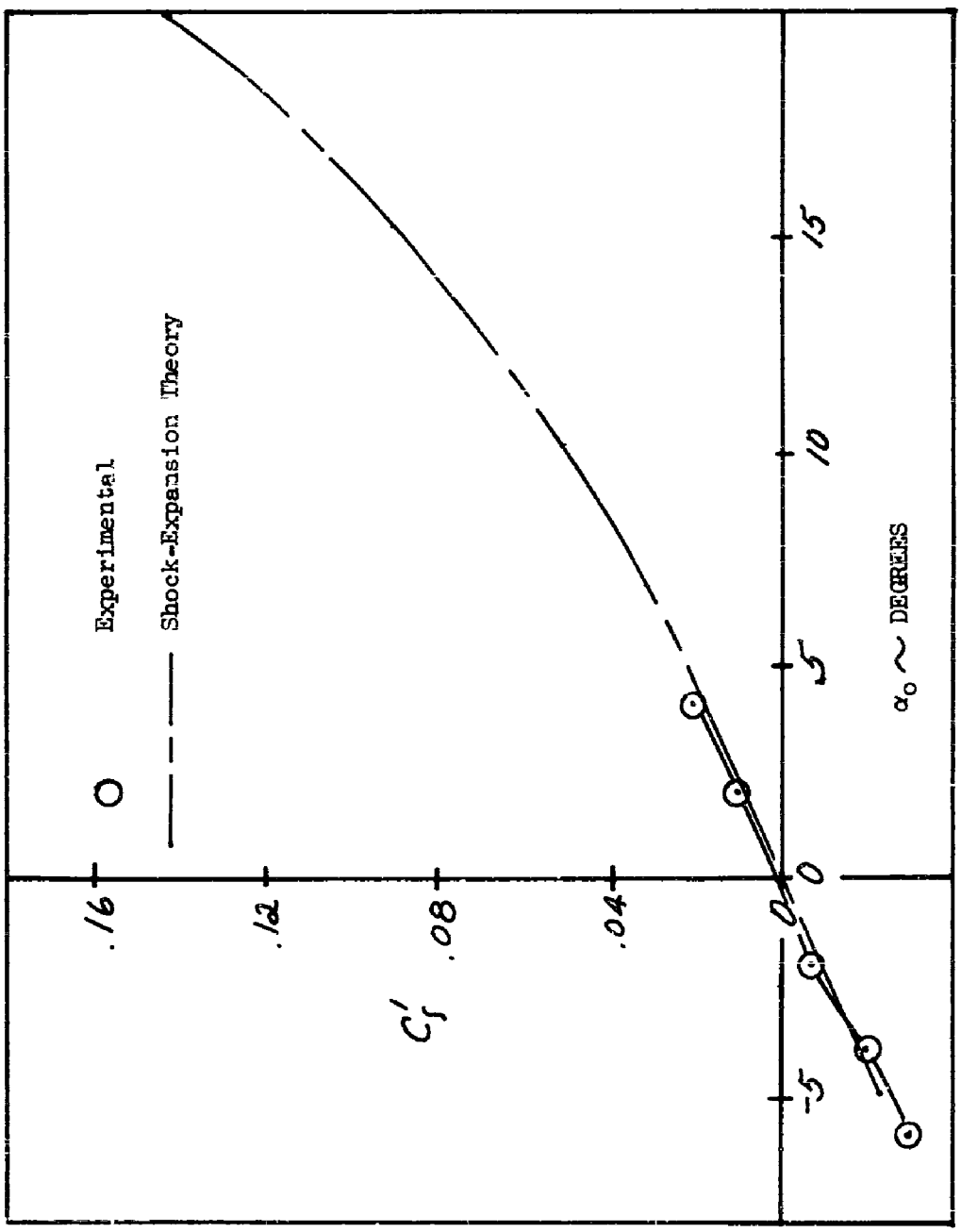

FIGURE 57 COMPARISON OF EXPERIMENTAL AND SHOCK EXPANSION ROLLING MOMENT COEFFICIENT VS. ANGLE-OF-ATTACK AT MACH NUMBER = 3.0; BASIC PLANFORM, t/c = .03

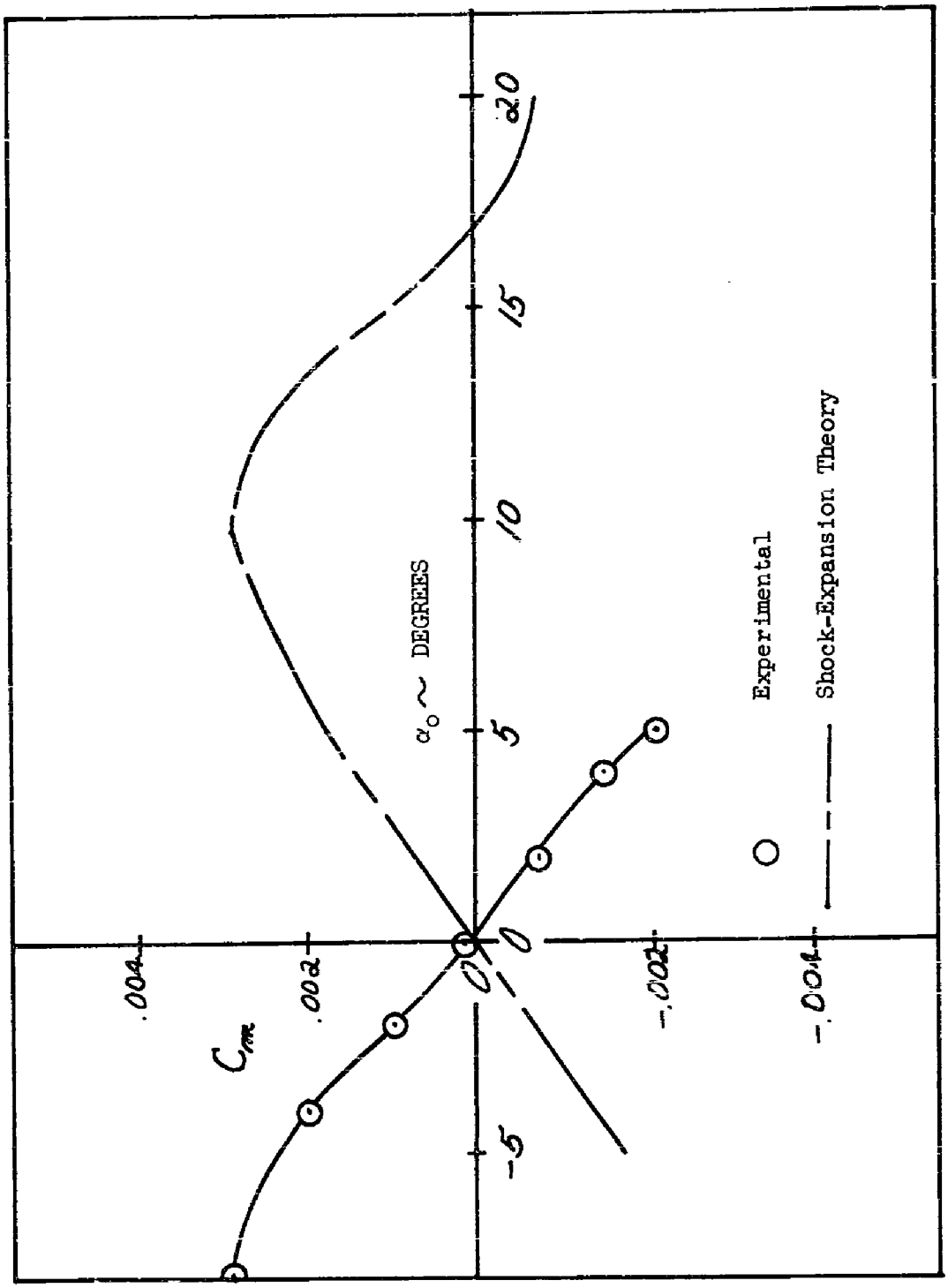

FIGURE 58 COMPARISON OF EXPERIMENTAL AND SHOCK EXPANSION PITCHING MOMENT COEFFICIENT VS. ANGLE-OF-ATTACK AT MACH NUMBER = 6.0; BASIC PLANFORM, t/c = .09

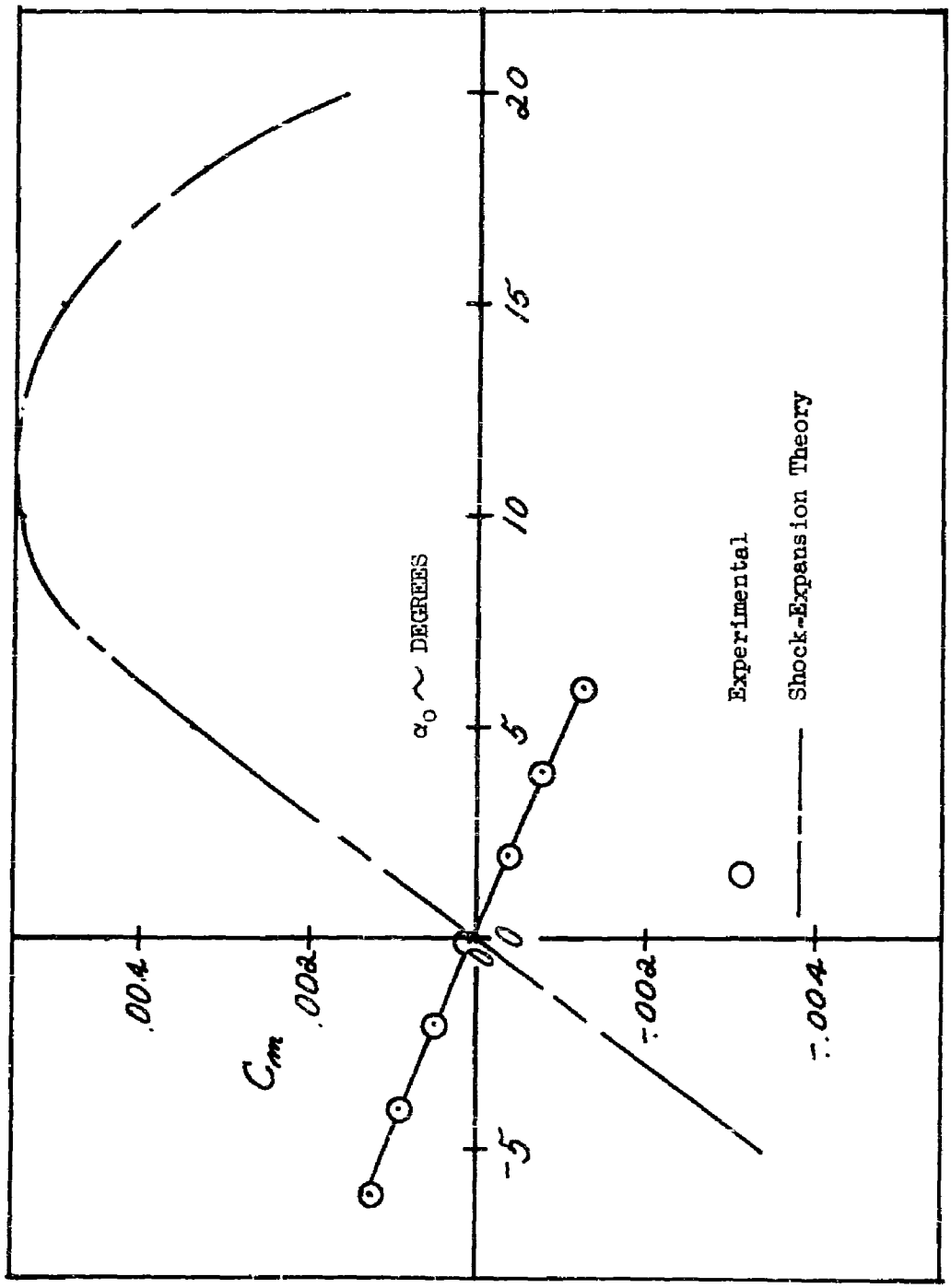

FIGURE 59 COMPARISON OF EXPERIMENTAL AND SHOCK EXPANSION PITCHING MOMENT COEFFICIENT VS. ANGLE-OF-ATTACK AT MACH NUMBER = 3.0; BASIC PLANFORM, t/c = .09

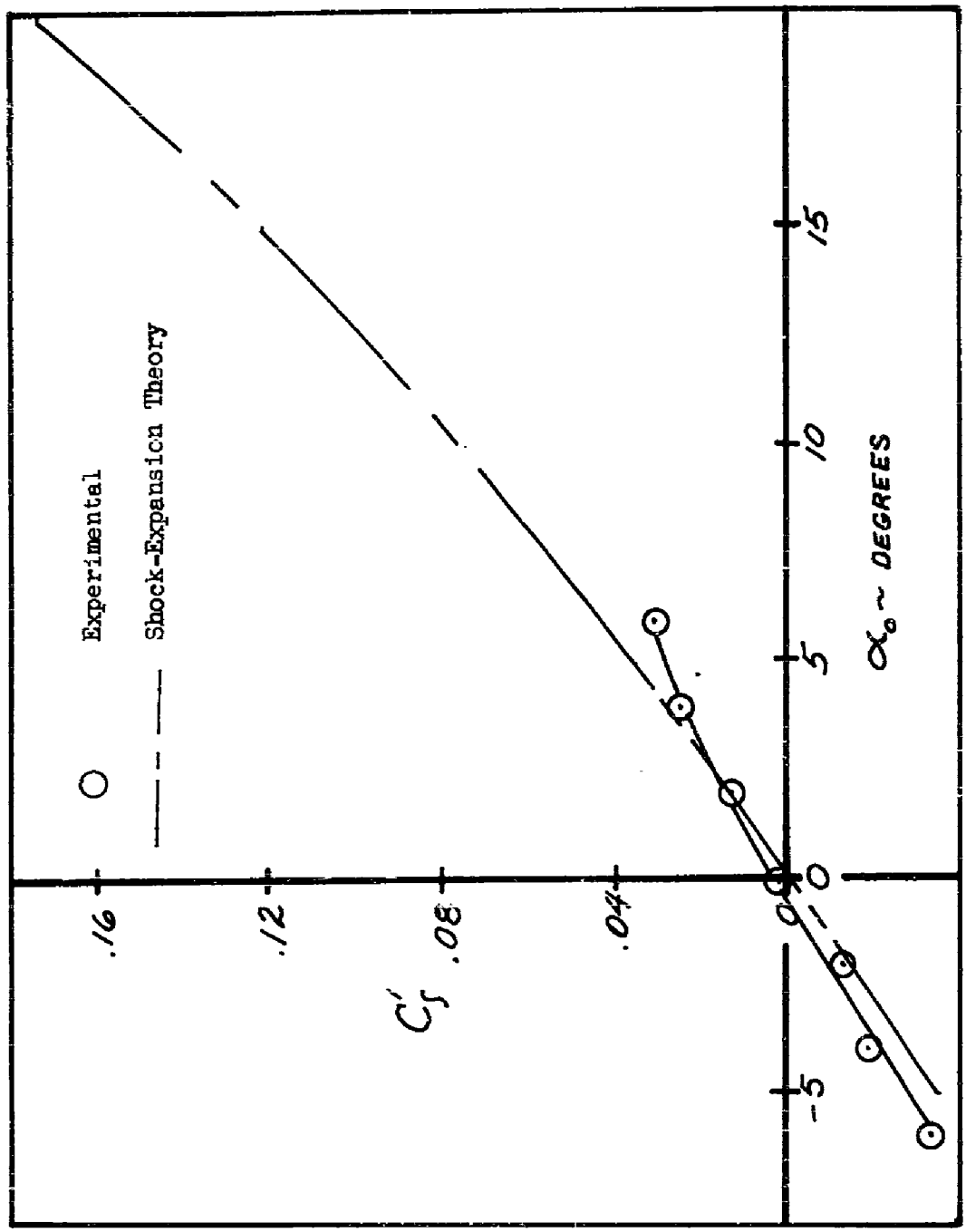

FIGURE 60 COMPARISON OF EXPERIMENTAL AND SHOCK EXPANSION ROLLING MOMENT COEFFICIENT VS ANGLE-OF-ATTACK AT MACH NUMBER = 6.0; BASIC PLANFORM, t/c = .09

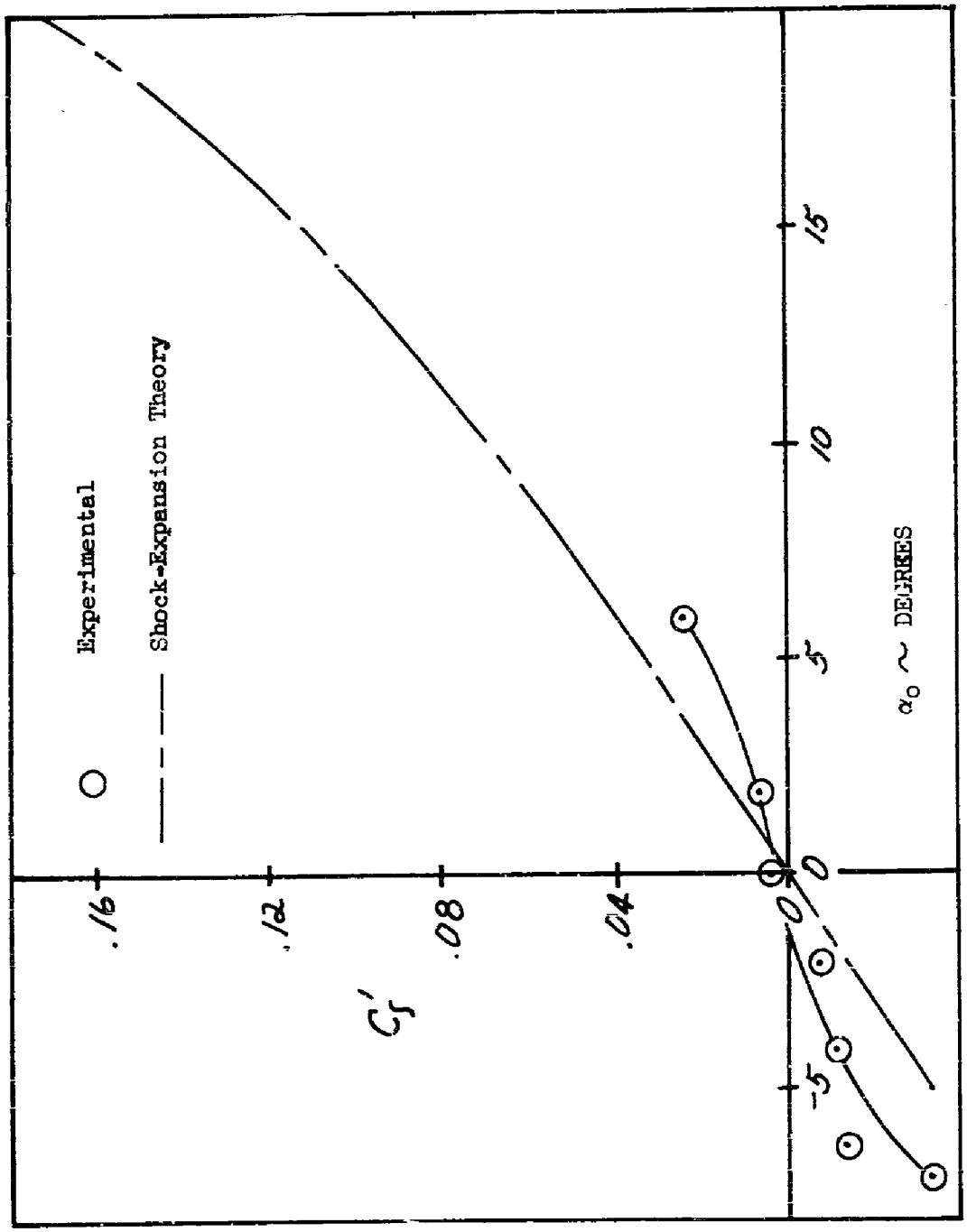

FIGURE 51 COMPARISON OF EXPERIMENTAL AND SHOCK EXPANSION ROLLING MOMENT COEFFICIENT VS. ANGLE-OF-ATTACK AT MACH NUMBER = 8.0; BASIC PLANFORM, t/c = .09

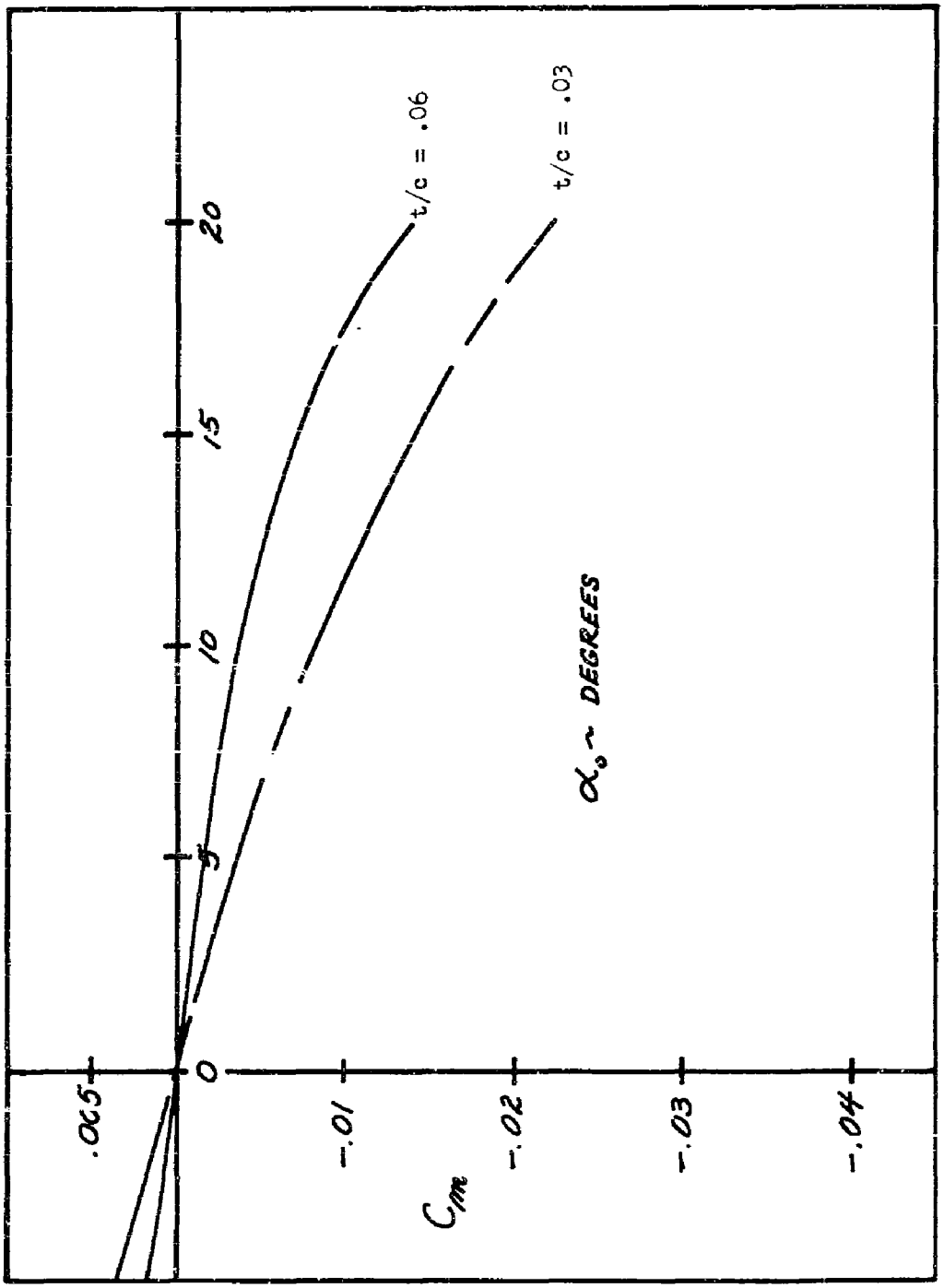

FIGURE 62 EFFECT OF THICKNESS RATIO ON PITCHING MOMENT COEFFICIENT VS. ANGLE-OF-ATTACK; "SHOCK-EXPANSION" THEORY - MACH NUMBER = 5.0

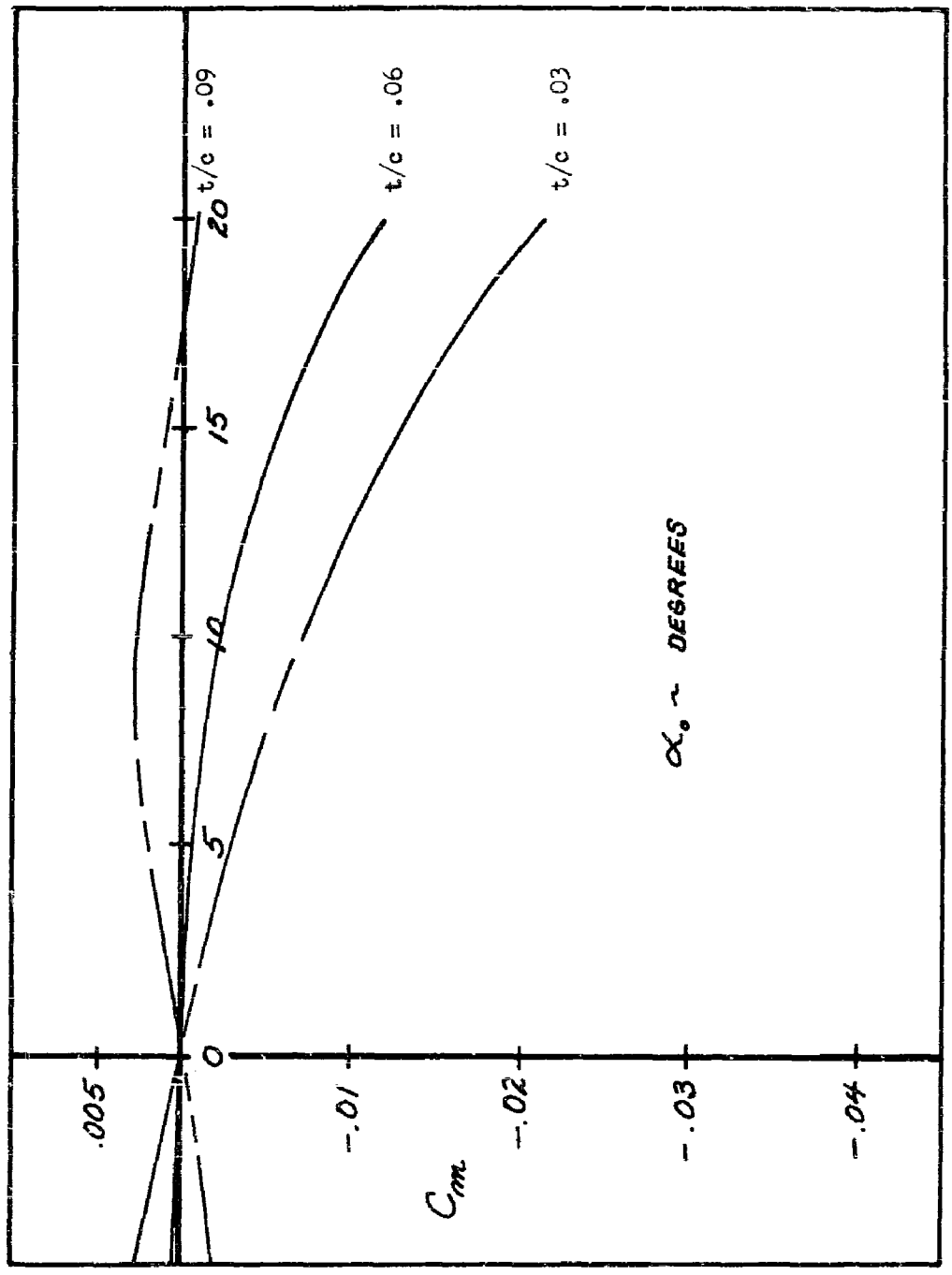

FIGURE 63 EFFECT OF THICKNESS RATIO ON PITCHING MOMENT COEFFICIENT VS. ANGLE-OF-ATTACK; "SHOCK-EXPANSION" THEORY - MACH NUMBER = 6.0

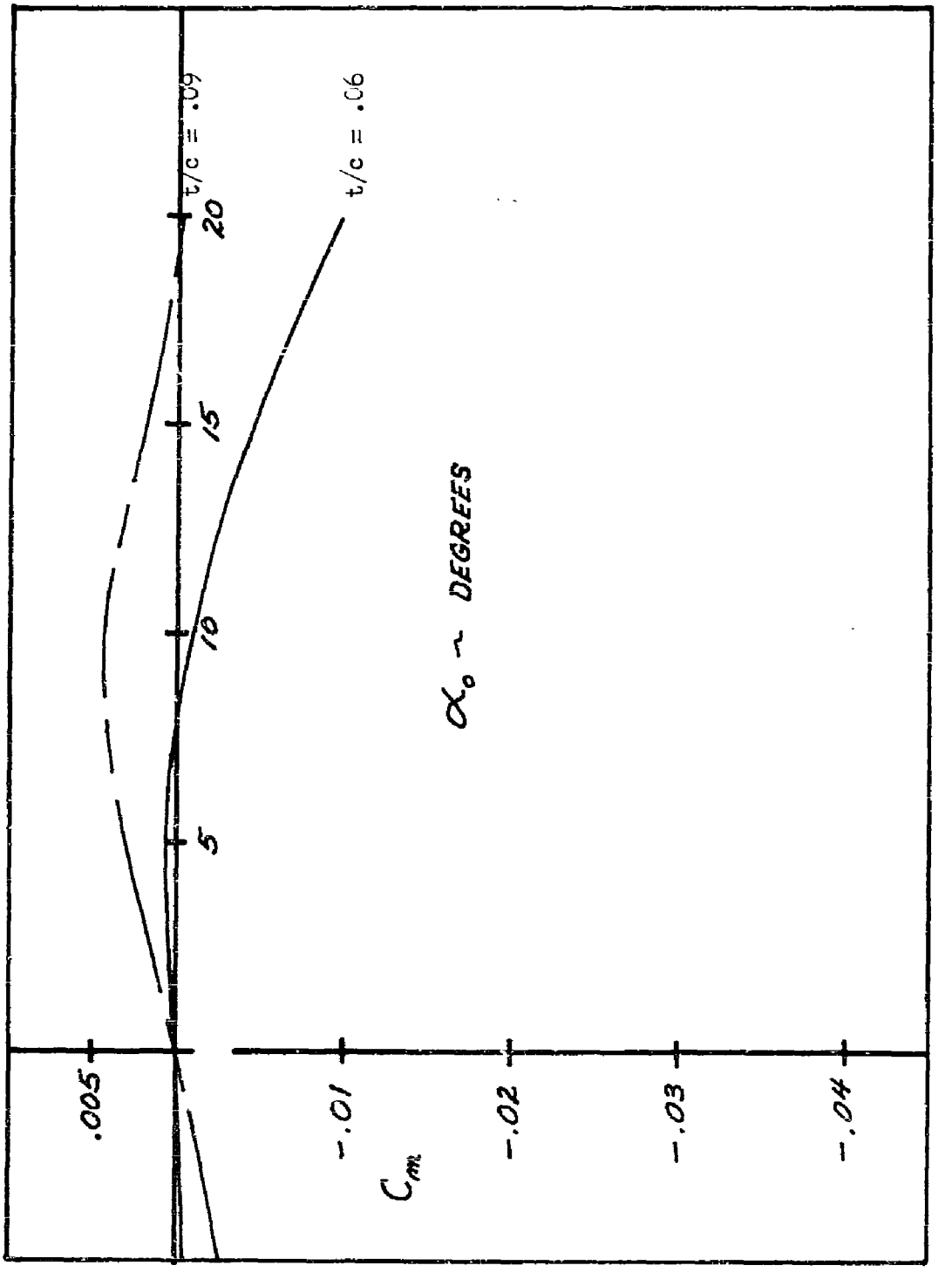

FIGURE 64 EFFECT OF THICKNESS RATIO ON PITCHING MOMENT COEFFICIENT VS. ANGLE-OF-ATTACK: "SHOCK-EXPANSION" THEORY - MACH NUMBER = 7.0

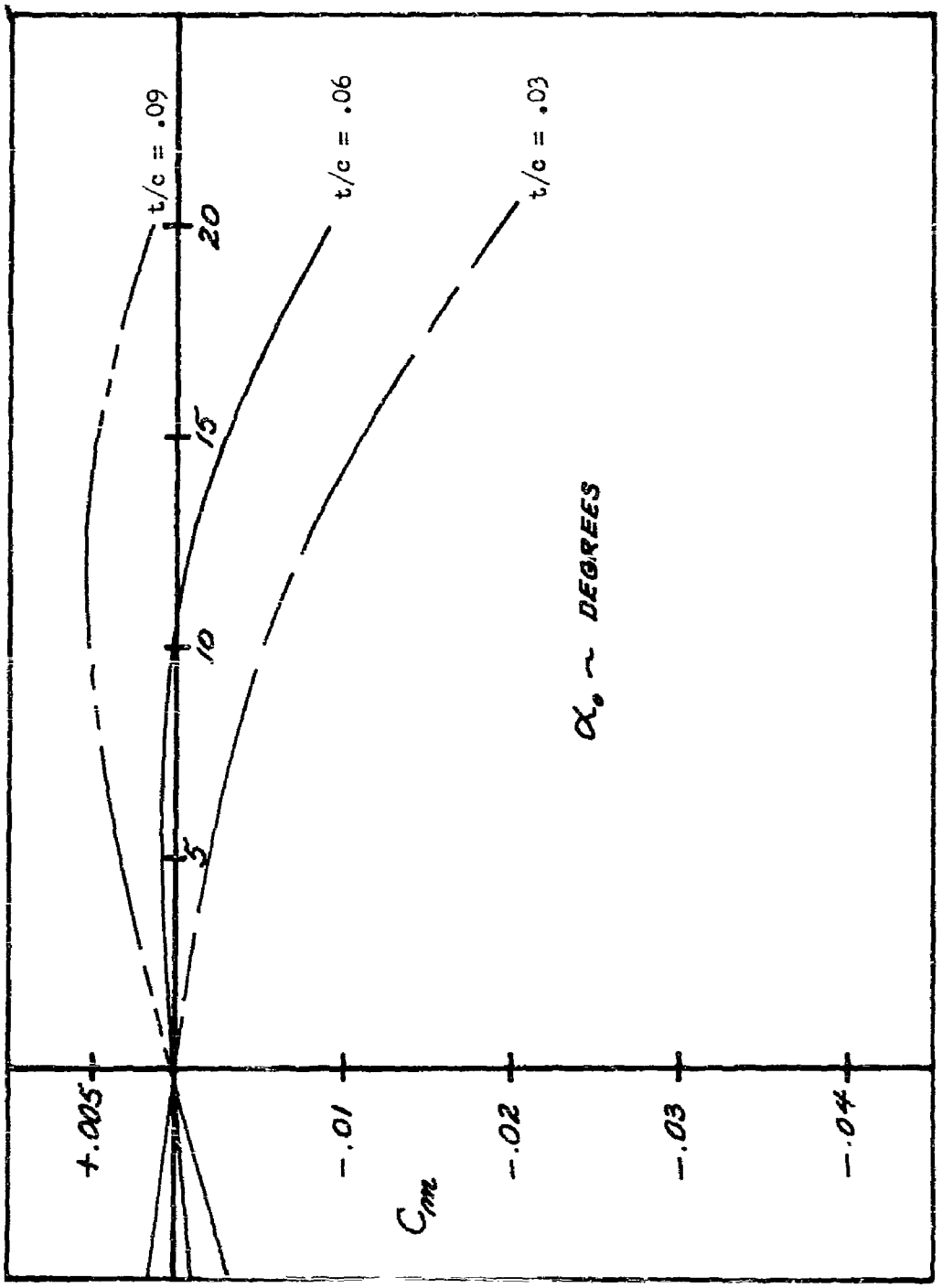

FIGURE 65 EFFECT OF THICKNESS RATIO ON PITCHING MOMENT COEFFICIENT VS. ANGLE-OF-ATTACK; "SHOCK-EXPANSION" THEORY - MACH NUMBER = 8.0

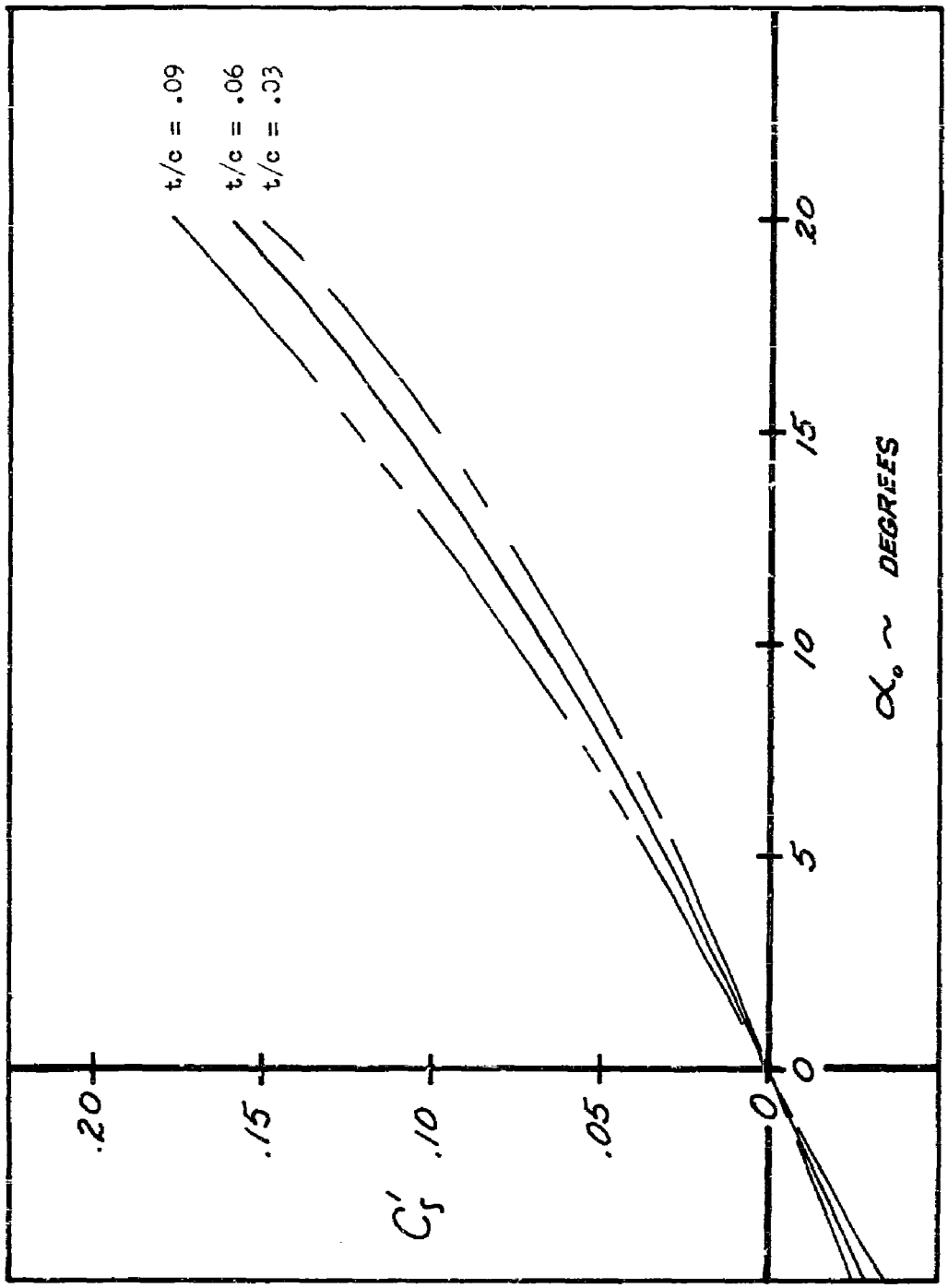

FIGURE 66 EFFECT OF THICKNESS RATIO ON ROLLING MOMENT COEFFICIENT VS. ANGLE-OF-ATTACK; "SHOCK-EXPANSION" THEORY - MACH NUMBER = 6.0

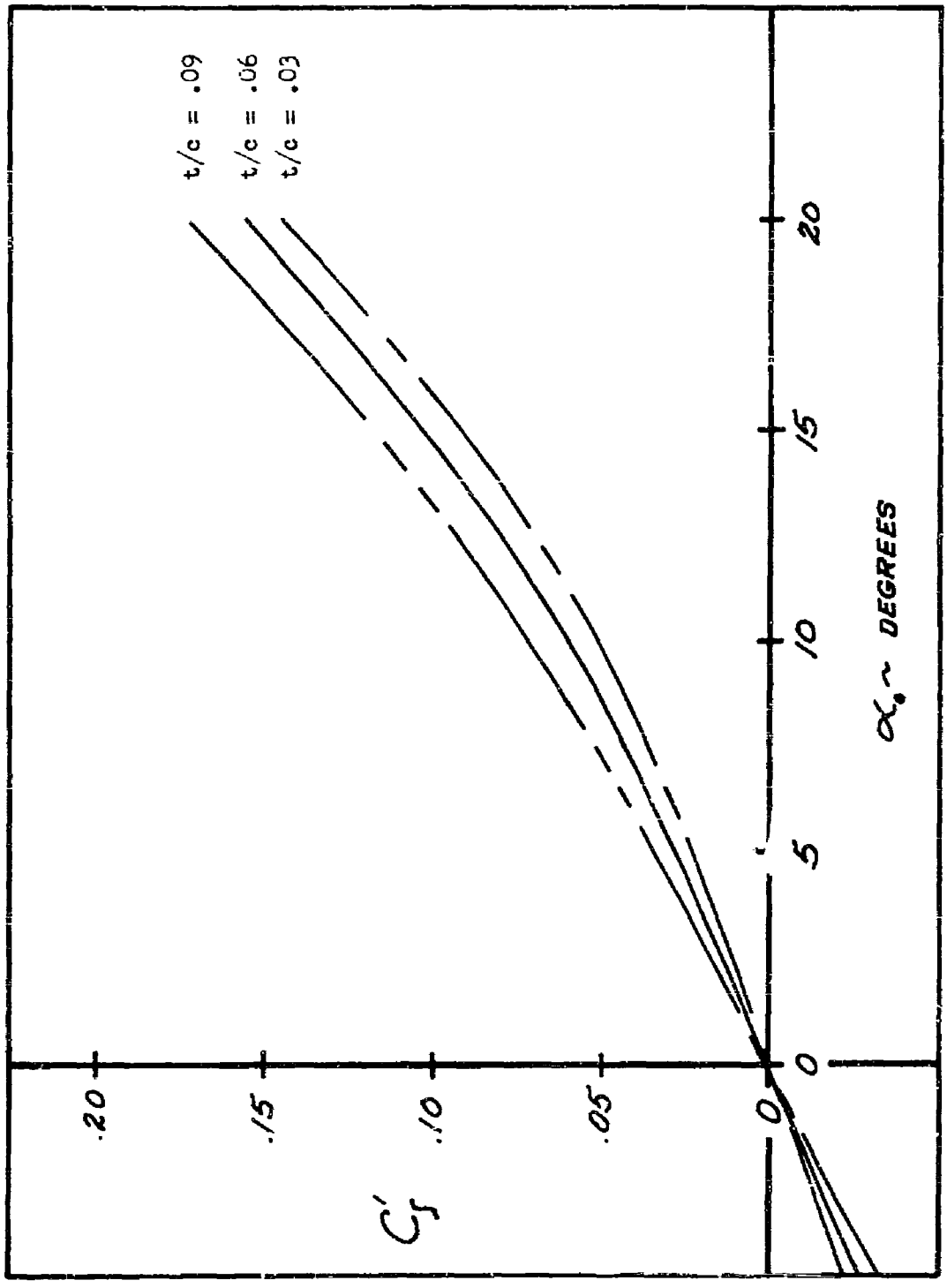

FIGURE 67 EFFECT OF THICKNESS RATIO ON ROLLING MOMENT COEFFICIENT VS. ANGLE-OF-ATTACK: "SHOCK-EXPANSION" THEORY - MACH NUMBER = 8.0

CONFIDENTIAL

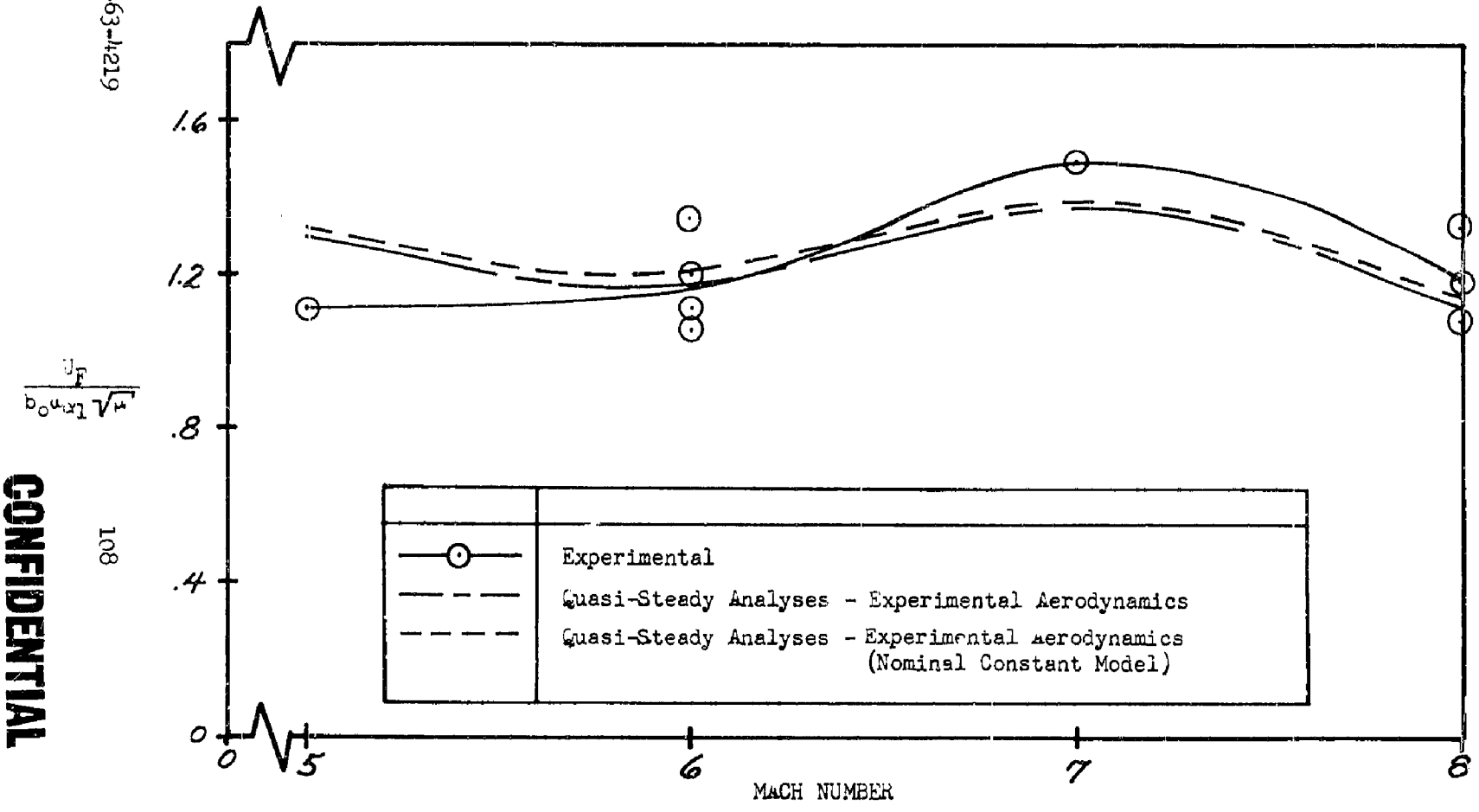

FIGURE 68 EXPERIMENTAL AND THEORETICAL, QUASI-STEADY (USING EXPERIMENTAL AERODYNAMICS) FLUTTER VELOCITY PARAMETER VS. MACH NUMBER; BASIC PLANFORM, t/c = .06, ω_h/ω_α = .6 α_0 = 0°

CONFIDENTIAL

CONFIDENTIAL

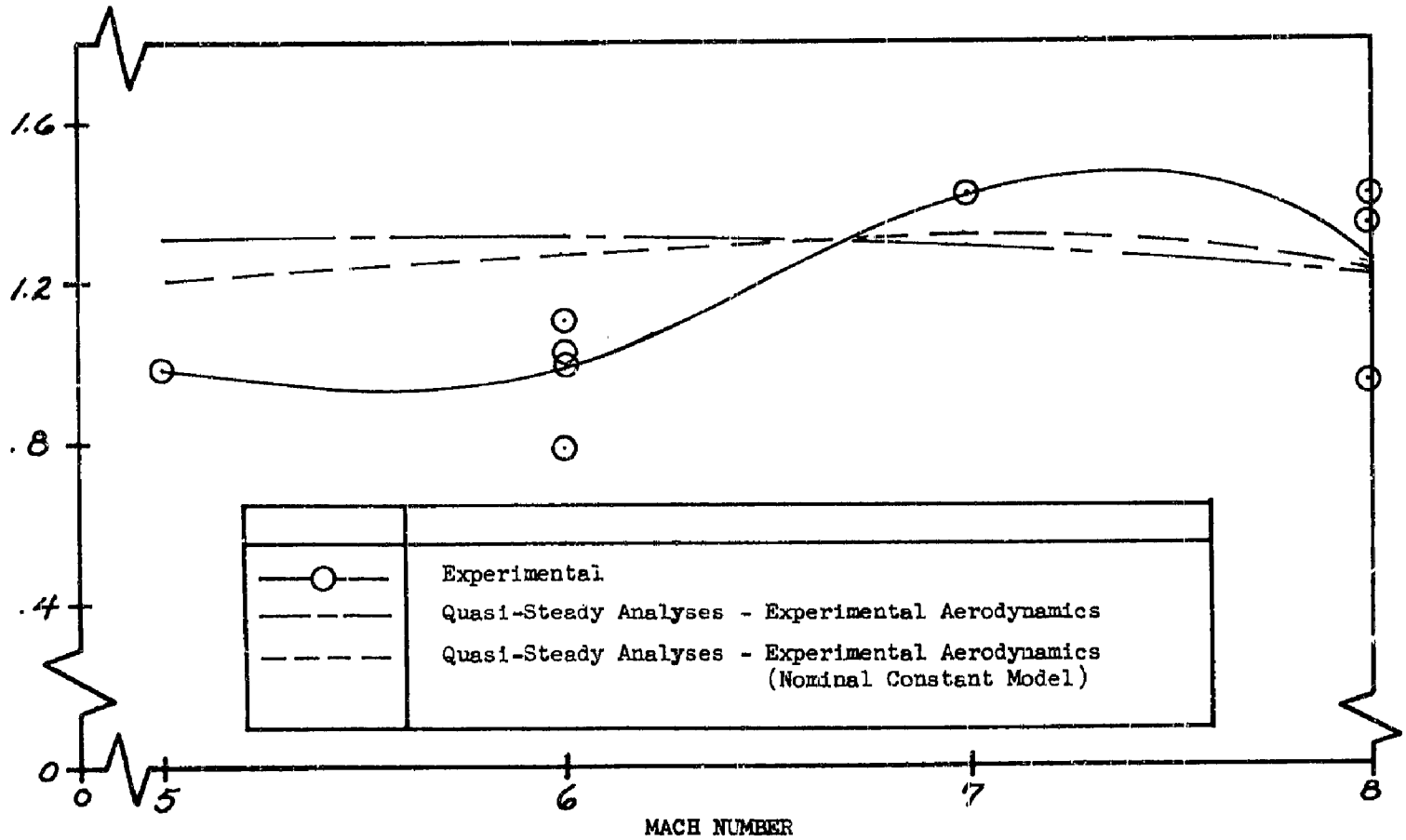

FIGURE 69 EXPERIMENTAL AND THEORETICAL, QUASI-STEADY (USING EXPERIMENTAL AERODYNAMICS) FLUTTER FREQUENCY RATIO VS. MACH NUMBER; BASIC PLANFORM, t/c = .06, $\omega_{h_1}/\omega_{\alpha_1}$ = .60, $\alpha_0 = 0°$

CONFIDENTIAL

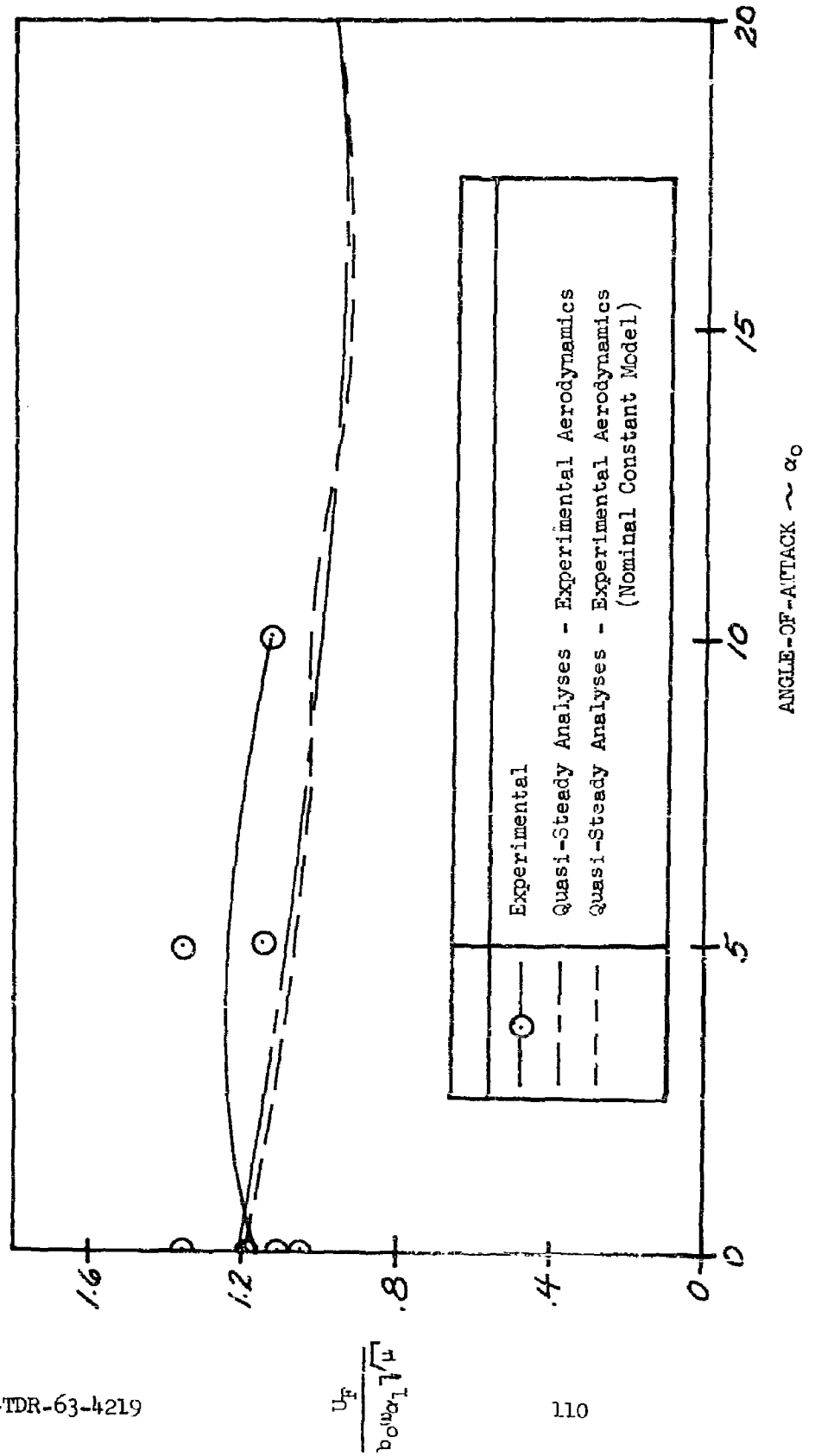

FIGURE 70 EXPERIMENTAL AND THEORETICAL, QUASI-STEADY (USING EXPERIMENTAL AERODYNAMICS) FLUTTER VELOCITY PARAMETER VS. ANGLE-OF-ATTACK AT MACH NUMBER = 6.0; BASIC PLANFORM, t/c = .06, $\omega_{h_0}/\omega_{\alpha_0}$ = .60

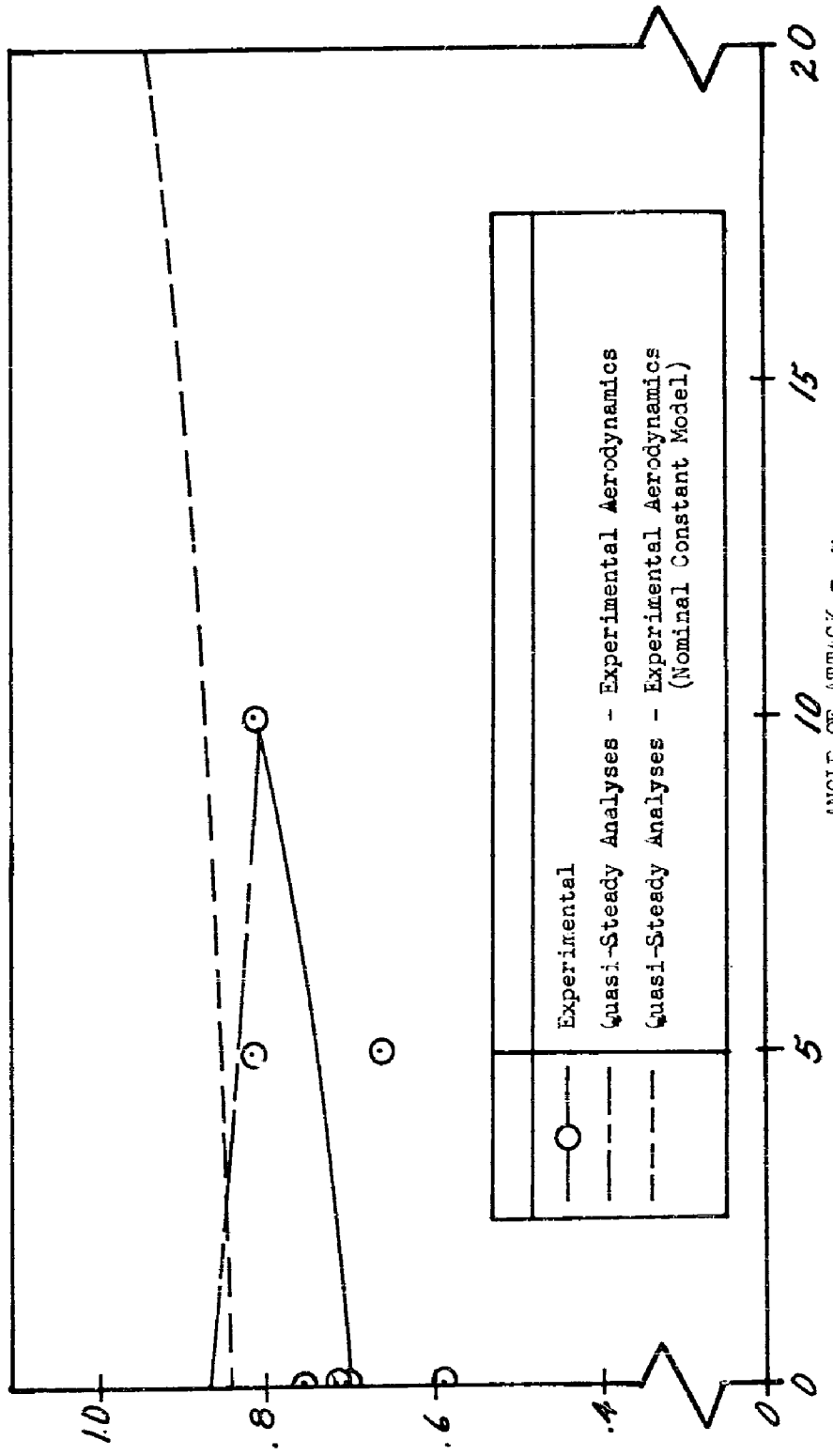

FIGURE 71 EXPERIMENTAL AND THEORETICAL, QUASI-STEADY (USING EXPERIMENTAL AERODYNAMICS) FLUTTER FREQUENCY RATIO VS. ANGLE-OF-ATTACK AT MACH NUMBER = 6.0; BASIC PLANFORM, $t/c = .06$, $\omega_h/\omega_\alpha = .60$

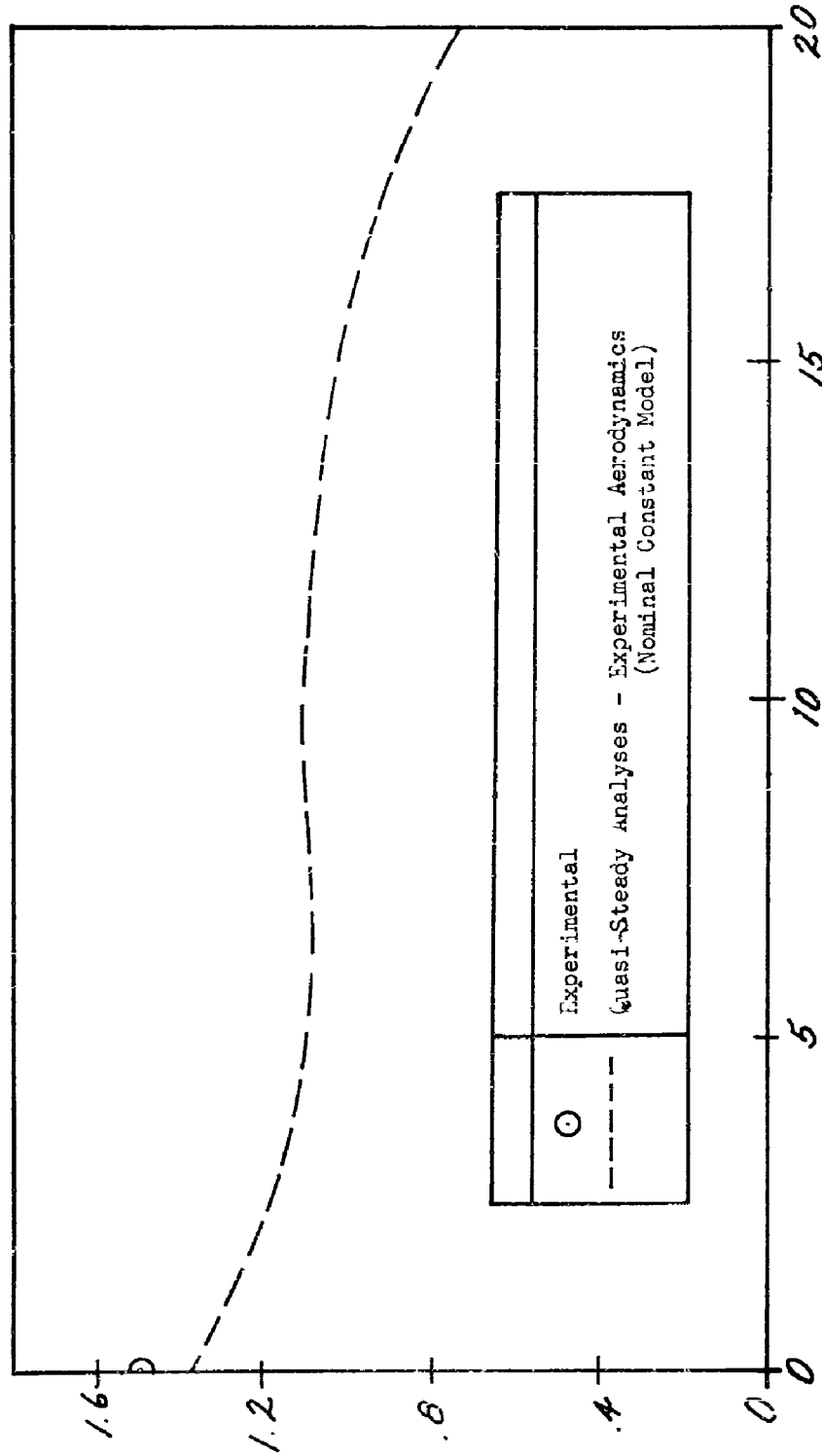

FIGURE 72 THEORETICAL, QUASI-STEADY (USING EXPERIMENTAL AERODYNAMICS) FLUTTER VELOCITY PARAMETER VS. ANGLE-OF-ATTACK AT MACH NUMBER = 7.0; BASIC PLANFORM NOMINAL MODEL, t/c = .06, ω_h/ω_α = .60

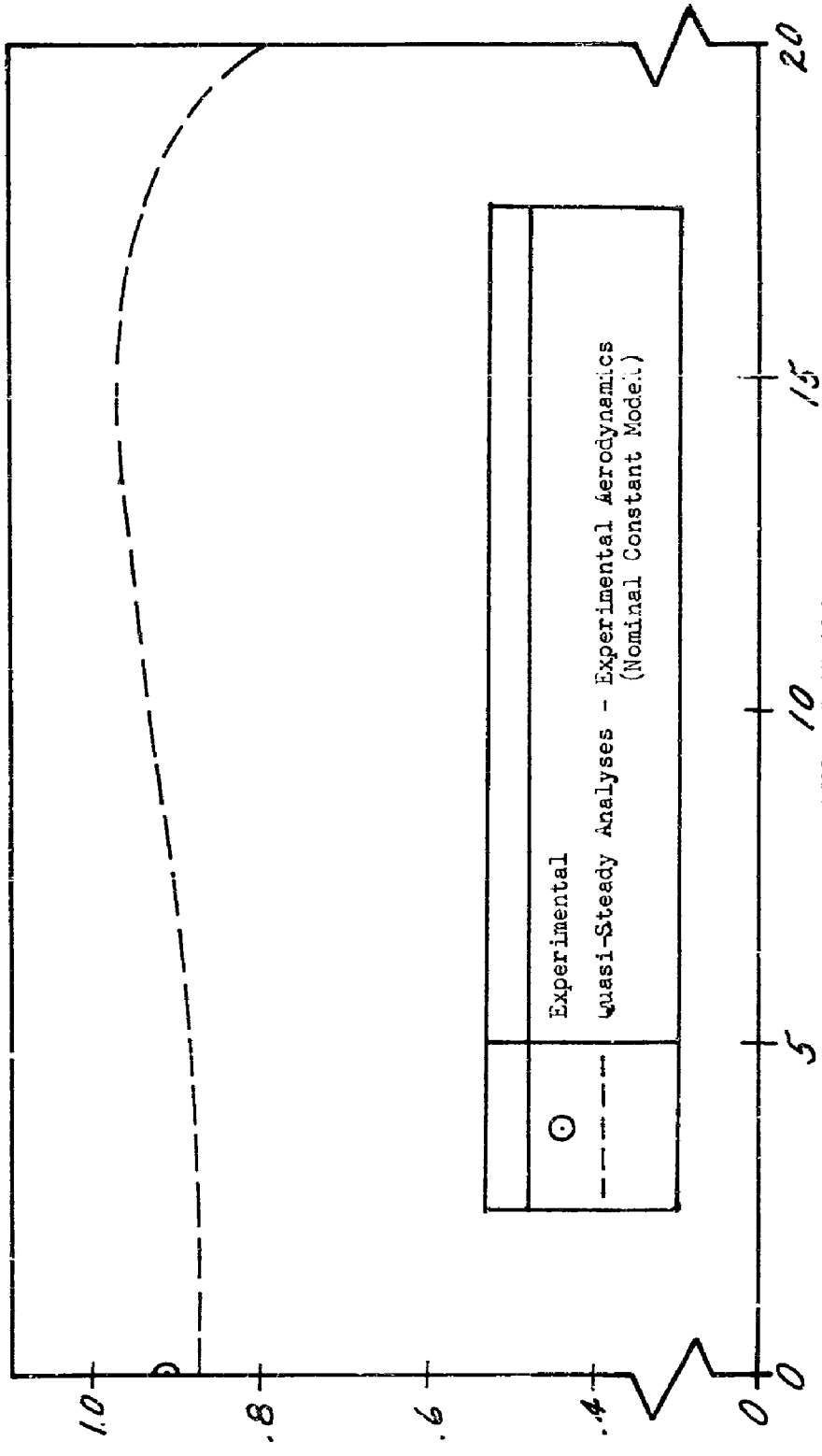

FIGURE 73 THEORETICAL QUASI-STEADY (USING EXPERIMENTAL AERODYNAMICS) FLUTTER FREQUENCY RATIO VS. ANGLE-OF-ATTACK AT MACH NUMBER = 7.0; BASIC PLANFORM, NOMINAL MODEL, t/c = .06, $\omega_h/\omega_{\alpha_1}$ = .60

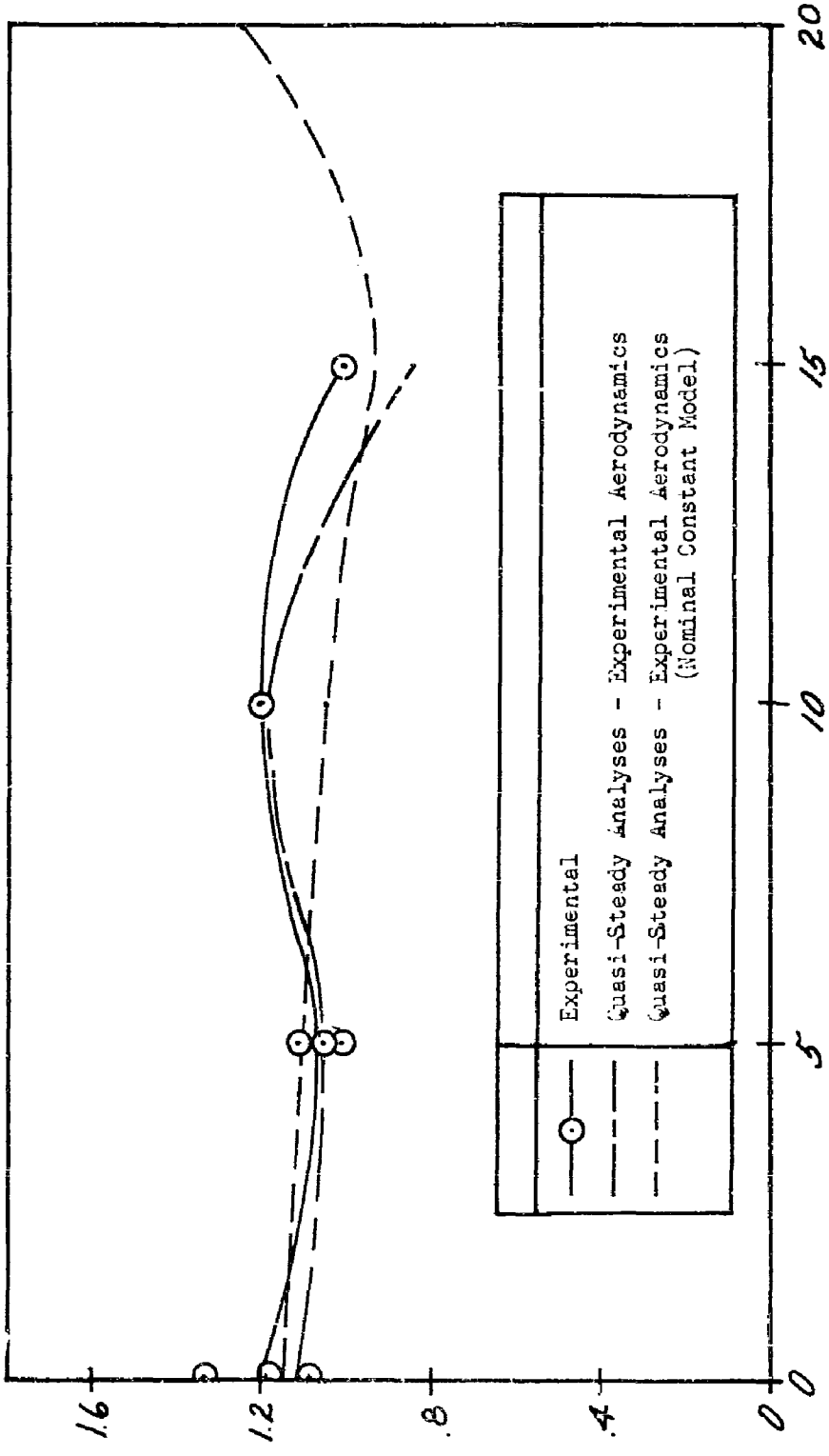

FIGURE 74 EXPERIMENTAL AND THEORETICAL, QUASI-STEADY (USING EXPERIMENTAL AERODYNAMICS) FLUTTER VELOCITY PARAMETER VS. ANGLE-OF-ATTACK AT MACH NUMBER = 8.0; BASIC PLANFORM, $t/c = .06$, $\omega_h/\omega_\alpha = .60$

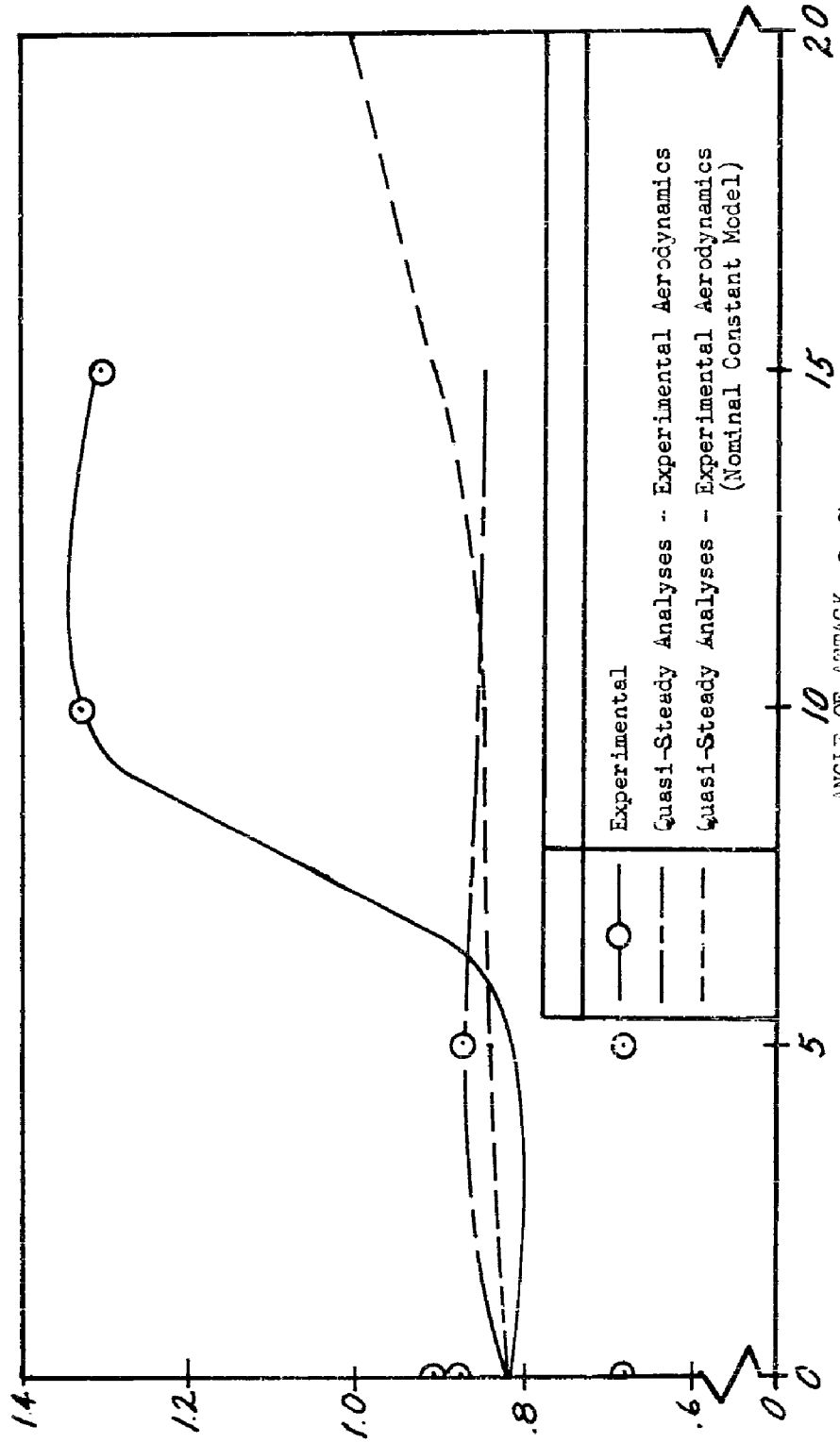

FIGURE 75 EXPERIMENTAL AND THEORETICAL, QUASI-STEADY (USING EXPERIMENTAL AERODYNAMICS) FLUTTER FREQUENCY RATIO VS. ANGLE-OF-ATTACK AT MACH NUMBER = 8.0; BASIC PLANFORM, t/c = .06, ω_h/ω_α = .60

CONFIDENTIAL

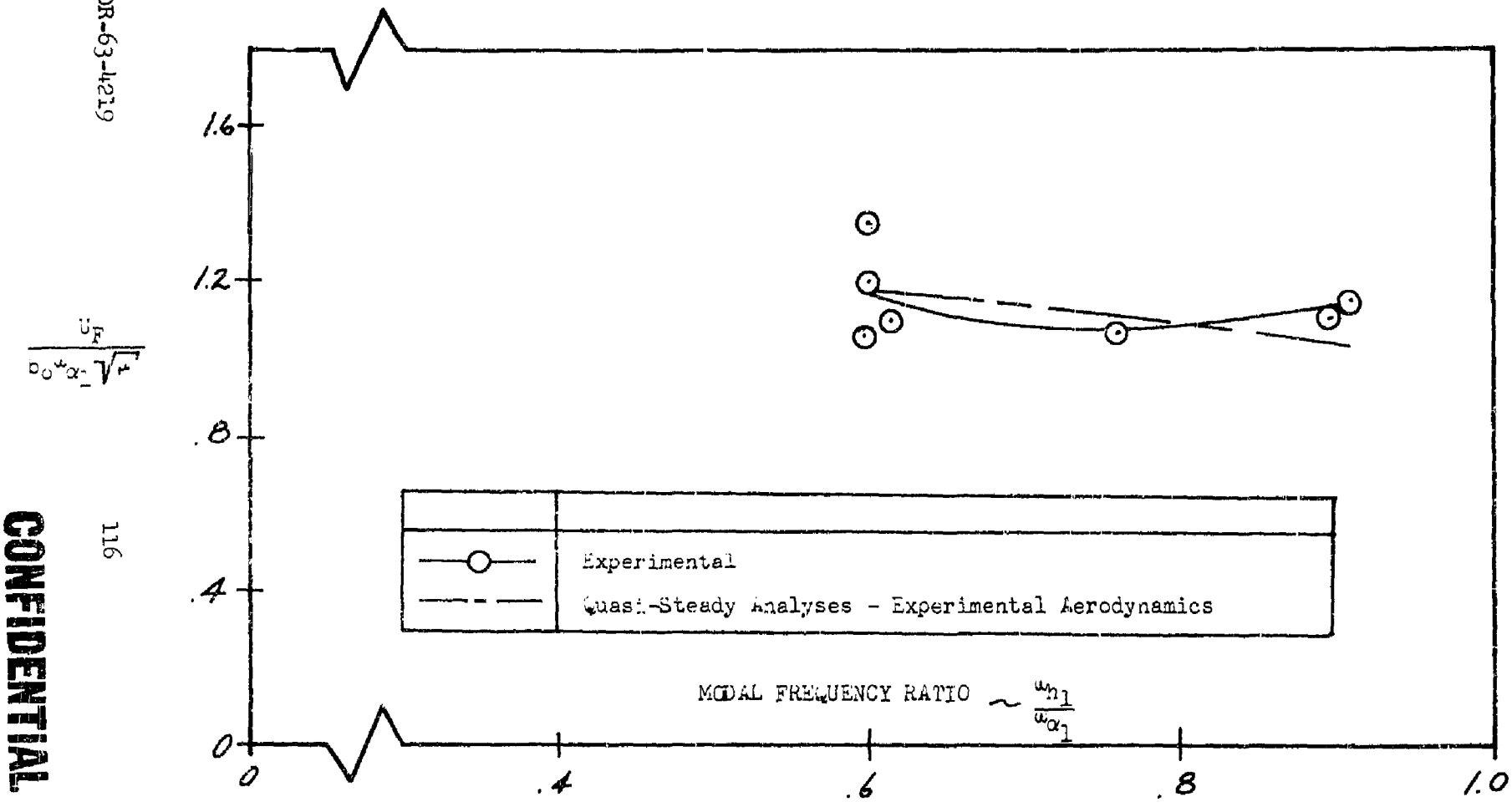

FIGURE 76 EXPERIMENTAL AND THEORETICAL, QUASI-STEADY (USING EXPERIMENTAL AERODYNAMICS) FLUTTER VELOCITY PARAMETER VS. MODAL FREQUENCY RATIO AT MACH NUMBER = 6.0; BASIC PLANFORM, t/c = .06, $\alpha_0 = 0°$

CONFIDENTIAL

CONFIDENTIAL

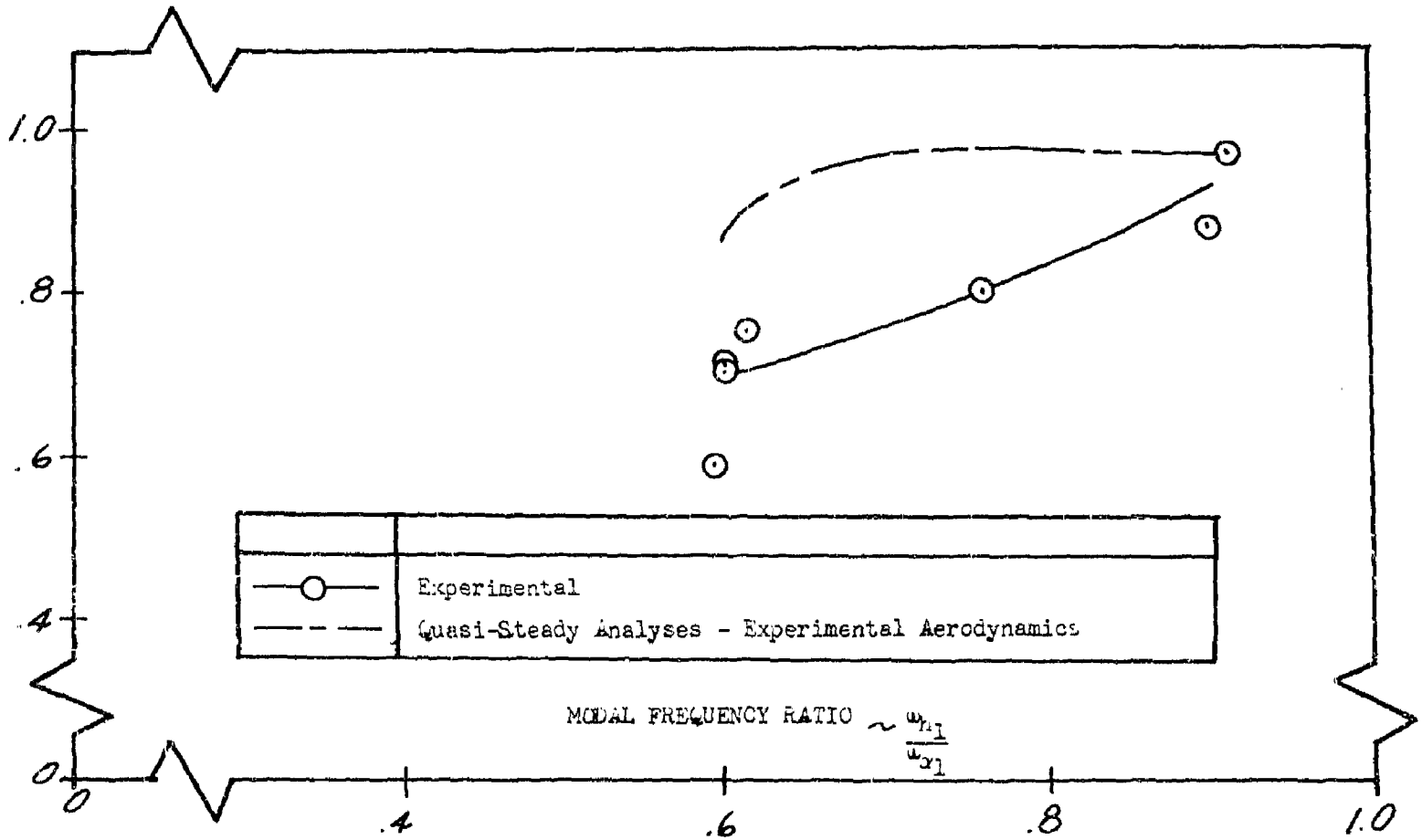

FIGURE 77 EXPERIMENTAL AND THEORETICAL, QUASI-STEADY (USING EXPERIMENTAL AERODYNAMICS) FLUTTER FREQUENCY RATIO VS. MODAL FREQUENCY RATIO AT MACH NUMBER = 6.0; BASIC PLANFORM, t/c = .06; $\alpha_o = 0°$

CONFIDENTIAL

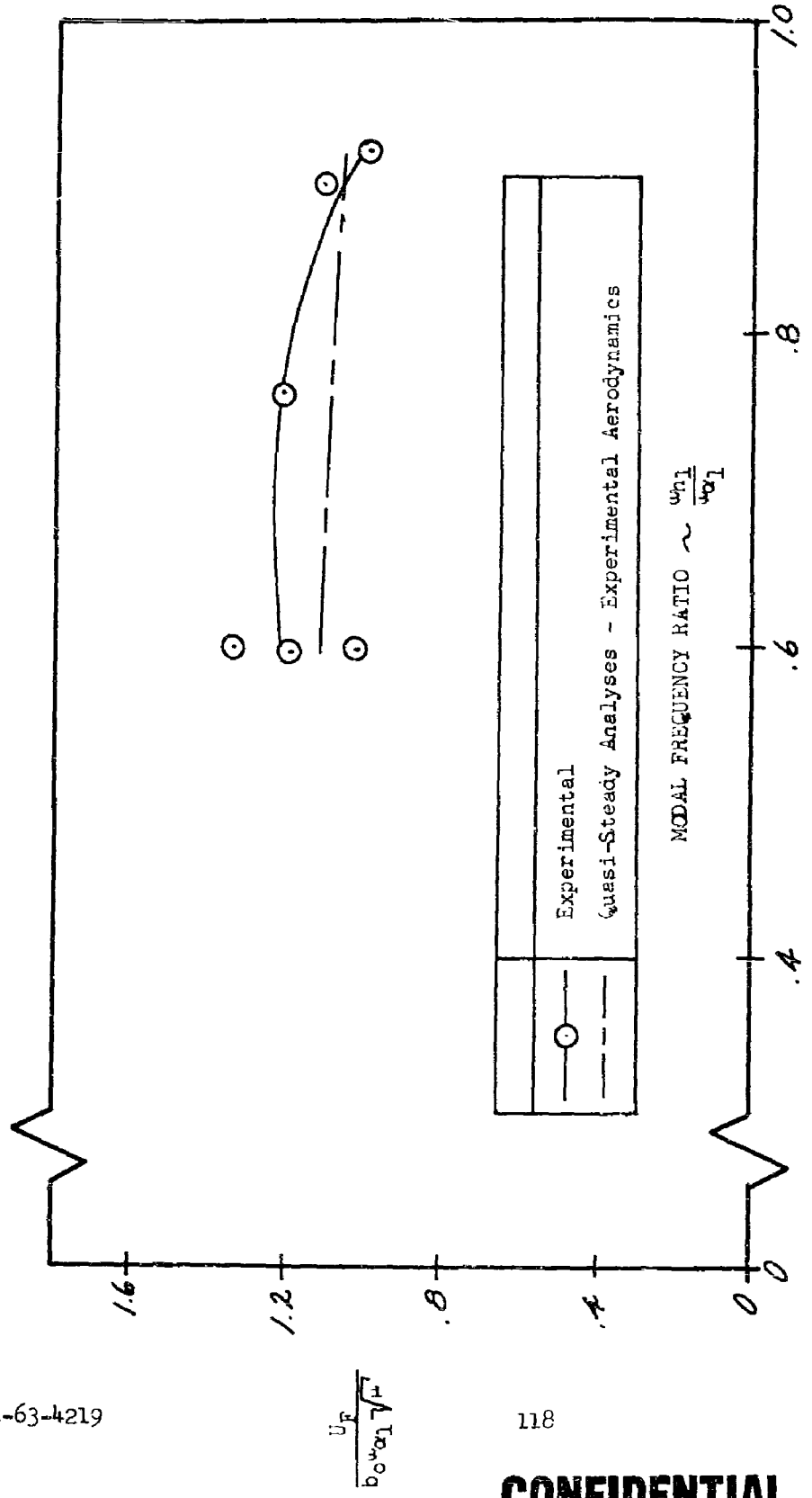

FIGURE 78 EXPERIMENTAL AND THEORETICAL, QUASI-STEADY (USING EXPERIMENTAL AERODYNAMICS) FLUTTER VELOCITY PARAMETER VS. MODAL FREQUENCY RATIO AT MACH NUMBER = 8.0; BASIC PLANFORM, t/c = .06, $\alpha_o = 0°$

CONFIDENTIAL

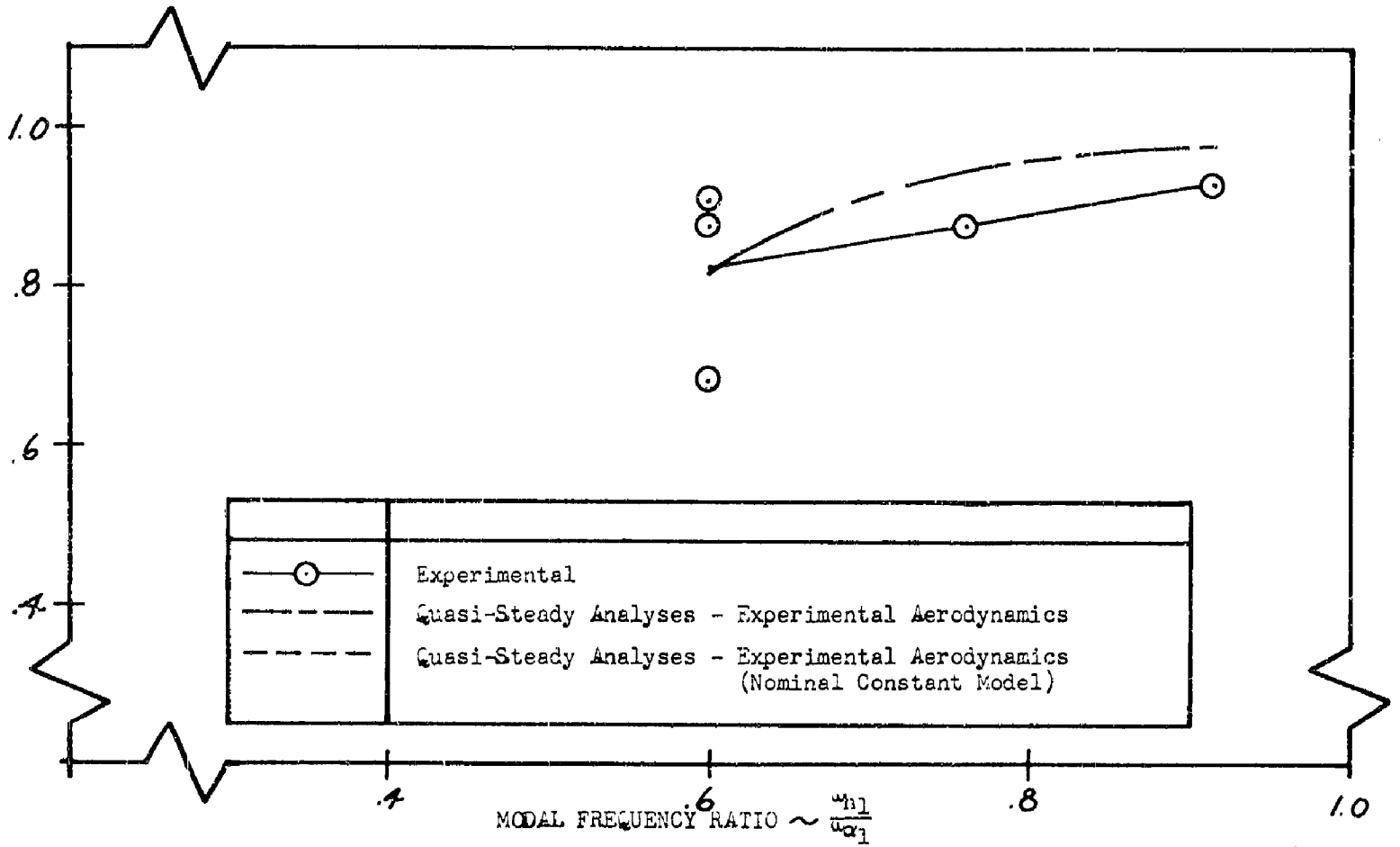

FIGURE 79 EXPERIMENTAL AND THEORETICAL, QUASI-STEADY (USING EXPERIMENTAL AERODYNAMICS) FLUTTER FREQUENCY RATIO VS. MODAL FREQUENCY RATIO AT MACH NUMBER = 8.0; BASIC PLANFORM, t/c = .06, α_o = 0°

CONFIDENTIAL

CONFIDENTIAL

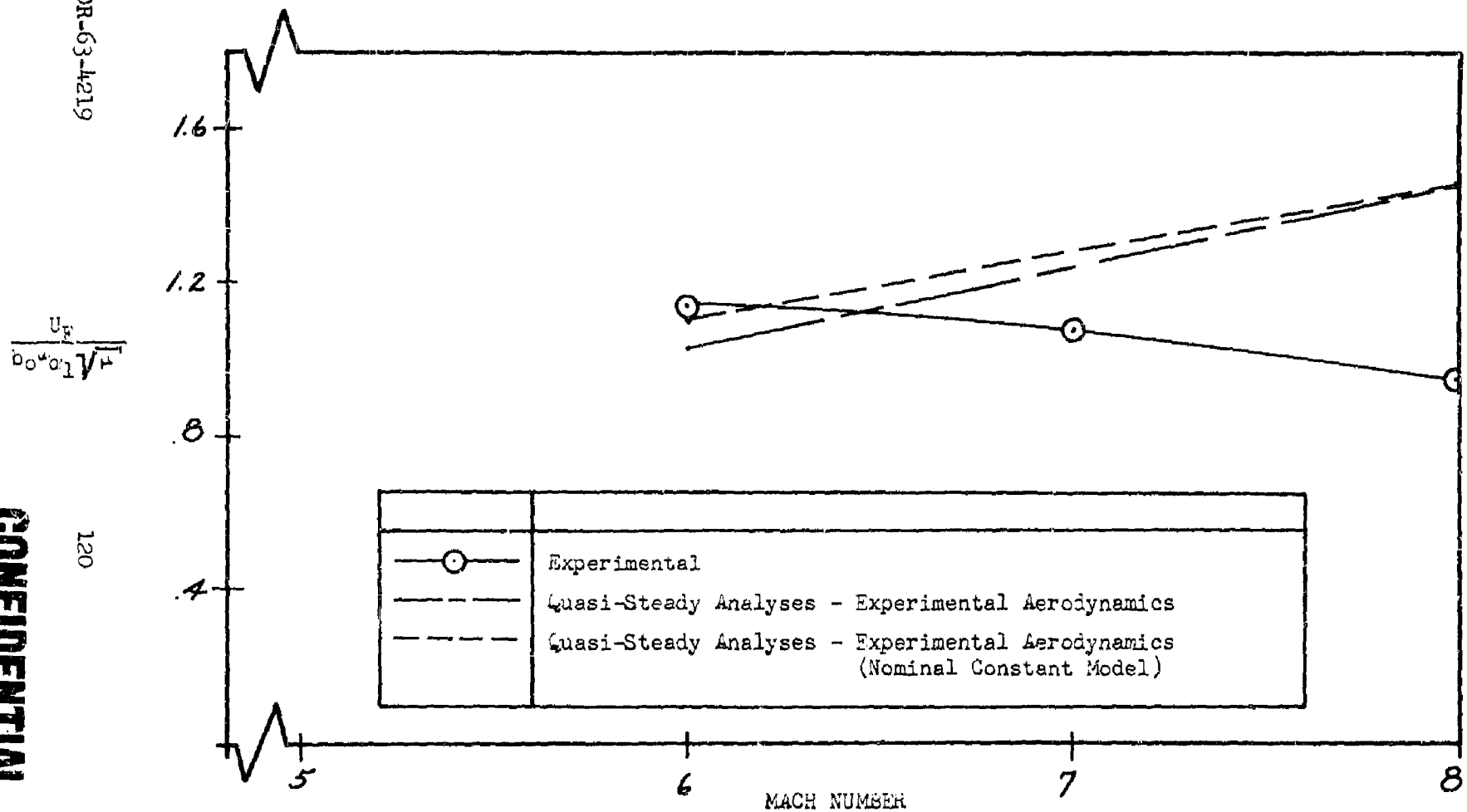

FIGURE 80 EXPERIMENTAL AND THEORETICAL, QUASI-STEADY (USING EXPERIMENTAL AERODYNAMICS) FLUTTER VELOCITY PARAMETER VS. MACH NUMBER; BASIC PLANFORM, t/c = .09, $\omega_{h_1}/\omega_{\alpha_1}$ = .60; α_0 = 0°

CONFIDENTIAL

CONFIDENTIAL

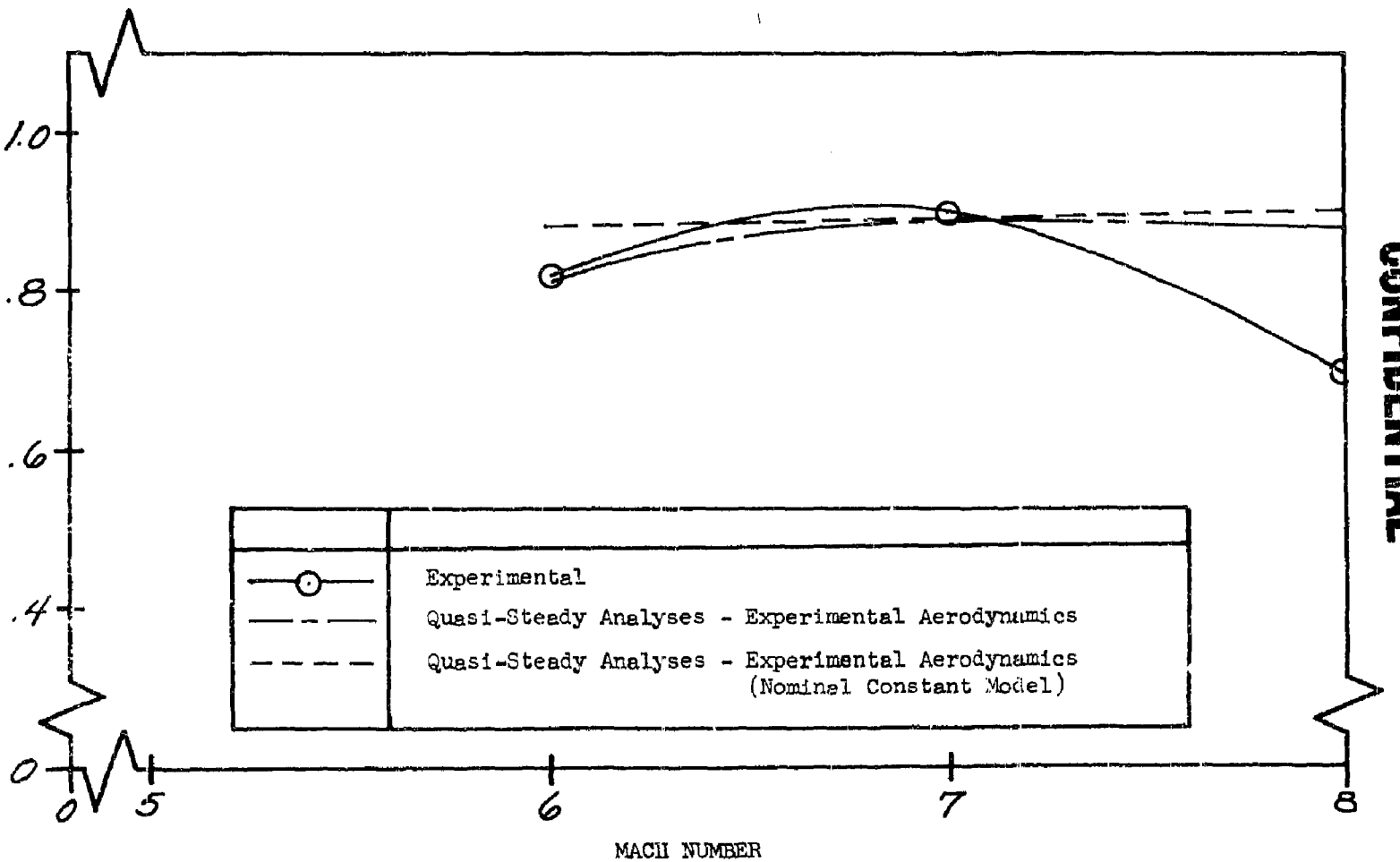

FIGURE 81 EXPERIMENTAL AND THEORETICAL, QUASI-STEADY (USING EXPERIMENTAL AERODYNAMICS) FLUTTER FREQUENCY RATIO VS. MACH NUMBER; BASIC PLANFORM, t/c = .09, $\omega_{h_1}/\omega_{\alpha_1}$ = .60; α_0 = 0°

CONFIDENTIAL

CONFIDENTIAL

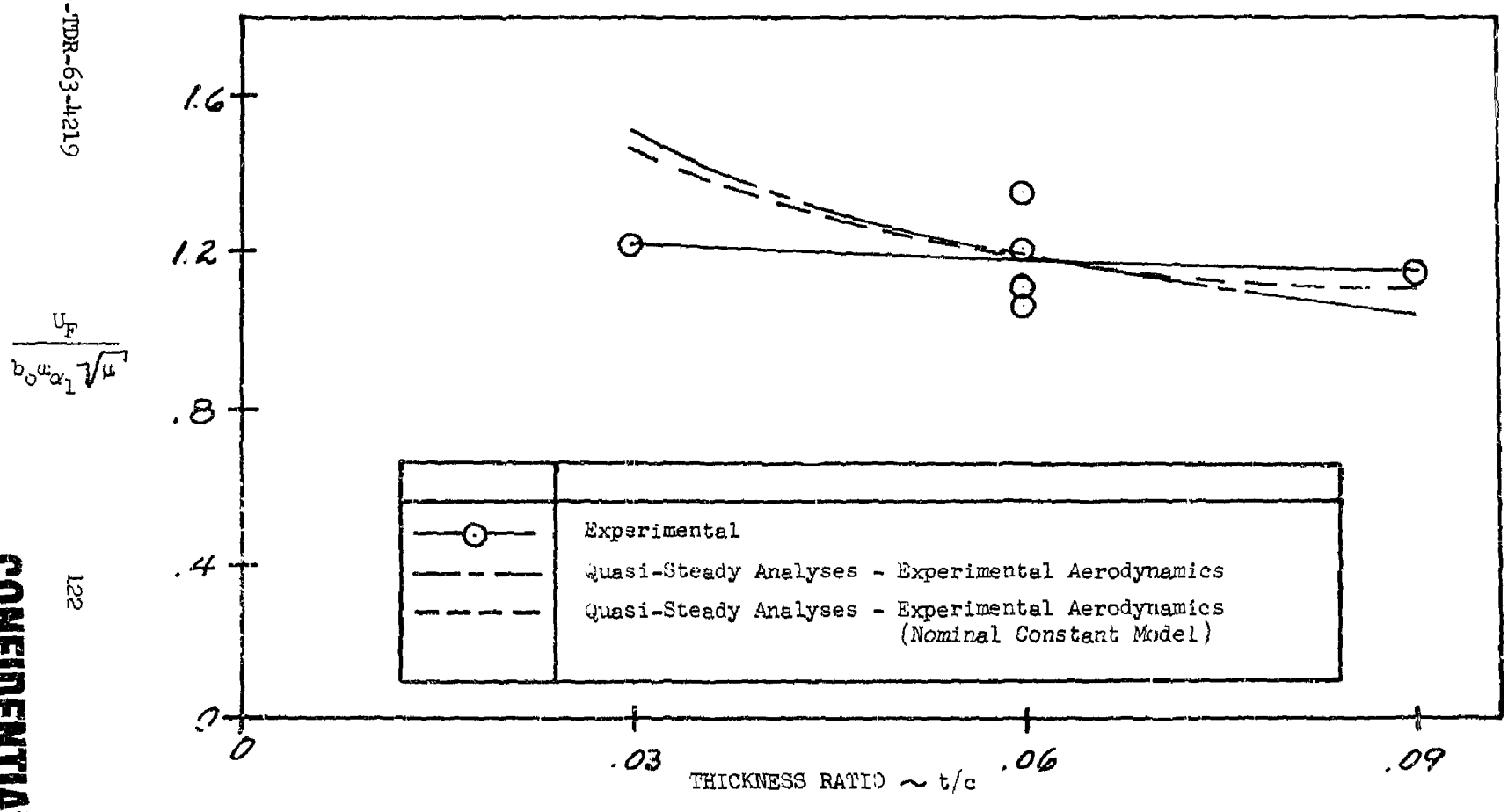

FIGURE 82 EXPERIMENTAL AND THEORETICAL, QUASI-STEADY (USING EXPERIMENTAL AERODYNAMICS) FLUTTER VELOCITY PARAMETER VS. THICKNESS RATIO AT MACH NUMBER = 6.0; BASIC PLANFORM, $\omega_{h_1}/\omega_{\alpha_1}$ = .60; $\alpha_0 = 0°$

CONFIDENTIAL

CONFIDENTIAL

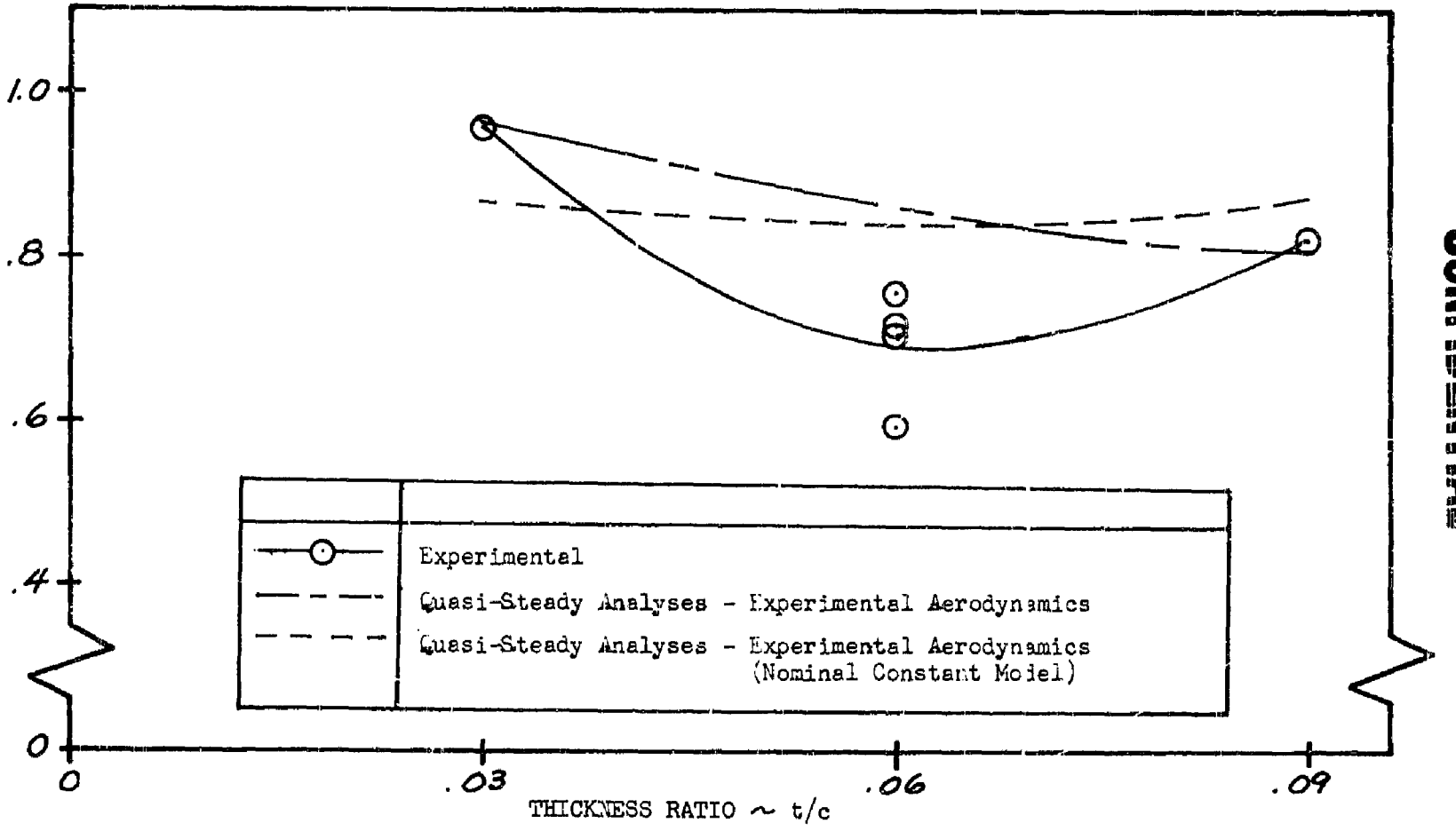

FIGURE 83 EXPERIMENTAL AND THEORETICAL, QUASI-STEADY (USING EXPERIMENTAL AERODYNAMICS) FLUTTER FREQUENCY RATIO VS. THICKNESS RATIO AT MACH NUMBER = 6.0; BASIC PLANFORM, ω_h/ω_α = .60; α_o = 0°

CONFIDENTIAL

CONFIDENTIAL

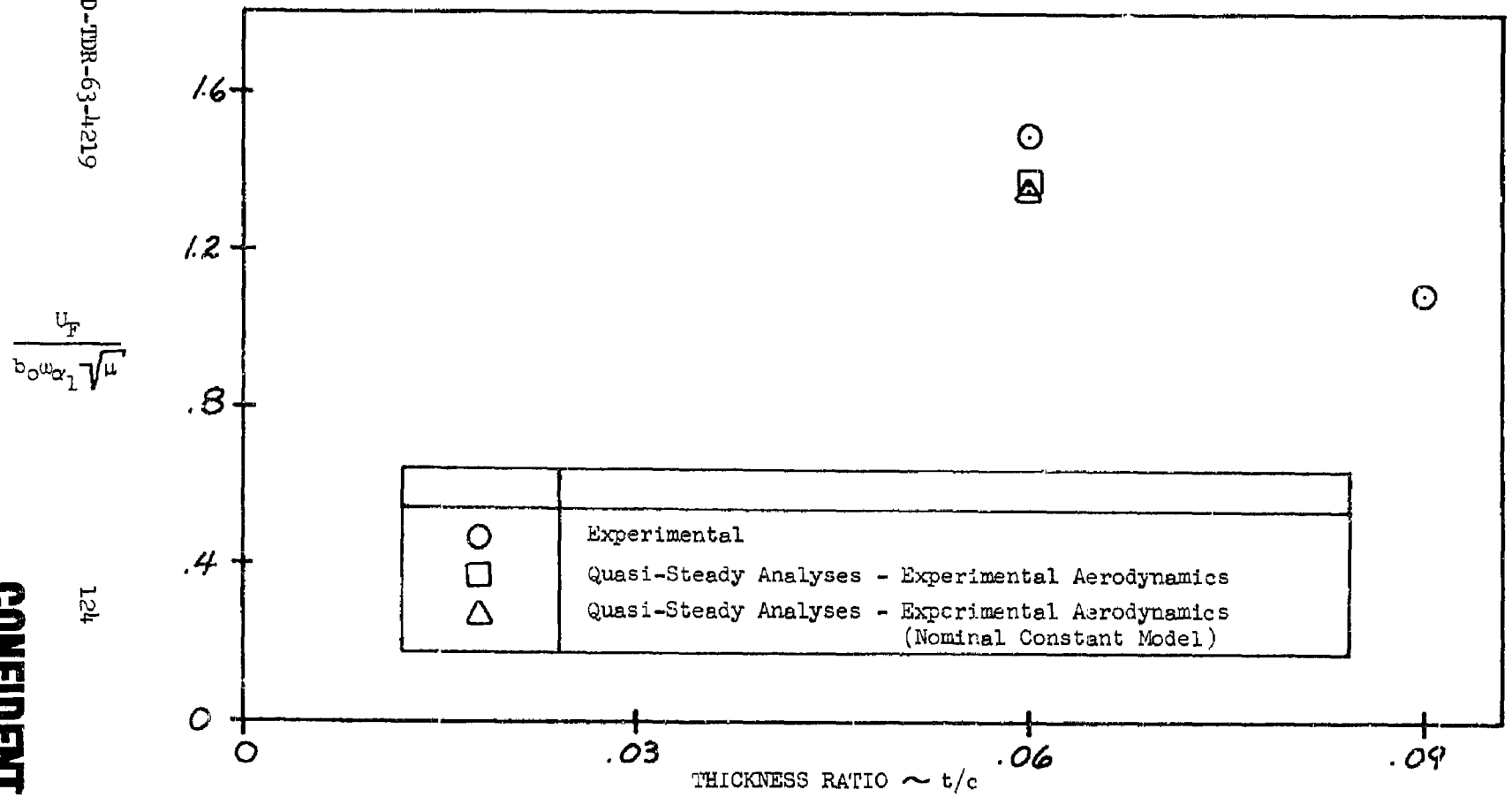

FIGURE 84 EXPERIMENTAL AND THEORETICAL, QUASI-STEADY (USING EXPERIMENTAL AERODYNAMICS) FLUTTER VELOCITY PARAMETER VS. THICKNESS RATIO AT MACH NUMBER = 7.0; BASIC PLANFORM, $\omega_{h_1}/\omega_{\alpha_1}$ = .60; $\alpha_o = 0°$

CONFIDENTIAL

CONFIDENTIAL

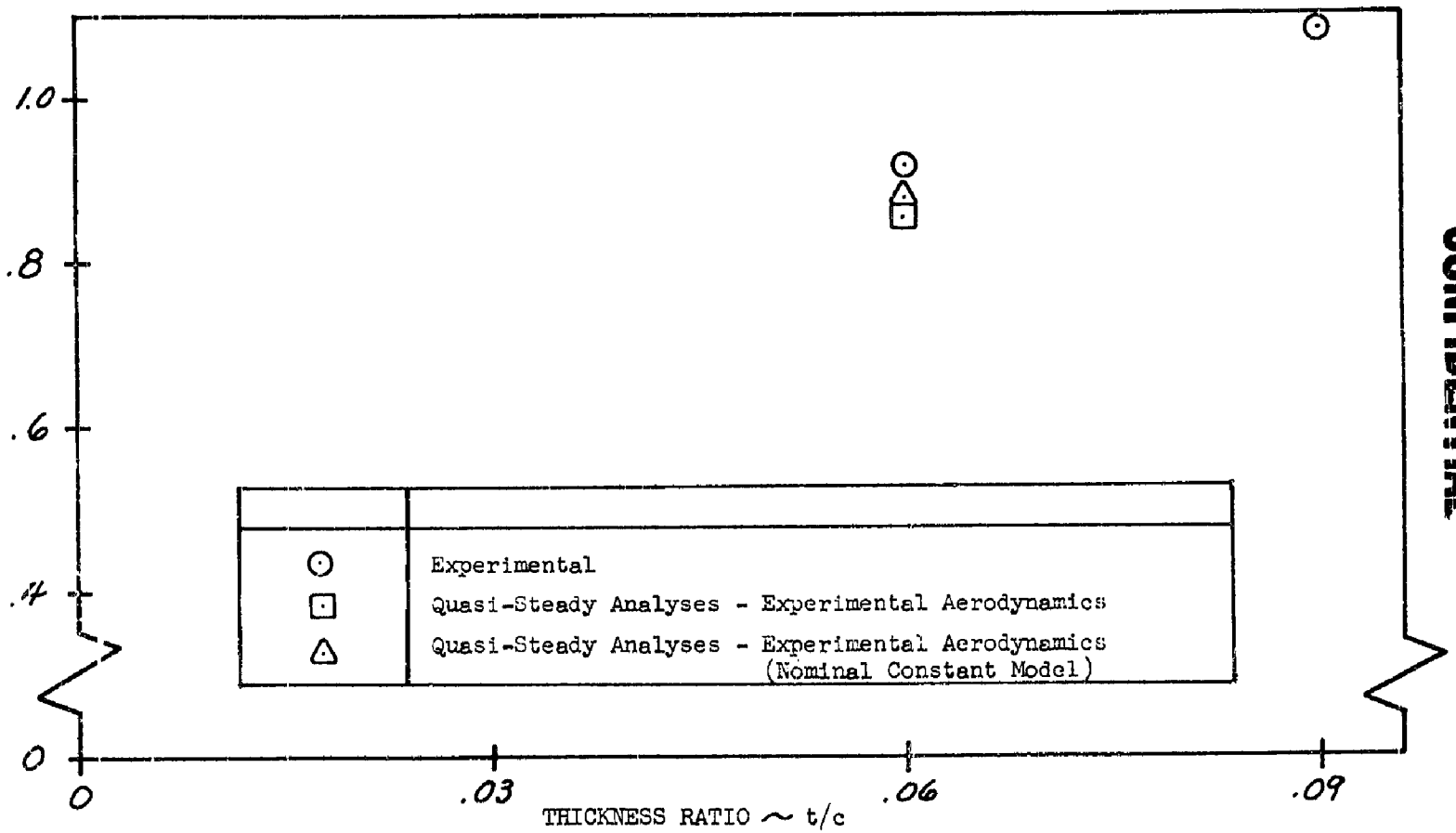

FIGURE 85 EXPERIMENTAL AND THEORETICAL, QUASI-STEADY (USING EXPERIMENTAL AERODYNAMICS) FLUTTER FREQUENCY RATIO VS. THICKNESS RATIO AT MACH NUMBER = 7.0, BASIC PLANFORM, $\omega_{h_1}/\omega_{\alpha_1}$ = .60; α_o = 0°

CONFIDENTIAL

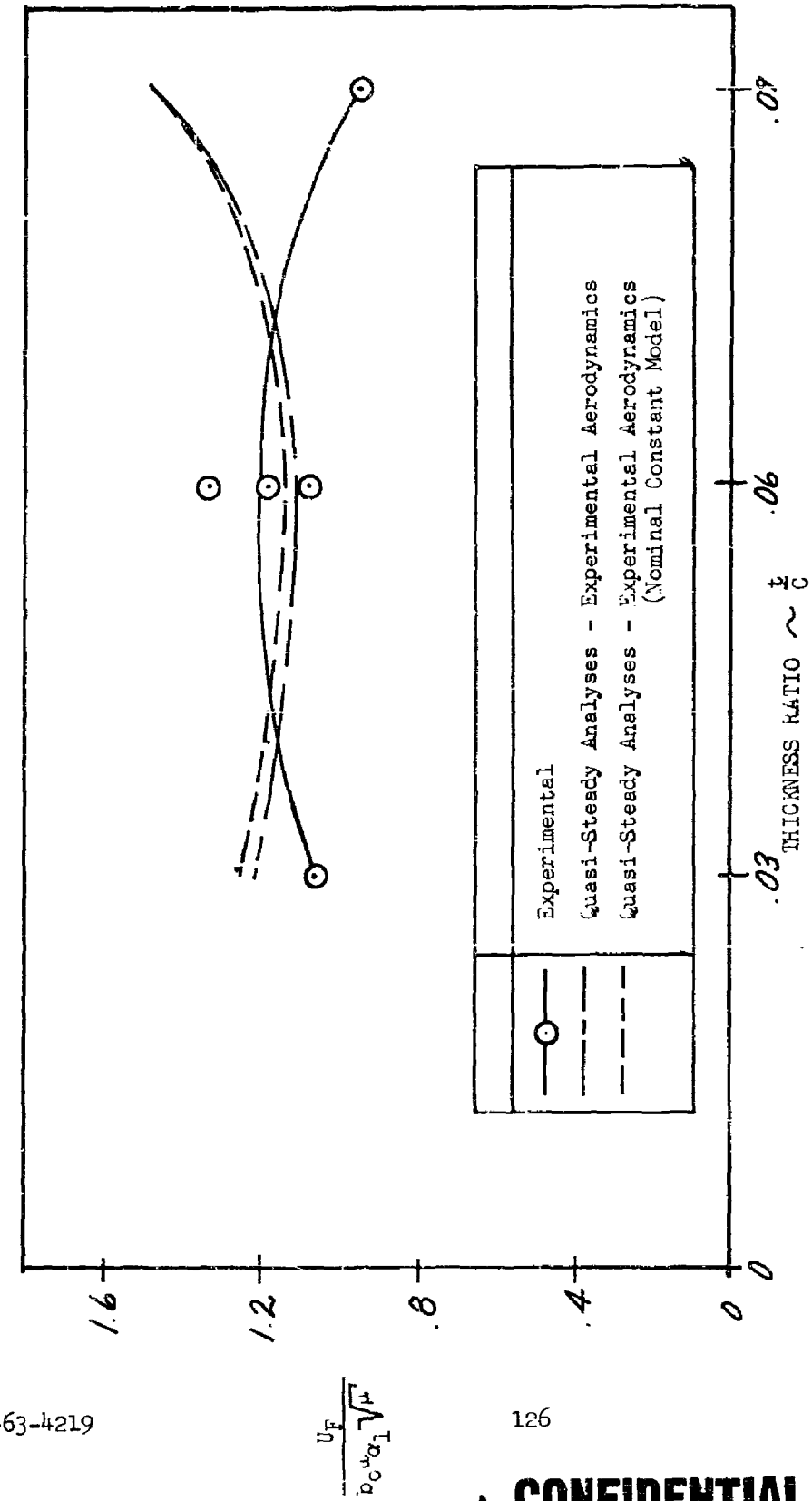

FIGURE 86 EXPERIMENTAL AND THEORETICAL, QUASI-STEADY (USING EXPERIMENTAL AERODYNAMICS) FLUTTER VELOCITY PARAMETER VS. THICKNESS RATIO AT MACH NUMBER = 8.0; BASIC PLANFORM, ω_h/ω_α, = .60; $\alpha_0 = 0°$

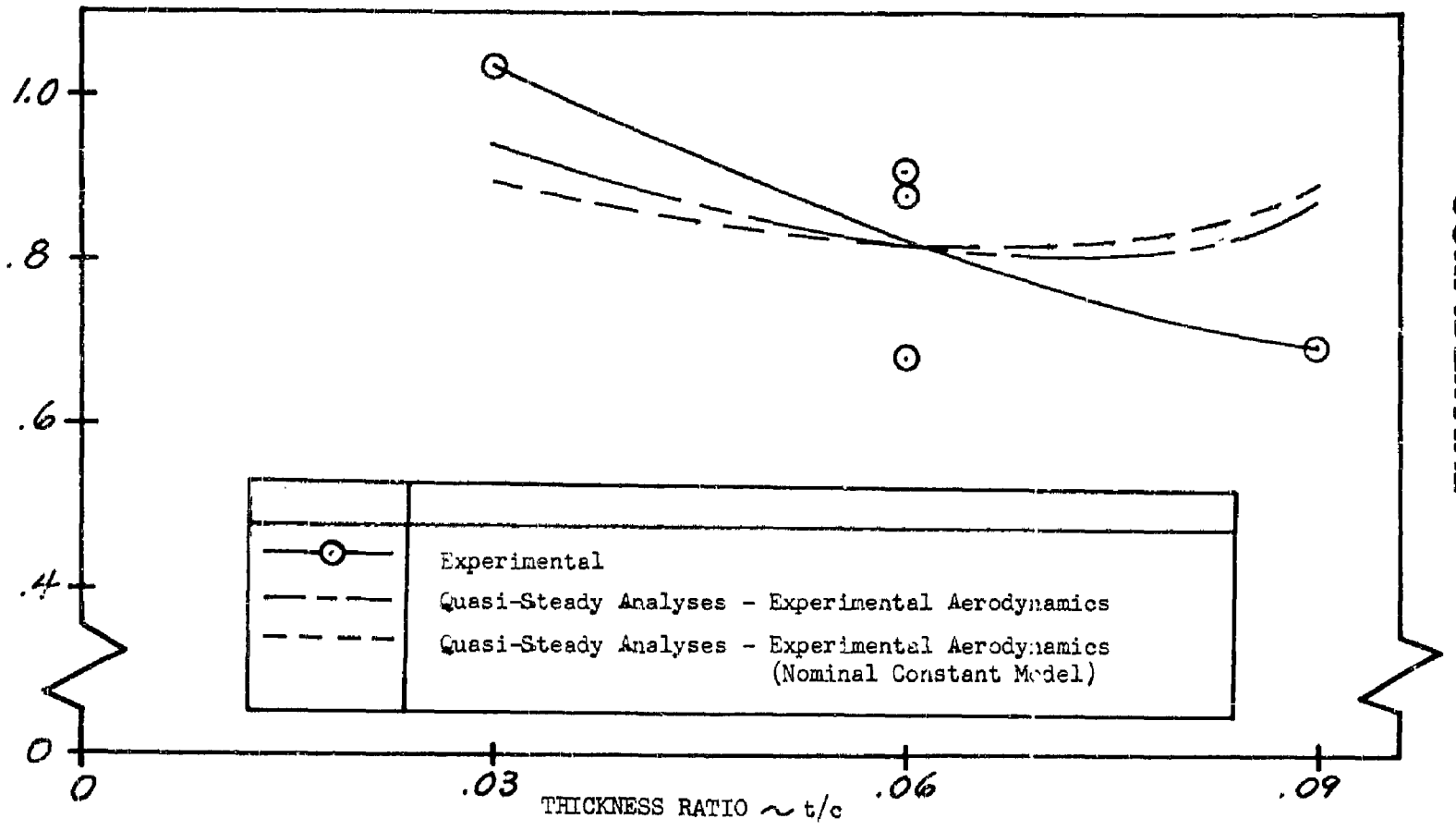

FIGURE 87 EXPERIMENTAL AND THEORETICAL, QUASI-STEADY (USING EXPERIMENTAL AERODYNAMICS) FLUTTER FREQUENCY RATIO VS. THICKNESS RATIO AT MACH NUMBER = 8.0; BASIC PLANFORM, ω_h/ω_α = .60; $\alpha_0 = 0°$

CONFIDENTIAL

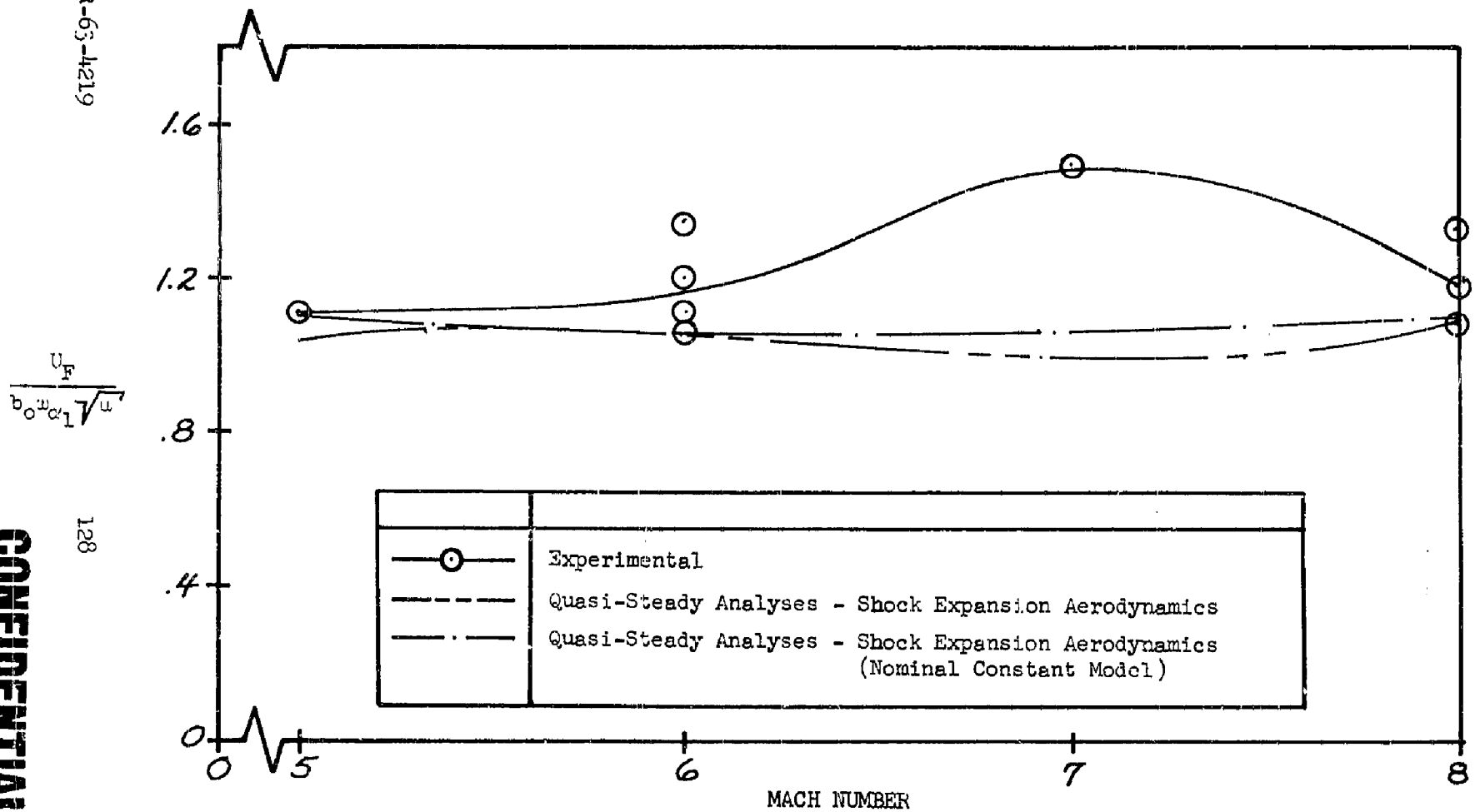

FIGURE 88 EXPERIMENTAL AND THEORETICAL, QUASI-STEADY (USING SHOCK-EXPANSION AERODYNAMICS) FLUTTER VELOCITY PARAMETER VS. MACH NUMBER; BASIC PLANFORM, t/c = .06, $\omega_{h_1}/\omega_{\alpha_1}$ = .60; α_o = 0°

CONFIDENTIAL

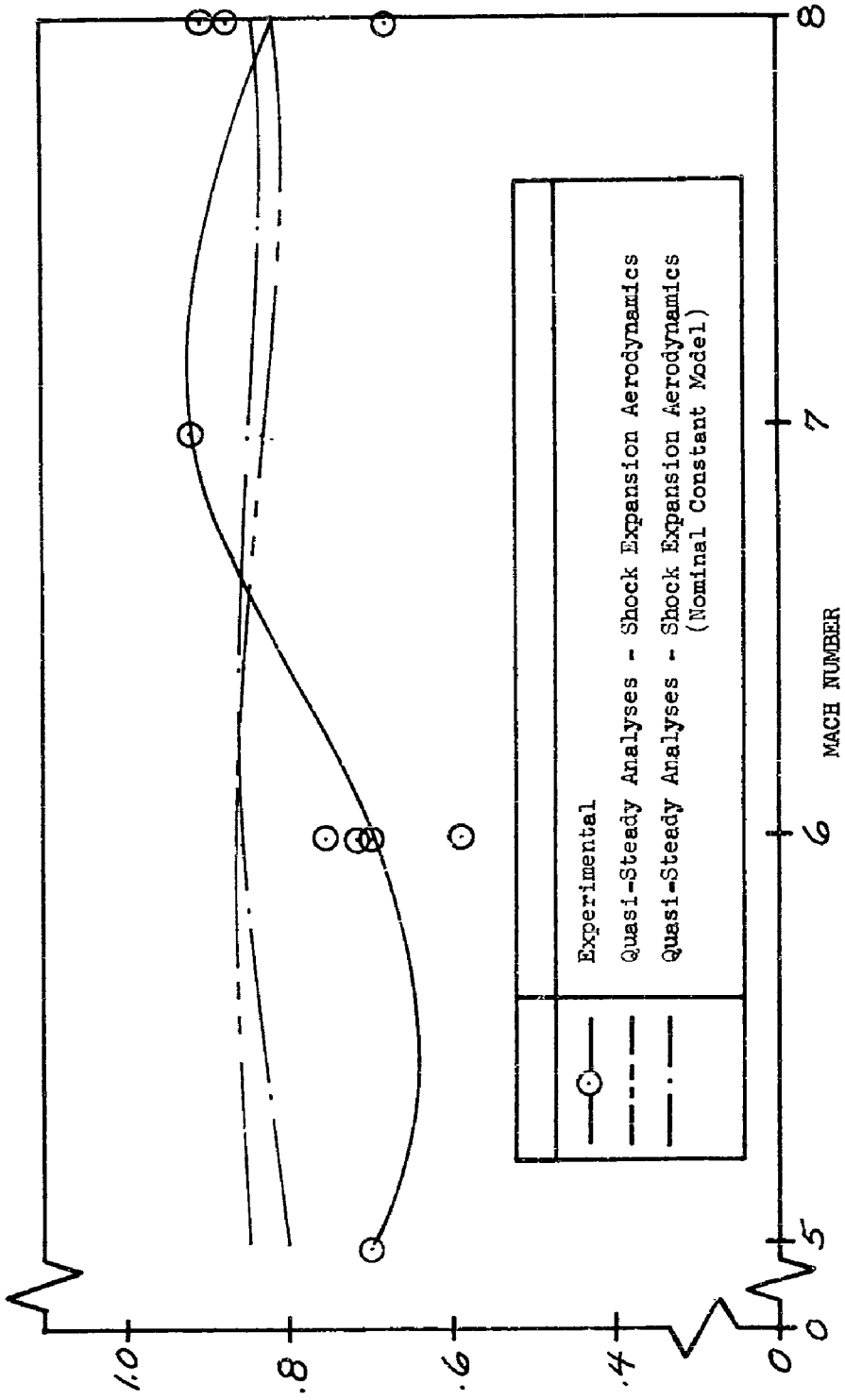

FIGURE 89 EXPERIMENTAL AND THEORETICAL, QUASI-STEADY (USING SHOCK-EXPANSION AERODYNAMICS) FLUTTER FREQUENCY RATIO VS. MACH NUMBER; BASIC PLANFORM, $t/c = .06$, $\omega_h/\omega_\alpha = .60$, $\alpha_o = 0°$

CONFIDENTIAL

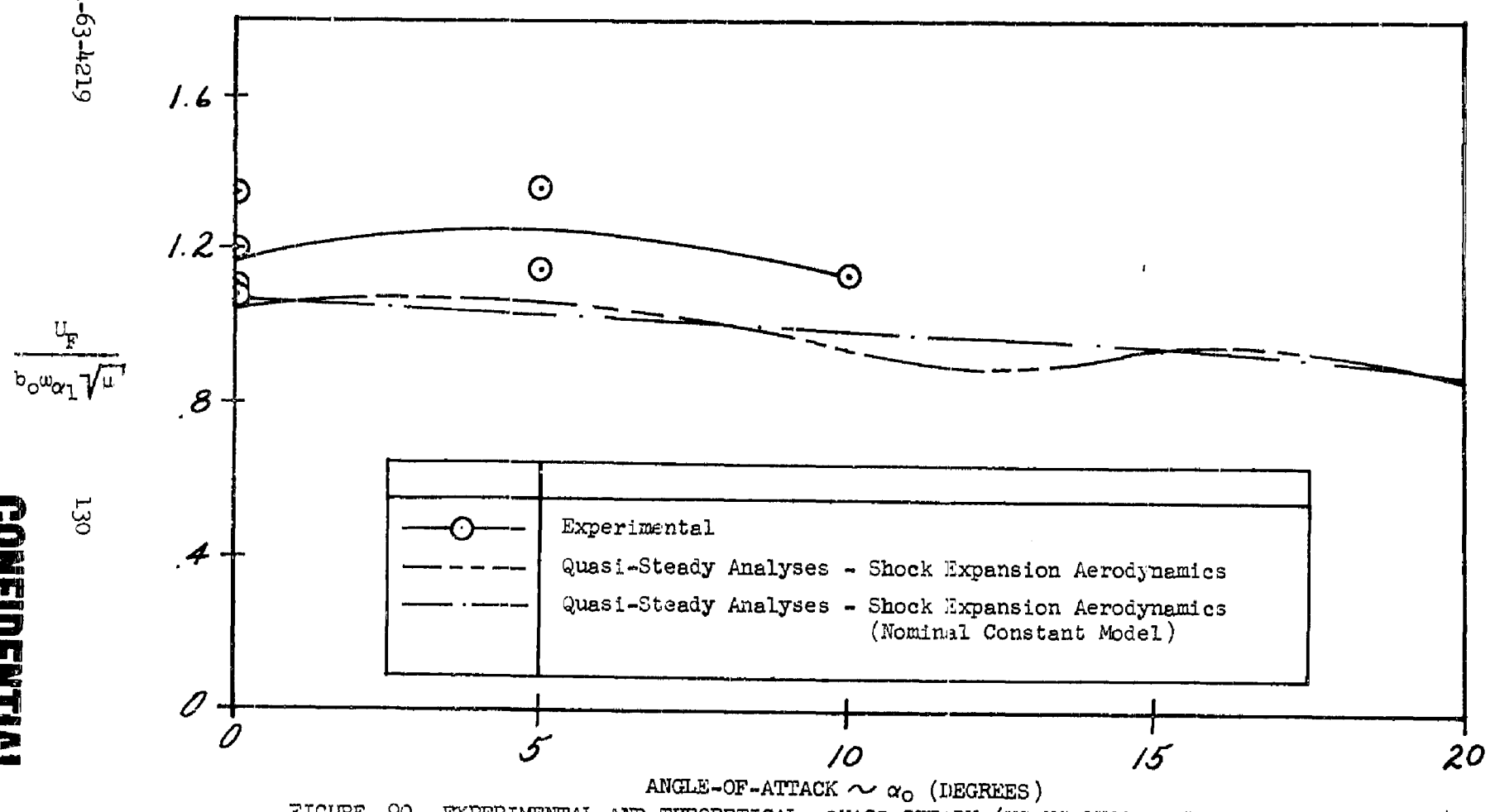

FIGURE 90 EXPERIMENTAL AND THEORETICAL, QUASI-STEADY (USING SHOCK-EXPANSION AERODYNAMICS) FLUTTER VELOCITY PARAMETER VS. ANGLE-OF-ATTACK AT MACH NUMBER = 6.0; BASIC PLANFORM, t/c = .06, $\omega_{h_1}/\omega_{\alpha_1}$ = .60

CONFIDENTIAL

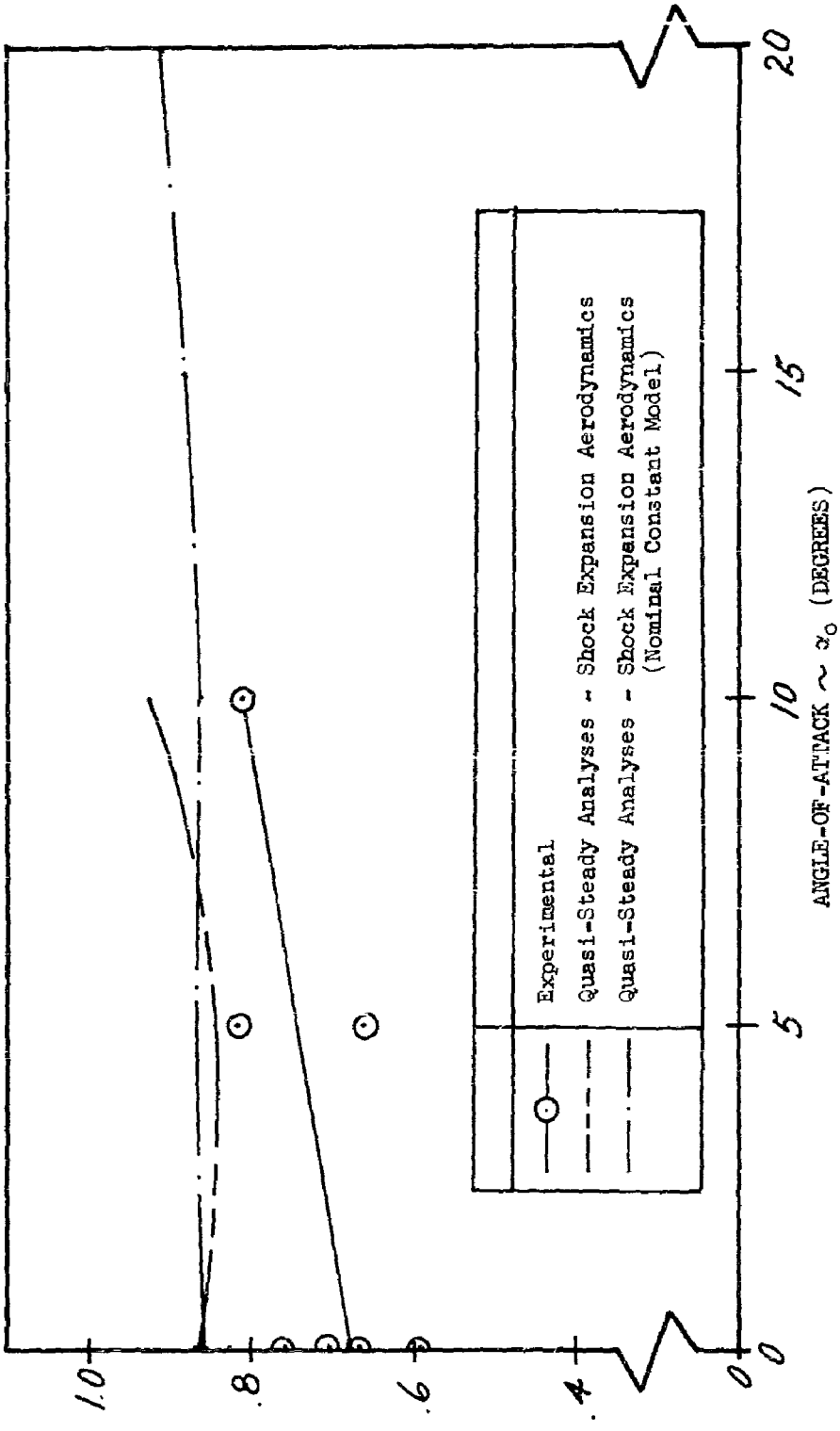

FIGURE 91 EXPERIMENTAL AND THEORETICAL, QUASI-STEADY (USING SHOCK-EXPANSION AERODYNAMICS) FLUTTER FREQUENCY RATIO VS. ANGLE-OF-ATTACK AT MACH NUMBER = 6.0; BASIC PLANFORM, t/c = .06, ω_h/ω_α = .60

CONFIDENTIAL

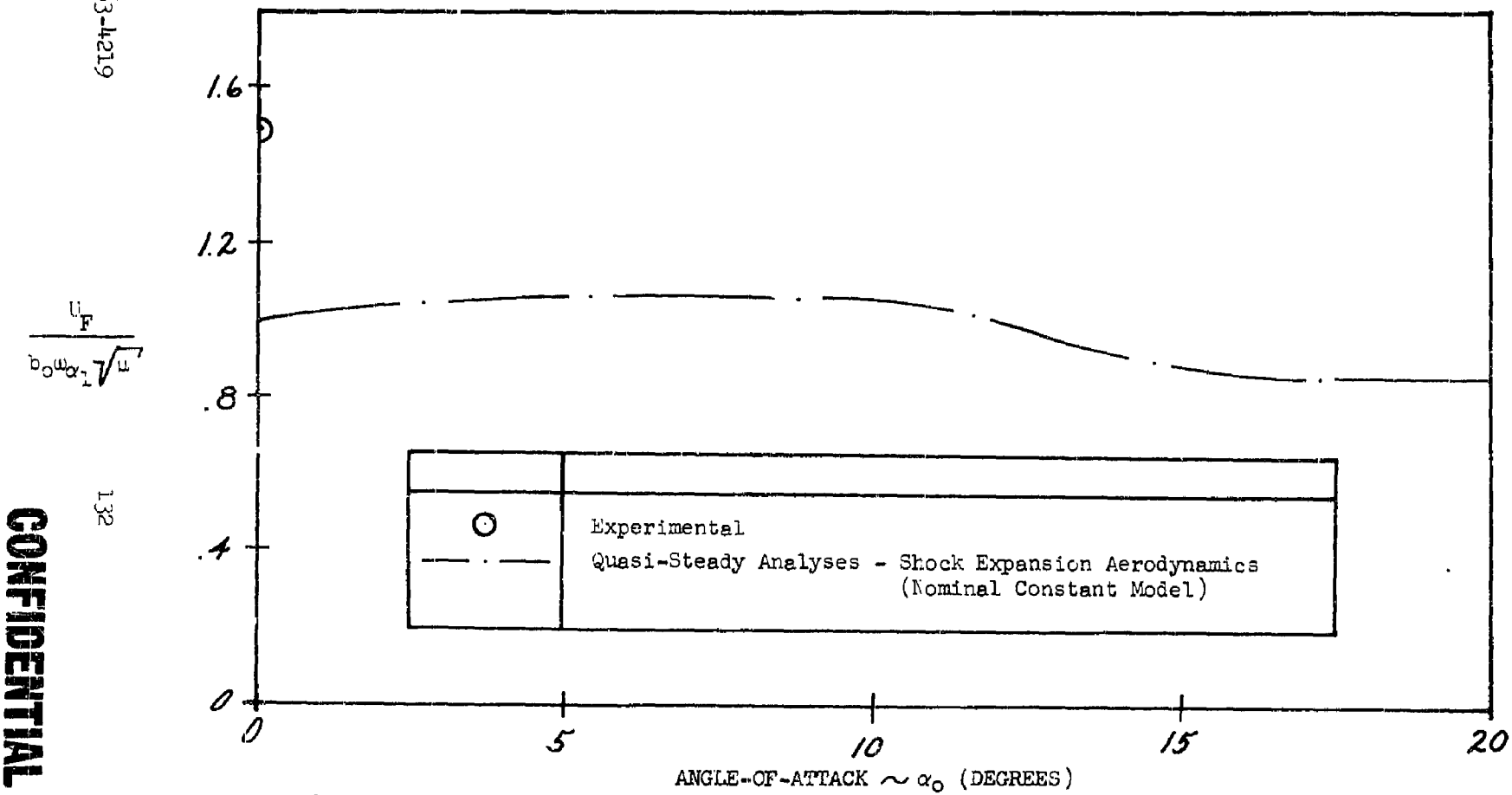

FIGURE 92 THEORETICAL, QUASI-STEADY (USING SHOCK-EXPANSION AERODYNAMICS) FLUTTER VELOCITY PARAMETER VS. ANGLE-OF-ATTACK AT MACH NUMBER = 7.0; BASIC PLANFORM, NOMINAL MODEL, t/c = .06, $\omega_{h_1}/\omega_{\alpha_1}$ = .60

CONFIDENTIAL

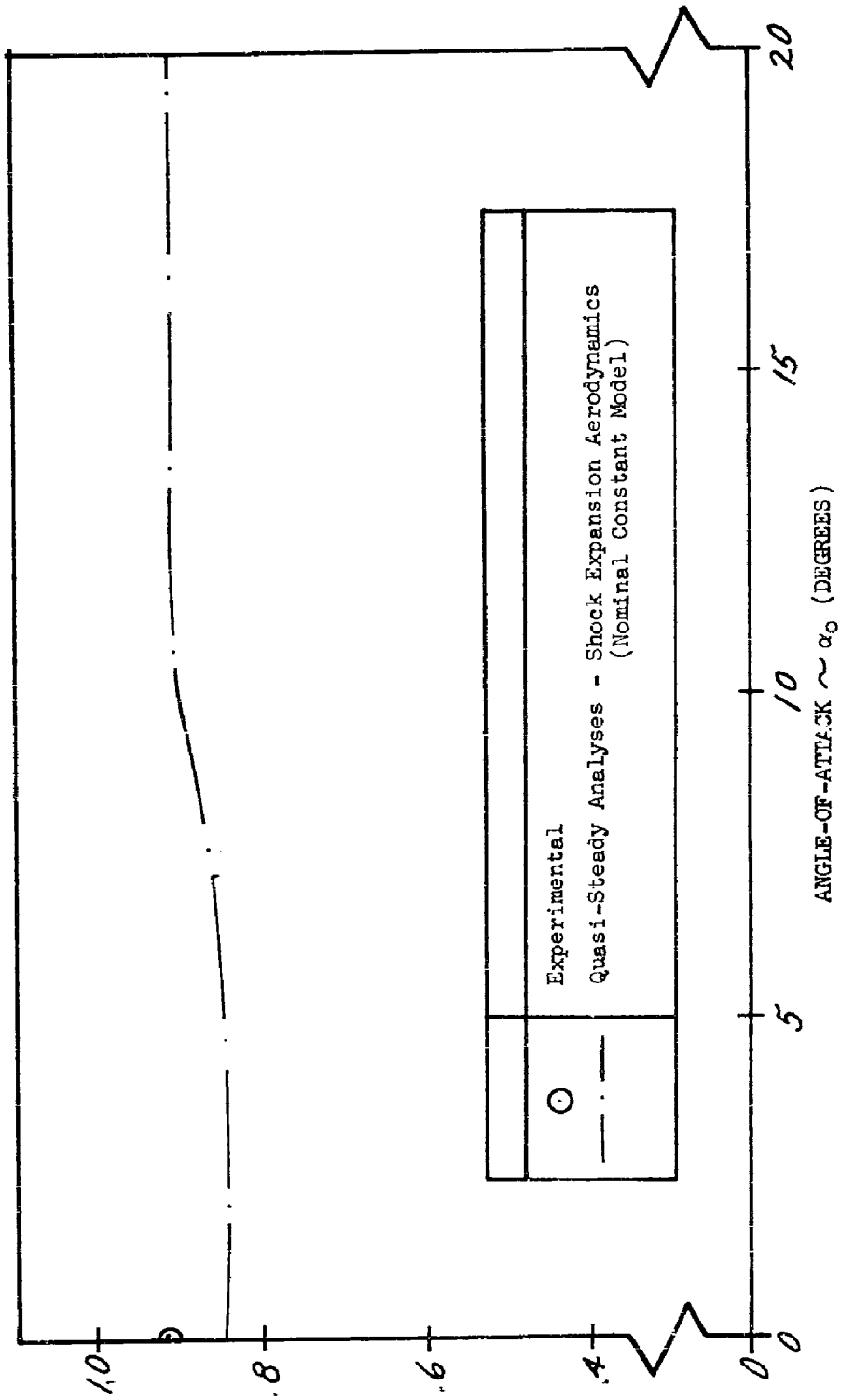

FIGURE 93 THEORETICAL, QUASI-STEADY (USING SHOCK-EXPANSION AERODYNAMICS) FLUTTER FREQUENCY RATIO VS. ANGLE-OF-ATTACK AT MACH NUMBER = 7.0; BASIC PLANFORM, t/c = .06, ω_h/ω_α = .60

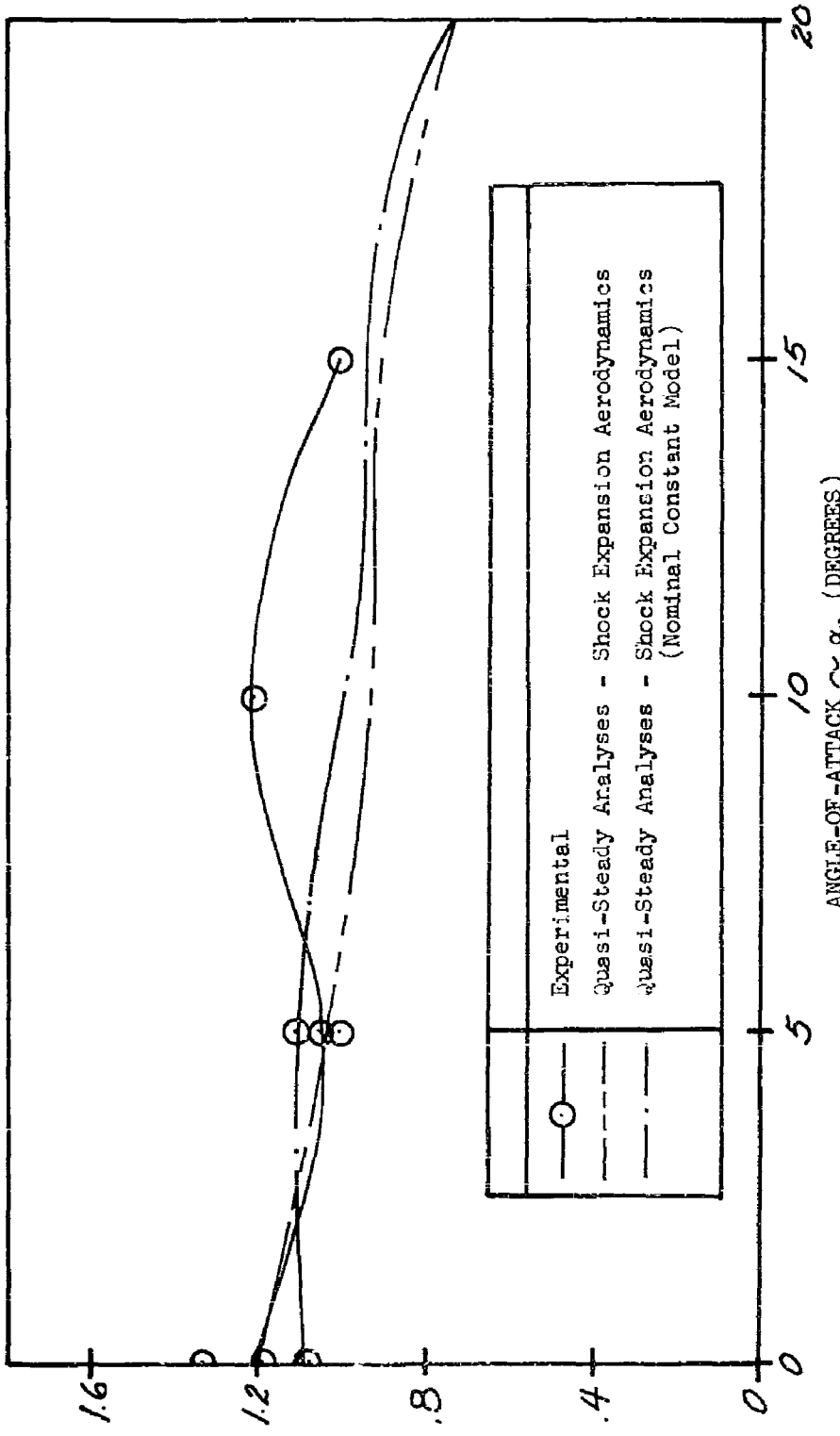

FIGURE 94 EXPERIMENTAL AND THEORETICAL, QUASI-STEADY (USING SHOCK-EXPANSION AERODYNAMICS) FLUTTER VELOCITY PARAMETER VS. ANGLE-OF-ATTACK AT MACH NUMBER = 8.0; BASIC PLANFORM, t/c = .06, ω_h/ω_α = .60

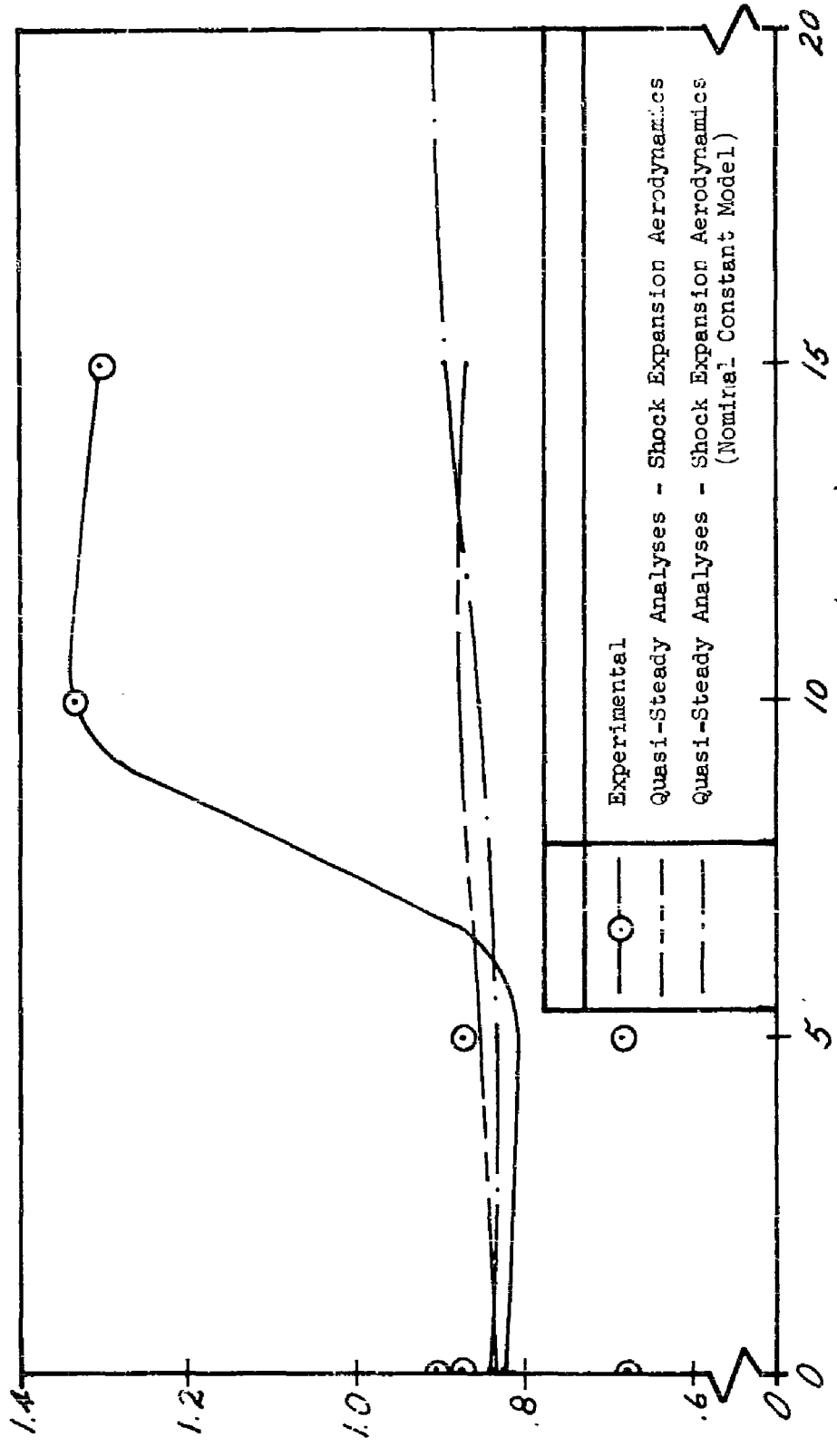

FIGURE 95 EXPERIMENTAL AND THEORETICAL, QUASI-STEADY (USING SHOCK-EXPANSION AERODYNAMICS) FLUTTER FREQUENCY RATIO VS. ANGLE-OF-ATTACK AT MACH NUMBER = 8.0; BASIC PLANFORM, $t/c = .06$, $\omega_h/\omega_\alpha = .60$

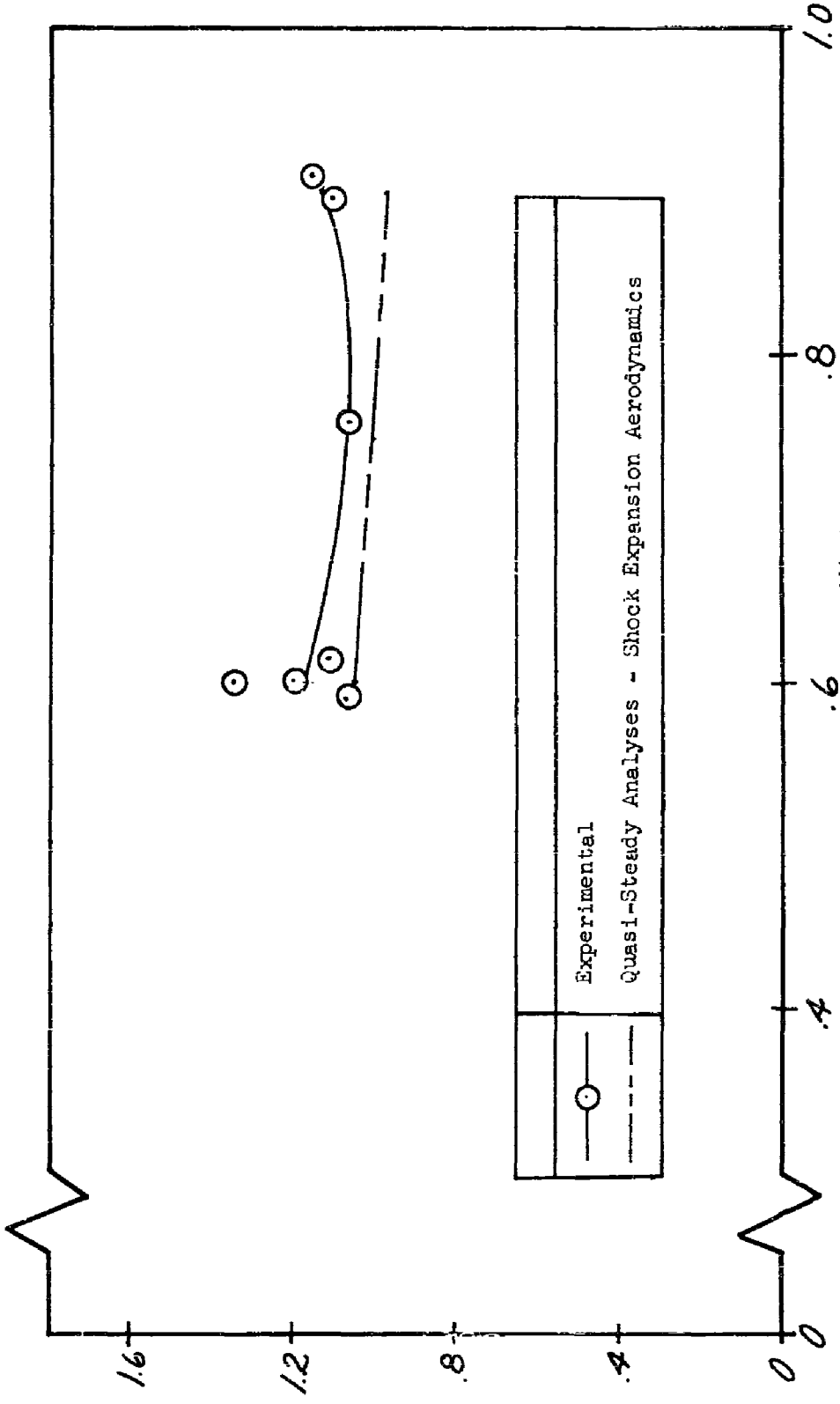

FIGURE 96 EXPERIMENTAL AND THEORETICAL, QUASI-STEADY (USING SHOCK-EXPANSION AERODYNAMICS) FLUTTER VELOCITY PARAMETER VS. MODAL FREQUENCY RATIO AT MACH NUMBER = 6.0; BASIC PLANFORM, t/c = .06, $\alpha_0 = 0°$

CONFIDENTIAL

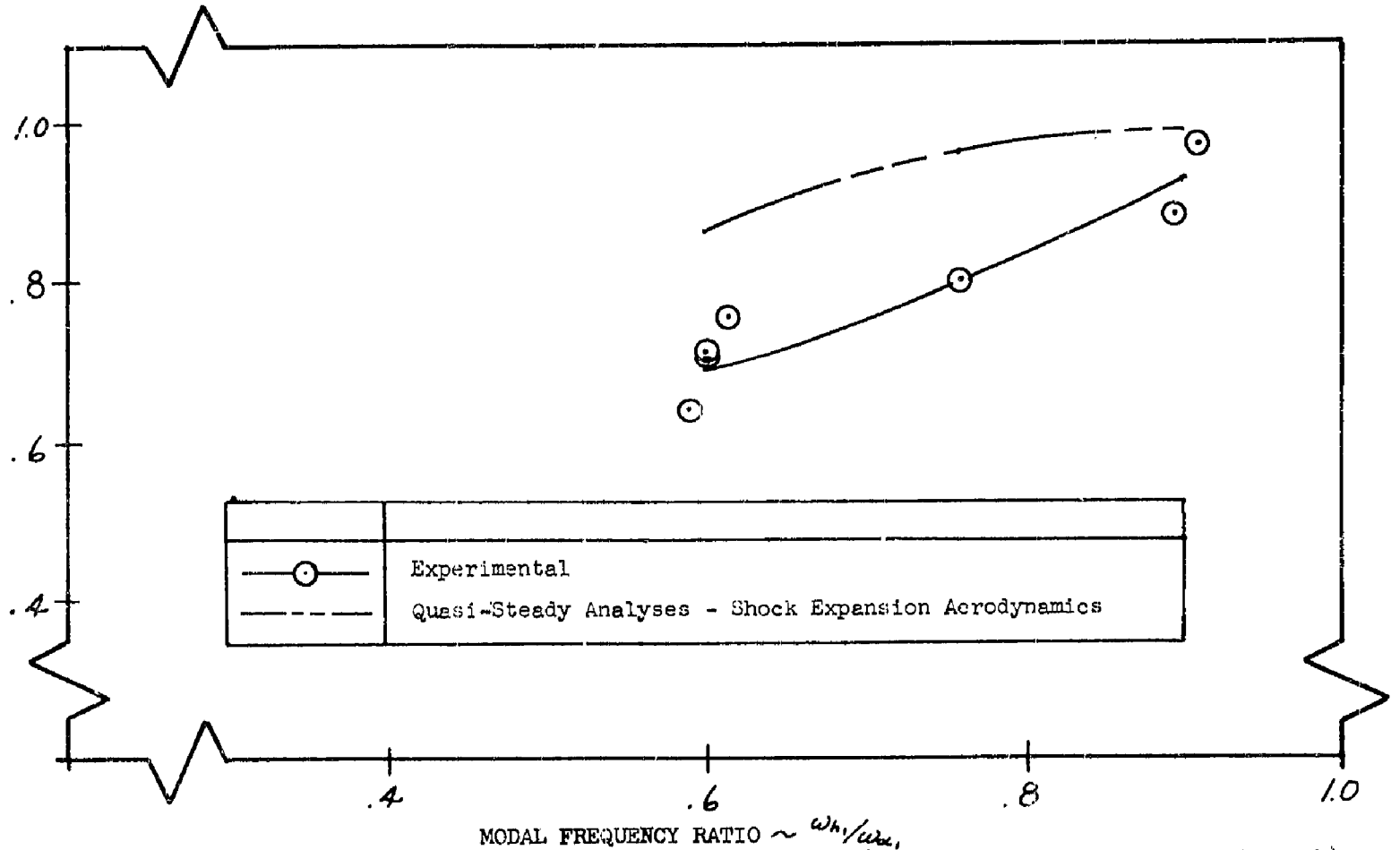

FIGURE 97 EXPERIMENTAL AND THEORETICAL, QUASI-STEADY (USING SHOCK-EXPANSION AERODYNAMICS) FLUTTER FREQUENCY RATIO VS. MODAL FREQUENCY RATIO AT MACH NUMBER = 6.0; BASIC PLANFORM, t/c = .06, $\alpha_o = 0°$

CONFIDENTIAL

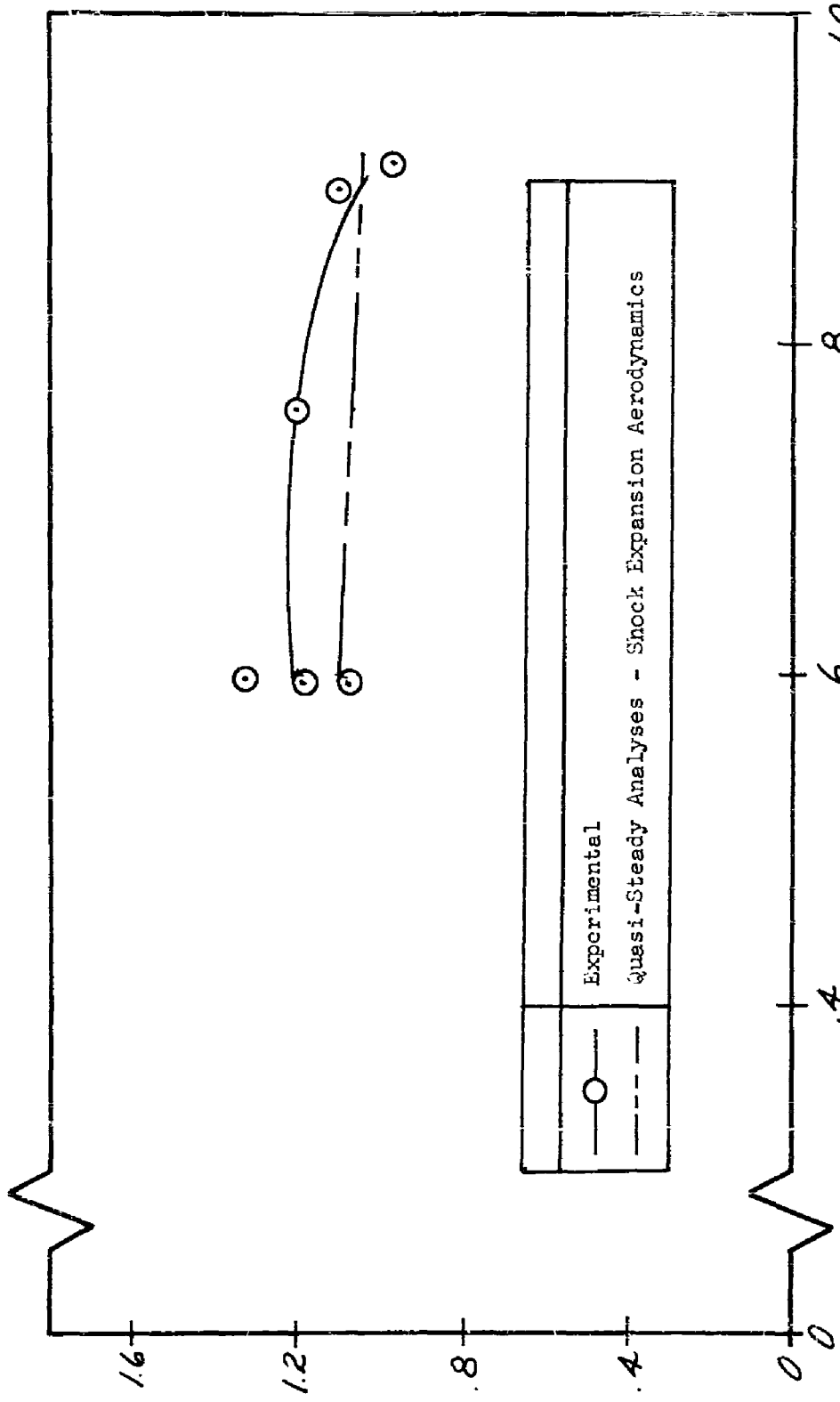

FIGURE 98 EXPERIMENTAL AND THEORETICAL, QUASI-STEADY (USING SHOCK-EXPANSION AERODYNAMICS) FLUTTER VELOCITY PARAMETER VS. MODAL FREQUENCY RATIO AT MACH NUMBER = 8.0; BASIC PLANFORM; t/c = .06, $\alpha_0 = 0°$

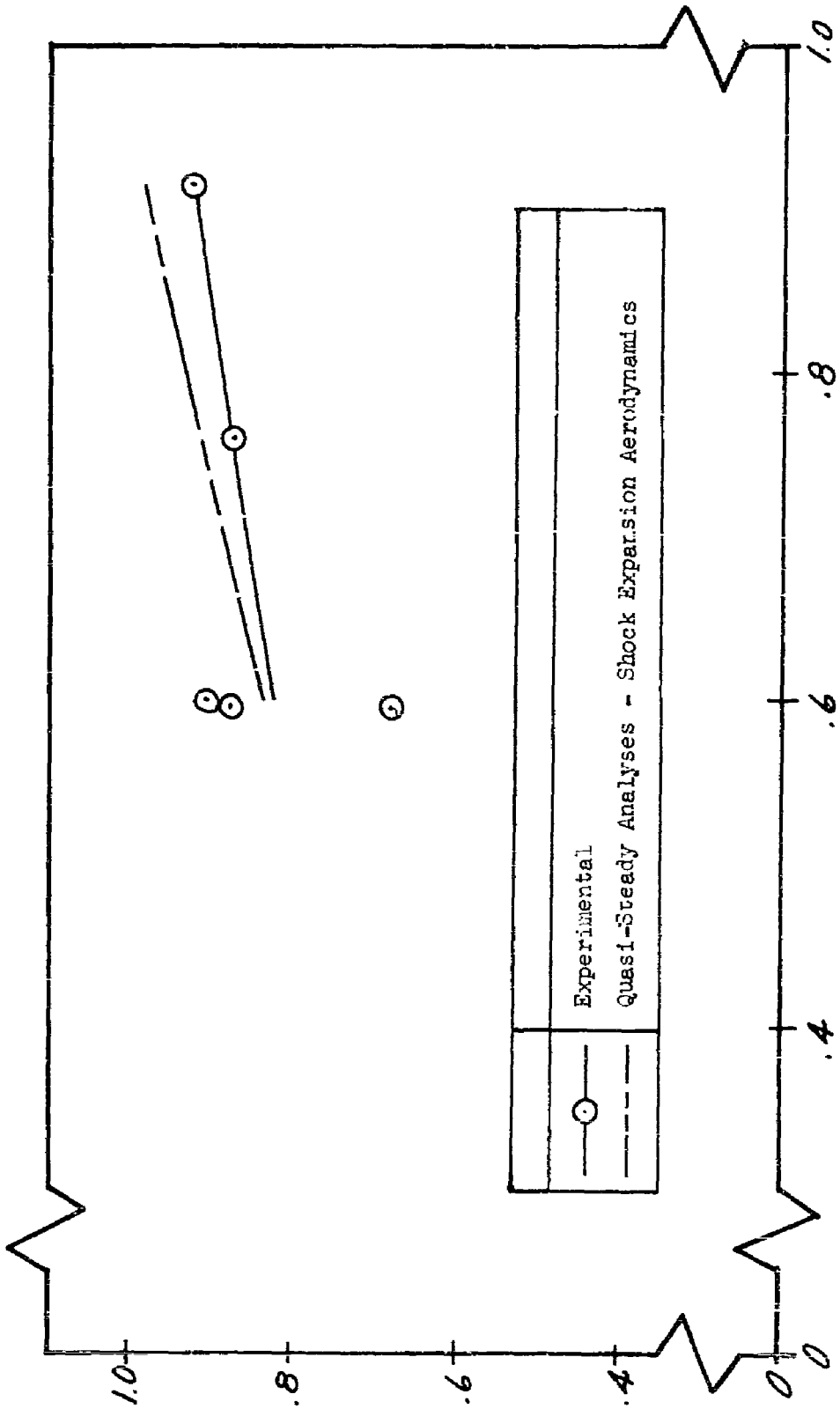

FIGURE 99 EXPERIMENTAL AND THEORETICAL, QUASI-STEADY (USING SHOCK-EXPANSION AERODYNAMICS) FLUTTER FREQUENCY RATIO VS. MODAL FREQUENCY RATIO AT MACH NUMBER = 8.0; BASIC PLANFORM, t/c = .06, α_0 = 0°

CONFIDENTIAL

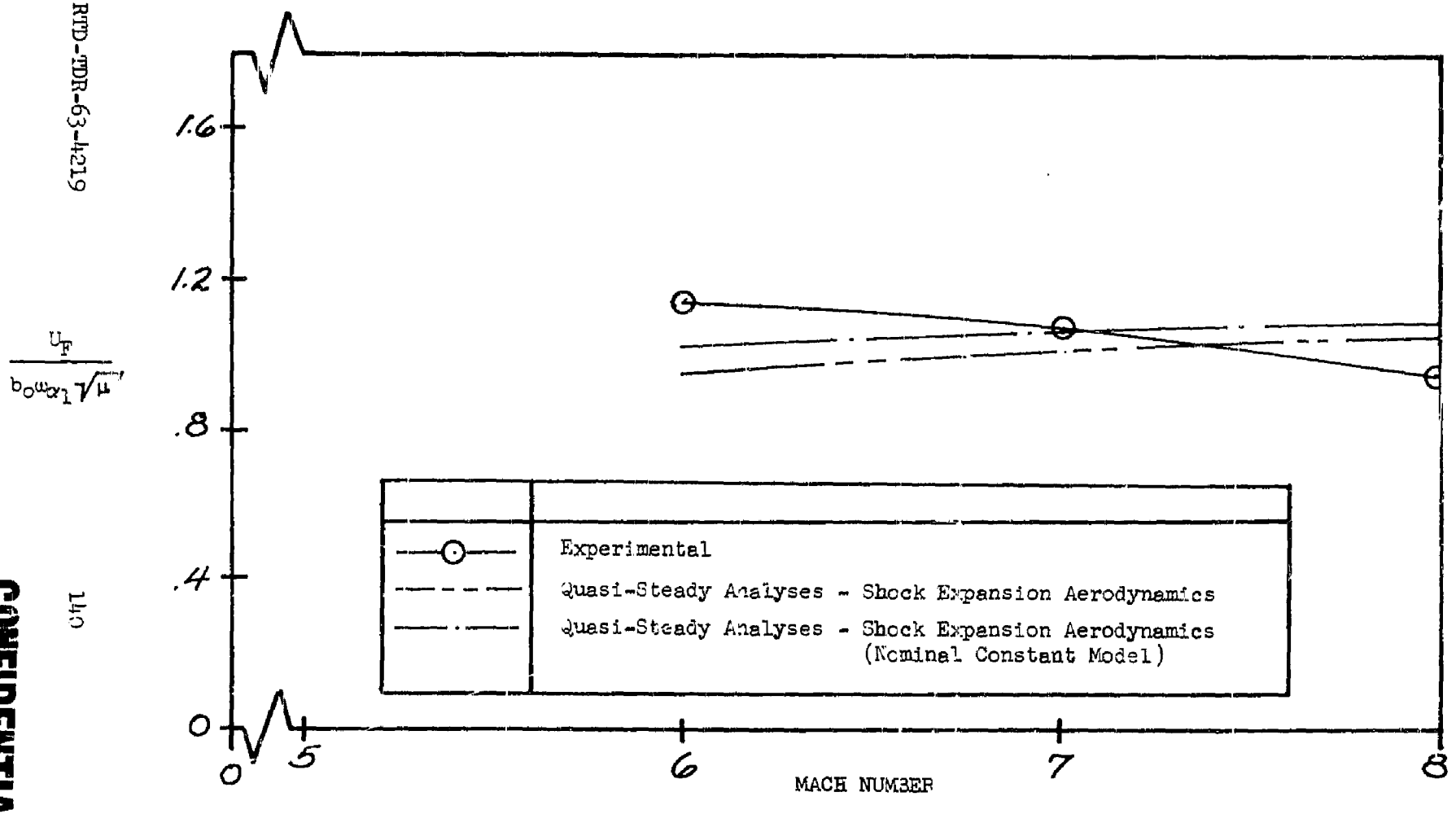

FIGURE 100 EXPERIMENTAL AND THEORETICAL, QUASI-STEADY (USING SHOCK-EXPANSION AERODYNAMICS) FLUTTER VELOCITY PARAMETER VS. MACH NUMBER; BASIC PLANFORM, t/c = .09, ω_h/ω_α = .60; $\alpha_0 = 0°$

CONFIDENTIAL

CONFIDENTIAL

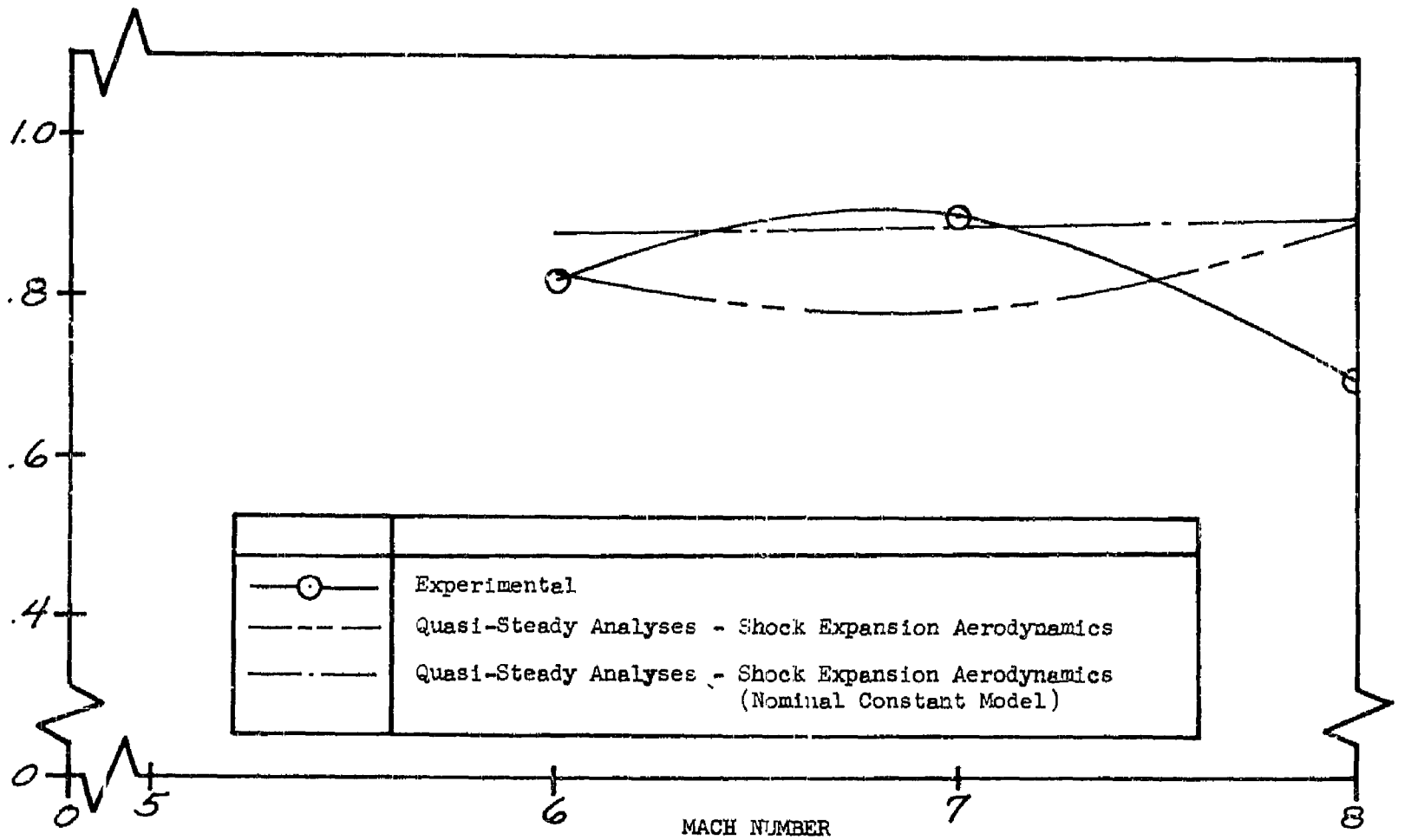

FIGURE 101 EXPERIMENTAL AND THEORETICAL, QUASI-STEADY (USING SHOCK-EXPANSION AERODYNAMICS) FLUTTER FREQUENCY RATIO VS. MACH NUMBER; BASIC PLANFORM, t/c = .09, $\omega_{h_1}/\omega_{\alpha_1}$ = .60, α_o = 0°

CONFIDENTIAL

CONFIDENTIAL

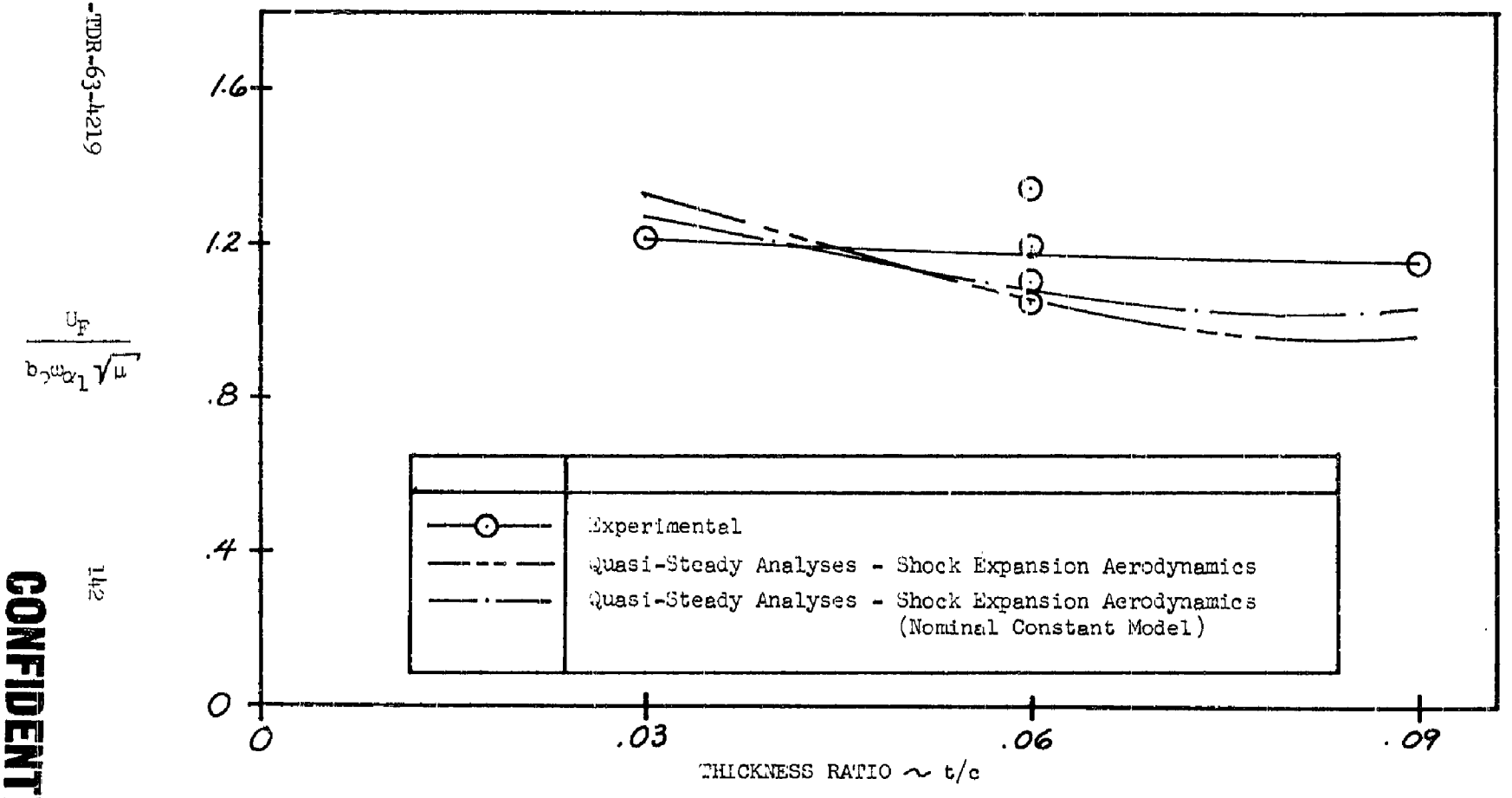

FIGURE 102 EXPERIMENTAL AND THEORETICAL, QUASI-STEADY (USING SHOCK EXPANSION AERODYNAMICS) FLUTTER VELOCITY PARAMETER VS. THICKNESS RATIO AT MACH NUMBER = 6.0; BASIC PLANFORM $\omega_{h_1}/\omega_{\alpha_1}$ = .6; α_o = 0°

CONFIDENTIAL

CONFIDENTIAL

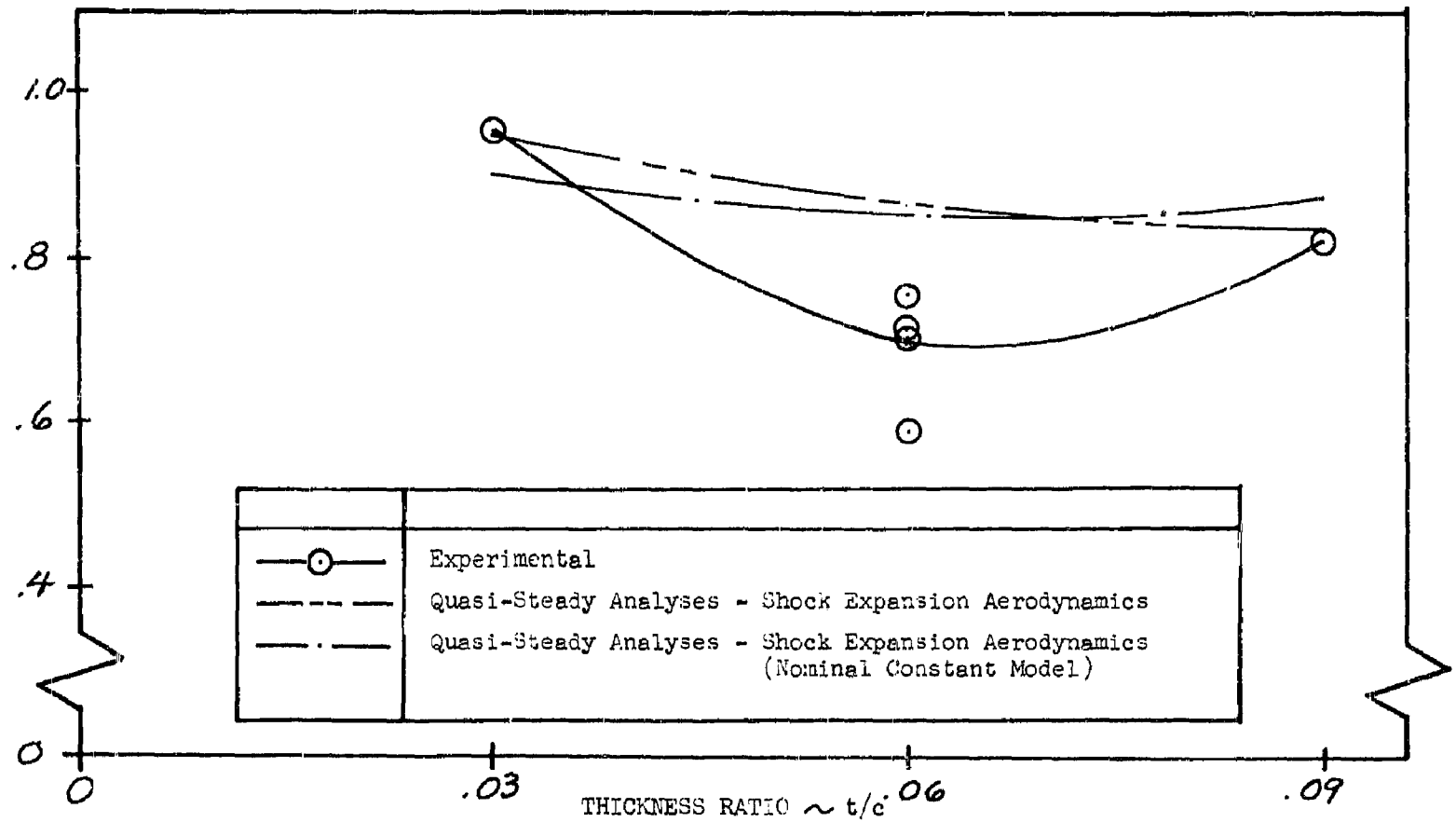

FIGURE 103 EXPERIMENTAL AND THEORETICAL, QUASI-STEADY (USING SHOCK EXPANSION AERODYNAMICS) FLUTTER FREQUENCY RATIO VS. THICKNESS RATIO AT MACH NUMBER = 6.0; BASIC PLANFORM $\omega_{h_1}/\omega_{\alpha_1}$ = .60; α_o = 0°

CONFIDENTIAL

CONFIDENTIAL

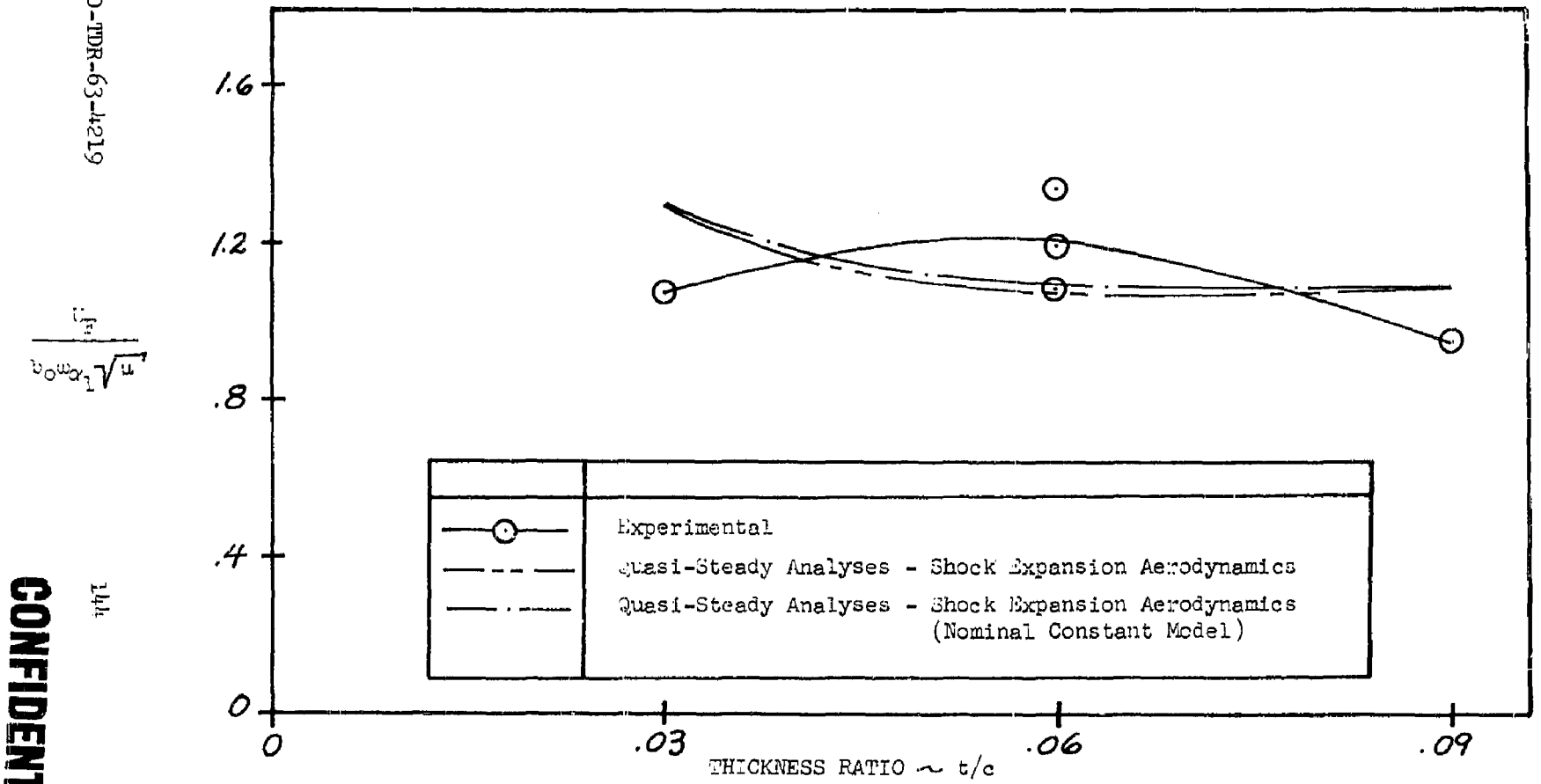

FIGURE 104 EXPERIMENTAL AND THEORETICAL, QUASI-STEADY (USING SHOCK-EXPANSION AERODYNAMICS) FLUTTER VELOCITY PARAMETER VS. THICKNESS RATIO AT MACH NUMBER = 8.0; BASIC PLANFORM $\omega_{h_1}/\omega_{\alpha_1} = .60$; $\alpha_0 = 0^\circ$

CONFIDENTIAL

CONFIDENTIAL

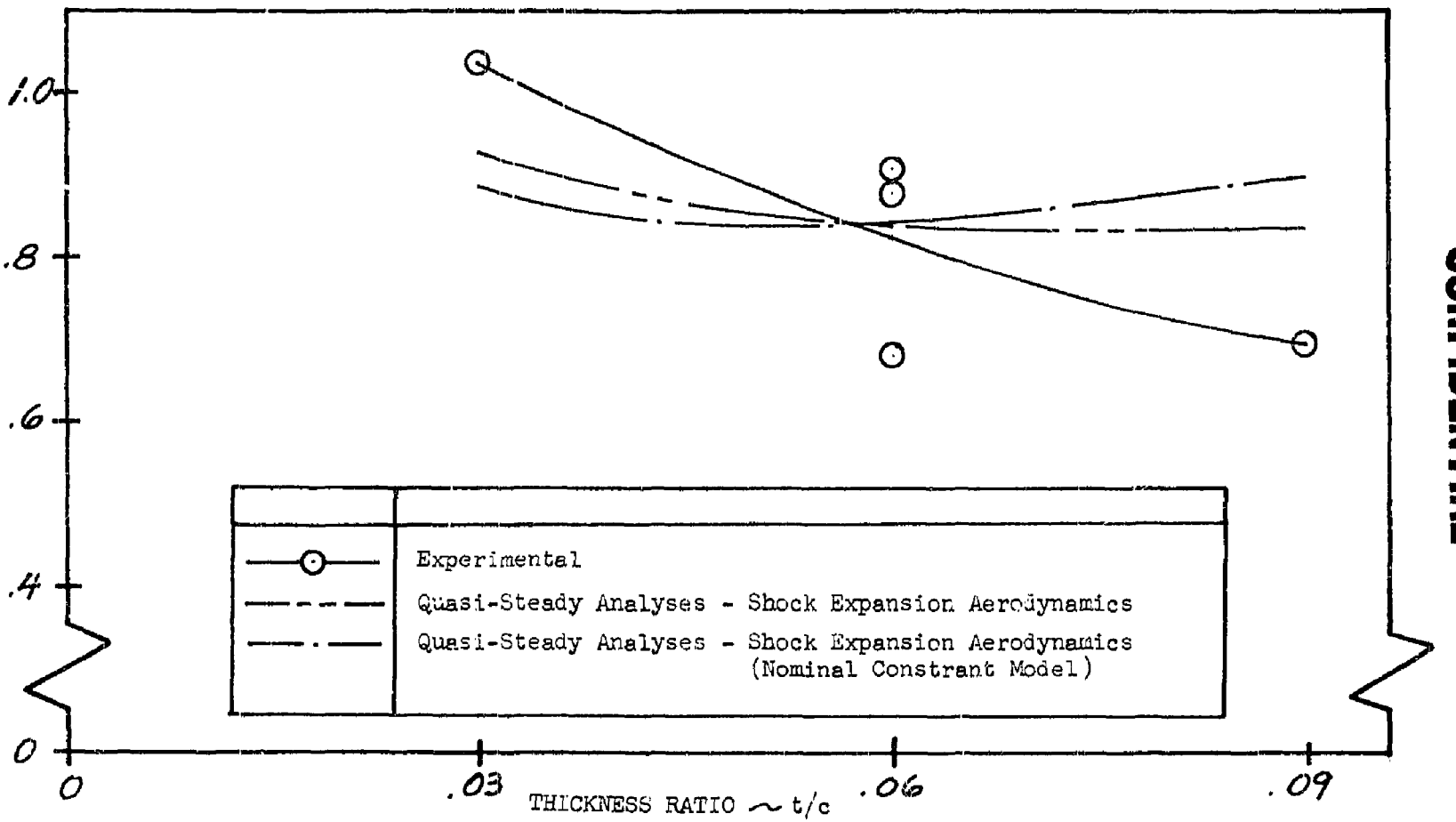

FIGURE 105 EXPERIMENTAL AND THEORETICAL, QUASI-STEADY (USING SHOCK-EXPANSION AERODYNAMICS) FLUTTER FREQUENCY RATIO VS. THICKNESS RATIO AT MACH NUMBER = 8.0; BASIC PLANFORM $\omega_{h_1}/\omega_{\alpha_1}$ = .60; α_o = 0°

CONFIDENTIAL

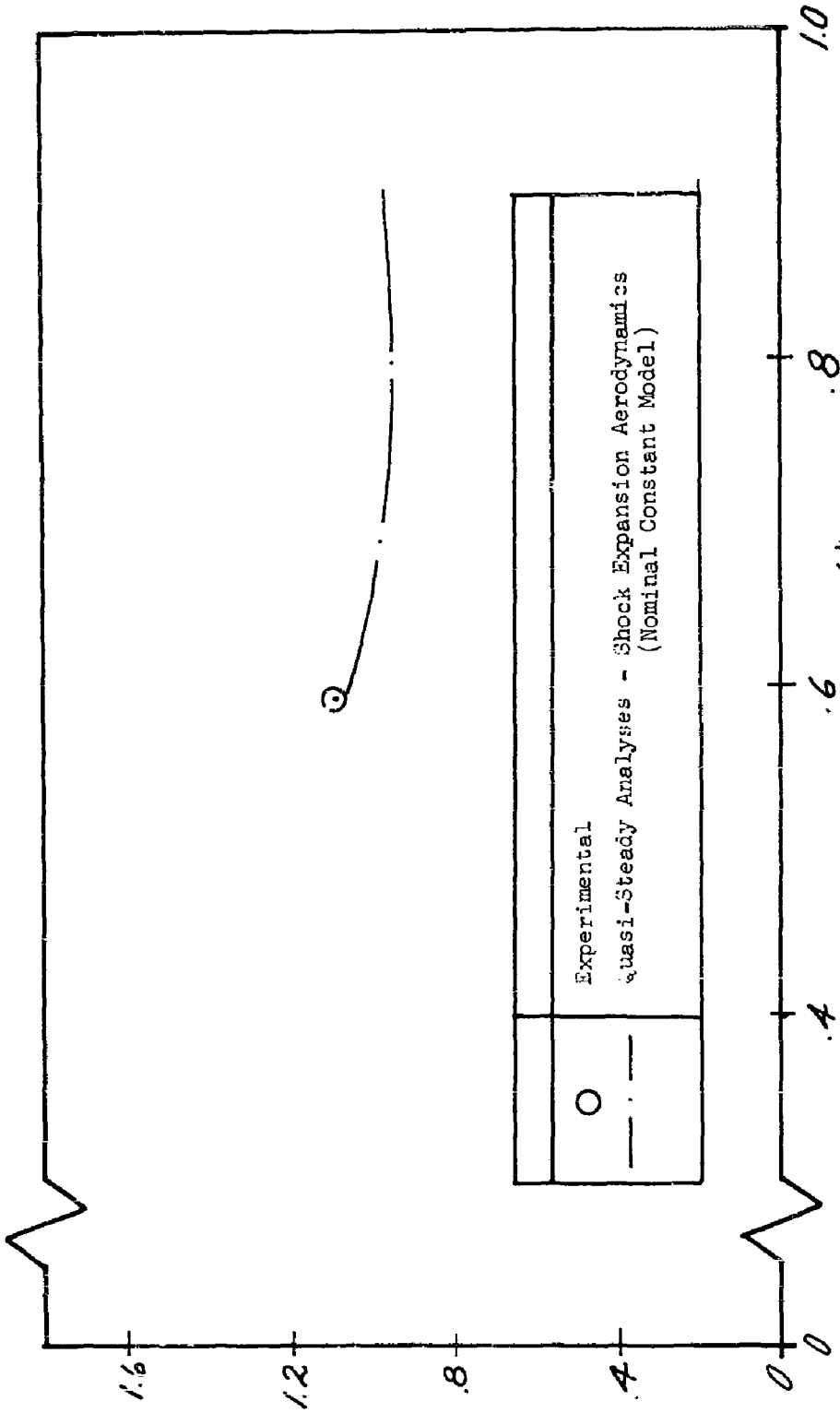

FIGURE 106 THEORETICAL, QUASI-STEADY (USING SHOCK-EXPANSION AERODYNAMICS) FLUTTER VELOCITY PARAMETER VS. MODAL FREQUENCY RATIO AT MACH NUMBER = 7.0; BASIC PLANFORM, t/c = .06, $\alpha_0 = 0°$

CONFIDENTIAL

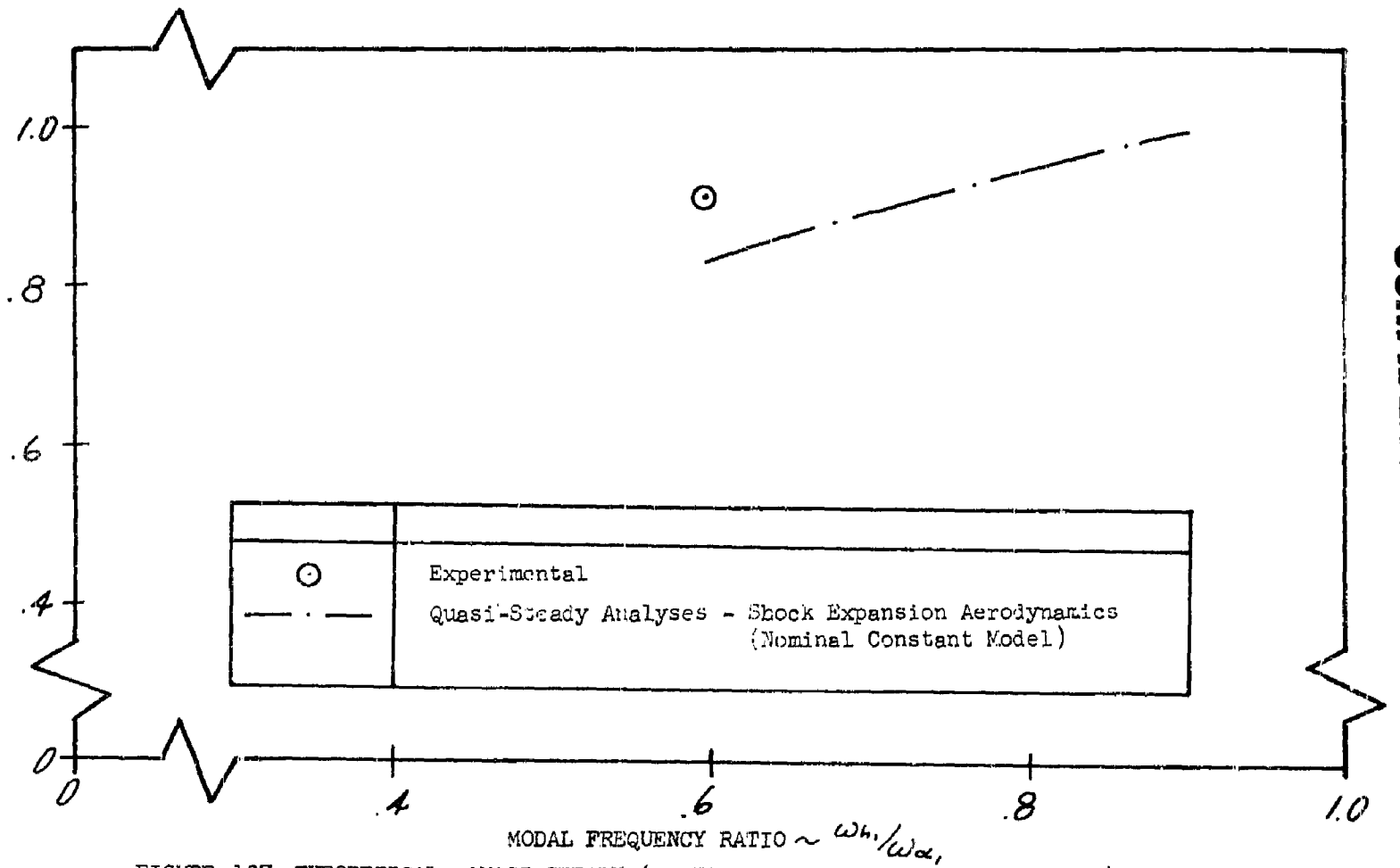

FIGURE 107 THEORETICAL, QUASI-STEADY (USING SHOCK-EXPANSION AERODYNAMICS) FLUTTER FREQUENCY RATIO VS. MODAL FREQUENCY RATIO AT MACH NUMBER = 7.0; BASIC PLANFORM, t/c = .06, $\alpha_o = 0°$

CONFIDENTIAL

CONFIDENTIAL

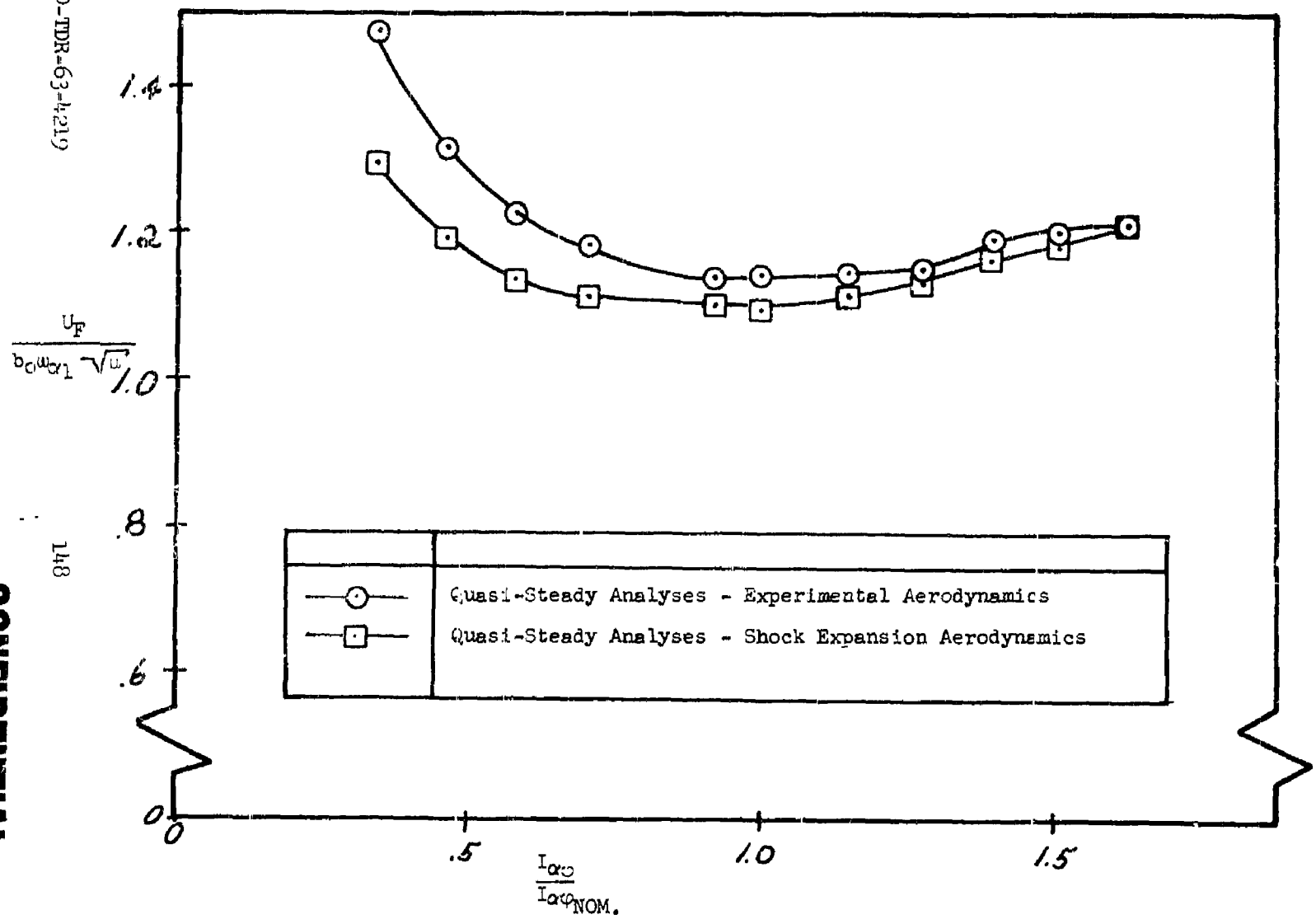

FIGURE 108 THEORETICAL QUASI-STEADY FLUTTER VELOCITY PARAMETER VS. PRODUCT OF INERTIA (USING SHOCK-EXPANSION AERODYNAMICS AND EXPERIMENTAL AERODYNAMICS) MACH NUMBER = 3.0, BASIC PLANFORM, t/c = .06

CONFIDENTIAL

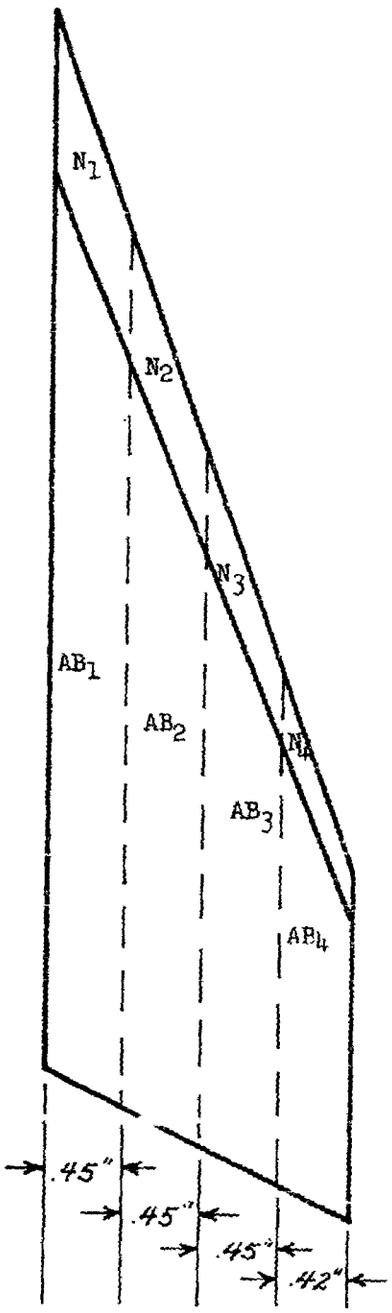

SEGMENT	AREA (IN^2)	$\bar{y}$ (IN)	C (IN)
N_1	.37040	.225	5.48746
N_2	.30121	.675	4.46238
N_3	.23202	1.125	3.43730
N_4	.15412	1.560	2.44638
AB_1	2.09895	.225	5.48746
AB_2	1.70686	.675	4.46238
AB_3	1.31477	1.125	3.43730
AB_4	0.87336	1.560	2.44638

FIGURE 109 SHOCK EXPANSION AERODYNAMIC AREAS OF INFLUENCE

APPENDIX A

The static aerodynamic force coefficients in pitch and roll are presented herein for configurations 4, 5, 6, and 7. These configurations were not investigated with respect to their associated flutter characteristics due to program reorientation.

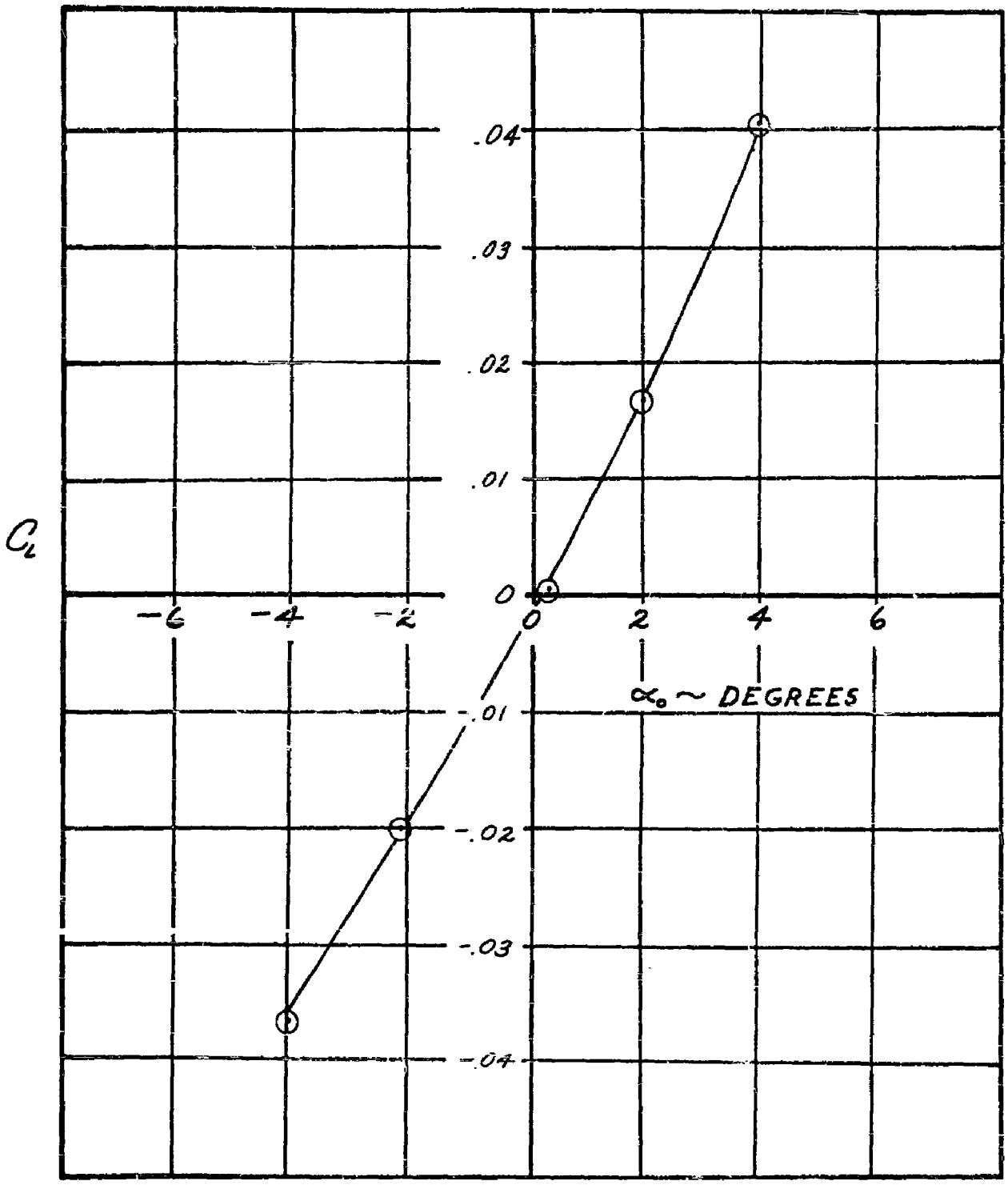

FIGURE A1 EXPERIMENTAL LIFT COEFFICIENT VS. ANGLE-OF-ATTACK; CONFIGURATION #4, MACH NUMBER = 6.0

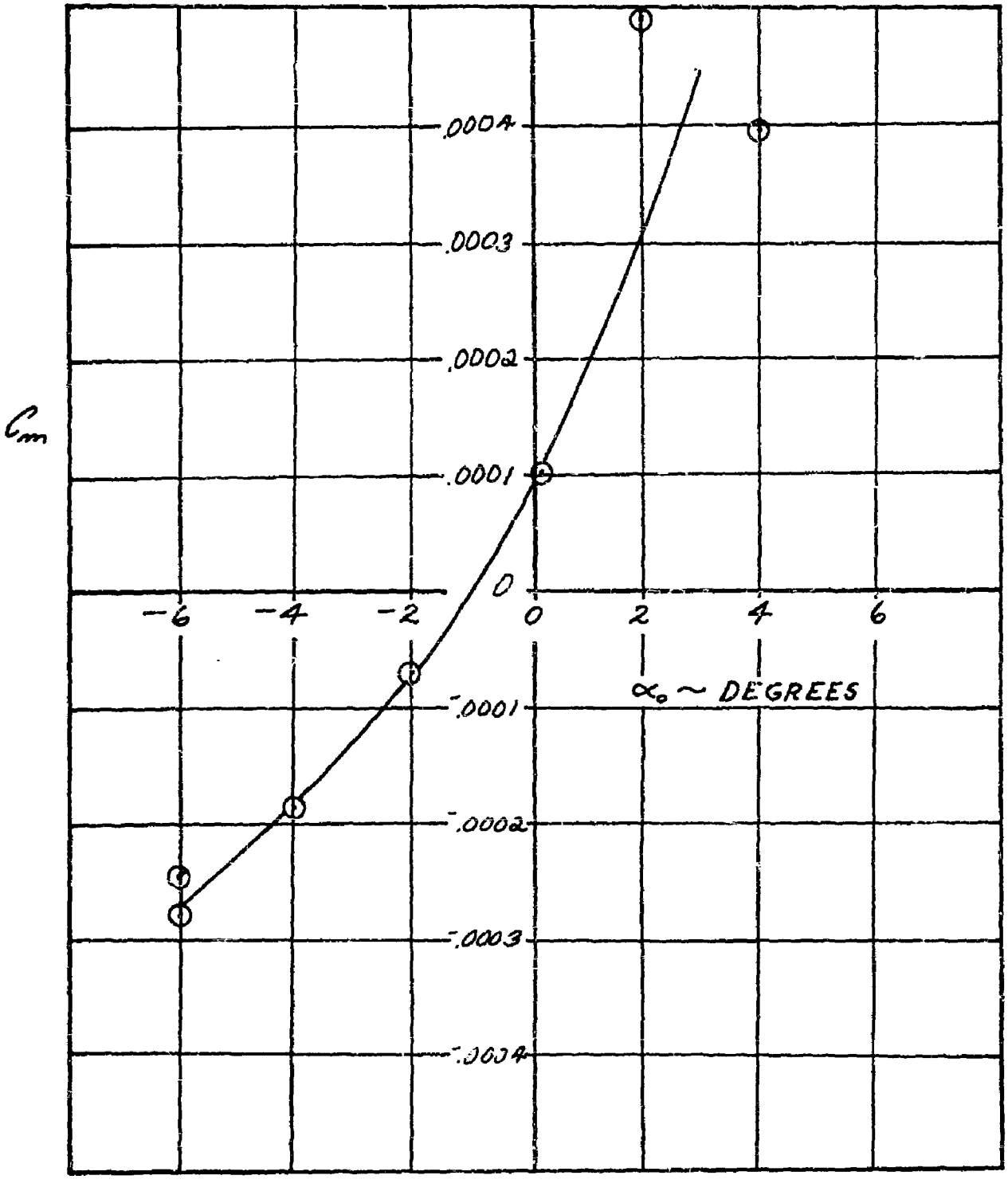

FIGURE A2 EXPERIMENTAL PITCHING MOMENT COEFFICIENT VS. ANGLE-OF-ATTACK; CONFIGURATION #4, MACH NUMBER = 6.0

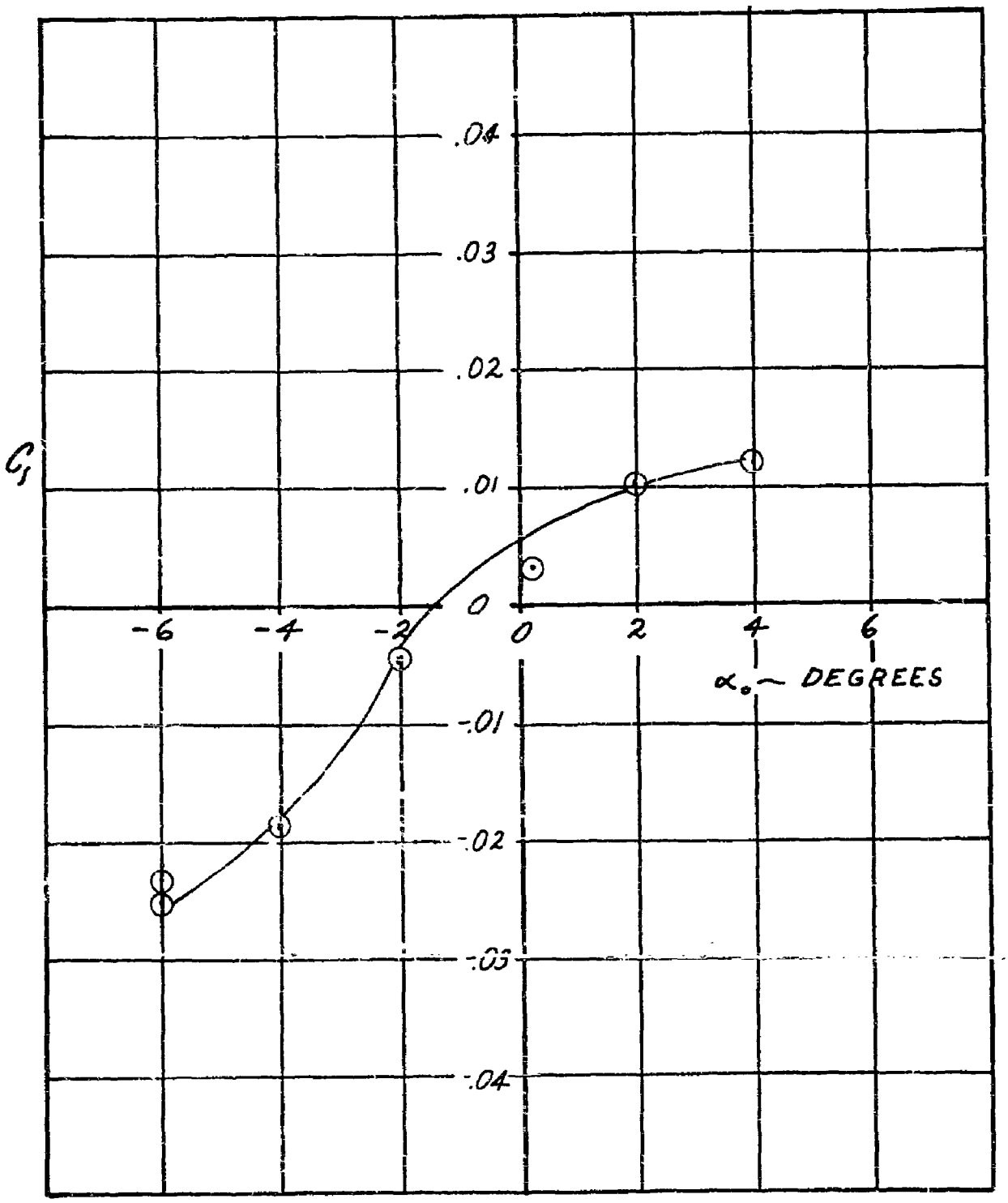

FIGURE A3 EXPERIMENTAL ROLLING MOMENT COEFFICIENT VS. ANGLE-OF-ATTACK; CONFIGURATION #4, MACH NUMBER = 6.0

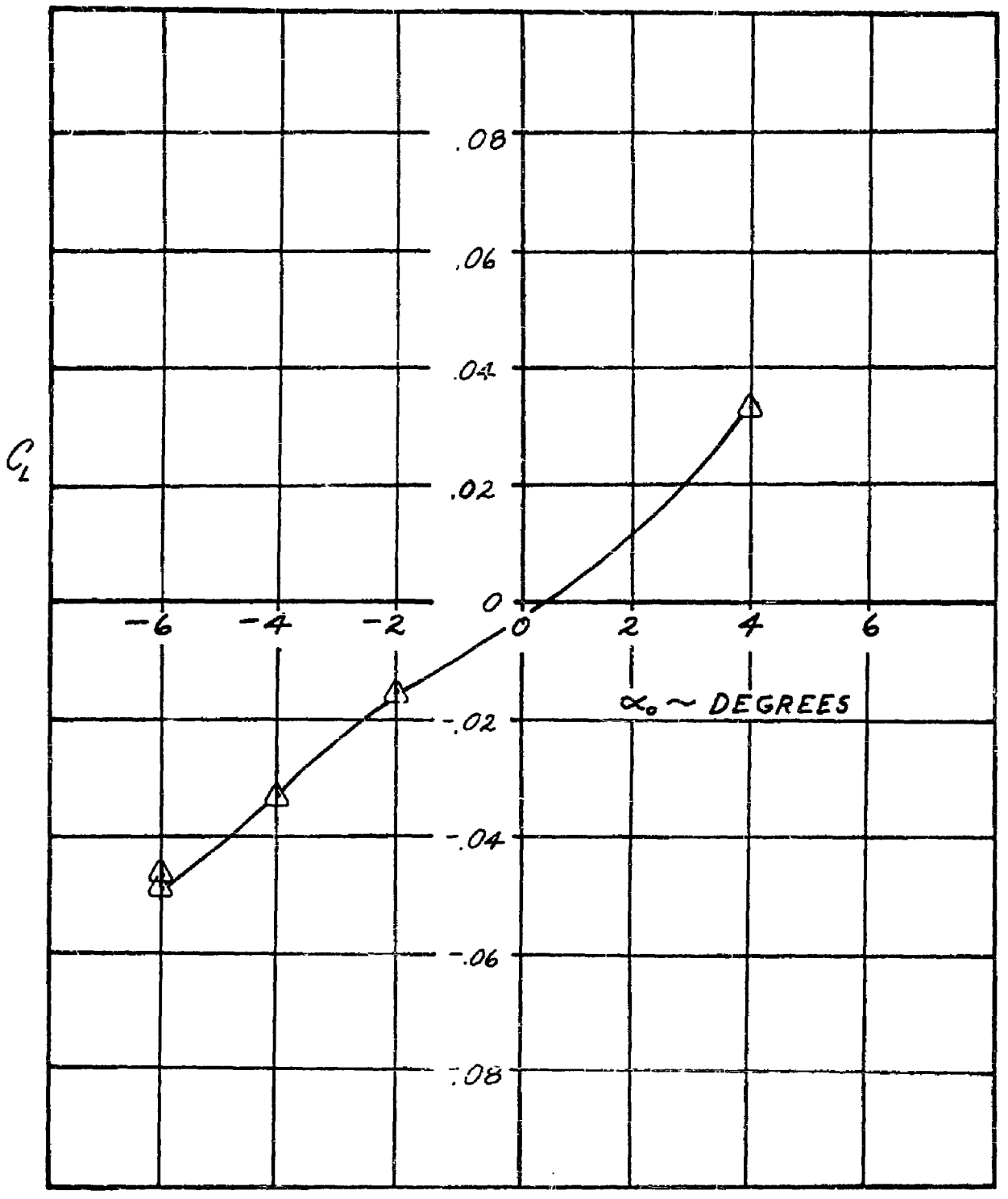

FIGURE A4 EXPERIMENTAL LIFT COEFFICIENT VS. ANGLE-OF-ATTACK; CONFIGURATION #4, MACH NUMBER = 8.0

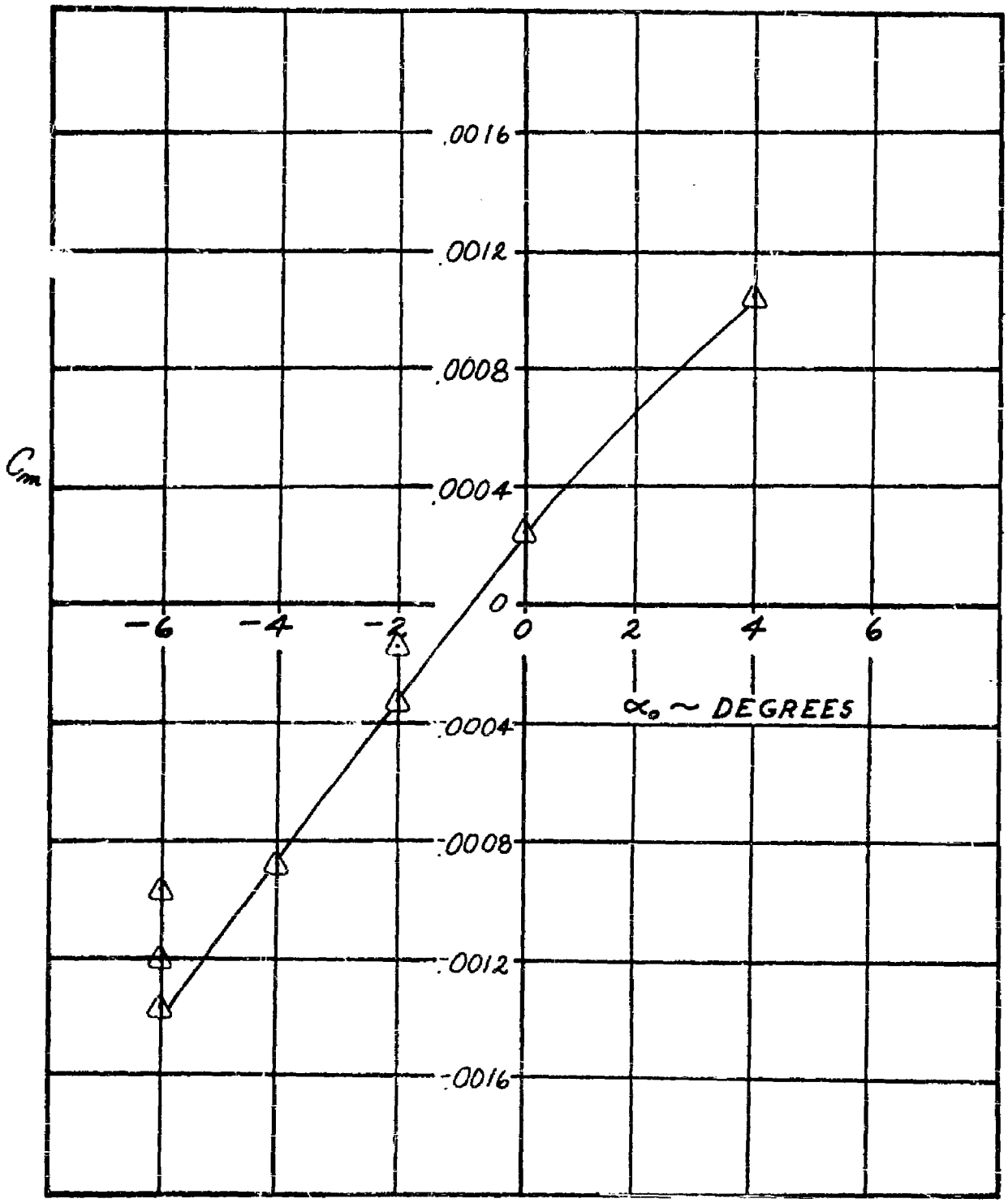

FIGURE A5 EXPERIMENTAL PITCHING MOMENT COEFFICIENT VS. ANGLE-OF-ATTACK; CONFIGURATION #4, MACH NUMBER = 8.0

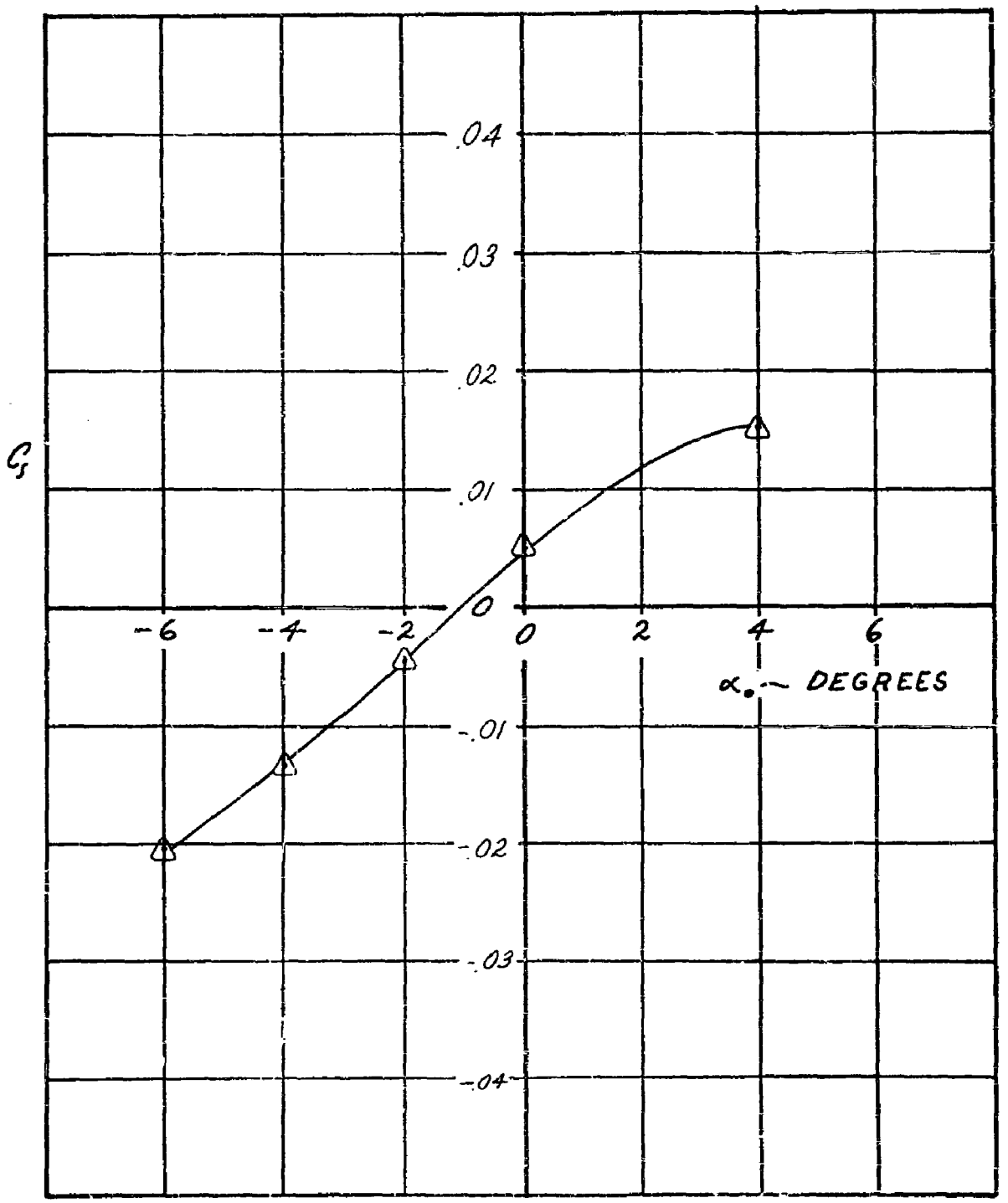

FIGURE A6 EXPERIMENTAL ROLLING MOMENT COEFFICIENT VS. ANGLE-OF-ATTACK; CONFIGURATION #4, MACH NUMBER = 8.0

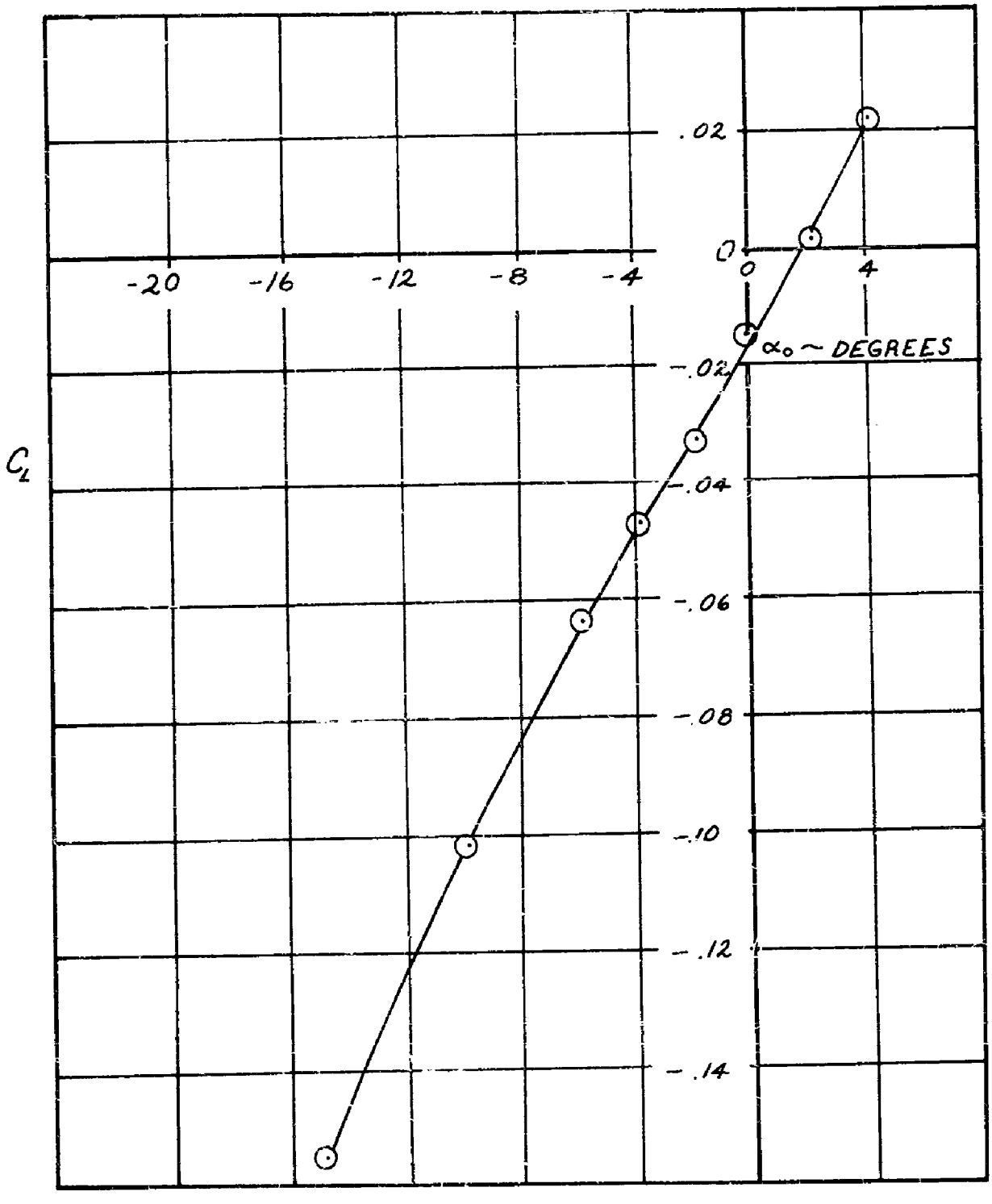

FIGURE A7 EXPERIMENTAL LIFT COEFFICIENT VS. ANGLE-OF-ATTACK; CONFIGURATION #5, MACH NUMBER = 6.0

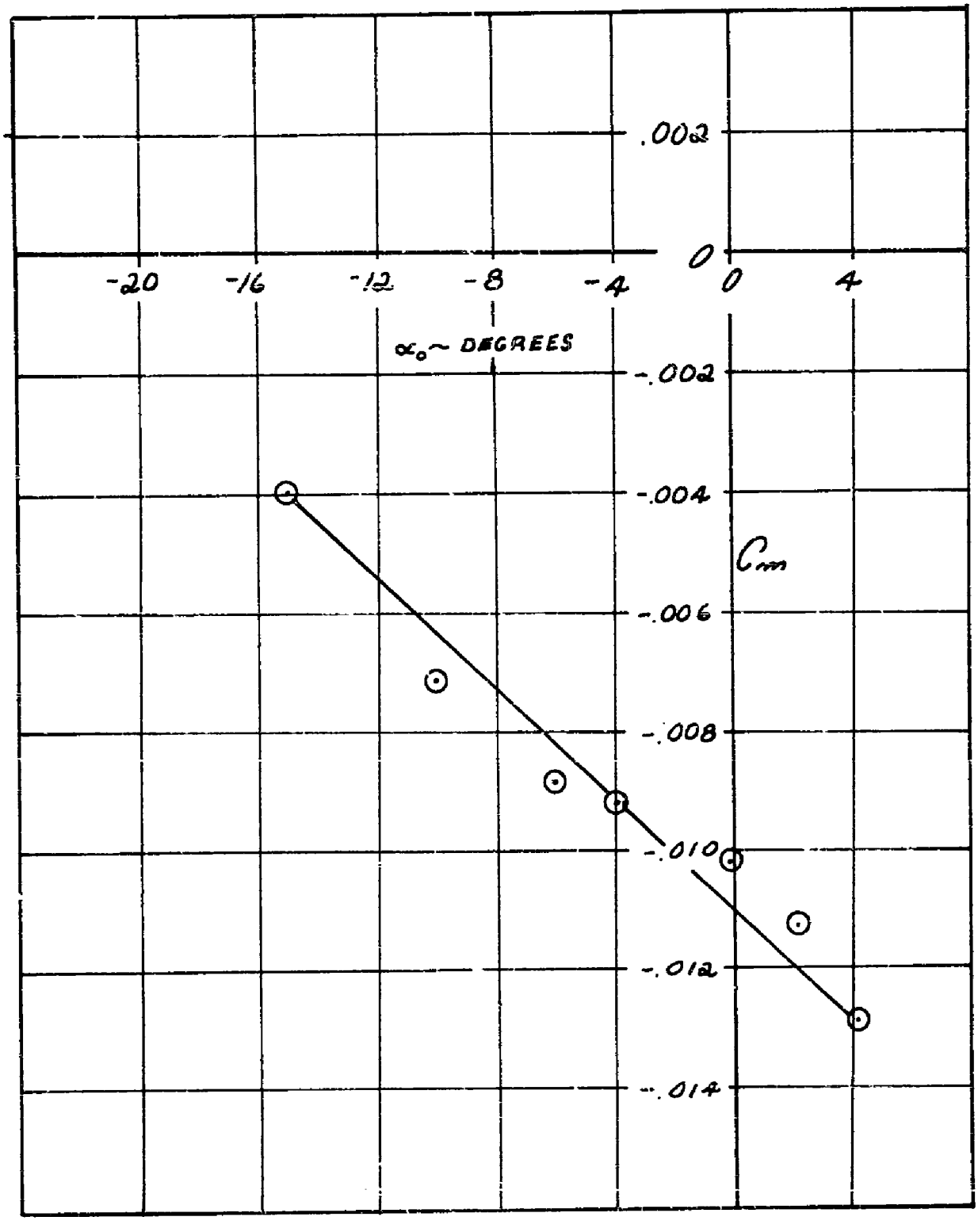

FIGURE A8 EXPERIMENTAL PITCHING MOMENT COEFFICIENT VS. ANGLE-OF-ATTACK; CONFIGURATION #5, MACH NUMBER = 6.0

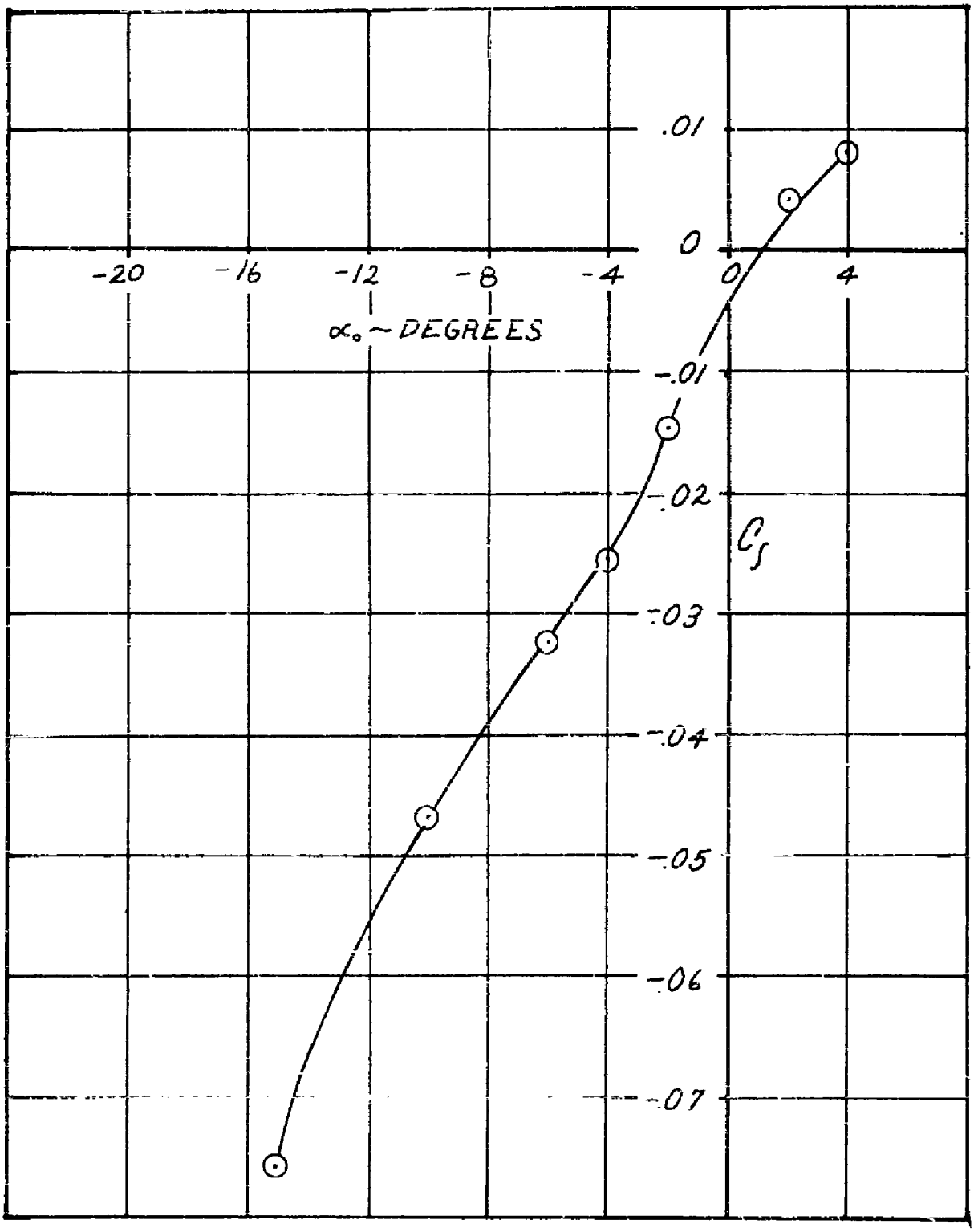

FIGURE A9 EXPERIMENTAL ROLLING MOMENT COEFFICIENT VS. ANGLE-OF-ATTACK; CONFIGURATION #5, MACH NUMBER = 6.0

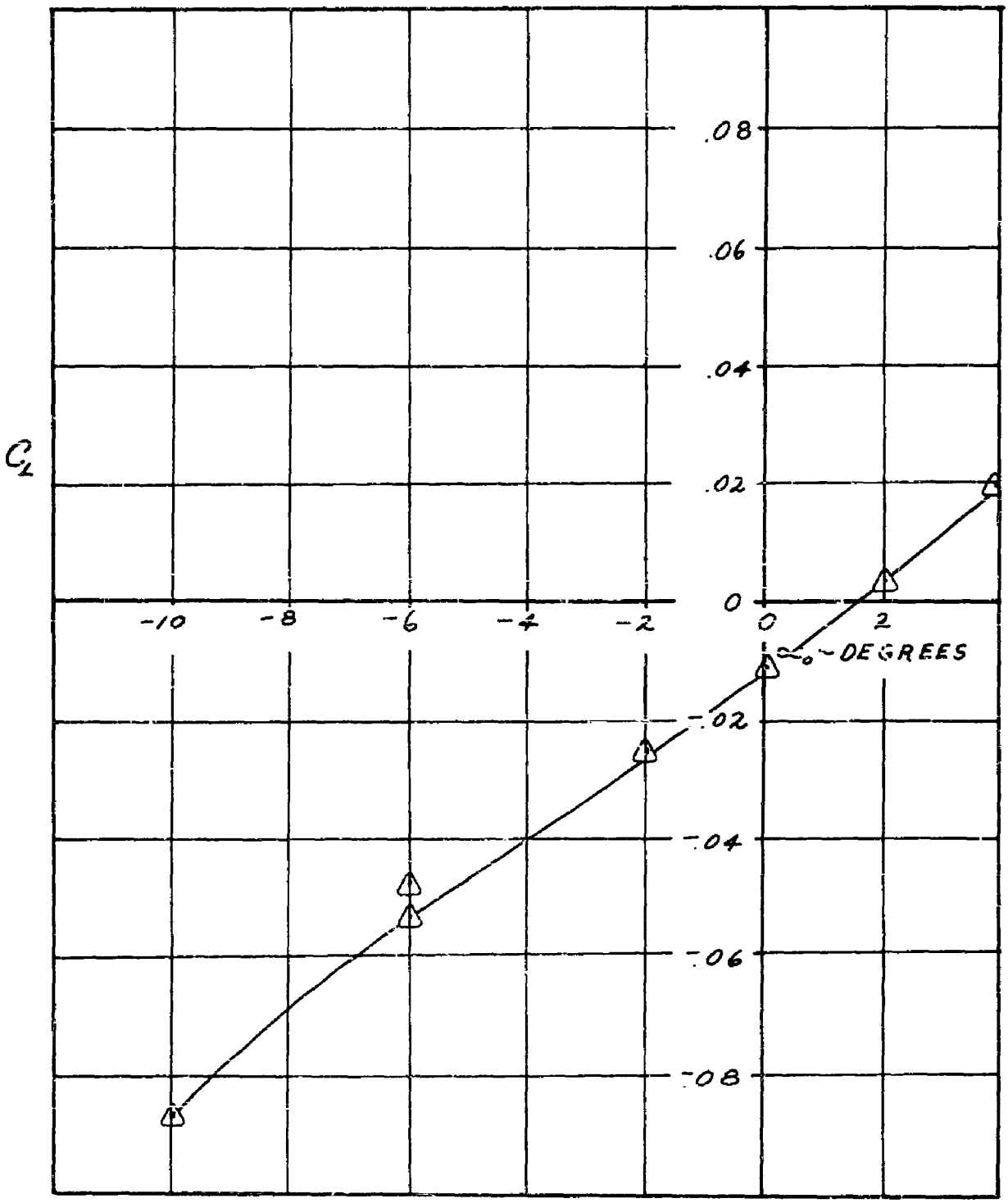

FIGURE A10 EXPERIMENTAL LIFT COEFFICIENT VS. ANGLE-OF-ATTACK; CONFIGURATION #5, MACH NUMBER = 8.0

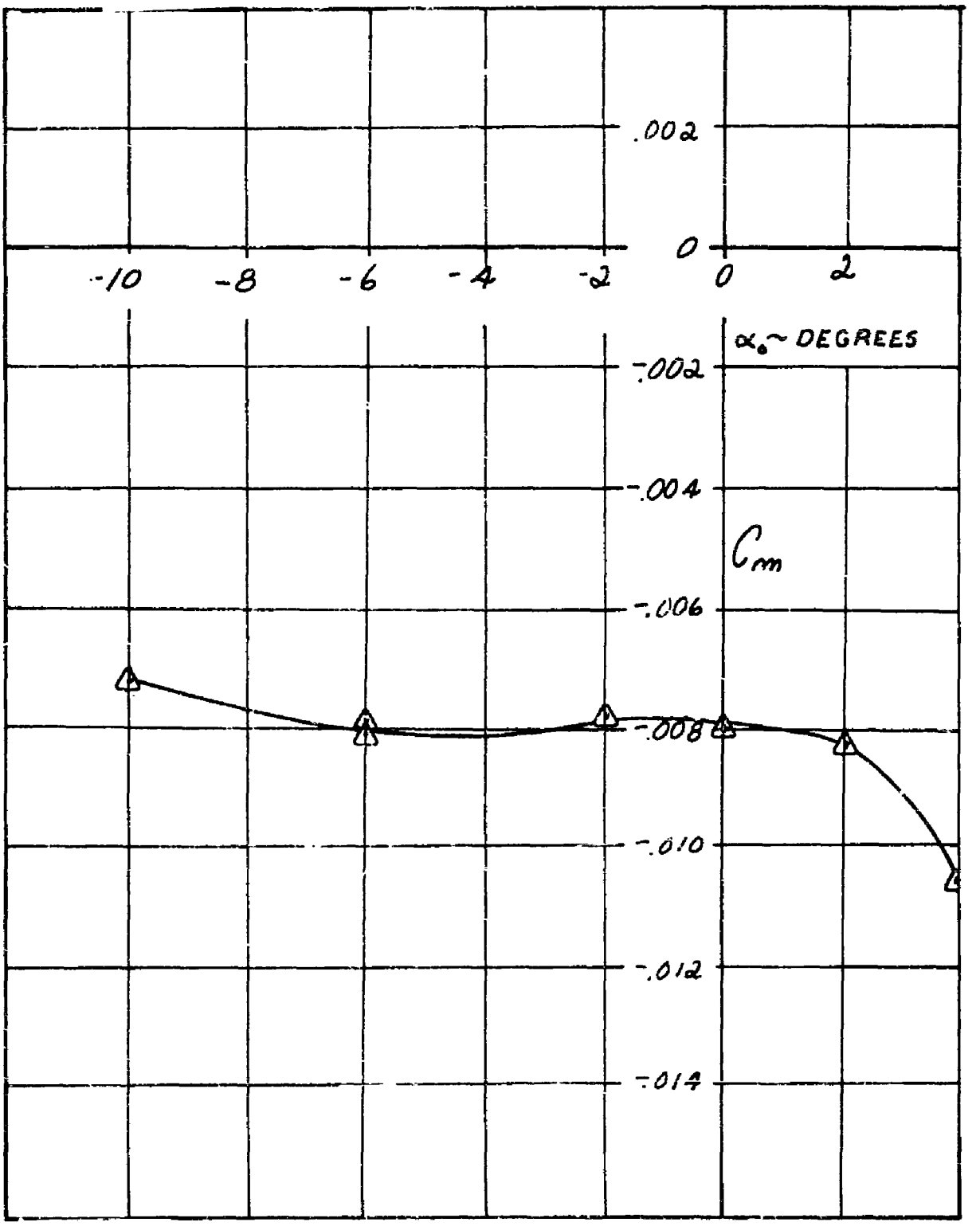

FIGURE A11 EXPERIMENTAL PITCHING MOMENT COEFFICIENT VS. ANGLE-OF-ATTACK; CONFIGURATION #5, MACH NUMBER = 8.0

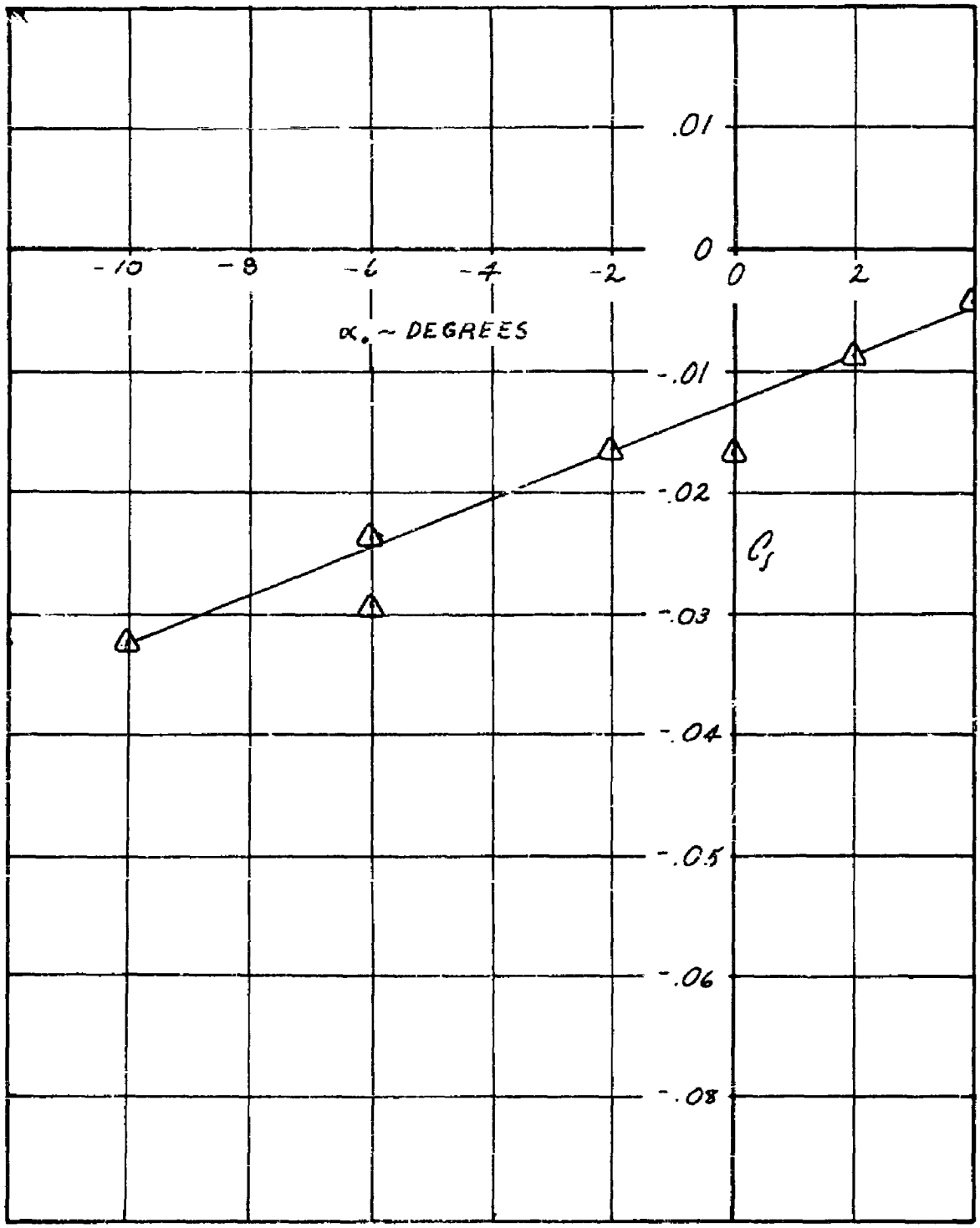

FIGURE A12 EXPERIMENTAL ROLLING MOMENT COEFFICIENT VS. ANGLE-OF-ATTACK; CONFIGURATION #5, MACH NUMBER = 8.0

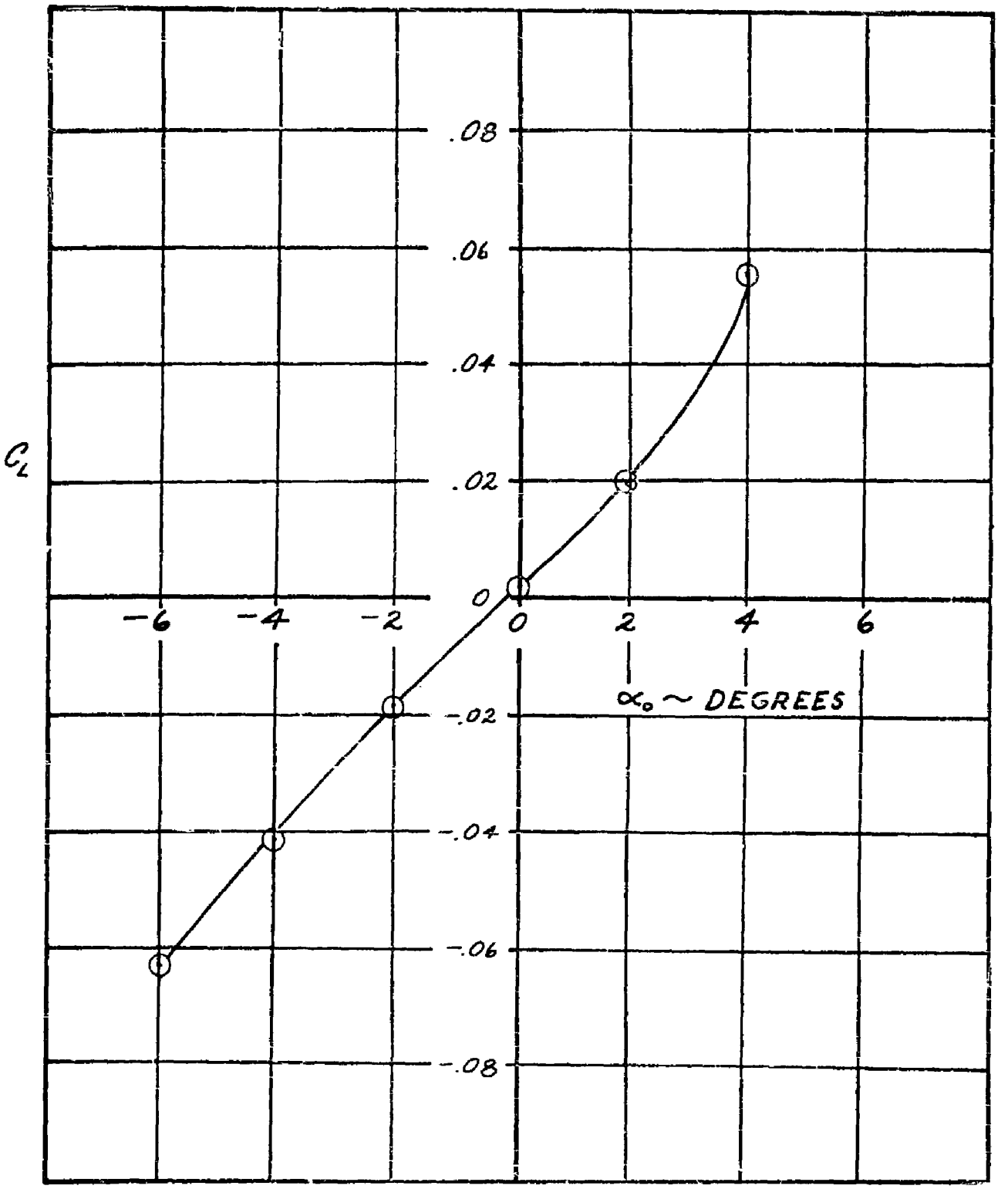

FIGURE A13 EXPERIMENTAL LIFT COEFFICIENT VS. ANGLE-OF-ATTACK; CONFIGURATION #6, MACH NUMBER = 6.0

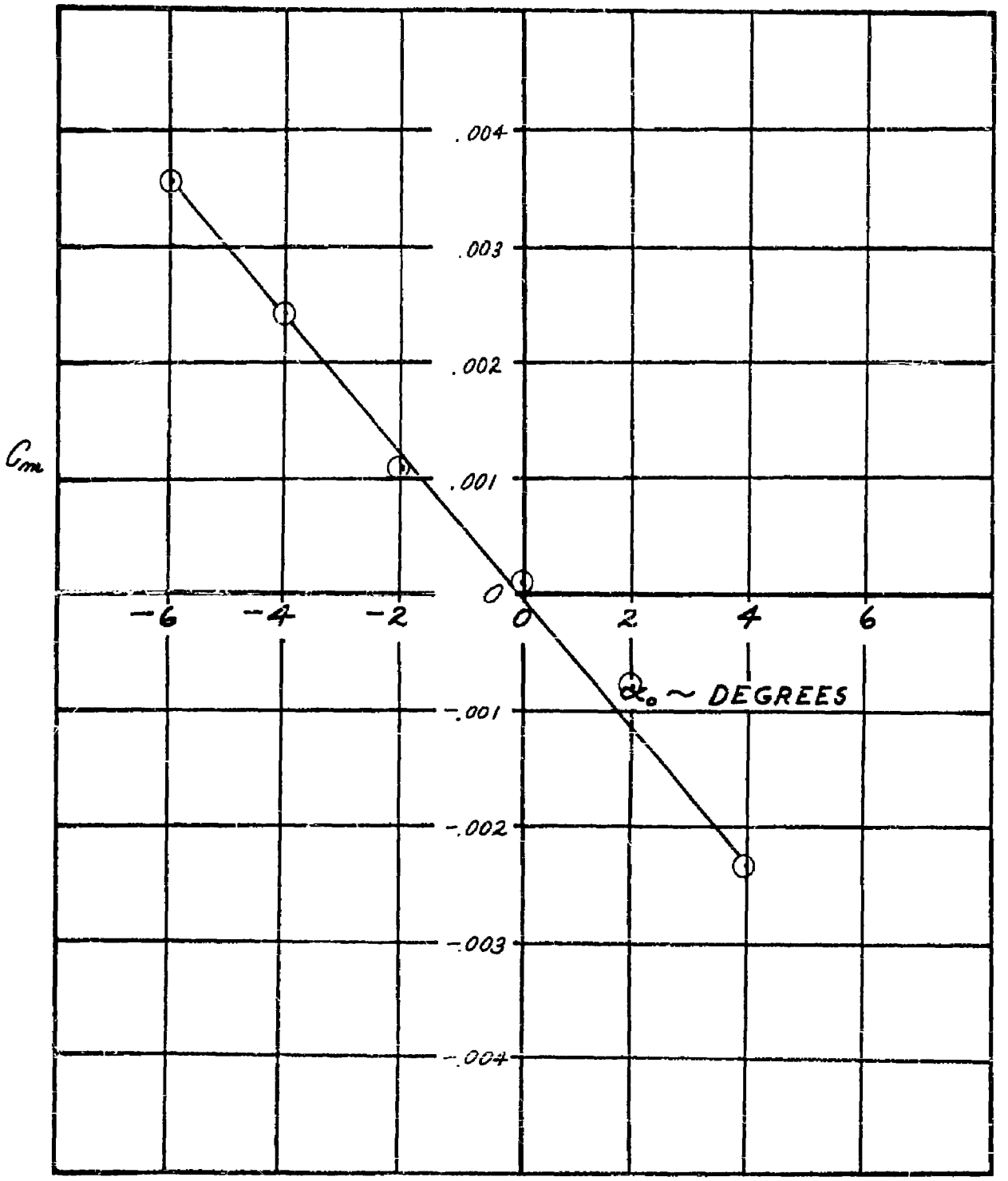

FIGURE A14 EXPERIMENTAL PITCHING MOMENT COEFFICIENT VS. ANGLE-OF-ATTACK; CONFIGURATION #6, MACH NUMBER = 6.0

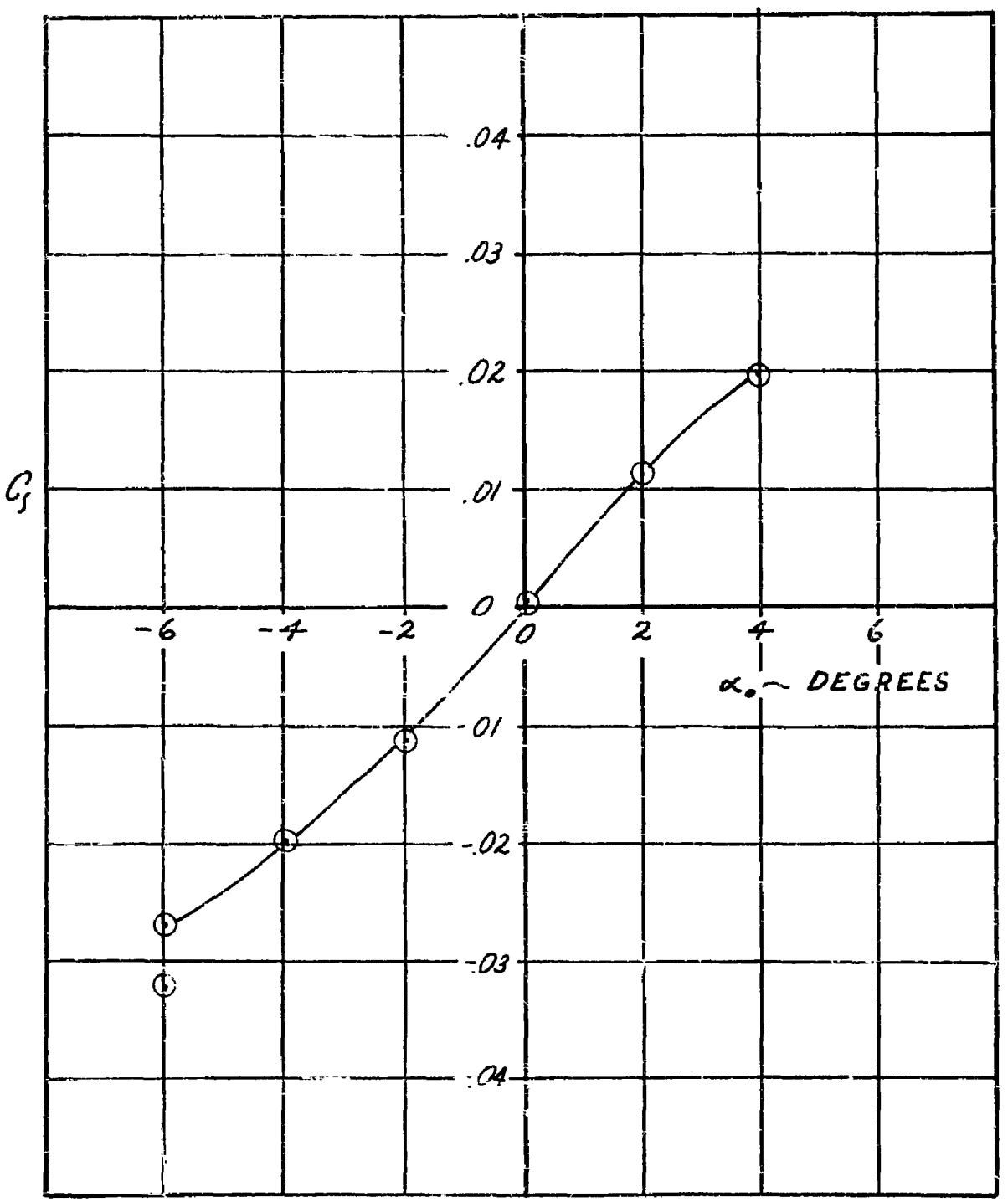

FIGURE A15 EXPERIMENTAL ROLLING MOMENT COEFFICIENT VS. ANGLE-OF-ATTACK; CONFIGURATION #6, MACH NUMBER = 6.0

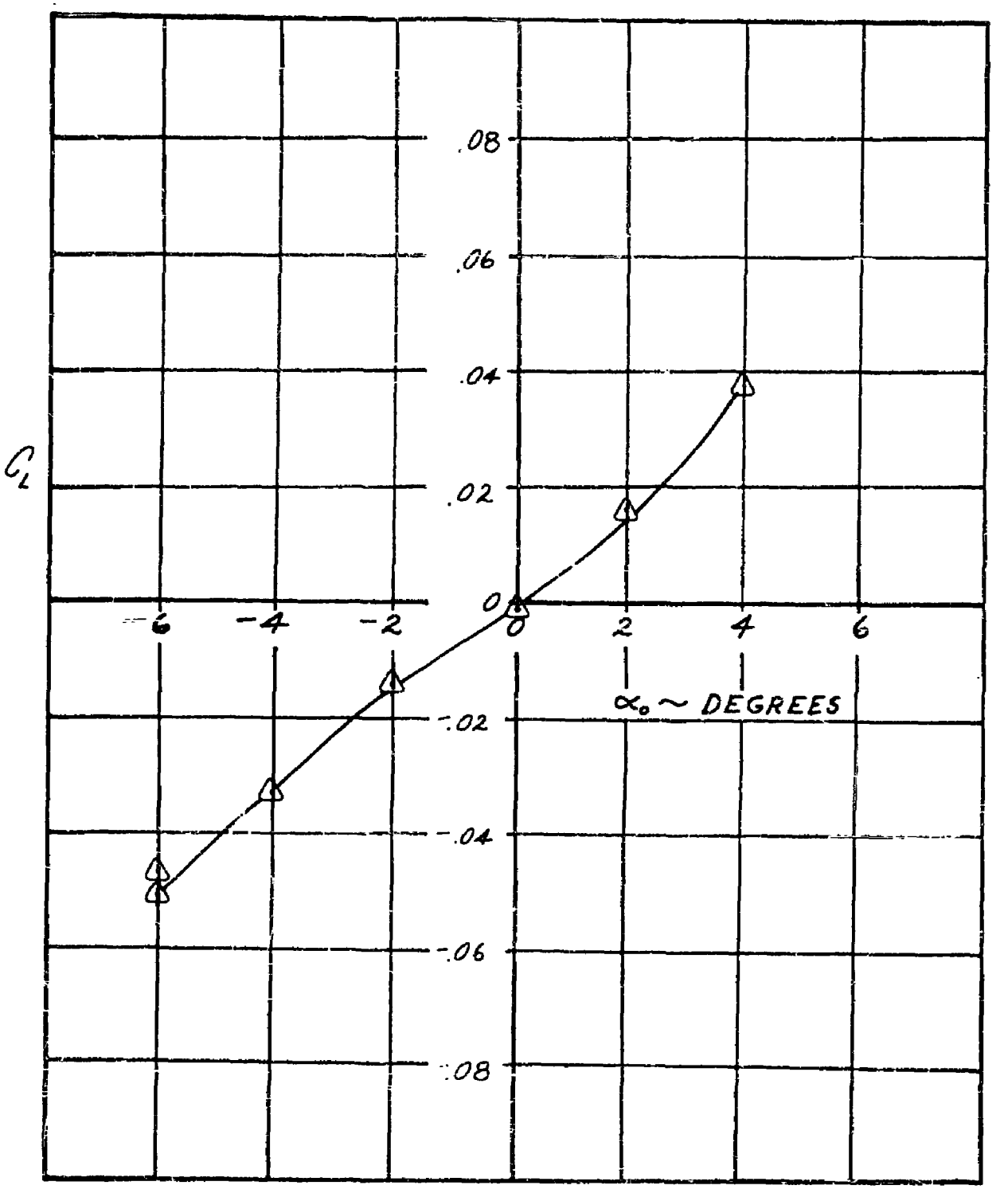

FIGURE A16 EXPERIMENTAL LIFT COEFFICIENT VS. ANGLE-OF-ATTACK; CONFIGURATION #6, MACH NUMBER = 8.0

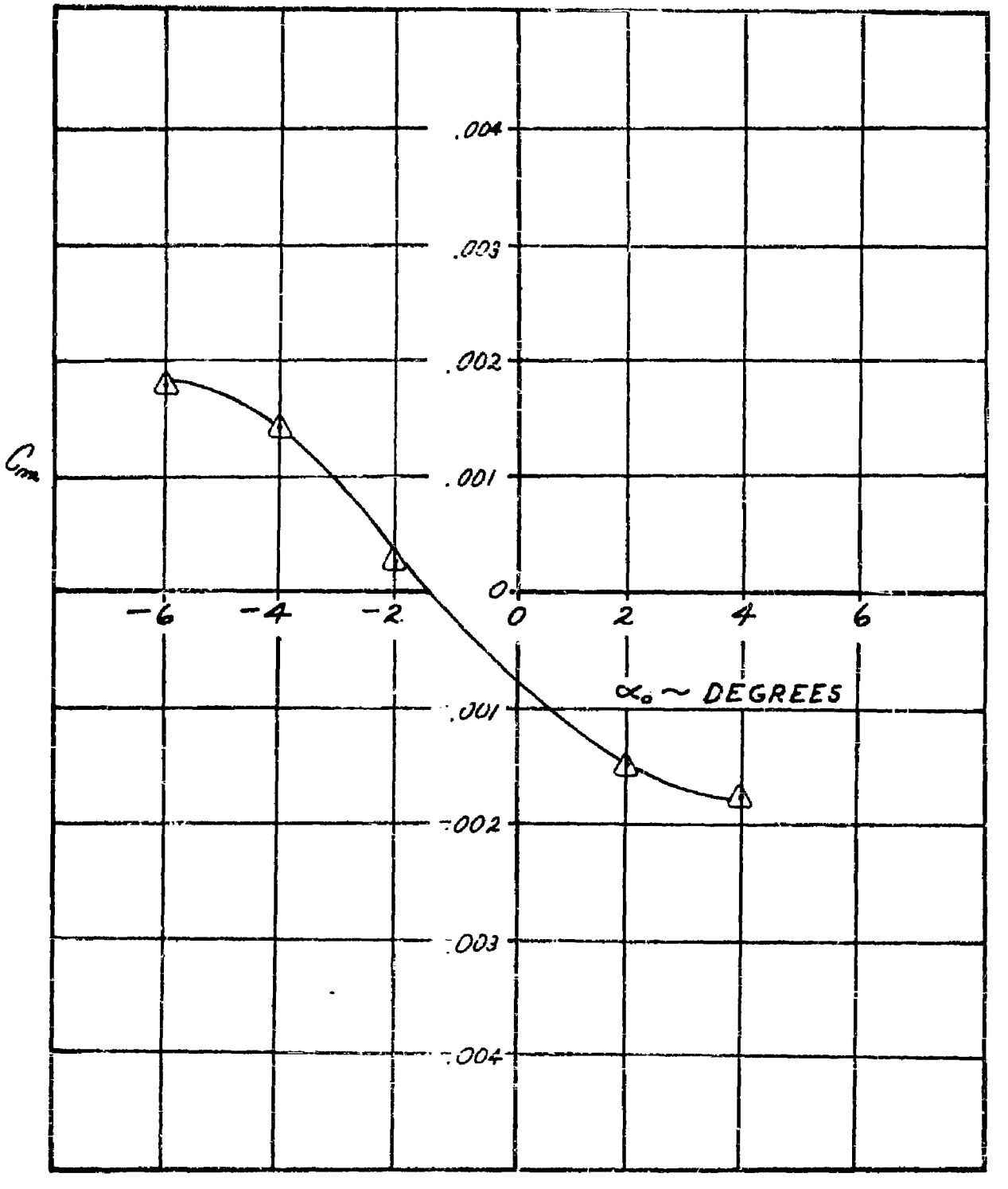

FIGURE A17 EXPERIMENTAL PITCHING MOMENT COEFFICIENT VS. ANGLE-OF-ATTACK; CONFIGURATION #6, MACH NUMBER = 8.0

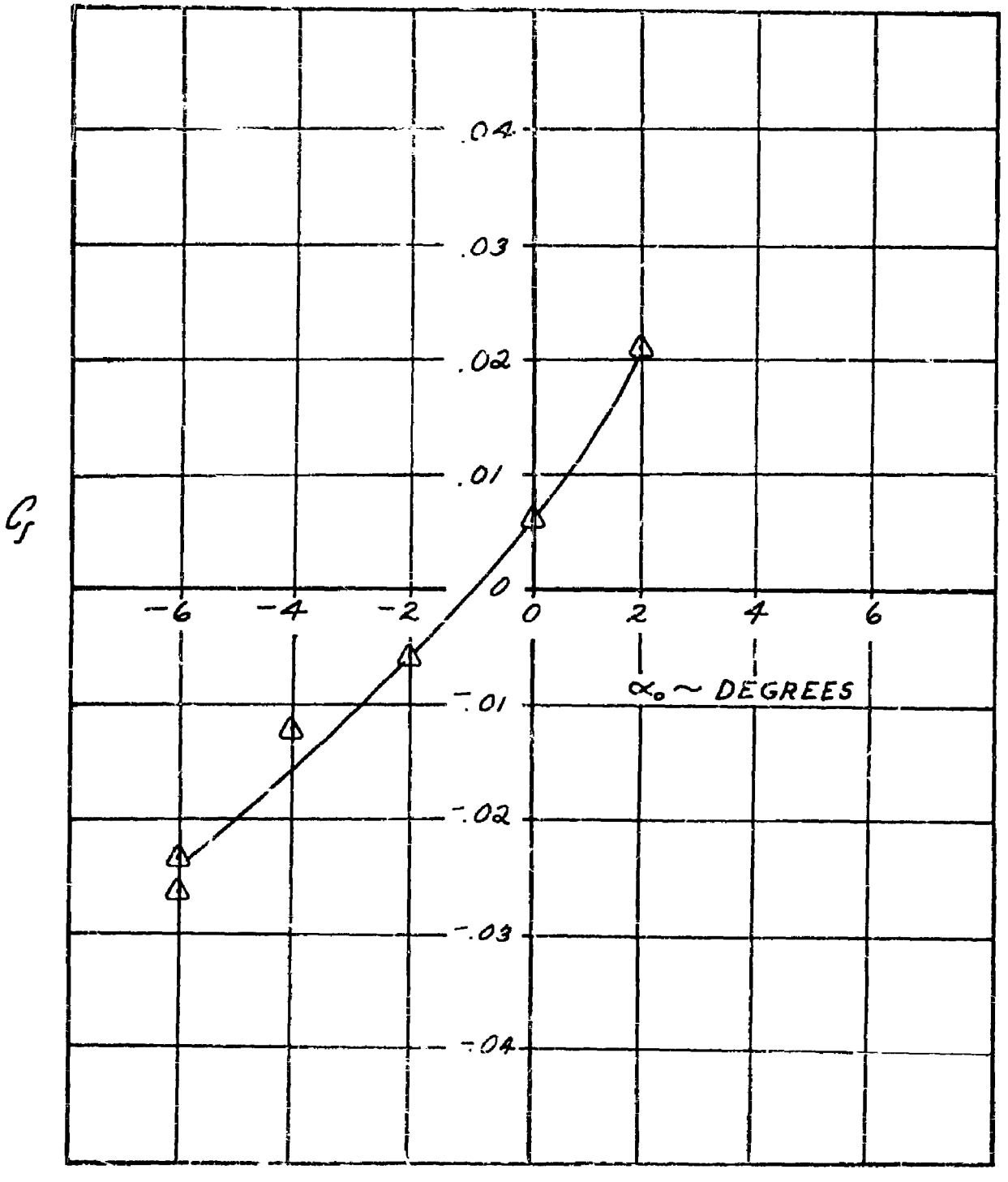

FIGURE A18 EXPERIMENTAL ROLLING MOMENT COEFFICIENT VS. ANGLE-OF-ATTACK; CONFIGURATION #6, MACH NUMBER = 8.0

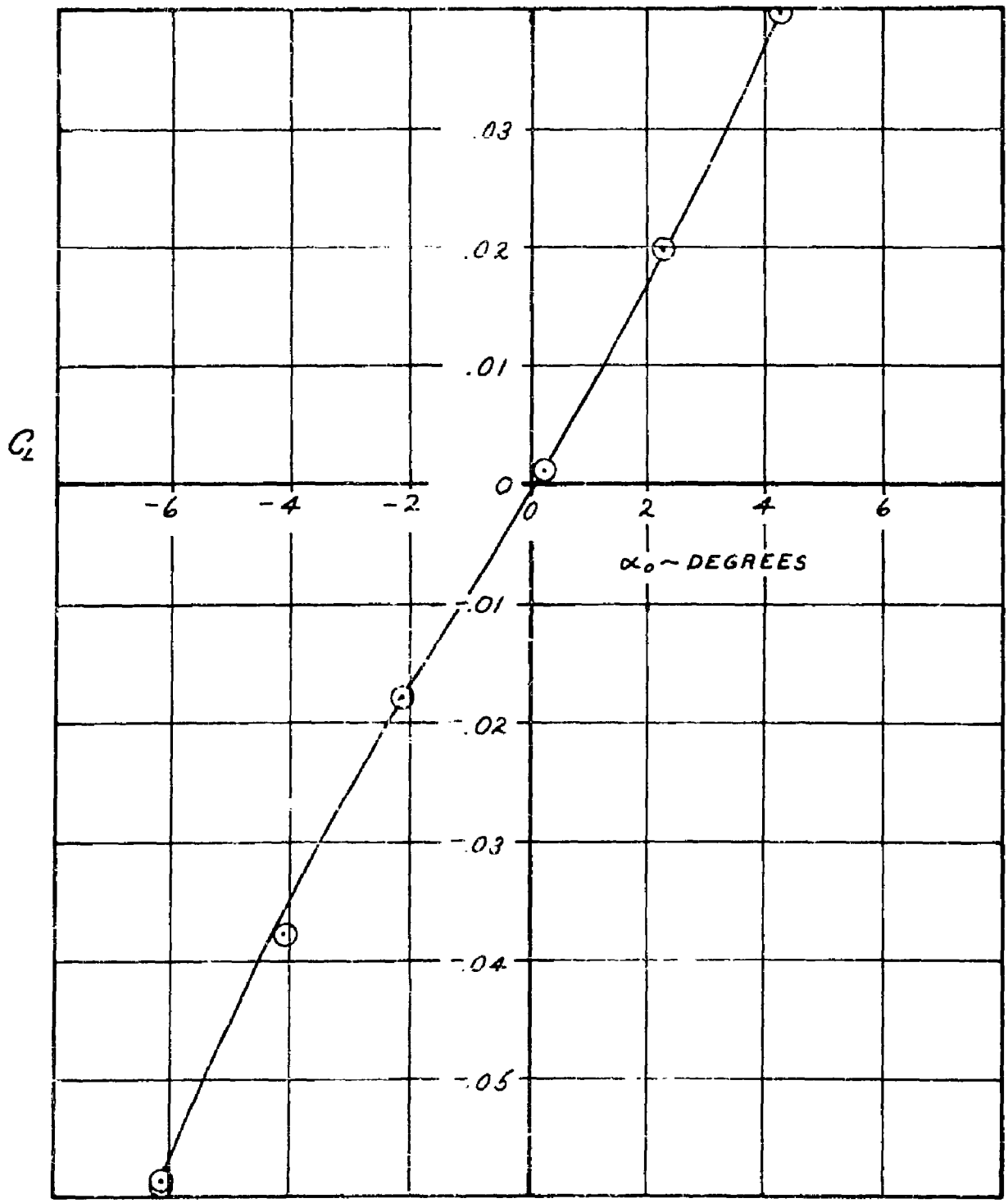

FIGURE A19 EXPERIMENTAL LIFT COEFFICIENT VS. ANGLE-OF-ATTACK; CONFIGURATION #7, MACH NUMBER = 6.0

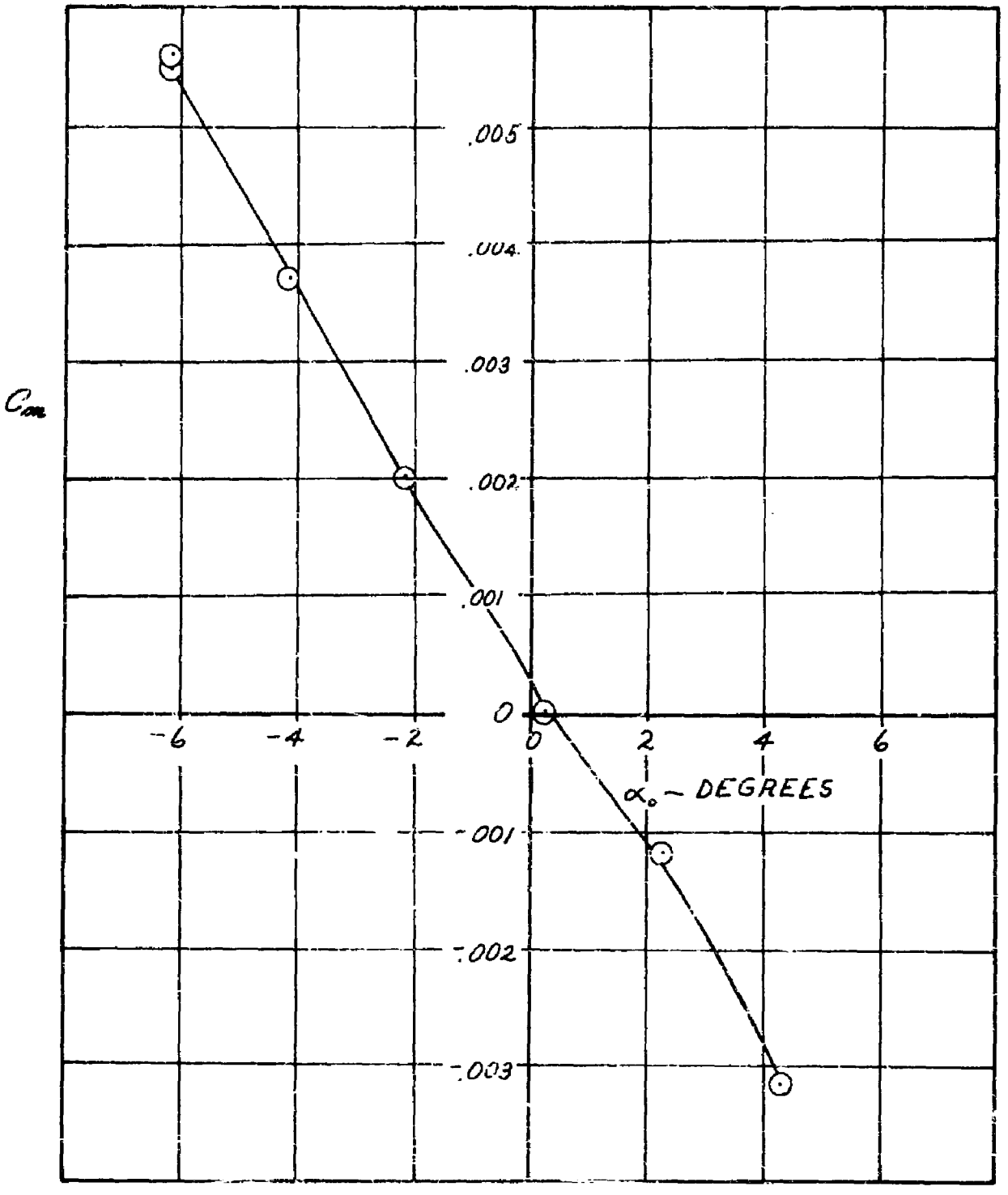

FIGURE A20 EXPERIMENTAL PITCHING MOMENT COEFFICIENT VS. ANGLE-OF-ATTACK; CONFIGURATION #7, MACH NUMBER = 6.0

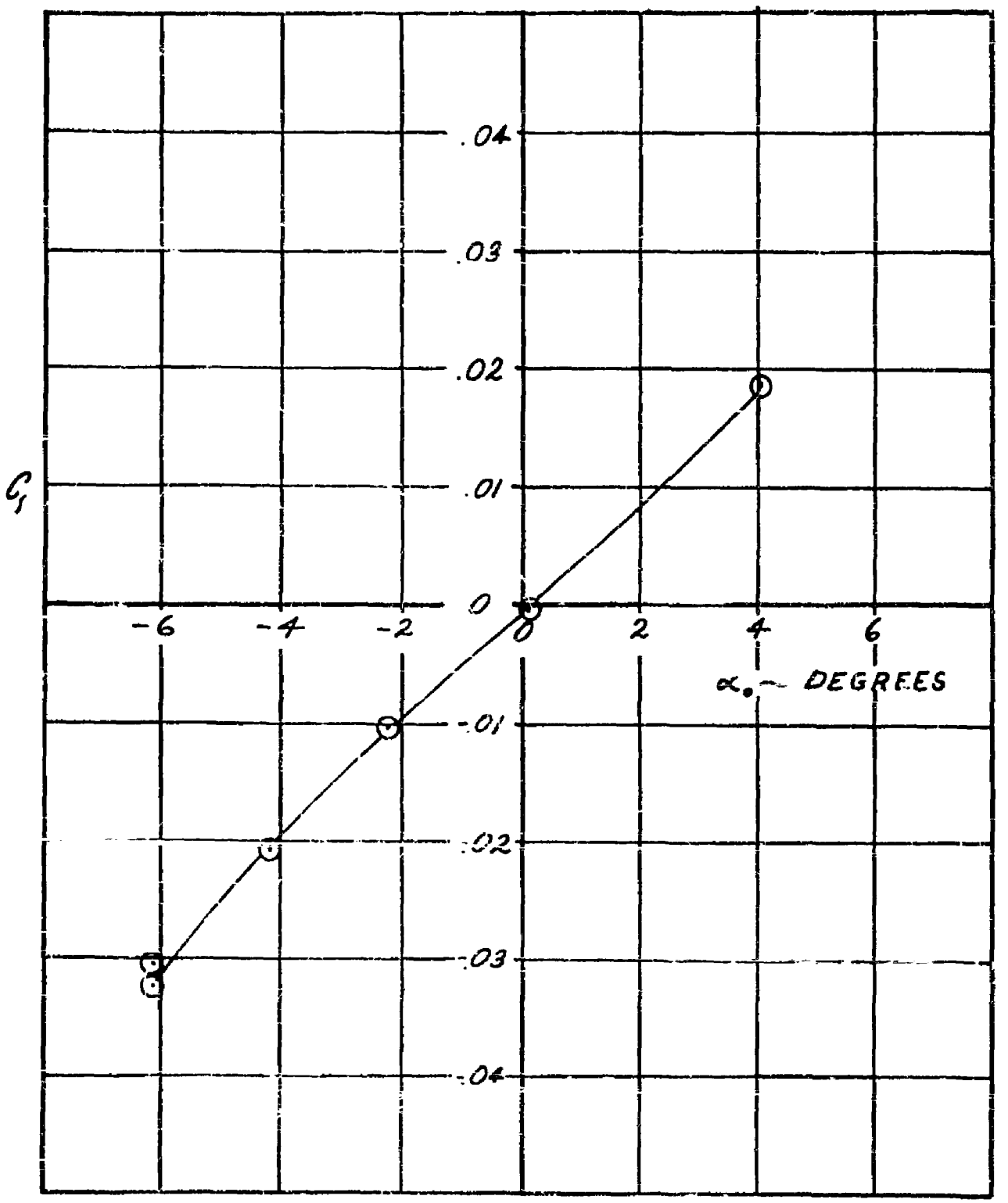

FIGURE A21 EXPERIMENTAL ROLLING MOMENT COEFFICIENT VS. ANGLE-OF-ATTACK; CONFIGURATION #7, MACH NUMBER = 6.0

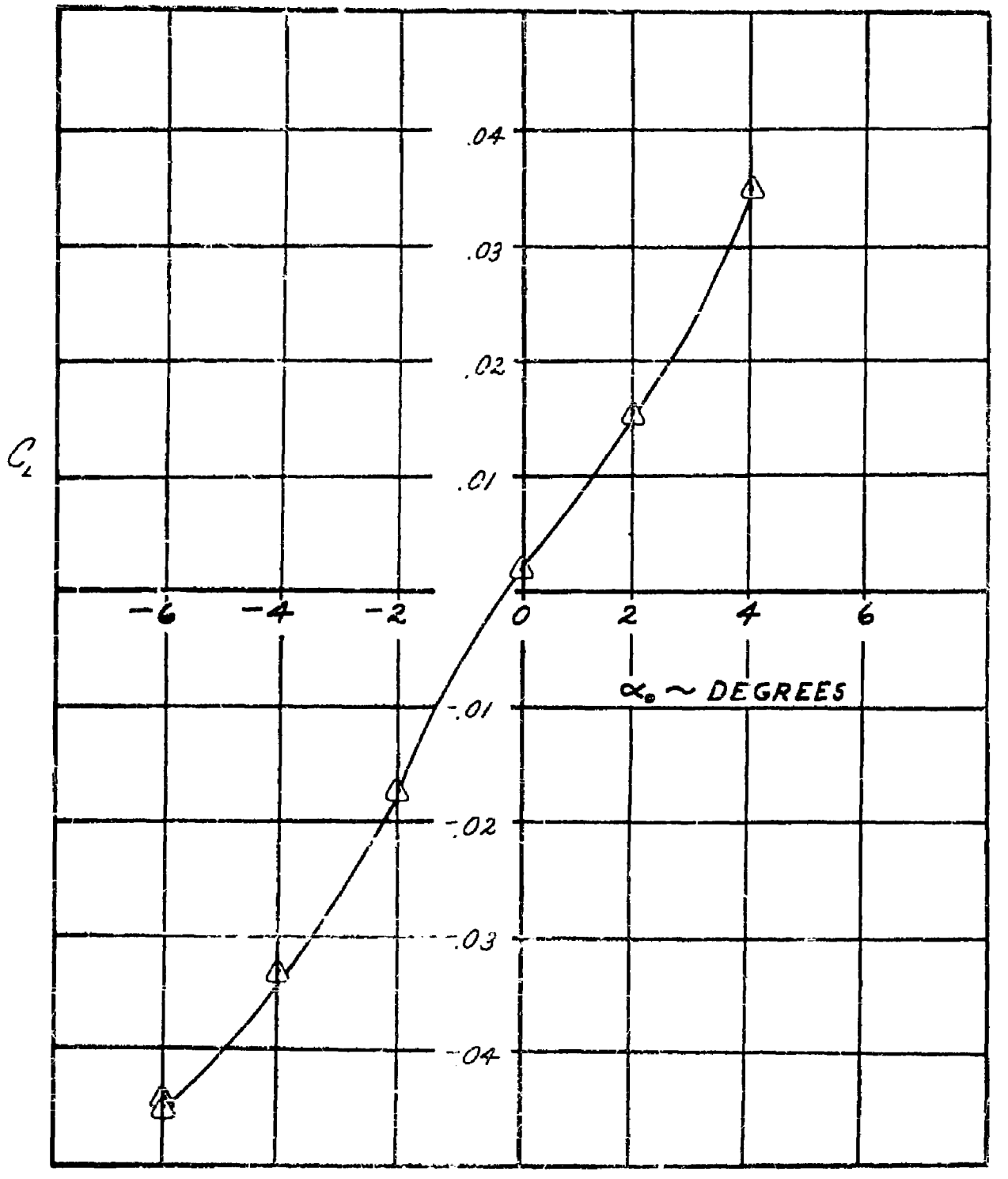

FIGURE A22 EXPERIMENTAL LIFT COEFFICIENT VS. ANGLE-OF-ATTACK; CONFIGURATION #7, MACH NUMBER = 8.0

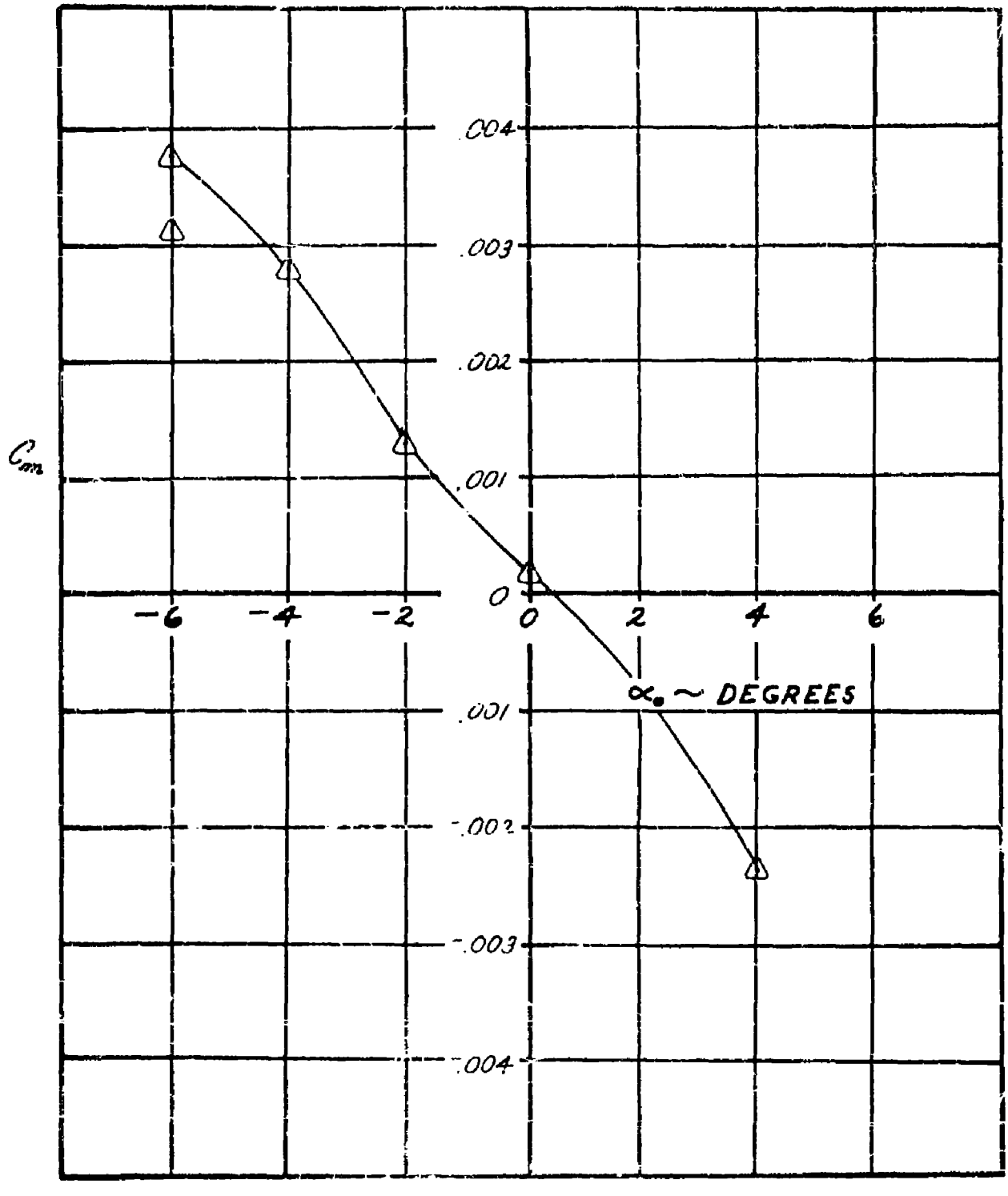

FIGURE A23 EXPERIMENTAL PITCHING MOMENT COEFFICIENT VS. ANGLE-OF-ATTACK; CONFIGURATION #7, MACH NUMBER = 8.0

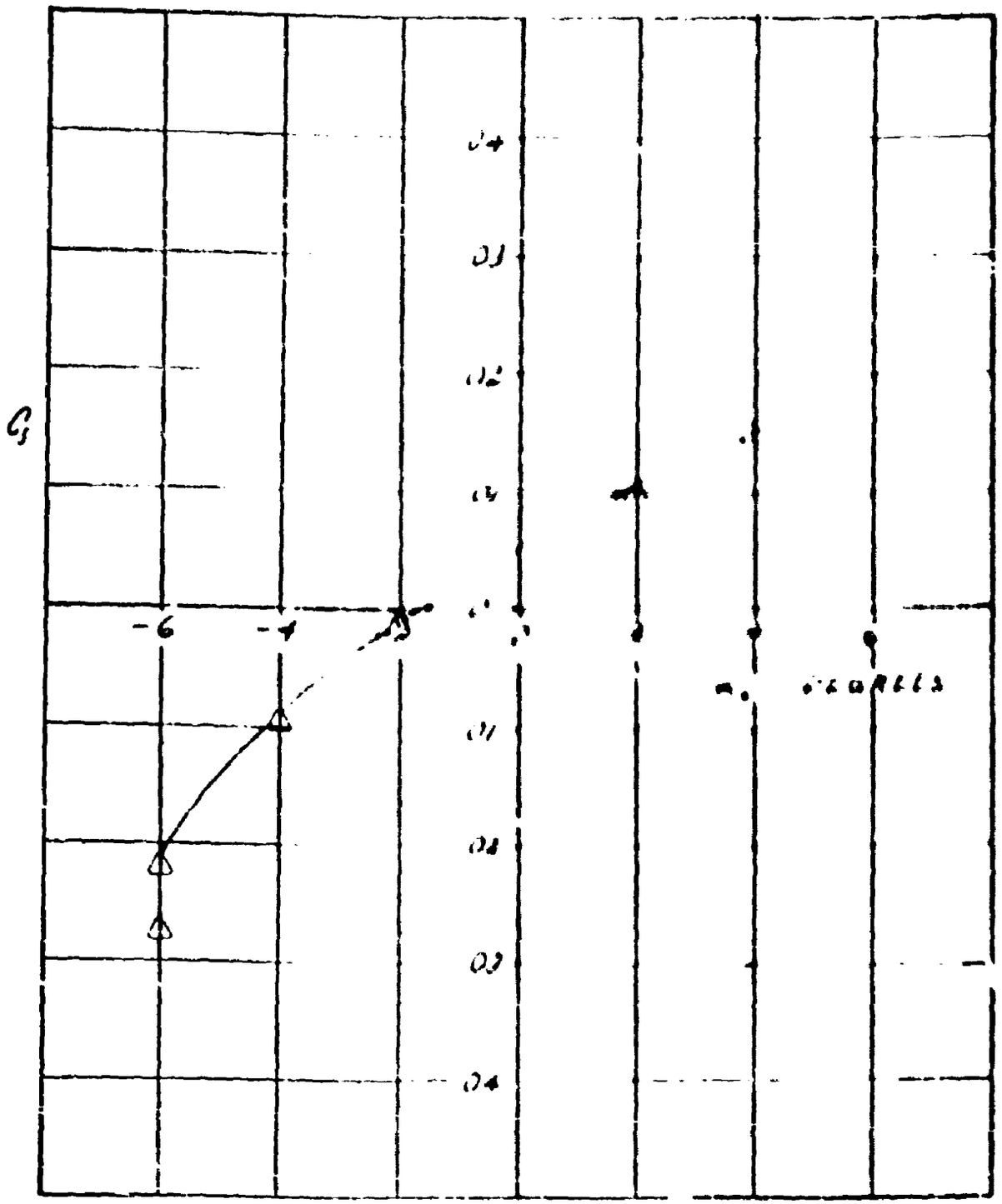

FIGURE A24 EXPERIMENTAL [illegible] V. ANGLE-OF-ATTACK; CONFIGURATION [illegible]

UNCLASSIFIED

UNCLASSIFIED